

# **Lysosomal Ca<sup>2+</sup> Signalling and Neurodegeneration**

***- A Global View***

---

Elizabeth Lucy Yates

A thesis submitted for the degree of Doctor of Philosophy

Department of Cell & Developmental Biology  
University College London

May 2017

## Declaration

I, Elizabeth Yates, confirm that the work presented in this thesis is my own. Where information has been derived from other sources, I confirm that this has been indicated in the thesis.

A handwritten signature in black ink, appearing to read 'Elizabeth Yates', with a long horizontal flourish extending to the right.

Elizabeth Yates

## Abstract

Dysfunction of the lysosomal  $\text{Ca}^{2+}$  channels TRPML1 and TPC2 has been implicated in neurodegenerative disease. However, there is little information about the involvement of these channels in cell-wide global  $\text{Ca}^{2+}$  signalling and it is unknown whether their dysfunction contributes to neurodegeneration by disturbing it.

First, by using synthetic compounds, I demonstrate that TRPML1 activation causes global  $\text{Ca}^{2+}$  signals. In contrast with the predominant lysosomal localisation of the channel these  $\text{Ca}^{2+}$  signals comprised a small lysosomal contribution and a large  $\text{Ca}^{2+}$  entry component. Examination of TRPML1-mediated  $\text{Fe}^{2+}$  entry posed the possibility that divalent cation entry can occur directly through TRPML1 on the plasma membrane.

Second, I identified enlarged and clustered lysosomes in fibroblasts derived from people with sporadic Parkinson's disease (PD). This was appropriately quantified from microscopy images by creating an automated sequence of image processing functions. By inhibiting TPC expression in fibroblasts I demonstrated their involvement in the propagation of physiological global  $\text{Ca}^{2+}$  signals evoked by bradykinin. In sporadic and familial PD patient fibroblasts these TPC-dependent  $\text{Ca}^{2+}$  signals were subtly modulated.

Finally, in a neuronal cell line, reduced TPC expression inhibited the propagation of physiological global  $\text{Ca}^{2+}$  signals evoked by carbachol. These  $\text{Ca}^{2+}$  signals were also blocked by a recently identified TPC blocker and by putative TPC blockers that were screened by collaborators. In cells expressing the PD-associated mutant, LRRK2 G2019S, these TPC-dependent  $\text{Ca}^{2+}$  signals were potentiated. In contrast, bradykinin-evoked  $\text{Ca}^{2+}$  signals in this neuronal cell line were not inhibited by TPC blockers, nor were they potentiated in the LRRK2 G2019S cells. Therefore, physiological global  $\text{Ca}^{2+}$  signalling in PD may be perturbed by TPC dysfunction, and be a compounding factor in neurodegeneration.

Collectively this research suggests that lysosomal  $\text{Ca}^{2+}$  signalling through TRPML1 and TPCs plays a role in global  $\text{Ca}^{2+}$  signalling and that this may be disturbed in neurodegenerative disease.

# Impact Statement

Neurodegenerative diseases hit the headlines regularly in societies with ageing populations. There are few people who are not affected by them - either directly, as relatives or as carers. Devastating neurodegenerative disorders also affect young people and deny a quality of life that many take for granted. Academia, pharma, government health departments and charities are bracing for the increasing social and economic burden of these diseases for which there are currently no cures.

Through endeavours to understand the cause of such diseases the lysosomes and lysosomal  $\text{Ca}^{2+}$  channels such as TRPML1 and TPC2 have received mounting attention. Lysosomes store and release intracellular  $\text{Ca}^{2+}$  which appears to be important for their own regulation.  $\text{Ca}^{2+}$  release from the lysosomes can also cause increases to  $\text{Ca}^{2+}$  levels throughout the cell. These global  $\text{Ca}^{2+}$  signals may impact many critical  $\text{Ca}^{2+}$ -sensitive processes and promote degeneration if they are disturbed. The global link between lysosomal  $\text{Ca}^{2+}$  signalling and neurodegeneration has been the focus of this thesis.

TRPML1 activation caused global  $\text{Ca}^{2+}$  signals which were largely composed of  $\text{Ca}^{2+}$  influx. These findings diverge from the perception that TRPML1 is a mediator of local  $\text{Ca}^{2+}$  signalling. It may also have implications for how the channel is studied in the context of neurodegenerative disorders such as Mucopolysaccharidosis type IV and how its dysfunction is understood to be pathogenic. This data has been published as part of an open access article (Kilpatrick and Yates et al., 2016) and has been cited by a handful of works.

Sporadic PD fibroblasts exhibited disturbed lysosome morphology. This adds weight to the idea that lysosomes have a role in PD. The image processing method used to quantify this defect has since been published in an open access article, and applied in the investigation of endolysosomal-ER contacts and growth factor signalling (Kilpatrick et al., 2017). Besides facilitating experimental work, this semi-automated image processing may be of use within a diagnostic assay for people presenting parkinsonian symptoms. This could enable timely administration of appropriate therapies.

TPCs were required for physiological global  $\text{Ca}^{2+}$  signalling. This supplements very limited data on this topic, and supports the notion that these channels may have cell-wide influence. Collaboration led to the identification of FDA-approved putative TPC blockers that inhibited physiological global  $\text{Ca}^{2+}$  signals. The same signals were augmented in a neuronal PD model. This



poses the possibility that TPC dysfunction contributes to neurodegeneration via potentiated global  $\text{Ca}^{2+}$  signalling. This could open up a new avenue for PD research and TPCs may emerge as suitable drug targets. Indeed, the putative TPC blockers may inform the development of PD-modifying drugs.

The data in this thesis have been shared with a wide audience in the form of annual reports to Parkinson's UK, publications, posters and talks. These have been presented at departmental seminars, the UCL Neuroscience Symposium, the International Meeting of the European Calcium Society, and a Parkinson's UK visit attended by people with PD and their families. Data, ideas and tools presented in this thesis continue to be developed within the Patel laboratory.

# Acknowledgments

First, I would like to thank my supervisors Professor Sandip Patel and Professor Anthony Schapira for granting me the opportunity to study at UCL. Both have unbounded enthusiasm and drive to improve the lives of others through their research. In particular, I would like to thank Professor Sandip Patel for imparting his immense knowledge, for his continuous guidance and support, and for creating a research environment where ideas, methods and laughter are freely shared.

I thank Parkinson's UK for my funding. This charity truly brings science to life and it is difficult not to be inspired by their work, nor the people with Parkinson's disease whom they involve in every aspect of what they do.

To the individuals who donated skin biopsies for the fibroblast cultures used in this thesis - thank you. Likewise I acknowledge Henrietta Lacks and the girl whose cells have formed the HeLa and SH-SY5Y cell lines respectively.

Numerous scientists have enabled my research, for which I am grateful. For this I extend my thanks to Drs Michelle Beavan, Alisdair McNeill, Jan-Willem Taanman and Tatiana Papkovskaia for generating the fibroblast cultures, to Drs Mark Cooper and Kai-Yin Chau for creating the stable LRRK2 SH-SY5Y cell lines, to Dr Stephen Mullin for murine neurons and Drs Taufiq Rahman, Christopher Penny and Prof Patel for their identification of putative TPC inhibitors. I would also like to recognise my graduate tutor Professor Michael Duchon, Dr Andrey Abramov and Professor Gyorgy Szabadkai for formative and stimulating discussion about my work, particularly on the topic of lysosome morphology quantification. I also thank Dr Bill Andrews for his technical advice on quantitative PCR.

To Dr Bethan Kilpatrick and Leanne Hockey, who showed me the ropes when I joined the Patel lab and beyond - your time, expertise and patience cannot be underestimated. To you, and Dr Alice Roycroft, Cara Yuan, Dr Christopher Penny, Dr Manuela Melchionda and Dr Sophie McLachlan, with whom I've shared an office for 3 years - thank you all for your technical support, your camaraderie and the endless baked goods, for which I have been reprimanded by the dentist. Thanks also to Dr Lewis Brayshaw, who as a chatty resident of the culture room provided light relief between cell counts, and similarly to Adam Shellard in the office next door, who truly sings "like no one is listening".

Finally, to my friends and family outside UCL life - your support and encouragement has been tremendous, and an essential part of this thesis. Thank you.

# Contents

<b>Declaration</b> .....	2
<b>Abstract</b> .....	3
<b>Impact Statement</b> .....	4
<b>Acknowledgments</b> .....	6
<b>Abbreviations</b> .....	15
<b>CHAPTER 1: Introduction</b> .....	18
<b>1.1 OVERVIEW</b> .....	18
<b>1.2 LYSOSOMES</b> .....	19
1.2.1 Lysosomes and Degradation .....	19
1.2.2 Lysosomal Ca <sup>2+</sup> .....	21
1.2.3 Lysosomal Ca <sup>2+</sup> and membrane fusion/fission.....	21
1.2.4 Lysosomal Ca <sup>2+</sup> release.....	23
1.2.4.1 TRPML1 .....	23
1.2.4.1.1 Structure and Discovery.....	23
1.2.4.1.2 Localisation .....	24
1.2.4.1.3 Channel Properties.....	24
1.2.4.1.4 Cellular Function .....	26
1.2.4.2 TPC1 & 2.....	27
1.2.4.2.1 Structure and Discovery.....	27
1.2.4.2.2 Localisation .....	28
1.2.4.2.3 Channel Properties.....	28
1.2.4.2.4 Cellular Function .....	30
1.2.5 Lysosomal Ca <sup>2+</sup> uptake .....	31
1.2.5.1 CAX .....	31
<b>1.3 Ca<sup>2+</sup> SIGNALLING</b> .....	31
1.3.1 Local and Global Ca <sup>2+</sup> signals.....	32
1.3.2 Membrane Contact Sites .....	32
1.3.3 Ca <sup>2+</sup> from the ER.....	33
1.3.4 Ca <sup>2+</sup> from the Golgi.....	34
1.3.5 Ca <sup>2+</sup> from the lysosomes .....	36
1.3.6 Ca <sup>2+</sup> from the extracellular space.....	44
1.3.7 Ca <sup>2+</sup> and mitochondrial function.....	45
1.3.8 Signal Silencing.....	47

<b>1.4 LYSOSOMES, Ca<sup>2+</sup> AND NEURODEGENERATION</b> .....	48
1.4.1 Mucopolidosis Type IV .....	49
1.4.2 Parkinson's Disease.....	52
1.4.2.1 Genetics and PD.....	53
1.4.2.1.1 GBA1 .....	53
1.4.2.1.2 ATP13A2.....	54
1.4.2.1.3 LRRK2 .....	55
1.4.2.1.4 SNCA.....	57
1.4.2.1.5 PINK1, PRKN and PARK7 .....	59
1.4.2.2 Environmental Factors and PD.....	60
1.4.2.3 Age and PD.....	61
<b>1.5 SUMMARY</b> .....	64
<b>1.6 AIMS</b> .....	66
<b>CHAPTER 2: TRPML1 and Global Ca<sup>2+</sup> Signalling</b> .....	68
<b>2.1 INTRODUCTION</b> .....	68
<b>2.2 METHODS and ANALYSIS</b> .....	71
2.2.1 Cell culture .....	71
2.2.1.1 HeLa .....	71
2.2.1.2 Fibroblast .....	71
2.2.1.3 SH-SY5Y .....	71
2.2.1.4 Neuronal .....	71
2.2.2 Transfection .....	72
2.2.3 Cell labelling.....	72
2.2.4 Microscopy: Confocal.....	73
2.2.4.1 Pearson's correlation coefficient.....	73
2.2.4.2 Percentage of colocalised vesicles.....	73
2.2.5 Microscopy: Epifluorescence .....	74
2.2.5.1 Ca <sup>2+</sup> - GCaMP3.....	75
2.2.5.2 Ca <sup>2+</sup> - Fura-2 .....	75
2.2.5.3 Fe <sup>2+</sup> - Fura-2.....	76
2.2.5.4 Acidic Organelles - LysoTracker Red.....	76
2.2.6 Data Presentation .....	76
<b>2.3 RESULTS</b> .....	77
2.3.1 The TRPML1 agonist ML-SA1 evokes global Ca <sup>2+</sup> signals in cells overexpressing GCaMP3-ML1 .....	77
2.3.2 The TRPML1 agonist ML-SA1 evokes global Ca <sup>2+</sup> signals in untransfected cells.....	79

2.3.3 Overexpressed TRPML1 and mutant TRPML1 colocalise with lysosomes.....	81
2.3.4 Overexpressed TRPML1 WT potentiates agonist-evoked global Ca <sup>2+</sup> signals but TRPML1 mutant does not .....	83
2.3.5 Extracellular Ca <sup>2+</sup> contributes to TRPML1-mediated global Ca <sup>2+</sup> signals .....	85
2.3.6 Lysomotropic GPN inhibits TRPML1-mediated global Ca <sup>2+</sup> signals.....	86
2.3.7 SOCE blocker BTP2 does not inhibit TRPML1-mediated global Ca <sup>2+</sup> signals.....	88
2.3.8 TRPML1 agonists permit divalent cation entry.....	90
2.3.9 Divalent cation entry is inhibited by SOCE blocker BTP2, but is not induced by ER Ca <sup>2+</sup> depletion .....	93
2.3.10 The TRPML1 agonist ML-SA1 evokes global Ca <sup>2+</sup> signals in multiple untransfected cell types.....	94
<b>2.4 DISCUSSION.....</b>	<b>95</b>
<b>CHAPTER 3: TPCs and Global Ca<sup>2+</sup> Signalling .....</b>	<b>100</b>
<b>3.1 INTRODUCTION.....</b>	<b>100</b>
<b>3.2 METHODS and ANALYSIS .....</b>	<b>103</b>
3.2.1 Recurrent methods .....	103
3.2.2 Cell culture .....	103
3.2.2.1 Fibroblast .....	103
3.2.3 Immunocytochemistry.....	103
3.2.4 Microscopy: Confocal.....	104
3.2.4.1 Automated image analysis for LAMP1 intensity.....	104
3.2.4.2 Automated image analysis for lysosome size and frequency.....	105
3.2.4.2.1 Generating binary images by local thresholding .....	105
3.2.4.2.2 Watershed segmentation .....	110
3.2.4.2.3 Distinguishing between lysosome morphotypes.....	114
3.2.5 siRNA transfection .....	114
3.2.6 Quantitative PCR.....	115
3.2.7 Microscopy: Epifluorescence .....	116
3.2.7.1 Ca <sup>2+</sup> - Fura-2 .....	116
3.2.8 Statistical Analysis.....	116
<b>3.3 RESULTS .....</b>	<b>117</b>
3.3.1 Disturbed lysosome morphology is associated with increased LAMP1 immunofluorescence in LRRK2-GS but not sporadic PD patient fibroblasts .....	117
3.3.2 Automated lysosome analysis confirms enlarged lysosomes in sporadic PD fibroblasts .....	119
3.3.3 NH <sub>4</sub> Cl as a tool to deplete lysosomal Ca <sup>2+</sup> .....	122

3.3.4 Inflammatory mediator bradykinin evokes concentration-dependent global Ca <sup>2+</sup> signals which are blocked by NH <sub>4</sub> Cl .....	125
3.3.5 Validation of TPC knockdown in fibroblasts by quantitative PCR.....	127
3.3.6 TPC knockdown inhibits bradykinin-evoked Ca <sup>2+</sup> signals .....	129
3.3.7 Bradykinin-evoked Ca <sup>2+</sup> signals are similar in LRRK2-GS PD and control fibroblasts	131
3.3.8 Bradykinin-evoked Ca <sup>2+</sup> signals are similar in sporadic PD and control fibroblasts.	133
<b>3.4 DISCUSSION</b> .....	<b>135</b>
<b>CHAPTER 4: TPCs and Global Ca<sup>2+</sup> Signalling</b> .....	<b>145</b>
<b>4.1 INTRODUCTION</b> .....	<b>145</b>
<b>4.2 METHODS and ANALYSIS</b> .....	<b>147</b>
4.2.1 Recurrent methods .....	147
4.2.2 Cell culture .....	147
4.2.2.1 SH-SY5Y .....	147
4.2.3 siRNA transfection .....	147
4.2.3.1 Standard protocol .....	147
4.2.3.2 Extended protocol.....	148
4.2.4 Microscopy: Epifluorescence .....	148
4.2.4.1 Ca <sup>2+</sup> - Fura-2 .....	148
4.2.5 Western blotting .....	149
4.2.6 Statistical analysis .....	149
<b>4.3 RESULTS</b> .....	<b>151</b>
4.3.1 Lysomotropic agent GPN evokes simple Ca <sup>2+</sup> signals in SH-SY5Y cells .....	151
4.3.2 Carbachol and bradykinin evoke concentration-dependent Ca <sup>2+</sup> signals .....	151
4.3.3 GPN inhibits carbachol but not bradykinin-evoked Ca <sup>2+</sup> signals .....	154
4.3.4 Carbachol but not bradykinin blocks GPN-evoked Ca <sup>2+</sup> signals .....	155
4.3.5 Thapsigargin inhibits both carbachol and bradykinin-evoked Ca <sup>2+</sup> signals .....	156
4.3.6 Validating TPC knockdown in SH-SY5Ys .....	158
4.3.7 TPC1 knockdown inhibits carbachol-evoked Ca <sup>2+</sup> signals .....	160
4.3.8 TPC2 siRNAs reduce TPC2 transcript levels in fibroblasts but not SH-SY5Ys .....	161
4.3.9 Recently identified TPC inhibitor tetrandrine blocks carbachol but not bradykinin-evoked Ca <sup>2+</sup> signals.....	163
4.3.10 Putative TPC blocker and MAO inhibitor L-deprenyl blocks carbachol but not bradykinin-evoked Ca <sup>2+</sup> signals .....	165
4.3.11 Putative TPC blockers sunitinib and pimozide block carbachol but not bradykinin-evoked Ca <sup>2+</sup> signals.....	166
4.3.12 Putative TPC blocker fluphenazine blocks carbachol but not bradykinin-evoked Ca <sup>2+</sup> signals.....	168

4.3.13 Carbachol but not bradykinin-evoked Ca <sup>2+</sup> signals are potentiated in LRRK2-GS cells.....	170
4.3.14TPC transcript levels are unaltered in LRRK2-GS cells .....	172
4.3.15 GPN and thapsigargin-evoked Ca <sup>2+</sup> signals are unchanged in LRRK2-GS cells.....	173
4.3.16 SOCE is inhibited in LRRK2-GS cells.....	174
<b>4.4 DISCUSSION</b> .....	175
<b>CHAPTER 5: Conclusions and Future Directions</b> .....	191
<b>Appendices</b> .....	199
Appendix A: Additional genes implicated in PD or parkinsonism.....	199
Appendix B: Example binary images for lysosome size and frequency analysis .....	202
Appendix C: In silico-based drug screens for FDA-approved, selective TPC blockers .....	207
<b>References</b> .....	210

## List of Figures

<b>Chapter 1: Introduction</b>		
1.1	The dynamic lysosome	20
1.2	TRPML1	23
1.3	TPCs	27
1.4	The Ca <sup>2+</sup> signalling network of the cell	35
1.5	Lysosomes, Ca <sup>2+</sup> and neurodegeneration	65
<b>Chapter 2: TRPML1 and Global Ca<sup>2+</sup> Signalling</b>		
2.1	Introduction	70
2.1	The TRPML1 agonist ML-SA1 evokes global Ca <sup>2+</sup> signals in cells overexpressing GCaMP3-TRPML1	78
2.2	The TRPML1 agonist ML-SA1 evokes global Ca <sup>2+</sup> signals in untransfected cells	80
2.3	Overexpressed TRPML1 and mutant TRPML1 colocalise with lysosomes	82
2.4	Overexpressed TRPML1 WT potentiates agonist-evoked global Ca <sup>2+</sup> signals, but TRPML1 mutant does not	84
2.5	Extracellular Ca <sup>2+</sup> contributes to TRPML1-mediated global Ca <sup>2+</sup> signals	85
2.6	Lysomotropic GPN inhibits TRPML1-mediated global Ca <sup>2+</sup> signals	87
2.7	The SOCE blocker BTP2 does not inhibit TRPML1-mediated global Ca <sup>2+</sup> signals	89
2.8	TRPML1 agonists permit divalent cation entry	91
2.9	Divalent cation entry is inhibited by SOCE blocker BTP2, but is not induced by ER Ca <sup>2+</sup> depletion	93
2.10	The TRPML1 agonist ML-SA1 evokes global Ca <sup>2+</sup> signals in multiple untransfected cell types	94
<b>Chapter 3: TPCs and Global Ca<sup>2+</sup> Signalling - in Familial and Sporadic PD Fibroblasts</b>		
3.1	Introduction	102
3.M.1	Macro commands for LAMP1 intensity analysis	105
3.M.2	LAMP1-positive structures are enlarged in fibroblasts treated with vacuolin	105
3.M.3	Schematic of global thresholding in ImageJ	107
3.M.4	Immunofluorescence images converted to binary by global thresholding	108
3.M.5	Schematic of Bernsen local thresholding in ImageJ	109
3.M.6	Schematic of watershed segmentation in ImageJ	111
3.M.7	Immunofluorescence images converted to binary by Bernsen local thresholding and watershed segmentation	112
3.M.8	Macro commands for lysosome size and frequency analysis	112
3.M.9	Automated image processing and analysis confirms enlarged lysosomes in vacuolin-treated fibroblasts	113
3.1	Disturbed lysosome morphology is associated with increased LAMP1 immunofluorescence in LRRK2-GS but not sporadic PD patient fibroblasts	118
3.2	Automated lysosome analysis confirms enlarged lysosomes in sporadic PD fibroblasts	120



3.3	NH <sub>4</sub> Cl as a tool to deplete lysosomal Ca <sup>2+</sup>	123
3.4	Inflammatory mediator bradykinin evokes concentration-dependent global Ca <sup>2+</sup> signals, which are blocked by NH <sub>4</sub> Cl	126
3.5	Validation of TPC knockdown in fibroblasts by quantitative PCR	128
3.6	TPC knockdown inhibits bradykinin-evoked Ca <sup>2+</sup> signals	130
3.7	Bradykinin-evoked Ca <sup>2+</sup> signals are similar in LRRK2-GS PD and control fibroblasts	132
3.8	Bradykinin-evoked Ca <sup>2+</sup> signals are similar in sporadic PD and control fibroblasts	134

#### **Chapter 4: TPCs and Global Ca<sup>2+</sup> Signalling – in a Neuronal PD Model**

4.1	Introduction	146
4.1	Lysomotropic agent GPN evokes simple Ca <sup>2+</sup> signals in SH-SY5Y cells	152
4.2	Carbachol and bradykinin evoke concentration-dependent Ca <sup>2+</sup> signals	153
4.3	GPN inhibits carbachol but not bradykinin-evoked Ca <sup>2+</sup> signals	154
4.4	Carbachol but not bradykinin blocks GPN-evoked Ca <sup>2+</sup> signals	156
4.5	Thapsigargin inhibits both carbachol and bradykinin-evoked Ca <sup>2+</sup> signals	157
4.6	Validating TPC knockdown in SH-SY5Ys	159
4.7	TPC1 knockdown inhibits carbachol-evoked Ca <sup>2+</sup> signals	160
4.8	TPC2 siRNAs reduce TPC2 transcript levels in fibroblasts but not SH-SY5Ys	162
4.9	Recently identified TPC inhibitor tetrandrine blocks carbachol but not bradykinin-evoked Ca <sup>2+</sup> signals	164
4.10	Putative TPC blocker and MAO inhibitor L-deprenyl blocks carbachol but not bradykinin-evoked Ca <sup>2+</sup> signals	166
4.11	Putative TPC blockers sunitinib and pimozide block carbachol but not bradykinin-evoked Ca <sup>2+</sup> signals	167
4.12	Putative TPC blocker fluphenazine blocks carbachol but not bradykinin-evoked Ca <sup>2+</sup> signals	169
4.13	Carbachol but not bradykinin-evoked Ca <sup>2+</sup> signals are potentiated in LRRK2-GS cells	171
4.14	TPC transcript levels are unaltered in LRRK2-GS cells	172
4.15	GPN and thapsigargin-evoked Ca <sup>2+</sup> signals are unchanged in LRRK2-GS cells	173
4.16	SOCE is inhibited in LRRK2-GS cells	174

#### **Chapter 5: Conclusions and Future Directions**

5.1	Recently identified TPC inhibitor tetrandrine preferentially inhibits histamine-evoked Ca <sup>2+</sup> signals in fibroblasts	196
5.2	Lysosomal Ca <sup>2+</sup> Signalling and Neurodegeneration – <i>A Global View</i> . Conclusions and Future Directions	197

## List of Tables

<b>Chapter 1: Introduction</b>		
1.1	Extracellular stimuli associated with NAADP generation	38
1.2	Ca <sup>2+</sup> signals induced by extracellular stimuli with inferred NAADP/lysosomal involvement	40
1.3	Additional genes implicated in PD or parkinsonism	60

<b>Chapter 2: TRPML1 and Global Ca<sup>2+</sup> Signalling</b>		
2.1	Plasmids	72
2.2	Confocal microscopy excitation/emission wavelengths	73
2.3	SQUASSH parameters	74
2.4	Epifluorescence microscopy excitation/emission wavelengths	74
2.5	Epifluorescence microscopy excitation/emission wavelengths	74

<b>Chapter 3: TPCs and Global Ca<sup>2+</sup> Signalling - in Familial and Sporadic PD Fibroblasts</b>		
3.1	Patient-derived fibroblasts	103
3.2	Confocal microscopy excitation/emission wavelengths	104
3.3	TPC-targeting siRNAs	115
3.4	Quantitative PCR primers	115
3.5	Epifluorescence microscopy excitation/emission wavelengths	116
3.6	TPC-dependent, stimulus-evoked Ca <sup>2+</sup> signals	142

<b>Chapter 4: TPCs and Global Ca<sup>2+</sup> Signalling – in a Neuronal PD Model</b>		
4.1	TPC-targeting siRNAs	148

# Abbreviations

7-ket	7-ketocholesterol
$\alpha$ -syn	$\alpha$ -synuclein
Ab	Antibody
ALG	Apoptosis linked gene
AM	Acetoxymethyl ester
ATC	Arginine thiazolidine carboxylate
ATP	Adenosine triphosphate
BAPTA	1,2-Bis(2-aminophenoxy)ethane-N,N,N',N'-tetraacetic acid
BiP	Binding immunoglobulin protein
BSA	Bovine serum albumin
BTP2	<i>N</i> -[4-[3,5-Bis(trifluoromethyl)-1 <i>H</i> -pyrazol-1-yl]phenyl]-4-methyl-1,2,3-Thiadiazole-5-carboxamide
cADPR	Cyclic adenosine diphosphate ribose
CAMKK	Calcium/calmodulin-dependent protein kinase kinase
Cav	Voltage-operated Ca <sup>2+</sup> channel
CB <sub>2</sub>	Cannabinoid receptor type 2
CHO	Chinese hamster ovary
CICR	Ca <sup>2+</sup> -induced Ca <sup>2+</sup> release
CMA	Chaperone-mediated autophagy
DA	Dopamine
DABCO	1,4 diazabicyclo[2,2,2]octane
DAPI	4',6-diamidino-2-phenylindole
DHP	Dihydropyridine
DMEM	Dulbecco's Modified Eagle Medium
DMSO	Dimethyl sulfoxide
DNA	Deoxyribonucleic acid
ECL	Enhanced chemiluminescence
EDM	Euclidean distance map
EDTA	Ethylenediaminetetraacetic acid
EGF	Epidermal growth factor
EGTA	Ethylene glycol-bis( $\beta$ -aminoethyl ether)-N,N,N',N'-tetraacetic acid
EMA	European Medicines Agency
ER	Endoplasmic reticulum
ERK	Extracellular signal-regulated kinase 1/2
ERM	Ezrin/radixin/moesin
ET	Endothelin
FasL	Fas ligand
FBS	Foetal bovine serum
FDA	US Food and Drug Administration
GAP	GTPase activating protein
GAPDH	Glyceraldehyde 3-phosphate dehydrogenase
GBA	Glucocerebrosidase beta
GCaMP3	GFP Calmodulin Peptide 3
GD	Gaucher's disease
GDF	GDI displacement factor
GDI	GDP dissociation inhibitor
GDP	Guanosine diphosphate

GECO	Genetically encoded calcium indicator for optimal imaging
GEF	Guanine nucleotide exchange factor
GFP	Green fluorescent protein
GLP	Glucagon-like peptide
GPN	Glycyl-L-phenylalanine-beta-naphthylamide
GRP75	75kDa glucose-related protein
GS	G2019S mutation
GTP	Guanosine
HBS	HEPES-buffered saline
HCN	Hyperpolarisation and cyclic nucleotide gated cation
HEK293T	Human embryonic kidney cells 293, with SV40 large T-antigen
HEPES	(4-(2-hydroxyethyl)-1-piperazineethanesulfonic acid
HIV	Human immunodeficiency virus
HRP	Horseradish peroxidase
ID	Identifier
IICR	IP <sub>3</sub> -induced Ca <sup>2+</sup> entry
IL	Interleukin
INAD	Infantile neuroaxonal dystrophy
IP <sub>3</sub>	Inositol triphosphate
iPSC	Induced pluripotent stem cells
LAMP	Lysosome-associated membrane protein
LC3	Microtubule-associated protein 1A/1B-light chain 3
LDS	Lithium dodecyl sulphate
LRRK	Leucine-rich repeat kinase
LSD	Lysosomal storage disorder
LTR	Lysotracker Red
M6P	Mannose-6-phosphate
M6PR	Mannose-6-phosphate receptor
MCS	Membrane contact site
MEF	Mouse embryonic fibroblasts
MFN	Mitochondrial dynamin-related family member mitofusin
MLIV	Mucopolidosis type IV
ML1	TRPML1
ML-SA	Mucolipin synthetic agonist
ML-SI	Mucolipin synthetic inhibitor
mRFP	Monomeric red fluorescent protein
mTOR	Mammalian target of rapamycin
MxA	Interferon-induced protein MxA
NAADP	Nicotinic acid adenine dinucleotide phosphate
NAD	Nicotinamide adenine dinucleotide
NADP	Nicotinamide adenine dinucleotide phosphate
NBIA	Neurodegeneration with brain iron accumulation
NPC	Niemann-Pick type C disease
NSF	N-ethylmaleimide-sensitive factor
PAGE	Polyacrylamide gel electrophoresis
PBS	Phosphate-buffered saline
PCR	Polymerase chain reaction
PD	Parkinson's disease
PI(3,5)P <sub>2</sub>	Phosphatidylinositol 3,5-bisphosphate
PI(4,5)P <sub>2</sub>	Phosphatidylinositol 4,5-bisphosphate

PKB	Protein kinase B
PMCA	Plasma membrane Ca <sup>2+</sup> ATPase
PML	Promyelocytic leukaemia tumour suppressor
P <sub>o</sub>	Open probability
PSF	Point spread function
PT	Permeability transition
PTPIP	Protein tyrosine phosphatase-interacting protein
PVDF	Polyvinylidene difluoride
QPCR	Quantitative PCR
RCF	Relative centrifugal force
RNA	Ribonucleic acid
ROI	Region of interest
ROS	Reactive oxygen species
RT	Reverse transcriptase
SDS	Sodium dodecyl sulphate
SERCA	Sarco/endoplasmic reticulum Ca <sup>2+</sup> -ATPase
siRNA	Short interfering RNA
SNARE	Soluble N-ethylmaleimide-sensitive factor activating protein
SOCE	Store-operated Ca <sup>2+</sup> entry
SPCA	Secretory pathway Ca <sup>2+</sup> -ATPase
SQUASSH	Segmentation and quantification of subcellular shapes
Syt	Synaptotagmin
TBS	Tris-buffered saline
TBS-T	Tris-buffered saline plus Tween
TIFF	Tagged image file format
TMPH	2-[(3-Trifluoromethyl)phenyl] histamine dimaleate
TMR	Transmembrane region
TPC	Two-pore channel
TRP	Transient receptor potential
TRPC	Transient receptor potential canonical
TRPML	Transient receptor potential mucolipin
UBC	Ubiquitin C
UEP	Ultimate eroded point
UPR	Unfolded protein response
VAMP	Vesicle-associated membrane protein
VAP	Vesicle-associated membrane protein-associated protein
V-ATPase	Vacuolar ATPase
VDAC	Voltage-dependent anion channel
VEGF	Vascular endothelial growth factor
VICR	Voltage-induced Ca <sup>2+</sup> release
VOCC	Voltage-operated Ca <sup>2+</sup> channel
VOKC	Voltage-operated K <sup>+</sup> channel
VONC	Voltage-operated Na <sup>+</sup> channel
VPS35	Vacuolar protein sorting-associated protein 35
VTA	Ventral tegmental area
WT	Wildtype

# CHAPTER 1: Introduction

## 1.1 OVERVIEW

Inside our cells the signalling ion  $\text{Ca}^{2+}$  regulates a wide array of processes. Various patterns of  $\text{Ca}^{2+}$  movement around the cell can determine which specific processes are effected at a given moment. These  $\text{Ca}^{2+}$  signals are coordinated by a collection of intracellular  $\text{Ca}^{2+}$  stores, channels, pumps, exchangers and buffers. If any of these components of the  $\text{Ca}^{2+}$  signalling network dysfunction,  $\text{Ca}^{2+}$  signals may be disrupted and cause numerous  $\text{Ca}^{2+}$ -dependent processes to falter. This may lead to cell damage or cell death.

The lysosomes are a component of the  $\text{Ca}^{2+}$  signalling network, storing  $\text{Ca}^{2+}$  at a high concentration inside our cells. These small membrane-bound organelles have long been regarded as the waste-disposal unit of the cell, ridding any unwanted and potentially harmful materials. Now their job of  $\text{Ca}^{2+}$  storage and  $\text{Ca}^{2+}$  release is also more widely appreciated and is understood to influence their waste-disposal function too. Importantly,  $\text{Ca}^{2+}$  channels that enable lysosomal  $\text{Ca}^{2+}$  release have been associated with neurodegenerative disease – namely TRPML1 and TPC2. These lysosomal  $\text{Ca}^{2+}$  channels are believed to raise the local concentration of  $\text{Ca}^{2+}$  around the lysosomes to regulate lysosome function. In the associated neurodegenerative diseases there is evidence that this local  $\text{Ca}^{2+}$  signalling is disturbed. However, there is also evidence that  $\text{Ca}^{2+}$  release from the lysosomes can induce cell-wide rises in  $\text{Ca}^{2+}$  concentration known as global  $\text{Ca}^{2+}$  signals. Any changes to global  $\text{Ca}^{2+}$  signals have the potential to disrupt  $\text{Ca}^{2+}$ -sensitive processes throughout the cell. Currently though there is limited knowledge about whether TRPML1 and TPCs contribute to such global  $\text{Ca}^{2+}$  signals. Furthermore, it is unknown whether dysfunctional TRPML1 and TPCs contribute to neurodegeneration in their capacity to influence global  $\text{Ca}^{2+}$  signalling. This thesis explores this possible global relationship between lysosomal  $\text{Ca}^{2+}$  signalling and neurodegeneration.

## 1.2 LYSOSOMES

Lysosomes were discovered over 60 years ago when researchers investigating carbohydrate metabolism were drawn in by an enigmatic enzyme - acid phosphatase (de Duve, 2005). They eventually determined that acid phosphatase was “attached to a special type of cytoplasmic granules” that we know today as lysosomes (Appelmans et al., 1955). They went on to find a further four acid hydrolases associated with this fraction, signposting to the lysosome’s role in degradation (de Duve et al., 1955).

The creation of a lysosome combines classical biosynthesis and cooperation with the endocytic pathway (Fig. 1.1). Although various models exist, mature lysosomes are thought to arise from a dynamic cascade of fusion/transition events that begins with endocytosis (Luzio et al., 2007a): Vesicles bud off internally from the plasma membrane and fuse with each other or to pre-formed early endosomes (Bucci et al., 1992). This fusion occurs under the regulation of GTPase Rab5, which is subsequently replaced by Rab7, marking the conversion from early to late endosome (Rink et al., 2005). This transition is associated with luminal acidification which continues as these vesicles mature into lysosomes (Johnson et al., 2016; Mindell, 2012; Yamashiro, 1987). On the way, soluble hydrolases and lysosomal membrane proteins such as lysosome-associated membrane protein 1 (LAMP1) are delivered to the endolysosomal system (lv et al., 2011; Luzio et al., 2007a). The best understood delivery system is that of the hydrolases. Once synthesised at the endoplasmic reticulum (ER), they acquire a mannose-6-phosphate (M6P) tag at the Golgi which is recognised by M6P receptors (M6PR) at the *trans* Golgi network (TGN) (Braulke and Bonifacino, 2009). TGN vesicles subsequently bud off and shuttle the enzymes to the endosomes. M6PR are recycled back to the Golgi via retrograde transport and the hydrolases function optimally in the acidic environment of the lysosome to degrade unwanted material.

### 1.2.1 Lysosomes and Degradation

Lysosomes fuse with other organelles so that lysosomal hydrolases can access and degrade material from multiple trafficking routes. For example, lysosome fusion with endosomes gives access to extracellular material or membrane lipids brought in via endocytosis (Kolter and Sandhoff, 2010). In the process of autophagy lysosomes fuse with autophagosomes which envelope unwanted intracellular material (Feng et al., 2014b). Alternatively, lysosomes can directly receive intracellular material brought to them in chaperone-mediated autophagy (CMA) (Cuervo and Wong, 2014).

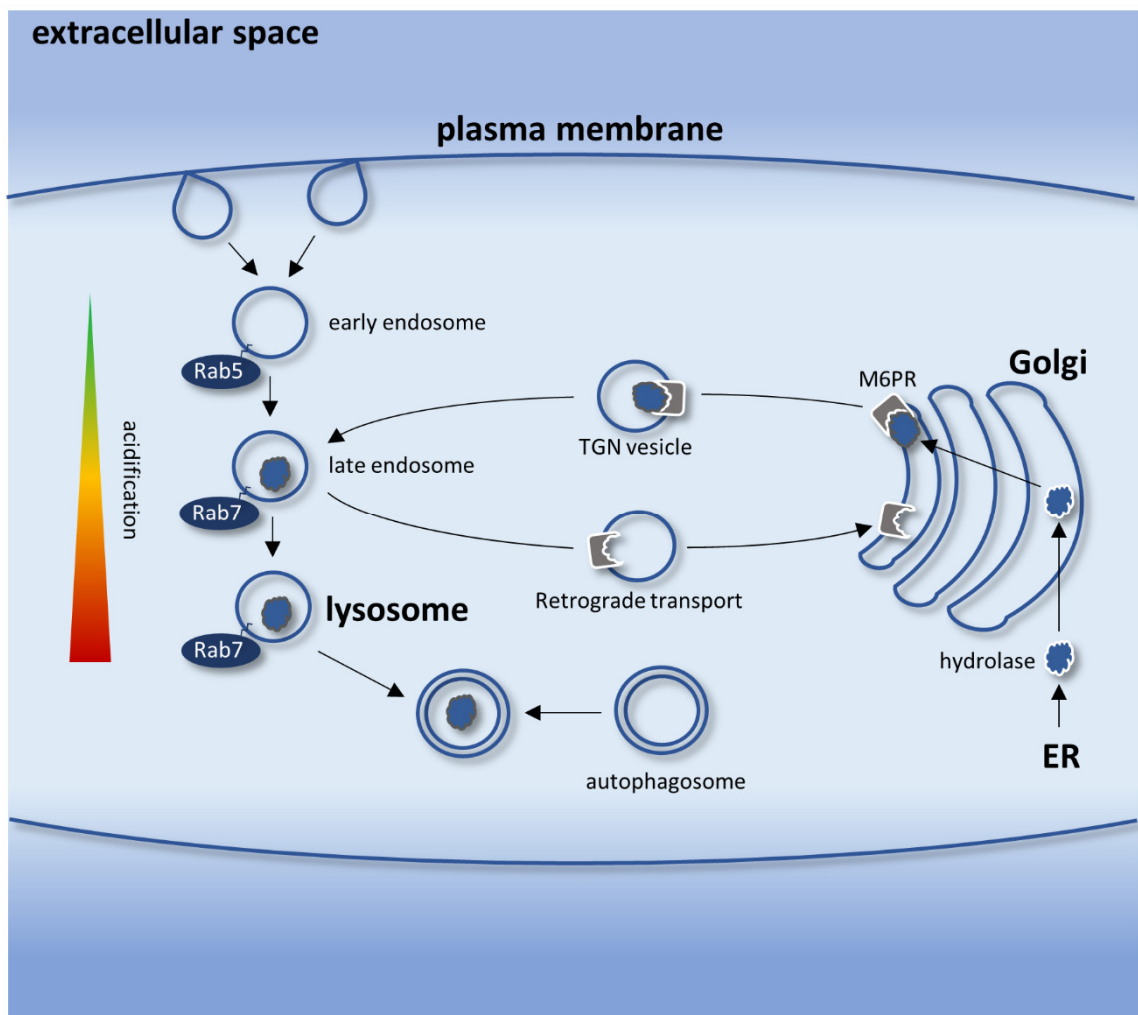


**Figure 1.1 The dynamic lysosome**

Lysosomes arise from a dynamic cascade of fusion/transition events that begins with endocytosis. Vesicles bud off internally from the plasma membrane and fuse with each other or to pre-formed early endosomes under the regulation of GTPase Rab5, which is subsequently replaced by Rab7, marking the conversion from early to late endosome. This is accompanied by luminal acidification which continues as these vesicles mature into lysosomes. Once a lysosomal hydrolyase is synthesised at the ER it acquires an M6P tag at the Golgi (grey outline), which is recognised by M6PR. TGN vesicles containing the hydrolyase and the M6PR bud off and shuttle the enzymes to the endosomes. M6PR are recycled back to the Golgi via retrograde transport. The lysosomal hydrolyases function optimally in acidic environments to degrade material that is delivered directly to the lysosomes, or can be accessed by fusing with other organelles such as autophagosomes.

The degradative function of lysosomes and their interconnectivity with other organelles establishes the importance of maintaining good lysosomal health: If there is a defect in lysosomal function there are likely to be knock-on consequences elsewhere in the cell and vice versa. Whilst this degradative and cooperative behaviour is widely appreciated as essential to maintain cellular well-being it is now becoming clearer that it is intertwined with another



important lysosomal function - that of storing and releasing  $\text{Ca}^{2+}$ . Indeed, there is evidence that autophagy is regulated by lysosomal  $\text{Ca}^{2+}$  release (La Rovere et al., 2016).

### **1.2.2 Lysosomal $\text{Ca}^{2+}$**

Early identification of lysosomal  $\text{Ca}^{2+}$  was demonstrated in absorptive cells of the duck duodenum and in the epithelia of a fresh-water mollusc (Davis et al., 1979b; Jones and Davis, 1982). The authors hypothesised that “these organelles play an important role in intracellular calcium homeostasis and/or calcium transport mechanisms”. Since then lysosomal  $\text{Ca}^{2+}$  has been measured using fluorescent indicators and is reported to be approximately 400-700  $\mu\text{M}$  (Christensen et al., 2002; Lloyd-Evans et al., 2008); higher than that of the surrounding cytosol ( $\sim 100\text{nM}$ ) (Berridge et al., 2000). This ability to store pools of  $\text{Ca}^{2+}$  and release it is important for lysosome fusion and fission, between themselves and other organelles (Pryor et al., 2000). This in turn is vital for lysosomes to carry out their degradative function.

### **1.2.3 Lysosomal $\text{Ca}^{2+}$ and membrane fusion/fission**

In a cell-free system fusion between lysosomes and late endosomes is inhibited by the  $\text{Ca}^{2+}$  chelator BAPTA but not by EGTA (Pryor et al., 2000). These contrasting results indicate that the  $\text{Ca}^{2+}$  required for lysosome membrane fusion comes from a local source. This conclusion is reached by considering the different speeds at which BAPTA and EGTA chelate  $\text{Ca}^{2+}$ : BAPTA binds  $\text{Ca}^{2+}$  quickly whereas EGTA binds  $\text{Ca}^{2+}$  approximately 150-fold slower (Naraghi, 1997). For instance, if the  $\text{Ca}^{2+}$  that is required for lysosome membrane fusion comes from a local source its movement from source to target (i.e. the lysosome membrane) would last for a relatively short length of time. As BAPTA can bind  $\text{Ca}^{2+}$  quickly it would be able to intercept this short-lived movement of  $\text{Ca}^{2+}$  and therefore prevent lysosome fusion. In contrast, by the time the more sluggish EGTA has chelated its  $\text{Ca}^{2+}$ , the short-lived movement of  $\text{Ca}^{2+}$  from local source to target will have already taken place and lysosome fusion may proceed. If, on the other hand, the  $\text{Ca}^{2+}$  required for lysosome membrane fusion came from a more distant source, even the slow-binding EGTA may have time to chelate and intercept the  $\text{Ca}^{2+}$  as it moves from source to target and consequently prevent lysosome fusion. In addition to this result, Pryor and colleagues found that lysosome fusion was also inhibited by chelating luminal  $\text{Ca}^{2+}$  with membrane-permeable EGTA (Pryor et al., 2000). Together, this pointed to lysosomal  $\text{Ca}^{2+}$  release as a requisite for lysosomal membrane fusion. Membrane fission was also reported to require luminal  $\text{Ca}^{2+}$ . However, fission was not inhibited by BAPTA suggesting that  $\text{Ca}^{2+}$  release was not required.

The exact mechanisms of lysosomal fusion and fission are not known but  $\text{Ca}^{2+}$ -dependent membrane fusion can be categorised into stages of tethering, docking and fusion. One of the key components of membrane fusion is the Rab GTPase. These small proteins can interact with motors to move vesicles along actin filaments or microtubules (Hales et al., 2002; Jordens et al., 2001). Rabs also recruit tethers which hold opposing donor and target membranes together (Balderhaar and Ungermann, 2013). This tethering is followed by docking which requires the interlacing of SNAREs (N-ethylmaleimide-sensitive factor activating protein receptors) from donor and target membranes to lock the two membranes in place (Pryor et al., 2004). It is thought that after this docking, luminal  $\text{Ca}^{2+}$  release, and increases in cytosolic  $\text{Ca}^{2+}$  facilitate membrane fusion (Jaiswal et al., 2002; Peters and Mayer, 1998). It is unclear how exactly this  $\text{Ca}^{2+}$  event triggers lysosomal membrane fusion with intracellular organelles but fusion with the plasma membrane requires both an increase in intracellular  $\text{Ca}^{2+}$  and the  $\text{Ca}^{2+}$  sensor Synaptotagmin7 (Syt 7) (Reddy et al., 2001). Work on neuronal Synaptotagmin 1 (Syt1) proposes that upon binding  $\text{Ca}^{2+}$ , it inserts into the plasma membrane to induce membrane curvature and promote membrane mixing (Hui et al., 2009). Although Syts have not been reported to mediate fusion between lysosomes and other intracellular organelles,  $\text{Ca}^{2+}$  sensors calmodulin and ALG-2 (apoptosis linked protein 2) have been proposed for this role (Cao et al., 2015a; Peters and Mayer, 1998; Pryor et al., 2000; Vergarajauregui et al., 2009). It is unlikely that these sensors need to induce membrane curvature to the same degree as at the plasma membrane. This is due to the more severe bend of intracellular vesicle membranes as a correlate of their relatively small size compared with the shallow bend of the plasma membrane which encompasses the relatively large cell.

Why luminal  $\text{Ca}^{2+}$  is needed for membrane fission is unclear. The reformation of lysosomes from lysosome-autophagosome hybrids is known to involve the generation of LAMP1-positive tubules and requires the GTPase dynamin-2 (Schulze et al., 2013). Notably, dynamin-2 can be dephosphorylated by  $\text{Ca}^{2+}$ -activated calcineurin in a similar way to dynamin-1, which is important for endocytosis (Ferguson and De Camilli, 2012).

With evidence that lysosome fusion and fission is dependent on lysosomal  $\text{Ca}^{2+}$ , any disturbances to the latter may affect the lysosomes' ability to cooperate with other organelles. In turn this could be highly detrimental to the lysosomes' degradative function and the cell as a whole. Therefore, understanding how lysosomes release and take up  $\text{Ca}^{2+}$  is pertinent.

## 1.2.4 Lysosomal Ca<sup>2+</sup> release

A handful of Ca<sup>2+</sup>-permeable channels are reported to localise at the lysosome (Patel and Cai, 2015; Tian et al., 2015). Whilst some are rather ubiquitous in their localisation TRPML1 and TPC channels are predominantly expressed in the endolysosomal system. In the last twenty years information about these channels has grown significantly.

### 1.2.4.1 TRPML1

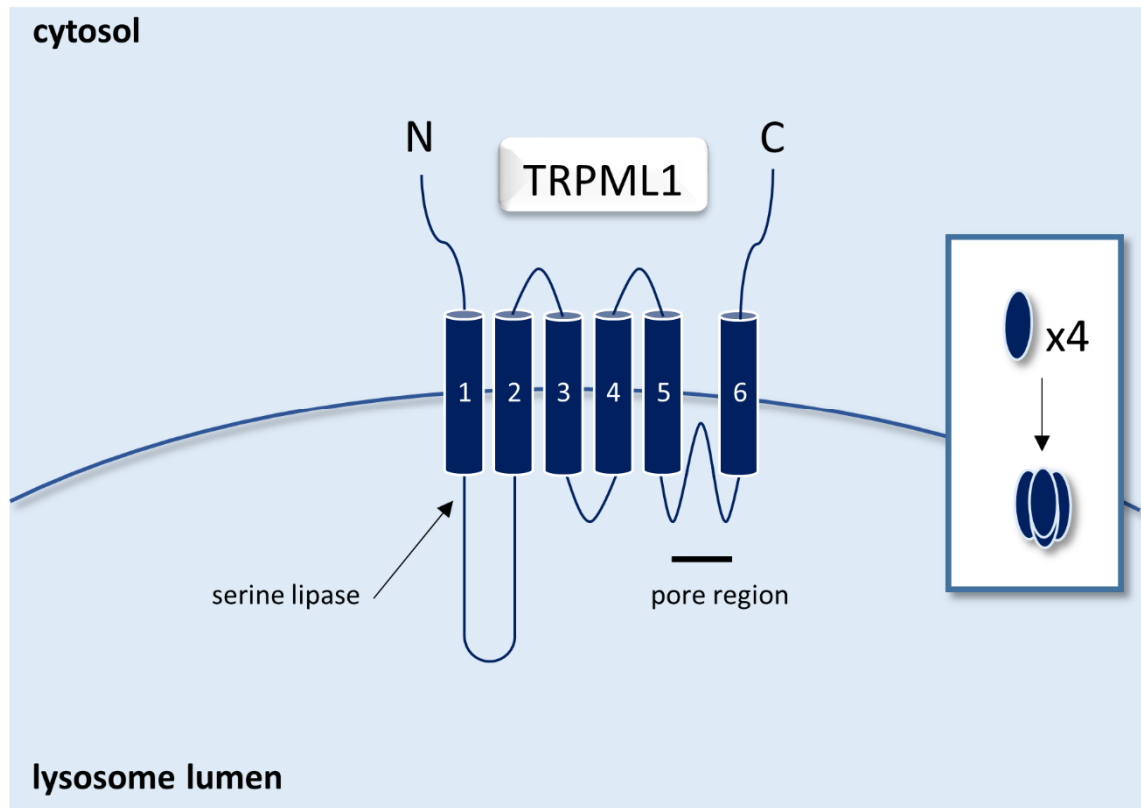


**Figure 1.2 TRPML1**

Adapted from diagrams in Li et al., 2011 and Venkatachalam and Montell, 2007. TRPML1 possesses 6 membrane spanning regions (MSR; labelled 1-6). The N and C termini face into the cytosol and a pore region is positioned between MSRs 5 and 6. The luminal linker between MSRs 1 and 2 confers regulation by luminal pH and Ca<sup>2+</sup> and is home to a serine lipase domain. TRPML1 forms tetramers (x4).

#### 1.2.4.1.1 Structure and Discovery

The lysosomal Ca<sup>2+</sup> release channel TRPML1 belongs to the family of TRP (transient receptor potential) channels. These ion channels can form tetramers and have diverse regulatory properties (Li et al., 2011; Venkatachalam and Montell, 2007). Within this TRP family a sub-group of mucolipin (ML) channels exists, composed of 3 isoforms (TRPML1-3) in humans. TRPML1, the first isoform discovered, was found as the defective protein responsible for the devastating

neurodegenerative disease mucopolidosis type IV (MLIV) (Bargal et al., 2000; Bassi et al., 2000; Sun et al., 2000). Topologically, TRPML1 is predicted to possess 6 membrane spanning regions (MSR) with both terminus tails positioned on the cytosolic face of the membrane (Sun et al., 2000) (Fig. 1.2). Predictions also identify the pore region between MSRs 5 and 6 and a functional serine lipase domain on the luminal linker between MSRs 1 and 2 (LaPlante et al., 2011). Very recently, the crystal structure of this luminal linker has been published, providing further insight to TRPML1 activity (Li et al., 2017).

#### 1.2.4.1.2 Localisation

Expression of TRPML1 has been detected in a variety of tissues, and the protein is predominantly situated in the endolysosomal system, colocalising with LAMP1 and Rab7 (Falardeau et al., 2002; Thompson et al., 2007; Zeevi et al., 2009). Its localisation here is thought to be determined by dileucine motifs at both termini (Vergarajauregui and Puertollano, 2006). Following its synthesis TRPML1 may take a direct route from the TGN to the endolysosomes or an indirect route via the plasma membrane (Vergarajauregui and Puertollano, 2006).

#### 1.2.4.1.3 Channel Properties

The lysosomal localisation of TRPML1 meant that electrophysiology experiments to characterise its behaviour were not simple. Instead, another isoform, TRPML3 paved the way for TRPML1 characterisation. TRPML3 has been shown to localise in the endolysosomal system but also in the plasma membrane and as such it permits small whole cell currents (Kim et al., 2009; Xu et al., 2007). Constitutive TRPML3 activity was subsequently established by introducing the A419P mutation that causes deafness and pigmentation loss in the murine varitint-waddler phenotype (Palma et al., 2002; Xu et al., 2007). By mutating the corresponding amino acid in TRPML1 (V432P) TRPML1 activity could also be observed when measuring whole cell currents (Dong et al., 2008; Xu et al., 2007). With this new tool studies into TRPML1 activity and regulation could advance. Later, biotinylation assays confirmed that TRPML1(V432P) exhibited increased plasma membrane localisation compared to the wildtype (WT) (Dong et al., 2009). The development of patch clamp methods directly onto whole lysosomes also verified increased channel currents of TRPML1(V432P) (Dong et al., 2008). This whole-lysosome technique requires the use of vacuolin to enlarge endolysosomes and has since allowed the measurement of endogenous and overexpressed WT TRPML1 currents (Cerny et al., 2004; Dong et al., 2010). Furthermore, it has facilitated the development of TRPML1 agonists ML-SA1 and MK6-83 which were modified from molecules originally identified in a TRPML3 screen (Chen et al., 2014; Grimm et al., 2010; Shen

et al., 2012). As a consequence of this TRPML1 inhibitors (ML-SI1-3) have also been generated (Samie et al., 2013).

The question of what regulates TRPML1 activity endogenously remains incompletely answered. One candidate agonist is phosphatidylinositol 3,5-bisphosphate (PI(3,5)P<sub>2</sub>), a low abundance endolysosomal phosphoinositide (McCartney et al., 2014). PI(3,5)P<sub>2</sub> has been shown to bind TRPML1 at its N terminus and activate endogenous TRPML1 currents (Dong et al., 2010). However, there is not yet evidence that it can cause TRPML1-mediated Ca<sup>2+</sup> signals. A candidate for TRPML1 inhibition is plasma membrane resident phosphatidylinositol 4, 5 bisphosphate (PI(4,5)P<sub>2</sub>) which is also thought to bind TRPML1 on its N terminus (Zhang et al., 2012). Although this species has previously been shown to activate a host of plasma membrane channels Zhang and colleagues propose that TRPML1 is inhibited by PI(4,5)P<sub>2</sub> at the plasma membrane (Suh and Hille, 2005). Constitutively active and WT TRPML1 is also reported to be regulated by extracytosolic/lysosomal pH, with optimal activity at an acidic ~pH 4.5 (Chen et al., 2014; Dong et al., 2008; Feng et al., 2014a; Xu et al., 2007). Conversely, TRPML3 WT is inhibited by acidic pH which could favour its activation at the plasma membrane (Kim et al., 2008b). The combination of activating endolysosomal PI(3,5)P<sub>2</sub> and acidic lysosome pH is likely to favour TRPML1 activity on the lysosomes compared to its activity at the plasma membrane where inhibitory PI(4,5)P<sub>2</sub> resides and the extracellular pH is neutral. Furthermore, constitutively active TRPML1 is inhibited by high extracytosolic Ca<sup>2+</sup> concentrations. As the concentration of Ca<sup>2+</sup> is greater in the extracellular space compared to the interior of the lysosome this too implies preferential TRPML1 activity at the lysosomes (Li et al., 2017).

Recent studies have deduced that TRPML1 is an inwardly rectifying (ions flow into the cytosol) Ca<sup>2+</sup>-permeable channel (for example: Dong et al., 2009; Li et al., 2017; Xu et al., 2007). In line with this, exogenous TRPML1 agonist ML-SA1 has been shown to cause local Ca<sup>2+</sup> signals in cells overexpressing genetically encoded Ca<sup>2+</sup> indicators fused to the N-terminus of the WT channel (Cao et al., 2015b; Medina et al., 2015; Shen et al., 2012). However, it should be noted that earlier research proposed TRPML1 as an outwardly rectifying (ions flow out of the cytosol) channel permeable to monovalent cations and inhibited by low pH (Kiselyov et al., 2005; Raychowdhury et al., 2004; Soyombo et al., 2006). Of note, these WT TRPML1 currents were recorded using whole-cell patches or reconstituted lipid bilayers. How this observation might reconcile these two contradicting current characterisations remains unknown. TRPML1 is a non-selective cation channel and accordingly it has been reported to be permeable to Fe<sup>2+</sup>, Zn<sup>2+</sup>, Mn<sup>2+</sup>, Mg<sup>2+</sup>, K<sup>+</sup> and Na<sup>+</sup> as well as Ca<sup>2+</sup> (Dong et al., 2008; Raychowdhury et al., 2004; Venkatachalam et al., 2015).

#### 1.2.4.1.4 Cellular Function

As the cellular role of TRPML1 has been explored its function as a  $\text{Ca}^{2+}$  release channel has been linked to regulation of lysosomal fusion and membrane trafficking. In cells with MLIV-related mutant TRPML1, reduced lysosome-endosome fusion, and delayed lysosome-autophagosome fusion has been reported (LaPlante et al., 2004; Vergarajauregui et al., 2008). The lysosome-endosome fusion defect could be recapitulated by membrane-permeable BAPTA in control cells, therefore implicating the  $\text{Ca}^{2+}$  release activity of TRPML1 in the regulation of membrane fusion and lysosomal homeostasis (LaPlante et al., 2004). Impaired endocytosis, receptor degradation, retrograde trafficking and lysosome reformation from hybrid organelles have also been associated with mutant TRPML1 (Chen et al., 1998; Pryor et al., 2006; Treusch et al., 2004; Vergarajauregui et al., 2008), so too has enhanced lipid endocytosis directed to the lysosomes (Chen et al., 1998). In addition, TRPML1 has been implicated in lysosomal exocytosis which is involved in phagocytosis and sarcolemma repair (Cheng et al., 2014; LaPlante et al., 2006; Samie et al., 2013). TRPML1's role in lysosomal exocytosis is supported by the upregulated exocytosis observed with constitutively active TRPML1(V432P) (Dong et al., 2009). In contrast, a recent study has shown that the absence of TRPML1 upregulates exocytosis and is associated with increased interactions between the SNAREs Vamp2 and SNAP25 (Park et al., 2016). There have also been observations of decreased lysosomal pH in TRPML1-deficient cells which would support the idea that TRPML1 also acts as a  $\text{H}^+$  release channel (Miedel et al., 2008; Soyombo et al., 2006). Soyombo et al also reported that abnormal storage in MLIV patient fibroblasts could be corrected by increasing the lysosomal pH. However, in contradicting work, MLIV TRPML1 has been associated with an increase in lysosomal pH and raising lysosomal pH does not correct storage defects (Bach et al., 1999; Kogot-Levin et al., 2009). The link between TRPML1, membrane trafficking and  $\text{Ca}^{2+}$  is further supported by interactions between TRPML1 and the  $\text{Ca}^{2+}$  sensor ALG-2 which has been shown to regulate lysosomal trafficking defects induced by overexpressed TRPML1 (Vergarajauregui et al., 2009). A more recent study has shown that similar defects could be reversed by membrane-permeable BAPTA and that ALG-2 may regulate TRPML1-mediated trafficking by interacting with the microtubule motor protein dynein (Li et al., 2016).

In non-MLIV models the correction of lysosomal trafficking defects has been achieved by treating cells with ML-SA1 which reportedly causes local  $\text{Ca}^{2+}$  signals (Cao et al., 2015b; Shen et al., 2012). Despite these measurements of local TRPML1-mediated  $\text{Ca}^{2+}$  release there has been little investigation into whether TRPML1 can also generate global  $\text{Ca}^{2+}$  signals. In Chapter 2 I address this question using ML-SA1 alongside other pharmacological and molecular tools.

### 1.2.4.2 TPC1 & 2

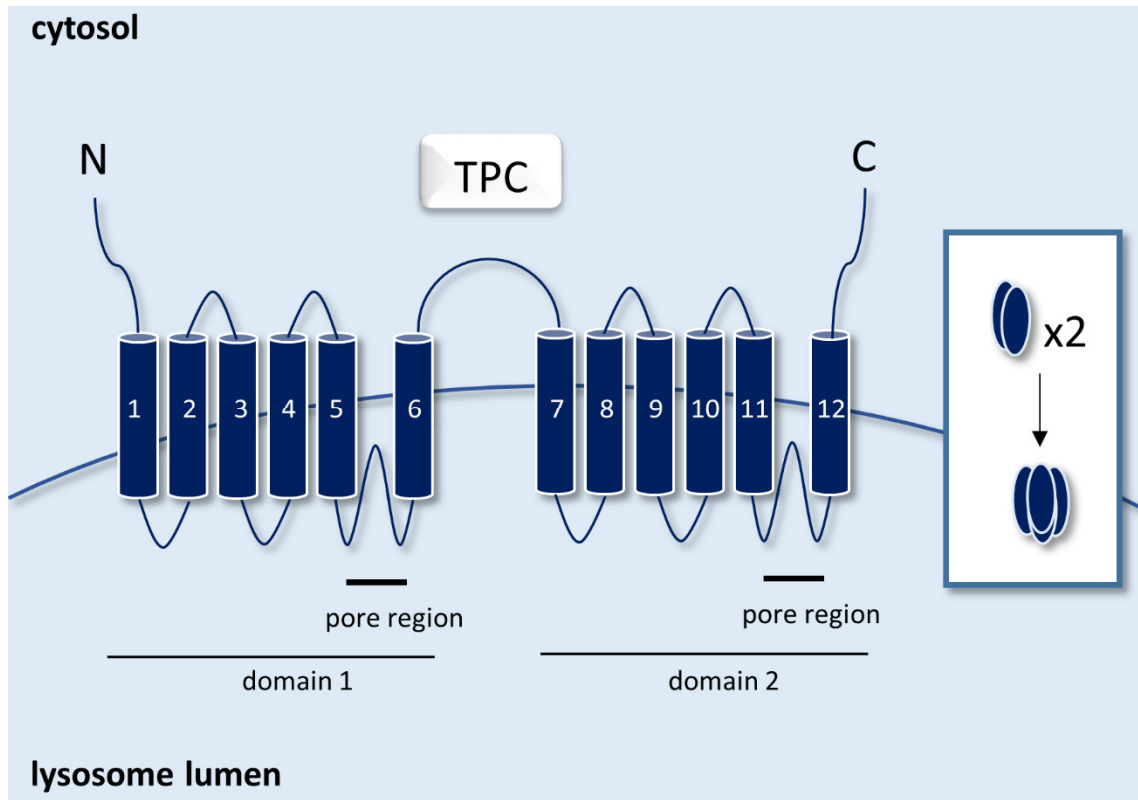


**Figure 1.3. TPCs**

Adapted from Guo et al., 2016 and Hooper et al., 2011. TPCs possess 12 membrane spanning regions (MSR; labelled 1-12) split into 2 domains of 6. The N and C termini face into the cytosol and two pore regions are positioned between MSRs 5 and 6, and MSRs 11 and 12. TPCs form dimers (x2).

#### 1.2.4.2.1 Structure and Discovery

TPCs are  $\text{Ca}^{2+}$  release channels that possess 12 MSRs in total, split into 2 domains of 6 (Guo et al., 2016; Hooper et al., 2011; Kintzer and Stroud, 2016) (Fig. 1.3). Both termini are cytosolic and the two pore regions that give these channels their name (two pore channels) lie between MSRs 5 and 6, and MSRs 11 and 12. This 2x6 MSR configuration is indicative of the TPCs' position in the evolution of voltage-operated ion channels: Through one round of duplication TPCs likely evolved from the 1x6 MSR voltage-operated  $\text{K}^+$  channels (VOKC), and through a second round of duplication evolved into the 4x6 MSR voltage-operated  $\text{Na}^+$  channels (VONC) and voltage-operated  $\text{Ca}^{2+}$  channels (VOCC) (Ishibashi et al., 2000). Given that VOKC channels function as tetramers and VONC/VOCC channels can function as monomers, TPCs were predicted to form dimers for a final 4x6 MSR configuration, which has since been demonstrated (Churamani et al., 2012; Guo et al., 2016; Kintzer and Stroud, 2016; Larisch et al., 2016; Rietdorf et al., 2011).

TPC1 was first discovered in rat kidney by identifying cDNA clones with similar amino acid sequences to VONCs (Ishibashi et al., 2000). Subsequently the plant homologue was identified in *Arabidopsis thaliana* (Furuichi et al., 2001). Since then *TPC1* and an additional TPC gene (*TPC2*) have been identified in humans whilst other organisms possess three TPC genes (*TPC1-3*) (Brailoiu et al., 2009; Calcraft et al., 2009).

#### 1.2.4.2.2 Localisation

TPCs are expressed in a variety of tissues with high levels in the liver and kidney (Calcraft et al., 2009; Ishibashi et al., 2000; Zong et al., 2009). At the cellular level TPC1 and TPC2 localise to the endolysosomal system with different distribution patterns. TPC2 exhibits some favourability towards the lysosomes and is targeted there through its N-terminal dileucine motif (Arredouani et al., 2015; Brailoiu et al., 2009, 2010a; Calcraft et al., 2009; Pereira et al., 2014; Zong et al., 2009). In contrast, TPC1 localisation is skewed somewhat to the endosomes and its position here requires a segment of its N-terminus but not specifically its N or C-terminus dileucine motifs (Brailoiu et al., 2009, 2010a; Calcraft et al., 2009; Churamani et al., 2013; Ruas et al., 2014).

#### 1.2.4.2.3 Channel Properties

As with TRPML1, the endolysosomal localisation of TPCs has meant characterisation of the channels has not been simple. As such, similar techniques have been used including patch clamping directly onto enlarged lysosomes (Cang et al., 2014; Grimm et al., 2014; Jha et al., 2014; Ruas et al., 2015; Schieder et al., 2010; Wang et al., 2012) or incorporating the channels into lipid bilayers (Pitt et al., 2010, 2014; Rybalchenko et al., 2012). TPC2 directed to the plasma membrane has also been exploited but by disruption of its N-terminal dileucine motif and not by causing constitutive activity as for TRPML1 (Brailoiu et al., 2010a; Jha et al., 2014; Wang et al., 2012; Yamaguchi et al., 2011). Many of these studies used the Ca<sup>2+</sup> mobilising messenger nicotinic acid adenine dinucleotide phosphate (NAADP) to assess the regulation of activated TPCs.

NAADP was first discovered when a derivative of nicotinamide adenine dinucleotide phosphate (NADP) caused Ca<sup>2+</sup> release in sea urchin egg homogenates (Clapper et al., 1987). The source of this Ca<sup>2+</sup> release was insensitive to other Ca<sup>2+</sup> mobilisers, inositol triphosphate (IP<sub>3</sub>) and cyclic adenosine diphosphate ribose (cADPR) (Clapper et al., 1987; Lee and Aarhus, 1995). The canonical ER was ruled out as the source of NAADP-induced Ca<sup>2+</sup> signals and it was demonstrated that these signals were perturbed when lysosomes were disrupted (Churchill et al., 2002; Genazzani and Galione, 1996; Lee and Aarhus, 1995). The contemporary identification of TPCs



then led to the discovery that human TPC2, localised to the endolysosomal system, was required for NAADP-mediated global  $\text{Ca}^{2+}$  signalling (Calcraft et al., 2009). This was followed by similar results with TPC1 (Brailoiu et al., 2009). The mechanism by which NAADP activates TPCs is unclear but NAADP appears to bind an unidentified binding protein and not to TPCs directly (Lin-Moshier et al., 2012; Walseth et al., 2012a, 2012b).

In early electrophysiology studies of NAADP-activated TPC2 the channel was demonstrated to be a voltage-independent  $\text{Ca}^{2+}$ -permeable channel (Brailoiu et al., 2010a; Pitt et al., 2010; Schieder et al., 2010). Furthermore, TPC2 required an acidic lumen for conductance thus advocating its suitability as a lysosomal channel (Schieder et al., 2010). Pitt and colleagues also demonstrated that the open probability of TPC2 ( $P_o$ ) was regulated by luminal pH (Pitt et al., 2010): In summary, the  $P_o$  at neutral pH plateaued at concentrations of NAADP above 1  $\mu\text{M}$ . At acidic pH however, the  $P_o$  of TPC2 was inhibited at 1  $\mu\text{M}$  NAADP and higher.

Electrophysiology studies of TPC1 followed, which suggested it was also permeable to  $\text{Ca}^{2+}$  (Pitt et al., 2014; Rybalchenko et al., 2012). Contrary to TPC2 however, TPC1 activity was voltage-dependent (Cang et al., 2014; Pitt et al., 2014; Rybalchenko et al., 2012). Optimal TPC1 activity reportedly required an acidic luminal pH and high concentrations of luminal  $\text{Ca}^{2+}$  (Pitt et al., 2014; Rybalchenko et al., 2012). Pitt and colleagues also showed that TPC1 could be activated by cytosolic  $\text{Ca}^{2+}$  and has proton permeability (Pitt et al., 2014). This proton permeability may contribute to NAADP-mediated alkalinisation of acidic stores (Morgan et al., 2013). Both TPC1 and TPC2 have also been reported to exhibit  $\text{K}^+$  permeability with TPC1 favouring its conductance compared to  $\text{Ca}^{2+}$  (Cang et al., 2014; Pitt et al., 2010, 2014; Rybalchenko et al., 2012).

Controversy about NAADP as the activating ligand for TPCs came in 2012, when a study demonstrated that TPCs were activated solely by  $\text{PI}(3,5)\text{P}_2$  (Wang et al., 2012). In cells from double knockout mice ( $\text{TPC1}^{-/-}/\text{TPC2}^{-/-}$ ) NAADP was still able to induce  $\text{Ca}^{2+}$  release but  $\text{PI}(3,5)\text{P}_2$ -induced currents were lost. In an effort to consolidate the controversy it was suggested that too high a concentration of NAADP had been used in the TPC knockout cells and that this could cause non-specific  $\text{Ca}^{2+}$  release (Jha et al., 2014). An additional proposal was that the TPC knockout (specifically TPC1) may not have been complete. The knockout involved the deletion of the first 69 amino acids of TPC1, which ran into an intron between exons 2 and 3. Deletion here in another knockout mouse however resulted in the expression of a variant TPC1 isoform (TPC1B) (Ruas et al., 2014). Ruas and colleagues have since shown that TPC1B is capable of eliciting

NAADP-induced  $\text{Ca}^{2+}$  release (Ruas et al., 2015). TPC2 knock out models have also displayed reduced NAADP-induced currents or  $\text{Ca}^{2+}$  signals (Grimm et al., 2014; Ruas et al., 2015). However, why  $\text{PI}(3,5)\text{P}_2$  currents disappeared in  $\text{TPC1}^{-1}/\text{TPC2}^{-1}$  cells when NAADP currents persisted is another point of contention which has not yet been resolved (Wang et al., 2012).

Another novel find by Wang and colleagues was that TPC2 was selective for  $\text{Na}^+$  over  $\text{Ca}^{2+}$  ions when activated by  $\text{PI}(3,5)\text{P}_2$ . Similar  $\text{Na}^+$  selectivity has since been reported for both TPC isoforms after either NAADP or  $\text{PI}(3,5)\text{P}_2$  activation (Cang et al., 2014; Pitt et al., 2014; Sakurai et al., 2015). In response to Wang et al (2012) the regulation of  $\text{Na}^+$  currents through TPC2 was addressed (Jha et al., 2014). Upon activation by NAADP or  $\text{PI}(3,5)\text{P}_2$ ,  $\text{Na}^+$  currents were present, although the NAADP-induced currents were weaker. NAADP-induced  $\text{Ca}^{2+}$  signals were also modulated by  $\text{PI}(3,5)\text{P}_2$  synthesis or inhibition, pointing to convergent regulation by the two messengers. In addition, TPC2 currents were regulated by  $\text{Mg}^{2+}$ , ATP and kinases. Reciprocal to the ligand controversy of TPCs activation of TRPML1 by NAADP has also been demonstrated (Zhang et al., 2009, 2011).

To summarise the channel properties of TPCs, it appears that they do differ somewhat between isoforms. The evidence so far points to both channels conducting  $\text{Ca}^{2+}$  and  $\text{Na}^+$  upon activation by NAADP or  $\text{PI}(3,5)\text{P}_2$ , and regulation by luminal pH and possibly  $\text{Ca}^{2+}$  (Pitt et al., 2016). However, TPC1 activity is also dependent on voltage and cytosolic  $\text{Ca}^{2+}$ , and is permeable to protons. Their differential regulation may hold clues about how they cooperate and segregate their functions.

#### 1.2.4.2.4 Cellular Function

Some differences in function between TPC1 and TPC2 have already been published, although caution should be heeded to allow for varied overexpression and knockdown efficiencies. For example, overexpression of sea urchin TPC1 in HEK293 cells caused more pronounced phenotypes of disturbed lysosome morphology and retrograde trafficking compared to TPC2 (Ruas et al., 2010). Another group found that overexpression of TPC2 but not TPC1 caused a pigmentation defect in *Xenopus* oocytes (Lin-Moshier et al., 2014). In a recent knockout study in mice a lack of TPC1 caused a more severe effect on retrograde transport compared to that of TPC2, but it was the TPC2 knockout that caused delayed endosome-lysosome trafficking (Ruas et al., 2014). In addition, knockdown of TPC2 but not TPC1 has been shown to improve defective lysosome morphology in Parkinson's disease (PD) cells (Hockey et al., 2015). These effects of TPCs on the endolysosomal system are likely to be conveyed by their association with Rab

GTPases and SNAREs (Grimm et al., 2014; Hockey et al., 2015; Lin-Moshier et al., 2014). TPC activity has also been linked to exocytosis (Davis et al., 2012), autophagy (Gómez-Suaga et al., 2012; Lin et al., 2015; Lu et al., 2013; Pereira et al., 2011), differentiation (Aley et al., 2010a; Zhang et al., 2013) and infectious disease (Sakurai et al., 2015). What is more, where increased TPC activity has been linked to trafficking defects and disease, treatment with cell-permeable BAPTA has improved the phenotype (Hockey et al., 2015; Lin-Moshier et al., 2014; Lu et al., 2013). Conversely, trafficking defects caused by reduced TPC activity in fatty liver disease were recapitulated with BAPTA (Grimm et al., 2014). These results therefore link TPC activity and local  $\text{Ca}^{2+}$  release to disease phenotypes.

## **1.2.5 Lysosomal $\text{Ca}^{2+}$ uptake**

### **1.2.5.1 CAX**

Despite steps forward in understanding the molecular nature of lysosomal  $\text{Ca}^{2+}$  release in humans, the components of lysosomal  $\text{Ca}^{2+}$  uptake have proved more elusive.  $\text{Ca}^{2+}$  uptake into the acidic organelles of non-mammalian cells has been attributed to both  $\text{Ca}^{2+}$ -ATPase pumps and  $\text{Ca}^{2+}/\text{H}^+$  exchangers (CAX) (Pittman, 2011). Although the machinery has not been identified ATPase-dependent and  $\text{H}^+$ -dependent  $\text{Ca}^{2+}$  accumulation in mammalian lysosome-related organelles has been reported (Patel and Docampo, 2010). Notably,  $\text{Ca}^{2+}/\text{H}^+$  exchange is reliant on the high concentration of  $\text{H}^+$  built up in the lumen by the vacuolar  $\text{H}^+$ -ATPase (V-ATPase) (Förster and Kane, 2000; Krebs et al., 2010; Morgan et al., 2011). Recently, putative mammalian CAX sequences were identified for the first time in the genomes of the platypus and Tasmanian devil (Melchionda et al., 2016). In the same study overexpressed CAX from *Xenopus laevis* was reported to localise at the endolysosomal system in human cells, and modulate cytosolic  $\text{Ca}^{2+}$  signals, pointing to a role in lysosomal  $\text{Ca}^{2+}$  uptake. Although this recent work supports the idea of  $\text{Ca}^{2+}/\text{H}^+$  exchange in human lysosomes the identity of the endogenous molecular component(s) remains unknown.

## **1.3 $\text{Ca}^{2+}$ SIGNALLING**

TRPML1 and TPC activity appear to influence vesicular trafficking, likely by releasing lysosomal  $\text{Ca}^{2+}$  into the vicinity of lysosomal membranes. It is understood that this type of local  $\text{Ca}^{2+}$  transient can be amplified by other components of the  $\text{Ca}^{2+}$  signalling network to produce large global  $\text{Ca}^{2+}$  signals that propagate throughout the cell. This network is an intricate system of organelles, channels, exchangers and buffers which together fine-tune the duration, amplitude,

location and pattern of  $\text{Ca}^{2+}$  signals so that this one ion can control an array of processes (Berridge et al., 2000) (Fig. 1.4).

### 1.3.1 Local and Global $\text{Ca}^{2+}$ signals

The generation of global  $\text{Ca}^{2+}$  signals is thought to arise from initial local signals which are short-lived and spatially restricted (Berridge et al., 2000). The generation of local  $\text{Ca}^{2+}$  signals themselves relies on a synergy between individual  $\text{Ca}^{2+}$  channels.  $\text{Ca}^{2+}$  release through  $\text{IP}_3$  receptors ( $\text{IP}_3\text{R}$ ) has been studied in depth to shed light on this process (Bootman et al., 1997; Dickinson and Parker, 2013).  $\text{IP}_3\text{R}$  are residents of the ER membrane and as their name suggests are activated by the phosphoinositide  $\text{IP}_3$  (Taylor and Tovey, 2010). However, they are also allosterically modulated by  $\text{Ca}^{2+}$  and support  $\text{Ca}^{2+}$ -induced  $\text{Ca}^{2+}$  release (CICR) (Bezprozvanny et al., 1991; Taylor and Tovey, 2010). Thus, if one  $\text{IP}_3$  receptor is activated, the  $\text{Ca}^{2+}$  it releases can diffuse into the cytosol and may induce the opening of a neighbouring channel. If a single channel is active the event is defined as a “blip”. If, however, activity spreads amongst a cluster of channels, the amplitude of intracellular  $\text{Ca}^{2+}$  increases, and the event is defined as a “puff” or local  $\text{Ca}^{2+}$  signal (Bootman et al., 1997).

This transition from “blip” to “puff” can then be followed by the generation of  $\text{Ca}^{2+}$  waves as has been observed when increasing  $\text{IP}_3$  levels in oocytes (Parker and Yao, 1996). Bootman and colleagues also showed that increasing concentrations of histamine (an  $\text{IP}_3$ -forming extracellular agonist (Bristow et al., 1991; Ishida et al., 2014; Johnson et al., 1990) turned “blips” or “puffs” into  $\text{Ca}^{2+}$  waves resembling global  $\text{Ca}^{2+}$  signals. This transition from local to global was correlated with increased frequency and amplitude of the local signal. This stage is often observed during whole-cell measurements as a smooth, slow-rising “pacemaker” region at the initiation of global  $\text{Ca}^{2+}$  signals (Bootman et al., 1997).

### 1.3.2 Membrane Contact Sites

In the above  $\text{IP}_3\text{R}$  model the generation of local and global  $\text{Ca}^{2+}$  signals is apparently reliant on diffusion of  $\text{Ca}^{2+}$  to nearby  $\text{IP}_3\text{R}$  channels on the same organelle. However, the targets of local  $\text{Ca}^{2+}$  signals are not always natural neighbours so the cell has to bring the intended targets close to the source of  $\text{Ca}^{2+}$  release. An example of this is the aforementioned use of SNAREs and tethers to dock vesicles together for  $\text{Ca}^{2+}$ -mediated membrane fusion. Regions of close apposition between membranes that do not fuse are termed membrane contact sites (MCS) (Prinz, 2014). Electron micrographs of human fibroblasts display MCS between lysosomes and the ER with less than 30 nm between their membranes (Kilpatrick et al., 2013, 2017). Whilst the

molecular composition of this MCS is currently understudied, the ER also shares MCS with endosomes, mitochondria and the plasma membrane, for which interacting proteins have been described (Eden, 2016; Eden et al., 2016; Phillips and Voeltz, 2016; Prinz, 2014). Interestingly, the GTPase Rab7 is found at MCS between late endosomes and the ER, and may therefore play a part in lysosome-ER MCS (Raiborg et al., 2015; Rocha et al., 2009). Besides facilitating the transmission of  $\text{Ca}^{2+}$  signals MCS also have a role in cholesterol homeostasis and membrane trafficking. For example, at low cholesterol levels the cholesterol sensor ORP1L binds vesicle-associated membrane protein-associated protein A (VAP-A) on the ER to form a stable ER-endosome MCS (Rocha et al., 2009). However, in high cholesterol, ORP1L binds through a Rab7 complex to microtubule motors to promote endosome trafficking. MCS have also been reported as sites of direct lipid transfer, independent of the vesicular pathway (Phillips and Voeltz, 2016).

### 1.3.3 $\text{Ca}^{2+}$ from the ER

The ER is perhaps the most appropriate starting point for understanding the  $\text{Ca}^{2+}$  signalling network. This is due to the relatively large portion of cell that it occupies and the variety of organelles it is known to share MCSs with (Phillips and Voeltz, 2016; Weibel et al., 1969). Therefore, it may be regarded as a central hub for  $\text{Ca}^{2+}$  signalling. The ER has a  $\text{Ca}^{2+}$  concentration of 60-600 $\mu\text{M}$  and is filled by the sarco/endoplasmic reticulum  $\text{Ca}^{2+}$ -ATPase (SERCA) on the ER membrane (Demaurex and Frieden, 2003; Miyawaki et al., 1997).

$\text{Ca}^{2+}$  signals emanating from the ER are generated through two types of large tetrameric channels, one being the  $\text{IP}_3\text{R}$  (Berridge et al., 2000; Seo et al., 2012). The activator  $\text{IP}_3$  binds to the receptor and is generated by phospholipase C (PLC) which cleaves  $\text{PI}(4,5)\text{P}_2$  into cytosolic  $\text{IP}_3$  and membrane-bound diacylglycerol (DAG).  $\text{PLC}\beta$  and  $\text{PLC}\gamma$  are activated by g-protein coupled receptors (GPCR) or receptor tyrosine kinases (RTK) respectively (Clapham, 2007). Extracellular agonists which stimulate  $\text{IP}_3$  generation include bradykinin (Ataei et al., 2013; Johnson et al., 1990), carbachol (Chen and Hsu, 1994; Piiper et al., 1994; Shin et al., 2003) and histamine (Bristow et al., 1991; Ishida et al., 2014; Johnson et al., 1990). There are three  $\text{IP}_3\text{R}$  isoforms (1-3) arising from three different genes, which are all expressed in mammals (Foskett et al., 2007). Multiple isoforms are often expressed in a given tissue, although not equally. For example,  $\text{IP}_3\text{R}1$  is the predominant isoform expressed in neurons (Ivanova et al., 2014). As well as the ER,  $\text{IP}_3\text{Rs}$  are also found in the plasma membrane and the Golgi.

At twice the size of  $\text{IP}_3\text{R}$  the ryanodine receptor (RyR) is the other major ER  $\text{Ca}^{2+}$  release channel. Like  $\text{IP}_3\text{Rs}$  there are three RyR gene isoforms which display overlapping but uneven tissue

expression (Kiviluoto et al., 2013). RyR is somewhat structurally and functionally homologous to IP<sub>3</sub>R but their modes of activation do differ (Seo et al., 2012). In the first instance RyRs appear to be regulated by cADPR (Lee, 2012). cADPR is synthesised from nicotinamide adenine dinucleotide (NAD) by ADP-ribosyl cyclase (ADPR-c) activity of membrane proteins CD38 and CD157. However, the pathway that activates these enzymes is unclear (Malavasi et al., 2008). Interestingly, IP<sub>3</sub>-forming bradykinin and histamine also induce cADPR production (Kip et al., 2006). In addition, acetylcholine, which activates the same receptors as carbachol, also causes cADPR synthesis (Kip et al., 2006; Yamasaki et al., 2005). Another difference between IP<sub>3</sub>Rs and RyRs is that no cADPR-binding site has been determined on the receptor and it is suspected that RyR activation is dependent upon an intermediate binding protein, akin to NAADP and TPC activation (Lee, 2012; Lin-Moshier et al., 2012; Walseth et al., 2012a, 2012b). Like IP<sub>3</sub>R, RyR is also activated by Ca<sup>2+</sup> so elicits CICR. Importantly, both channels are stimulated by relatively low concentrations of Ca<sup>2+</sup> but inhibited at higher concentrations (Bezprozvanny et al., 1991).

#### **1.3.4 Ca<sup>2+</sup> from the Golgi**

The Ca<sup>2+</sup> concentration of the Golgi is similar to that of the ER at ~150-600 μM, and it also possesses IP<sub>3</sub> and RyR activity (Aulestia et al., 2015; Lissandron et al., 2010; Missiaen et al., 2004; Pinton et al., 1998). Despite these similarities the contribution of the Golgi to Ca<sup>2+</sup> signalling appears to differ to that of the ER. For example, in response to histamine stimulation, the drop in luminal Golgi Ca<sup>2+</sup> is smaller than that of the ER, and in response to ATP Ca<sup>2+</sup> release from the Golgi terminates before that of the ER (Missiaen et al., 2004; Vanoevelen et al., 2004). The Golgi only contributes ~2-3% of total cell volume and ~2-5% of cellular Ca<sup>2+</sup> which may go some way to explain these findings (Chandra et al., 1991). However, as demonstrated by the lysosomes diminutive proportions do not necessarily preclude importance in Ca<sup>2+</sup> signalling.

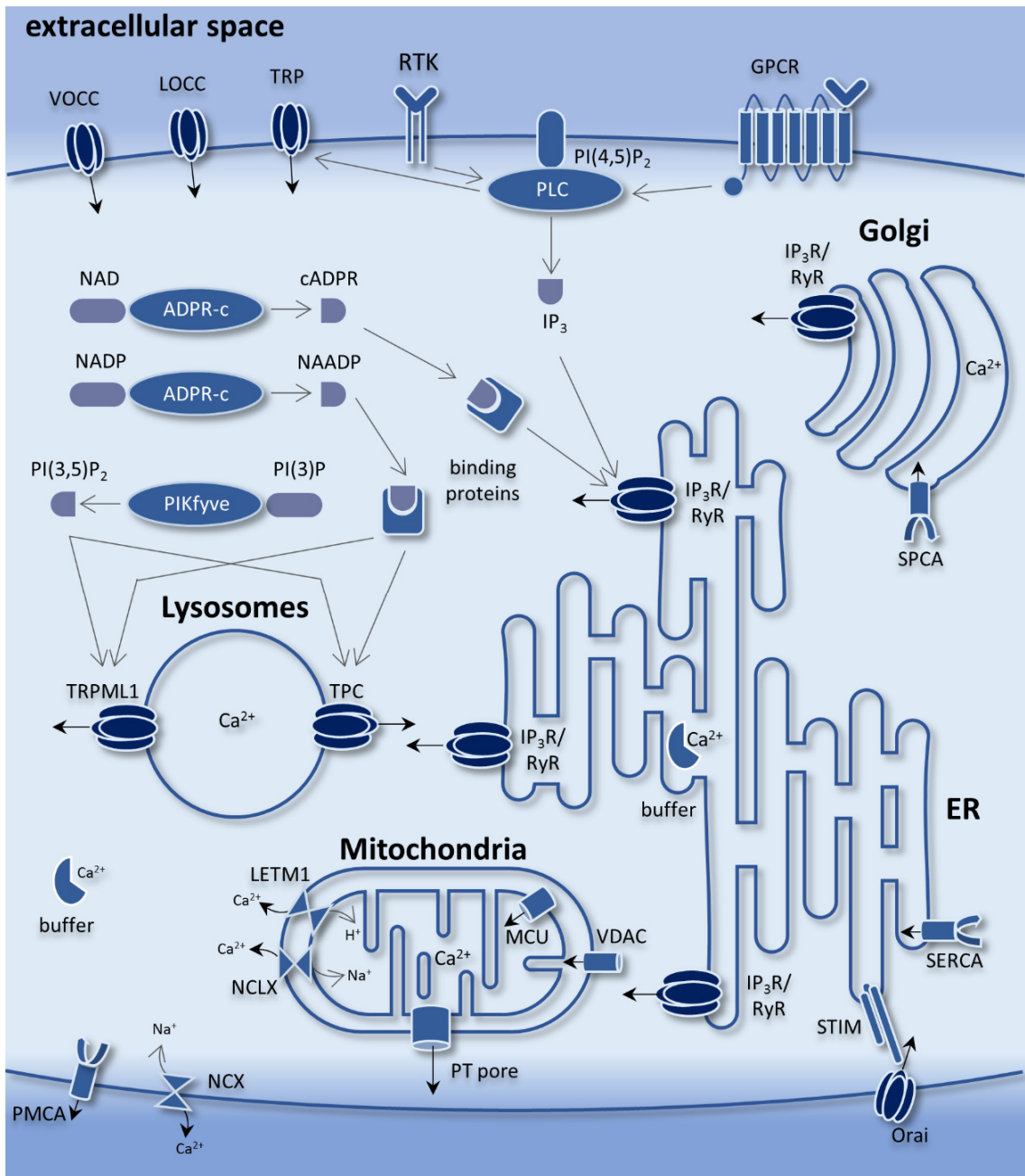


**Figure 1.4 The  $\text{Ca}^{2+}$  signalling network of the cell**

Extracellular  $\text{Ca}^{2+}$  can enter the cell when VOCC, LOCC or TRP channels are activated. It may also enter via STIM and Orai when ER  $\text{Ca}^{2+}$  is depleted.  $\text{Ca}^{2+}$  is extruded back out of the cell by PMCA and NCX.  $\text{Ca}^{2+}$  stored in the lysosomes, the Golgi and ER can be released when resident  $\text{Ca}^{2+}$  channels such as TRPML1, TPCs, IP<sub>3</sub>R and RyR are activated by the phosphoinositide PI(3,5)P<sub>2</sub> or mobilising messengers NAADP, cADPR or IP<sub>3</sub>. The synthesis of IP<sub>3</sub> by PLC is stimulated by activated RTKs or GPCRs on the plasma membrane. PLC can activate TRP channels. cADPR and NAADP are synthesised by ADPR-c and are thought to require accessory binding proteins to activate their target channels. PI(3,5)P<sub>2</sub> is synthesised by PIKfyve.  $\text{Ca}^{2+}$  is pumped into the Golgi by SPCA and into the ER by SERCA.  $\text{Ca}^{2+}$  enters the mitochondria through VDAC and MCU and leaves via NCLX, LETM1 and the PT pore. Cytosolic and ER buffers can modulate  $\text{Ca}^{2+}$  signals.

$\text{Ca}^{2+}$  release/uptake → ; other signalling paths → .

### 1.3.5 Ca<sup>2+</sup> from the lysosomes

Lysosomes have a luminal Ca<sup>2+</sup> concentration of 400-700 μM which is comparable to that of the ER (Christensen et al., 2002; Lloyd-Evans et al., 2008). However, the total cell volume occupied by lysosomes is smaller compared to the ER in mammalian cells and the two organelles contribute to Ca<sup>2+</sup> signalling differently (Weibel et al., 1969).

As discussed previously, TRPML1 and TPC channels mediate lysosomal Ca<sup>2+</sup> release and are likely under endogenous regulation by PI(3,5)P<sub>2</sub> and NAADP. PI(3,5)P<sub>2</sub> is synthesised from PI(3)P by the lipid kinase PIKfyve which can localise to endosomes and lysosomes (McCartney et al., 2014). Extracellular stimuli that trigger PI(3,5)P<sub>2</sub> synthesis are not extensively documented. However, insulin secretion has been shown to regulate PIKfyve activity, and osmotic shock in yeast increases PI(3,5)P<sub>2</sub> production.

NAADP can be synthesised from NADP via a base-exchange reaction which is catalysed by CD38 (Malavasi et al., 2008). Reported extracellular stimuli for NAADP synthesis are detailed in Table 1.1 and include receptor agonists histamine and carbachol. Of note, CD38 is not always required for these stimulus-evoked NAADP increases eluding to the presence of an as yet unidentified NAADP-synthesising enzyme (Gul et al., 2016; Park et al., 2015; Shaul et al., 2009; Soares et al., 2007). In lieu of direct NAADP measurements some stimuli have been linked to NAADP production if their Ca<sup>2+</sup> signals have been inhibited by desensitising concentrations of NAADP or NAADP antagonists (Table 1.2). NAADP involvement has also been implied when Ca<sup>2+</sup> signals are inhibited after disruption of the lysosomal Ca<sup>2+</sup> store (Table 1.2). This is achieved by the lysosomotropic agent glycyl-L-phenylalanine-beta-naphthylamide (GPN) or the V-ATPase inhibitor bafilomycin A. GPN is a weak hydrophobic base that can diffuse into the lysosomes where it is then cleaved by the pH-sensitive hydrolase cathepsin C. The resultant products cause disruption to the lysosomal membrane and can initiate Ca<sup>2+</sup> signals (Haller et al., 1996; Jadot et al., 1984). Bafilomycin A is thought to indirectly deplete lysosomal Ca<sup>2+</sup> by reducing the proton content of lysosomes and consequently inhibiting Ca<sup>2+</sup>/H<sup>+</sup> exchange, possibly mediated by CAX (Morgan et al., 2011). Although external triggers such as neurotransmitters and hormones have been reported to induce Ca<sup>2+</sup> signals via lysosomes or NAADP, evidence supporting TPC involvement is lagging behind. In Chapters 3 and 4 I investigate the requirement of TPCs in the generation of such physiological global Ca<sup>2+</sup> signals.

As research is ongoing to uncover the triggers and mechanisms of PI(3,5)P<sub>2</sub> and NAADP synthesis, so are efforts to understand how these stimuli elicit large Ca<sup>2+</sup> signals in mammalian



cells through a low-volume  $\text{Ca}^{2+}$  store. Isolated NAADP-induced  $\text{Ca}^{2+}$  signals from the lysosomes alone are very small and difficult to detect, eluding to their local nature (Morgan, 2016). In contrast, isolated NAADP-induced  $\text{Ca}^{2+}$  release in sea urchin egg homogenates generates relatively large  $\text{Ca}^{2+}$  transients. This is likely due to the relatively large cell volume that lysosome-related organelles occupy in sea urchin eggs (Morgan, 2011). However, in intact sea urchin eggs (where native MCS are presumably preserved) NAADP gives rise to an initial  $\text{Ca}^{2+}$  signal and a secondary  $\text{Ca}^{2+}$  wave by triggering further  $\text{Ca}^{2+}$  release from the ER (Churchill and Galione, 2001). In mammalian cells this functional coupling between the lysosomes and ER has also been demonstrated and is seemingly even more crucial for the production of global  $\text{Ca}^{2+}$  signals (Cancela et al., 1999; Morgan, 2016) .

As well as lysosome-to-ER  $\text{Ca}^{2+}$  coupling, communication between the two organelles can work in the reverse mode. Upon  $\text{Ca}^{2+}$  release from the ER lysosomes may take up  $\text{Ca}^{2+}$  and act as a buffer of global  $\text{Ca}^{2+}$  signals (Lopez-Sanjurjo et al., 2013). Alternatively, as detected by increases in lysosomal pH, ER  $\text{Ca}^{2+}$  release can cause further NAADP-dependent lysosomal  $\text{Ca}^{2+}$  release (Morgan et al., 2013).

**Table.1.1 Extracellular stimuli associated with NAADP generation**

<b>Stimulus</b>	<b>Concentration</b>	<b>Cell type</b>	<b>Species</b>	<b>Reference</b>
Angiotensin II	100 nM	Hepatic stellate cells	Mouse	(Kim et al., 2010)
Anti-CD3 Ab (OKT3)	5 µg/ml	Jurkat T lymphocytes (subclone JMP)	Human	(Gasser et al., 2006)
ATC	400 µM	Pancreatic β cell	Mouse	(Park et al., 2015)
ATP	100 µM	Cortical astrocytes	Rat	(Barceló-Torns et al., 2011)
Carbachol	100 µM	Tracheal rings	Guinea pig	(Aley et al., 2013)
Cholecystokinin	50 pM	Pancreatic acinar	Mouse	(Cosker et al., 2010)
Cholecystokinin	10 pM – 1 µM	Pancreatic acinar cells	Mouse	(Yamasaki et al., 2005)
ET-1	1 µM	Pulmonary arterial smooth muscle cell	Rat	(Kinnear et al., 2004)
ET-1	100 nM	Coronary arterial smooth muscle cells	Bovine	(Zhang et al., 2006)
FasL	10 ng/mL	Coronary arterial myocytes	Mouse	(Zhang et al., 2010)
GLP-1	10 nM	Pancreatic β cells	Mouse	(Kim et al., 2008a)
Glucose		Adipose tissue	Mouse	(Song et al., 2012)
Glucose	12 mM	Pancreatic Islets	Mouse	(Shawl et al., 2012)
Glucose	20 mM	Pancreatic β cells MIN6	Mouse	(Masgrau et al., 2003)
Glutamate	10 µM	Whole brain suspension	Rat	(Pandey et al., 2009)
Histamine	100 µM	Myometrial	Human	(Soares et al., 2007)
IL-8	10 pM	Lymphokine-activated killer cells	Mouse	(Rah et al., 2010)
Insulin	100 nM	3T3-L1 adipose-differentiated	Mouse	(Song et al., 2012)
Insulin	100 nM	Primary Adipocytes	Mouse	(Song et al., 2012)
Insulin	200 nM	Pancreatic β-cells	Mouse	(Shawl et al., 2009)
Ischemic reperfusion		Heart	Mouse	(Davidson et al., 2015)
Isoprenaline	100 nM	Heart	Guinea pig	(Lewis et al., 2012)
Isoprenaline	2 µM	Cardiomyocytes	Rat	(Gul et al., 2016)
Isoprenaline	60 nM	Heart	Guinea Pig	(Macgregor et al., 2007)
NF546 (P2Y11-R agonist)	1 and 100 µM	Neonatal Cardiomyocytes	Rat	(Djerada and Millart, 2013)
Rosiglitazone	1 µM	3T3-L1 adipose-differentiated	Mouse	(Song et al., 2012)
Sperm	~1-2 x10 <sup>8</sup> /ml	Eggs	Sea urchin	(Churchill et al., 2003)

Thrombin	0.5 units/ml	Platelets	Mouse	(Mushtaq et al., 2011)
TMPH	100 $\mu$ M	EA.hy926 endothelial cells	Human	(Esposito et al., 2011)

**Table 1.2. Ca<sup>2+</sup> signals induced by extracellular stimuli with inferred NAADP/lysosomal involvement**

Ca<sup>2+</sup> signals induced by the stimuli listed below were inhibited by GPN, Bafilomycin A (Baf), NAADP antagonists (N-ant), or desensitising concentrations of NAADP.

Stimulus	Concentration	Cell type	Species	GPN/ Baf/ N-ant/ NAADP	Reference
7-Ket	10 µg/ml	Coronary arterial myocytes	Mouse	N-ant	(Xu et al., 2015)
Acetylcholine	10 µM	Aortic endothelial cells (HAEC)	Human	Baf N-ant	(Brailoiu et al., 2010b)
Angiotensin II	100 nM	Hepatic stellate cells	Mouse	Baf NAADP	(Kim et al., 2010)
Anti-CD3 Ab (OKT3)	10 µg/ml	Jurkat T lymphocytes (subclone JMP)	Human	NAADP	(Berg et al., 2000)
Antigen (ESO 9C)-presenting cells	100nM ESO 9C	Cytotoxic T lymphocytes	Human	Baf N-ant NAADP	(Davis et al., 2012)
ATC	400 µM	Pancreatic β cell	Mouse	N-ant	(Park et al., 2015)
ATP	100 µM	Cortical astrocytes	Rat	GPN Baf N-ant	(Barceló-Torns et al., 2011)
ATP	10 µM	Hippocampal Neurons and Glia (separate results)	Rat	GPN	(Pandey et al., 2009)
Carbachol	100 µM	Tracheal smooth muscle cells	Guinea pig	N-ant	(Aley et al., 2013)
Carbachol	10 µM	Gastric Smooth muscle cells	Rat	NAADP	(Pereira et al., 2014)
Cholecystokinin	25 and 40 pM	Pancreatic acinar	Mouse	GPN	(Cosker et al., 2010)
Cholecystokinin	10 pM	Pancreatic acinar	Rat	NAADP	(Cosker et al., 2010)
Cholecystokinin	5 pM	Pancreatic acinar cells	Mouse	N-ant	(Gerasimenko et al., 2015)
Cholecystokinin	0.5-2.5 pM	Pancreatic acinar cells	Mouse	Baf GPN	(Yamasaki et al., 2004)
Cholecystokinin	2-5pM	Pancreatic acinar cells	Mouse	NAADP	(Cancela et al., 1999)

Cross-linked CD3	5 µg/ml αCD3; 50 µg/ml streptavidin	Naïve CD4 or CD8 T cells (Ned-19 only)	Mouse	Baf N-ant	(Ali et al., 2016)
Cross-linked CD3	5 µg/ml αCD3; 50 µg/ml streptavidin	Effector CD4 T cells	Mouse	N-ant	(Ali et al., 2016)
ET-1	10 nM	Cortical astrocytes	Rat	GPN Baf N-ant	(Barceló-Torns et al., 2011)
ET-1	100 nM	Pulmonary arterial smooth muscle cell	Rat	Baf	(Kinnear et al., 2004)
ET-1	100 nM	Coronary arterial smooth muscle cells	Bovine	Baf	(Zhang et al., 2006)
ET-1	100 nM	Renal afferent arterioles	Rat	Baf N-ant	(Thai et al., 2009)
ET-1 (following IRL1620)	10 nM	Peritubular smooth muscle cells	Rat	Baf NAADP	(Gambara et al., 2008)
Extracellular NAADP	3 µM	Naïve CD4 T cells	Mouse	Baf N-ant	(Ali et al., 2016)
Extracellular NAADP	3 µM	Effector CD4 T cells	Mouse	Baf N-ant	(Ali et al., 2016)
FasL	10 ng/mL	Coronary arterial myocytes	Mouse	Baf	(Zhang et al., 2010)
GLP-1	10 nM	Pancreatic β cells	Mouse	GPN Baf NAADP	(Kim et al., 2008a)
Glucose	5-15mM	Pancreatic Islets	Mouse	N-ant	(Wang et al., 2012)
Glucose	10 mM	Pancreatic β cells	Mouse	GPN Baf N-ant	(Arredouani et al., 2015)
Glucose	20 mM	Pancreatic β cells MIN6	Mouse	Baf	(Yamasaki et al., 2004)
Glucose	10 mM	Pancreatic β cells	Mouse	N-ant	(Naylor et al., 2009)
Glucose	20 mM	Pancreatic β cells MIN6	Mouse	NAADP	(Masgrau et al., 2003)

Glutamate	10 $\mu$ M	Hippocampal Neurons and Glia (separately)	Rat	Baf GPN	(Pandey et al., 2009)
Histamine	100 $\mu$ M	EA.hy926 endothelial cells	Human	N-ant	(Esposito et al., 2011)
Histamine	100 $\mu$ M	Umbilical vein endothelial cells (HUVEC)	Human	N-ant	(Favia et al., 2014)
Histamine	100 $\mu$ M	Myometrial	Human	Baf GPN	(Soares et al., 2007)
IL-8	10 pM	Lymphokine-activated killer cells	Mouse	Baf	(Rah et al., 2010)
Insulin	100 nM	3T3-L1 adipose-differentiated	Mouse	Baf, N-ant	(Song et al., 2012)
Insulin	200 nM	Pancreatic $\beta$ -cells	Mouse	NAADP	(Shawl et al., 2009)
Insulin	200 nM	Pancreatic Islet cells	Human	NAADP	(Johnson and Mislser, 2002)
IRL1620	100 nM	Peritubular smooth muscle cells	Rat	Baf NAADP	(Gambara et al., 2008)
Ischemic reperfusion	Anoxic, followed by normoxic buffer	Ventricular Cardiomyocytes	Rat	N-ant	(Davidson et al., 2015)
Isoprenaline	200 nM	Cardiac myocytes	Mouse	Baf N-ant	(Nebel et al., 2013)
Isoprenaline	2 $\mu$ M	Cardiomyocytes	Rat	Baf	(Gul et al., 2016)
Isoprenaline and Electrical stimulation	2 nM 1Hz	Ventricular myocytes	Guinea Pig	Baf N-ant	(Capel et al., 2015)
Noradrenaline	10 $\mu$ M	Renal afferent arterioles	Rat	Baf N-ant	(Thai et al., 2009)
Oxytocin	100 $\mu$ M	Myometrial	Human	Baf GPN	(Soares et al., 2007)
Oxytocin	10 nM	Uterine smooth muscle cells	Rat	Baf N-ant	(Aley et al., 2010b)
RANKL	1 nM	RAW	Mouse	Baf	(Notomi et al., 2012)
Sperm	$\sim 1-2 \times 10^8$ /ml	Eggs	Sea urchin	NAADP	(Churchill et al., 2003)

Thrombin	0.5 units/ml	Platelets	Mouse	Baf N-ant	(Mushtaq et al., 2011)
Thrombin	10 $\mu$ M	Aortic endothelial cells (HAEC)	Human	Baf N-ant	(Brailoiu et al., 2010b)
Thrombin	0.1 unit/ml	Platelets	Human	GPN	(López et al., 2005)
TMPH	100 $\mu$ M	EA.hy926 endothelial cells	Human	Baf N-ant, NAADP	(Esposito et al., 2011)
VEGF	100 $\mu$ g/L	Umbilical vein endothelial cells	Human	Baf N-ant	(Favia et al., 2014)

### 1.3.6 Ca<sup>2+</sup> from the extracellular space

Up to this point the focus has been on how Ca<sup>2+</sup> signals are generated from intracellular Ca<sup>2+</sup> stores. However, Ca<sup>2+</sup> is also maintained at high concentrations extracellularly (~1-2mM) and enters the cell through various channels at the plasma membrane (Thomas, 2000). An important route of Ca<sup>2+</sup> entry is that which serves to re-fill the ER when its Ca<sup>2+</sup> store has been depleted in order to sustain Ca<sup>2+</sup> signals (Shen et al., 2011). This store-operated calcium entry (SOCE) is mediated by three proteins working in concert: an ER membrane protein (STIM), a plasma membrane Ca<sup>2+</sup> channel (Orai) and the ER Ca<sup>2+</sup> uptake pump SERCA. STIM (stromal interaction molecule) controls the process through its interaction with luminal ER Ca<sup>2+</sup> (Stathopoulos et al., 2008). When ER Ca<sup>2+</sup> is released and luminal Ca<sup>2+</sup> levels drop STIM-Ca<sup>2+</sup> binding is reduced and STIM consequently undergoes conformational change. This leads to its oligomerisation, translocation and subsequent activation of Orai (Liou et al., 2007). As Ca<sup>2+</sup> enters the cell through Orai, SERCA re-fills the ER. These three SOCE proteins are enriched at ER-plasma membrane MCS although it is unclear whether the interaction between STIM and Orai modulates pre-existing MCS or creates new ones (Prinz, 2014). Extended synaptotagmins also have a role in ER-plasma membrane MCS formation that is dependent on Ca<sup>2+</sup> and PI(4,5)P<sub>2</sub> (Giordano et al., 2013).

In electrically excitable cells Ca<sup>2+</sup> also enters through voltage-operated Ca<sup>2+</sup> channels (VOCC). As the putative descendants of TPCs they possess a pore-forming  $\alpha$  subunit consisting of a 4x6 MSR configuration, with cytosolic termini (Simms and Zamponi, 2014). These channels open in response to membrane depolarisation and can be categorised according to voltage-sensitivity, kinetics, channel conductance and pharmacology. T-type VOCCs function autonomously as a single  $\alpha$  subunit and open in response to small electrical currents. Channel types L, N, P/Q or R are flanked by additional  $\beta$  and  $\alpha_2\delta$  subunits and open in response to large voltage changes. For the contraction of myofilaments in muscle, L-type VOCCs communicate to RyRs on the sarcoplasmic reticulum (SR) through specialised MCS which allow CICR or voltage-induced Ca<sup>2+</sup> release (VICR) (Burgoyne et al., 2015). In neurons a similar type of MCS is important for Ca<sup>2+</sup> communication between N-methyl-D-aspartate receptors (NMDAR) on the plasma membrane and RyR (Moriguchi et al., 2006). NMDAR are an example of ligand-operated Ca<sup>2+</sup> channels (LOCC) which also include nicotinic receptors (Pankratov and Lalo, 2014). These channels are gated by neurotransmitters glutamate and acetylcholine respectively.

Ca<sup>2+</sup> entry through the plasma membrane is also permitted by TRP channels. This family of channels has 28 members (including TRPML1) which are associated with diverse stimuli and functions (Nilius and Owsianik, 2011; Venkatachalam and Montell, 2007). Although TRPML1



localises to the lysosomes most TRPs are residents of the plasma membrane and their activity appears to be intertwined with other  $\text{Ca}^{2+}$  signalling events (Gees et al., 2010). For instance, members of the TRPC (TRP canonical) subgroup of channels are activated by PLC and therefore may be relevant to  $\text{IP}_3$ -mediated  $\text{Ca}^{2+}$  signals. It is unclear how TRPCs are activated by PLC but there is evidence in flies that the conversion of membrane bound  $\text{PI}(4,5)\text{P}_2$  to DAG physically alters the plasma membrane to mechanically open the channels (Hardie and Franze, 2012; Svobodova and Groschner, 2016). Alternatively,  $\text{PI}(4,5)\text{P}_2$  may inhibit TRPCs, thus  $\text{PI}(4,5)\text{P}_2$  metabolism might confer TRPC activation (Rohacs, 2013). In addition, TRPs may activate VOCCs by depolarising the cell, and be involved in SOCE (Gees et al., 2010; Yuan et al., 2009). The latter remains a contentious issue since the identification of Orai as a store-operated  $\text{Ca}^{2+}$  channel (SOCC).

### **1.3.7 $\text{Ca}^{2+}$ and mitochondrial function**

Unlike lysosomes and the ER, mitochondria do not rapidly release  $\text{Ca}^{2+}$  upon opening of ion channels in response to second messengers. However, they have important functions in the calcium signalling network including the shaping of  $\text{Ca}^{2+}$  transients and regulating cell death (Rizzuto et al., 2012). These organelles can take up local  $\text{Ca}^{2+}$  released from the ER via  $\text{IP}_3\text{Rs}$  or  $\text{RyRs}$  when the two organelles are in close proximity (Csordás et al., 2010; Szalai et al., 2000). To reach the mitochondrial matrix where  $\text{Ca}^{2+}$  regulates several downstream pathways  $\text{Ca}^{2+}$  ions must pass through an ion-permeable outer mitochondrial membrane (OMM) and an impermeable inner mitochondrial membrane (IMM). The OMM is permeable to ions  $\sim 5\text{kDa}$  and this is enabled by the presence of voltage-dependent anion channels (VDAC) (Colombini, 1980). To cross the IMM  $\text{Ca}^{2+}$  ions pass through the more selective mitochondrial  $\text{Ca}^{2+}$  uniporter (MCU) (De Stefani et al., 2011; Kirichok et al., 2004). As mitochondrial  $\text{Ca}^{2+}$  uptake relies on its closeness with the ER several studies have focussed on identifying the molecular components of the ER-mitochondrial MCS. One candidate, GRP75 (75kDa glucose-related protein), chaperones the interaction between  $\text{IP}_3\text{R}$  and VDAC (Szabadkai et al., 2006). MFN2 (mitochondrial dynamin-related family member mitofusin 2) has controversially been shown to both promote and inhibit ER-mitochondrial contacts and  $\text{Ca}^{2+}$  transfer (de Brito and Scorrano, 2008; Filadi et al., 2015; Naon et al., 2016). PML (promyelocytic leukaemia tumour suppressor) is reported to control  $\text{IP}_3\text{R}$   $\text{Ca}^{2+}$  release and mitochondrial uptake, possibly by regulating PKB (protein kinase B) activity (Giorgi et al., 2010). Interactions between ER VAP-B and OMM PTPIP51 (protein tyrosine phosphatase-interacting protein 51) are also important for maintaining ER-mitochondria MCS (De Vos et al., 2012). The importance of this MCS is perhaps highlighted by the neurodegenerative disorders Charcot-Marie Tooth disease and amyotrophic lateral sclerosis

(ALS) which can be caused by mutant forms of MFN2 and VAP-B (Chen et al., 2010; Züchner et al., 2004). Besides the ER, mitochondria can also take up  $\text{Ca}^{2+}$  from plasma membrane SOCE channels and VOCCs (Rizzuto et al., 2012). The makeup of mitochondria-plasma membrane MCS in mammals is currently unknown but in yeast Num1 and Mdm36 have been proposed as a tethering complex (Westermann, 2015).

The consequences of rising mitochondrial  $\text{Ca}^{2+}$  are numerous, ranging from helpful to the potentially disastrous. One of the more cooperative outcomes is an increase of dehydrogenase activity which contributes to increased ATP production (Denton, 2009; Glancy and Balaban, 2012). As many events triggered by rises in  $\text{Ca}^{2+}$  are energy-dependent this relationship may serve to keep ATP levels up with demand. The more sinister role of rising mitochondrial  $\text{Ca}^{2+}$  is in promoting cell death. First, increased ATP production may be accompanied by increased production of harmful reactive oxygen species (ROS) which damage proteins, lipids and nucleic acids (Turrens, 2003). Second, a cell's doom is often flagged by the increased permeability of the IMM in a phenomenon known as permeability transition (PT) (Biasutto et al., 2016). This can cause collapse of the mitochondrial electrochemical gradient that drives ATP synthesis, and release of pro-apoptotic factors such as cytochrome C into the cytosol. Many studies have shown that PT is preceded by increases in mitochondrial  $\text{Ca}^{2+}$ , whether it comes from excitotoxicity or cytosolic  $\text{Ca}^{2+}$  waves caused by physiological stimuli (Rizzuto et al., 2012).

The ability of mitochondria to take up  $\text{Ca}^{2+}$  is also important for shaping  $\text{Ca}^{2+}$  signals. For example, once  $\text{Ca}^{2+}$  is released through  $\text{IP}_3\text{R}$  there may be a high local  $\text{Ca}^{2+}$  concentration around the receptor. If this concentration is too high it will inhibit further release (Bezprozvanny et al., 1991). If, however, mitochondria are close by and buffer the  $\text{Ca}^{2+}$  to lower the local concentration further release from the ER may be permitted. In an alternative scenario mitochondria may reduce the local  $\text{Ca}^{2+}$  concentration around  $\text{IP}_3\text{R}$  to non-activating levels (Jouaville et al., 1995). The advantage of this is that more  $\text{IP}_3$  receptors will need to be stimulated simultaneously before  $\text{Ca}^{2+}$  levels are high enough to initiate CICR and produce a global  $\text{Ca}^{2+}$  signal. This prevents asynchronous firing of  $\text{IP}_3\text{Rs}$  which could result in the failure of a signal to propagate. The shaping of  $\text{Ca}^{2+}$  signals by mitochondria appears to be an active process whereby mitochondria move to the vicinity of  $\text{Ca}^{2+}$  release (MacAskill et al., 2009).

Of course  $\text{Ca}^{2+}$  entry into mitochondria, whatever the cause, must be balanced by  $\text{Ca}^{2+}$  extrusion. This is achieved by  $\text{Ca}^{2+}/\text{Na}^+$  and  $\text{Ca}^{2+}/\text{H}^+$  exchange activity conferred by NCLX and LETM1

respectively (Palty et al., 2010; Shao et al., 2016). The PT pore has also been reported to mediate mitochondrial  $\text{Ca}^{2+}$  release (Rizzuto, 2012).

### 1.3.8 Signal Silencing

$\text{Ca}^{2+}$  uptake by mitochondria provides one way of modulating and possibly terminating cytosolic  $\text{Ca}^{2+}$  signals. As discussed previously lysosomes can also take up  $\text{Ca}^{2+}$  via CAX activity. In addition, the pumps sarco/endoplasmic reticulum  $\text{Ca}^{2+}$ -ATPase (SERCA), secretory pathway  $\text{Ca}^{2+}$ -ATPase (SPCA) and plasma membrane  $\text{Ca}^{2+}$  ATPase (PMCA) can also remove  $\text{Ca}^{2+}$  from the cytosol to fill primarily the ER, Golgi and extracellular space respectively (Brini and Carafoli, 2009). These three pumps belong to the P-type family of ATPases that hydrolyse ATP to transport ions across a membrane. There are 3 gene isoforms for SERCA, with SERCA2 being the dominant presence in the brain (Baba-Aissa et al., 1996). All isoforms are predicted to have the same structure owing to highly conserved primary sequences (Periasamy and Kalyanasundaram, 2007). SERCA is functional as a monomer and possesses 10 helical MSRs which encompass two  $\text{Ca}^{2+}$  binding sites (Brini and Carafoli, 2009). The presence of two  $\text{Ca}^{2+}$  binding sites may explain the 2  $\text{Ca}^{2+}$  ions that are transported for every ATP that is hydrolysed. A distinguishing property of SERCA is its inhibition by the lactone thapsigargin which sits in a cavity created by the MSR helices. (Brini and Carafoli, 2009; Chen et al., 2017; Thastrup et al., 1990). SPCA has two isoforms, with SPCA1 evenly expressed in a wide variety of tissues (Vanoevelen et al., 2005). SPCA2 on the other hand has a more uneven expression pattern, with higher levels in the digestive system. The third P-type ATPase that reduces cytosolic  $\text{Ca}^{2+}$  is PMCA. Isoforms 1 and 4 are expressed ubiquitously whilst PMCA2 and 3 are restricted to the nervous system (Zacharias and Kappen, 1999). Both SPCA and PMCA are predicted to have similar structures to SERCA but they lack an acidic residue in MSR 5 which is crucial for  $\text{Ca}^{2+}$  binding (Brini and Carafoli, 2009). This reduces their number of binding sites to one which probably explains why they only transport one  $\text{Ca}^{2+}$  across the membrane for each hydrolysed ATP.

Cytosolic  $\text{Ca}^{2+}$  is also extruded by the  $\text{Ca}^{2+}/\text{Na}^{+}$  (NCX) exchanger in the plasma membrane. For every 3  $\text{Na}^{+}$  ions that enter the cytosol NCX exports one  $\text{Ca}^{2+}$  (Khananshvili, 2014). As well as pumps and exchangers, cytosolic  $\text{Ca}^{2+}$  levels can be reduced by other  $\text{Ca}^{2+}$  binding proteins. Although there are many molecules that bind  $\text{Ca}^{2+}$  in order to carry out their function they are not all present at large enough concentrations to be considered buffers (Schwaller, 2010). Examples of cytosolic  $\text{Ca}^{2+}$  sensors that are include parvalbumin, calbindins and calretinin. These buffers appear to modulate  $\text{Ca}^{2+}$  signals in unique ways. For instance, parvalbumin modulates the decay of global  $\text{Ca}^{2+}$  signals from a monophasic decay to biphasic - it increases the rate of

the initial drop but quickly the decay is slowed, causing the signal to plateau before returning to basal  $\text{Ca}^{2+}$  levels (Collin et al., 2005; Lee et al., 2000). Calbindin-D28K on the other hand has been shown to reduce the peak amplitude of  $\text{Ca}^{2+}$  transients (Airaksinen et al., 1997).  $\text{Ca}^{2+}$  buffers inside organelles are also important for shaping  $\text{Ca}^{2+}$  signals. ER resident calreticulin is one such buffer which affects the activity of SERCA and  $\text{Ca}^{2+}$  signals in response to bradykinin (John et al., 1998; Mesaeli et al., 1999). Calnexin is an ER membrane protein which also regulates SERCA in response to  $\text{IP}_3\text{R}$  activity (Roderick et al., 2000). These two  $\text{Ca}^{2+}$ -sensitive ER proteins function as chaperones, recognising polysaccharides tagged to misfolded nascent proteins (McCaffrey and Braakman, 2016). Another ER  $\text{Ca}^{2+}$  buffer, BiP, is also important in protein re-folding but binds instead to exposed hydrophobic protein patches. Problems may therefore arise if ER  $\text{Ca}^{2+}$  levels are disturbed as protein folding may be impaired. Depletion of ER  $\text{Ca}^{2+}$  and protein aggregation both contribute to ER stress and may trigger the unfolded protein response (UPR) which is regulated by BiP (Rutkowski and Kaufman, 2004). The UPR signalling cascades aim to restore ER homeostasis by pausing the majority of protein synthesis, increasing ER-associated protein degradation (ERAD), and increasing protein folding (Wang and Kaufman, 2016). If, however, UPR is prolonged and homeostasis is not reached, apoptosis ensues. This is mediated by increases in  $\text{IP}_3\text{R}$   $\text{Ca}^{2+}$  release and mitochondrial  $\text{Ca}^{2+}$  uptake.

In summary, the ability to fine-tune  $\text{Ca}^{2+}$  levels to prevent mitochondrial or ER stress is clearly important to prevent cell death. In addition, the control of  $\text{Ca}^{2+}$  is critical to avoid non-lethal disruption to a myriad of  $\text{Ca}^{2+}$  dependent processes including membrane trafficking and lysosome-mediated degradation. Therefore, understanding the upstream causes of de-regulated  $\text{Ca}^{2+}$  may be an essential part of understanding cell stress and degeneration.

## **1.4 LYSOSOMES, $\text{Ca}^{2+}$ AND NEURODEGENERATION**

Neurodegeneration is often accompanied by pathologies such as protein or lipid accumulation, mitochondrial dysfunction and oxidative stress. De-regulated  $\text{Ca}^{2+}$  is also now emerging as an important contributing factor.

Sustained  $\text{Ca}^{2+}$  influx through NMDAR is already linked to neurodegeneration in stroke, epilepsy, multiple sclerosis, Alzheimer's disease, Huntington disease and PD (Mehta et al., 2013). Caused by toxic levels of the excitatory neurotransmitter glutamate, this excitotoxicity is associated with mitochondrial  $\text{Ca}^{2+}$  overload. Although this may momentarily increase ATP synthesis it also increases ROS production and opens the mitochondrial PT pore leading to cell damage and cell

death. It is plausible that other changes to  $\text{Ca}^{2+}$  homeostasis may contribute to the same destructive pathway through the mitochondria. In addition, disruptive  $\text{Ca}^{2+}$  fluxes may impair proteostasis in the ER or membrane trafficking which may impact degradation or neurotransmission.  $\text{Ca}^{2+}$ -regulated ATP synthesis is also particularly important in neurons to keep up with the high energy demand of these large and electrically excitable cells (Surmeier et al., 2017a). It is conceivable that lysosomal  $\text{Ca}^{2+}$  release and its involvement in vesicular trafficking and global  $\text{Ca}^{2+}$  signalling is important in the context of neurodegeneration. Indeed, in lysosomal storage disorders such as mucopolysaccharidosis type IV, and in PD, there is accumulating evidence that  $\text{Ca}^{2+}$  and lysosomal channels are pivotal in bringing about phenotypic changes. Such changes include lipid accumulation, de-regulated autophagy, mitochondrial fragmentation, and even apoptosis. These are described in the following sections.

### **1.4.1 Mucopolysaccharidosis Type IV**

Mucopolysaccharidosis type IV (MLIV) is caused by mutations in the lysosomal  $\text{Ca}^{2+}$  channel TRPML1. It is an autosomal recessive disease and carrier frequency is relatively high (between 1:90 and 1:130) amongst Ashkenazi Jews (Bach, 2005; Bargal et al., 2001; Edelmann et al., 2002). In this population two founding mutations with origins in northern Poland and neighbouring Lithuania constitute 95% of MLIV mutant alleles, and both result in the loss of a functional protein (Edelmann et al., 2002). Diffuse neurodegeneration in MLIV is associated with psychomotor problems, ophthalmic degeneration and aberrant secretion of hydrochloric acid in the stomach (achlorhydria) (Bach, 2005). Pathogenesis likely begins before birth and symptoms are present from a very young age (Frei et al., 1998; Kohn et al., 1977). At present there is no medical treatment available. A range of therapies including physical, speech and vision are recommended as well as iron supplements to counter the effect of achlorhydria.

MLIV can be classed as a lysosomal storage disorder (LSD) and it is characterised by the accumulation of mucopolysaccharides, gangliosides and phospholipids (Bach et al., 1975, 1977; Bargal and Bach, 1997a). Before *MCOLN1* (encoding TRPML1) was identified as the causative gene this accumulation was linked to defects in membrane trafficking and not to dysfunctional lysosomal hydrolases which are responsible for many other LSDs (Bargal and Bach, 1997b; Chen et al., 1998). Since then a deeper understanding of TRPML1's role in membrane trafficking has evolved (see earlier section on TRPML1).

Perhaps particularly relevant to this neurodegenerative disorder are reports of aberrant autophagy. A growing number of studies have observed defective autophagy with associated

protein accumulation, ROS production or fragmented mitochondria in MLIV patient cells or disease models. Various mechanisms have been put forward to explain how these observations may be linked or how TRPML1 may cause them. Autophagic dysfunction was to blame for the accumulation of ubiquitinated proteins in MLIV cells (Curcio-Morelli et al., 2010a; Vergarajauregui et al., 2008). This impaired autophagy was reportedly due to 1) delayed fusion between autophagosomes and late endosomes/lysosomes and 2) sustained generation of autophagosomes. Elsewhere impaired autophagy in MLIV cells was reported to result in the accumulation of fragmented mitochondria (Jennings et al., 2006). They further demonstrated that the MLIV mitochondria did not have the usual capacity to buffer  $\text{Ca}^{2+}$  in response to  $\text{Ca}^{2+}$  signals stimulated by bradykinin. This, they showed, made MLIV cells more sensitive to  $\text{Ca}^{2+}$  - triggered apoptosis which could be inhibited by membrane-permeable BAPTA. Coblentz and colleagues also observed fragmented mitochondria in MLIV cells (Coblentz et al., 2014). However, in an alternative approach, Coblentz et al considered the iron-permeability of TRPML1 (Dong et al., 2008). They proposed that with no functional TRPML1,  $\text{Fe}^{2+}$  accumulates in the lysosomes. This re-distribution of iron then leads to increased ROS production which in turn causes mitochondrial fragmentation. Regulation of autophagy by TRPML1 has also been attributed to its ability to sense ROS (Zhang et al., 2016). Defective CMA has also been reported in MLIV cells, which may be due to impaired interactions between TRPML1 and chaperones Hsc70 and Hsc40 (Venugopal et al., 2009).

As the exact mechanisms linking TRPML1 to MLIV phenotypes are up for debate, the channel remains a focus of investigation. Promisingly, the activation of mutant TRPML1 (F408 $\Delta$ ) by synthetic agonist MK6-83 corrected the diffuse accumulation of lipids in MLIV fibroblasts (Chen et al., 2014). However, this highlights two issues. First and profoundly is that whilst the F408 $\Delta$  MLIV mutation still allows the formation of a functional lysosome-localised channel, many MLIV mutations do not (Chen et al., 2014; Edelmann et al., 2002). Therefore, activation of TRPML1 is not a viable universal therapy for MLIV patients. Secondly, although  $\text{Ca}^{2+}$  release through TRPML1 is understood to regulate membrane fusion there has been no investigation into whether activation of this  $\text{Ca}^{2+}$  channel can cause global  $\text{Ca}^{2+}$  signals in the same way that TPCs can and what the consequences may be (Brailoiu et al., 2009; Calcraft et al., 2009). This may be particularly important given the context of cells already under stress with impaired autophagy, damaged mitochondria, and an increased sensitivity to apoptosis.

Another neurodegenerative disease that may be associated with downregulated TRPML1 activity is Niemann-Pick Type C disease (NPC). As for MLIV, NPC is an autosomal recessive LSD

and pathogenesis may start before birth (Colin et al., 2015). It is caused by mutations in *NPC1* or *NPC2* which are thought to work together to extrude cholesterol from the endolysosomes (Infante et al., 2008; Kwon et al., 2009; Rosenbaum and Maxfield, 2011; Sleat et al., 2004; Storch and Xu, 2009; Vanier, 2010). Not only does cholesterol accumulate in NPC, but sphingomyelin, sphingosine and glycosphingolipids too (Davidson et al., 2009; Lloyd-Evans et al., 2008; Patterson et al., 2007; Vrucyte et al., 2004). Neurodegeneration in NPC is most notable in cerebella Purkinje neurons and is linked to difficulties with muscle movement, speech and dementia (Vanier, 2010).

Autophagy has been a focus of many NPC studies. Increased levels of the autophagosome marker, LC3, has been repeatedly reported in *NPC1*<sup>-/-</sup> mice, NPC human fibroblasts, iPSCs and other NPC models (Davidson et al., 2009; Ishibashi et al., 2009; Liao et al., 2007; Maetzel et al., 2014; Ordonez et al., 2012; Pacheco et al., 2007; Sarkar et al., 2013). Reduced lysosome hydrolase activity has also been reported (Elrick et al., 2012; Liao et al., 2007) and there are many more studies that demonstrate fusion and trafficking defects in NPC (Choudhury et al., 2004; Ganley and Pfeffer, 2006; Ko et al., 2001; Sobo et al., 2007; Tamari et al., 2013; Walter et al., 2003, 2009).

Mitochondrial damage also features in NPC neurons and fibroblasts, and may be a consequence of impaired autophagy (Ordonez et al., 2012). Interestingly, Ordonez and colleagues found that whilst protein levels of apoptosis inducing factor (AIF) were increased in NPC model neurons this was not mirrored in the NPC fibroblasts. An earlier study also identified aberrant mitochondria in NPC (Yu et al., 2005): Mitochondrial membrane cholesterol was elevated and membrane potential and ATP synthesis was reduced. Furthermore, this was linked to shortened neurites which could be lengthened by the addition of ATP.

Regarding lysosomal Ca<sup>2+</sup> and NPC, it has been reported that Ca<sup>2+</sup> release evoked by GPN or bafilomycin A is reduced in NPC fibroblasts, lymphocytes and Purkinje neurons (Lee et al., 2010a; Lloyd-Evans et al., 2008). In addition, Lloyd-Evans and colleagues demonstrated that NAADP-induced Ca<sup>2+</sup> signals were inhibited in NPC fibroblasts. Reduced lysosomal Ca<sup>2+</sup> in NPC fibroblasts and Purkinje Neurons has since been confirmed (Höglinger et al., 2015; Lee et al., 2014; Visentin et al., 2013; Xu et al., 2012). Reduced lysosomal Ca<sup>2+</sup> release has also been reported in NPC Natural Killer cells, Chinese Hamster Ovary (CHO) cells and mouse macrophages (Shen et al., 2012; Speak et al., 2014). However, Shen et al found that lysosomal Ca<sup>2+</sup> release evoked by GPN or ammonium chloride (NH<sub>4</sub>Cl) was no different in cells lacking NPC1 (*NPC1*<sup>-/-</sup>) compared to

controls (Shen et al., 2012). What they did find though was that  $\text{Ca}^{2+}$  release in response to the TRPML1 agonist, ML-SA1, was reduced. Shen and colleagues also showed that the membrane trafficking defects in NPC1<sup>-/-</sup> cells could be reversed by ML-SA1. The same research group has since linked TRPML1 to NPC as a regulator of autophagy (Wang et al., 2015b).

Given that the activation of TRPML1 may hold therapeutic potential for MLIV and NPC, as well as other diseases of the nervous system, it is important to understand the consequences fully (Bae et al., 2014; Zou et al., 2015). This includes finding out whether TRPML1 activation can generate global  $\text{Ca}^{2+}$  signals which may have deleterious effects in neurons that are already compromised by disease.

### **1.4.2 Parkinson's Disease**

Upon some grounds Parkinson's disease (PD) appears dissimilar to MLIV and NPC. First, PD is a disease associated with old age whereas MLIV and NPC appear in children and young adults. In predominantly Caucasian populations the prevalence of PD increases from ~1/1000 at 50-59 years of age, to 30/1000 at 80+ (Pringsheim et al., 2014). Secondly, MLIV and NPC are caused by inherited mutations in one or two select genes. In PD however, only the minority of cases are caused this way, and the rest are seemingly sporadic (Gandhi and Wood, 2010). However, all three disorders have been connected with defective autophagy and dysfunctional mitochondria. Furthermore, mutations in lysosomal proteins have been linked to PD, and disturbed  $\text{Ca}^{2+}$  homeostasis has emerged as part of PD pathology. Moreover, meta-analysis of expression data and genome-wide association studies (GWAS) has highlighted the relevance of the  $\text{Ca}^{2+}$  signalling network to PD (Edwards et al., 2011).

The motor symptoms of PD such as rigidity, bradykinesia, ataxia and tremor are associated with severe neurodegeneration of the substantia nigra pars compacta (SNc) and the consequential depletion of dopamine (DA). As such, neurodegeneration of the SNc has been the focus of much research. However, PD pathology is not limited to the SNc nor even the brain (Braak et al., 2003; Sampson et al., 2016). Critically there is no cure for PD. Treatment focuses on replenishing DA or mimicking its action, which can only stave off the motor symptoms for so long (Brichta et al., 2013). Non-motor symptoms including depression and insomnia are treated separately, as and when they manifest.



### 1.4.2.1 Genetics and PD

The route into describing PD pathogenesis is often guided by the genetic mutations that have been linked to familial PD. This brings some order to describing numerous discoveries which are often complex and interrelated. It should be noted that with the rapid accumulation of PD-linked genes it is no longer possible to classify them all into one simple system (Kalinderi et al., 2016; Marras et al., 2012). Some of the PD-linked genetic mutations have been associated with monogenic PD repeatedly and are widely accepted as causative. However, some are found in unaffected family members too. Many of the most recently identified genes have only been reported in a single family and are awaiting further reports for confirmation. In addition, some mutations are associated with parkinsonism that does not fit a classical PD diagnosis (Edvardson et al., 2012; Lesage et al., 2016; Quadri et al., 2013; Ramirez et al., 2006). Another issue complicating PD diagnosis is that Lewy deposits, which are held as the canonical PD hallmark, can only be viewed at autopsy (Spillantini et al., 1997). Furthermore, there are exceptions where Lewy bodies are not present in people who have been diagnosed with familial PD (Poulopoulos et al., 2012). Of particular relevance here mutations in the lysosomal genes *GBA1* and *ATP13A2* have been linked to PD. In addition, mutant *LRRK2* in PD has been linked to lysosome and  $\text{Ca}^{2+}$  de-regulation.

#### 1.4.2.1.1 *GBA1*

*GBA1* encodes the lysosomal enzyme glucocerebrosidase (GCSase) which catabolises glucocerebroside (GlcCer). Mutations in *GBA1* can cause Gaucher's disease (GD) which is the most common LSD (Stern, 2014). Like *MLIV* and *NPC*, GD is inherited in an autosomal recessive manner, presents early on in life and is a disease of neurodegeneration. Importantly, *GBA1* mutations also increase the risk of developing PD (Nichols et al., 2009; Sidransky et al., 2009). *GBA1*'s link to PD is further strengthened by the appearance of its locus in genome-wide association studies (GWAS) (Nalls et al., 2014).

In GD improper folding of GCSase is connected to its retention in the ER, degradation by the proteasome and impaired trafficking to the lysosomes (Ron and Horowitz, 2005). Interestingly, it has been reported that not only are GCSase levels reduced in the SNc of *GBA1*-PD patients but in sporadic PD patients too (Gegg et al., 2012). In the same study levels of  $\text{Ca}^{2+}$ -sensitive BiP, a protein of the unfolded protein response (UPR), were found to be increased in the PD putamen. Elsewhere, in the anterior cingulate cortex of late stage PD, a reduction in GCSase is associated with decreased levels of cathepsins and CMA protein LAMP2 (Murphy et al., 2014). In addition, this was accompanied by increased levels of  $\alpha$ -synuclein ( $\alpha$ -syn), a major constituent of Lewy deposits (Spillantini et al., 1997). Accumulation of  $\alpha$ -syn has also been reported in iPSC neurons

from people with *GBA1*-PD, accompanied by GlcCer build-up, disturbed autophagic flux and heightened sensitivity to mitochondrial complex 1 inhibition (Schöndorf et al., 2014).

An association between GCSase and  $\text{Ca}^{2+}$  signalling has also been established. In a neuronal model of GCSase inhibition,  $\text{Ca}^{2+}$  release induced by glutamate or caffeine was augmented compared to controls (Korkotian et al., 1999). Furthermore, this model was more sensitive to glutamate-induced cell death. Later, enhanced  $\text{Ca}^{2+}$  release induced by the RyR agonist, palmitoyl CoA, was reported in rat brain microsomes that were treated with exogenous GlcCer, and in microsomes derived from GD patient brain tissue (Lloyd-Evans et al., 2003). In the *GBA1*-PD neurons investigated by Schöndorf and colleagues RyR dysfunction was once again associated with increased GlcCer levels; both basal  $\text{Ca}^{2+}$  and caffeine-stimulated  $\text{Ca}^{2+}$  release through RyRs were raised (Schöndorf et al., 2014). More recently it was reported that fibroblasts from *GBA1*-PD patients exhibit enhanced ER  $\text{Ca}^{2+}$  content and cADPR-evoked  $\text{Ca}^{2+}$  signals, again supporting a *GBA1*-RyR link (Kilpatrick et al., 2016b). What is more, augmented ER  $\text{Ca}^{2+}$  appeared to be balanced by reduced lysosomal  $\text{Ca}^{2+}$  content, and was associated with altered lysosome morphology. Taken together, these reports form a case for the involvement of lysosomes and disturbed  $\text{Ca}^{2+}$  in PD pathogenesis.

#### 1.4.2.1.2 *ATP13A2*

Another gene that supports a role for lysosomes and  $\text{Ca}^{2+}$  in PD is *ATP13A2*. Mutations in this lysosomal P-type ATPase can cause PD or hereditary parkinsonism known as Kufor-Rakeb syndrome (Djarmati et al., 2009; Fonzo et al., 2007; Ramirez et al., 2006). Similarly to *GBA1*, pathogenic mutations result in the synthesis of truncated proteins that are retained in the ER and degraded by the proteasome (Ramirez et al., 2006). This has been supported in more recent work which also demonstrates that expression of  $\text{Ca}^{2+}$ -sensitive BiP and other UPR proteins are increased in Kufor-Rakeb patient cells (Park et al., 2011). This upregulation of  $\text{Ca}^{2+}$ -sensitive proteins may disturb  $\text{Ca}^{2+}$  signalling. In yeast and *Caenorhabditis elegans*, *ATP13A2* has been shown to be protective in the presence of toxic  $\alpha$ -syn (Gitler et al., 2009).

Reduced expression of *ATP13A2* in various models has been linked to mitochondrial dysfunction and increased ROS production, which was attributed to impaired autophagic flux (Gusdon et al., 2012). Indeed, dysfunctional *ATP13A2* has been associated with increased numbers of LC3-positive vesicles, impaired lysosome-mediated degradation, accumulation of  $\alpha$ -syn and decreased cell viability (Usenovic et al., 2012). Elsewhere, in fibroblasts from *ATP13A2*-PD patients the levels of multiple lysosome markers are raised, lysosomal pH is increased and cathepsin activity is reduced (Dehay et al., 2012). Recent work proposes that lysosome and

autophagy defects caused by the loss of a functional *ATP13A2* are the result of decreased Synaptotagmin 11 expression which is regulated in part by mammalian target of rapamycin (mTOR) and transcription factor EB (TFEB) (Bento et al., 2016). Such trafficking defects may also result from disturbed  $\text{Ca}^{2+}$  fluxes, which appear to be important in inter-organellar fusion and fission (Pryor et al., 2000). Whilst there is not yet a plethora of evidence that pathogenic *ATP13A2* affects cellular  $\text{Ca}^{2+}$ , overexpression and silencing of *ATP13A2* does cause a drop in basal  $\text{Ca}^{2+}$  in neurons (Ramonet et al., 2012).

#### 1.4.2.1.3 LRRK2

A third PD-linked gene that has been associated with lysosomal function is *LRRK2*. *LRRK2* mutations that cause autosomal dominant PD are positioned within the kinase and GTPase domains of the protein (Martin et al., 2014a). The G2019S mutation increases kinase activity and is the most common PD-associated mutation found in ~5% of familial PD cases and ~1% of sporadic (Bardien et al., 2011; Healy et al., 2008). Unlike some other PD-related genes *LRRK2* function cannot be easily pigeon-holed. In order to delineate its role in PD numerous studies have sought to identify *LRRK2* binding partners, and works offering digestible visualisations of this data have been published (Manzoni et al., 2015; Porras et al., 2015).

Repeatedly, *LRRK2* is implicated in vesicular trafficking. A host of *LRRK2* interactors are associated with synaptic vesicle endocytosis (Gallop et al., 2006; Lee et al., 2005; Matta et al., 2012; Piccoli et al., 2011) and *LRRK2* has been shown to bind with and phosphorylate Rab GTPases to modulate its function (Dodson et al., 2012; Gómez-Suaga et al., 2014; MacLeod et al., 2013; Shin et al., 2008; Steger et al., 2016). For example, the slowing of synaptic vesicle endocytosis caused by overexpression of *LRRK2* wildtype (WT) or mutant *LRRK2* could be reversed by overexpression of Rab5b (Shin et al., 2008). Neurite shortening and DA neuron survival in *LRRK2* G2019S cells could also be improved by overexpressing Rab7 or retromer component Rab7L1 (MacLeod et al., 2013). In addition, disturbed retrograde trafficking and lysosome swelling in *LRRK2* G2019S neurons could be reversed by overexpressed Rab7L1 or VPS35. In contrast to the data published by Macleod and colleagues, overexpressed Rab7L1 exacerbated Golgi clustering in cells transfected with *LRRK2* G2019S due to upregulated autophagy (Beilina et al., 2014). Like Rab7L1, VPS35 is a retromer component, but VPS35 is also associated with monogenic PD (Kalinderi et al., 2016). Besides retrograde transport VPS35 is involved in CMA and the formation of mitochondria-derived vesicles (MDVs) which transport cargo to lysosomes for degradation (Sugiura et al., 2014). In models with reduced or mutant VPS35 expression observations of impaired autophagy (Zavodszky et al., 2014), mitochondrial

fragmentation (Wang et al., 2016), disrupted recycling of neurotransmitter receptors (Munsie et al., 2015), accumulation of  $\alpha$ -syn, reduced locomotor scores and SNc neuronal loss (Tang et al., 2015) have all been reported.

Research in flies has further added to the LRRK2-Rab link: It was demonstrated that overexpression of Rab7 or LRRK2 G2019S promotes perinuclear lysosome clustering (Dodson et al., 2012). In human patient fibroblasts LRRK2 G2019S has also been associated with disturbed lysosome morphology that could be improved by inhibiting Rab7 (Hockey et al., 2015). Interestingly, this phenotype was associated with augmented global  $\text{Ca}^{2+}$  signals in response to NAADP. Furthermore, knockdown of TPC2 or treatment of the fibroblasts with membrane-permeable BAPTA also appeared to improve lysosome morphology.

The link between LRRK2 and TPCs has been reported elsewhere in relation to impaired autophagy. In HEK293T cells both LRRK2 WT and LRRK2 G2019S increase the number of LC3-positive vesicles (Gómez-Suaga et al., 2012). Notably, this LRRK2-induced autophagy was independent of mTOR and instead worked through calcium/calmodulin-dependent protein kinase kinase (CaMKK) signalling. Moreover, this disturbed autophagy could be blocked by overexpressing mutant TPC2, and recapitulated by treating cells with NAADP. Gómez-Suaga et al. also found that LRRK2 upregulated  $\text{Ca}^{2+}$ -dependent protein synthesis and that inhibition of mTOR alleviated the autophagy disturbance. Importantly, LRRK2 activity sensitized cells to death when the proteasome was blocked, which could be significant in the context of proteasome block by  $\alpha$ -syn (Stefanis et al., 2001; see SNCA section). Contrary to this study, inhibition of mTOR has been shown to exacerbate autophagy defects in LRRK2 G2019S cells and inhibition of LRRK2 kinase activity has been shown to increase protein synthesis and autophagic markers (Manzoni et al., 2013; Plowey et al., 2008). Extracellular-signal regulated kinase (ERK) has also been proposed as part of the LRRK2-autophagy pathway (Plowey et al., 2008). In addition, LRRK2 has been implicated in the turnover of the TGN via autophagy (Beilina et al., 2014) and degradation of pathogenic LRRK2 via CMA is impaired (Orenstein et al., 2013). The latter causes accumulation of  $\alpha$ -syn around the lysosomes (Orenstein et al., 2013).

LRRK2,  $\text{Ca}^{2+}$  and mitochondria have also been functionally linked (Cherra et al., 2013): In neurons expressing LRRK2 G2019S mitochondrial membrane potential was reduced, as was  $\text{Ca}^{2+}$  buffering capacity in response to depolarisation. Cellular mitochondrial content was reduced and autophagy was increased. Remarkably,  $\text{Ca}^{2+}$  chelation by cell-permeable BAPTA reversed the defects of mitochondrial membrane potential, mitochondrial content, autophagy, and

restored dendrite length in the LRRK2 G2019S neurons. Chelation of extracellular  $\text{Ca}^{2+}$  or block of L-type  $\text{Ca}^{2+}$  channels also restored mitochondrial content and neurite length.

Exactly how LRRK2 interacts with its effectors is not always clear. In some studies its kinase activity has been implicated (Gómez-Suaga et al., 2012; Matta et al., 2012). As the LRRK2 G2019S mutation increases its kinase activity, this could be a veritable mode of LRRK2 pathogenesis (Greggio and Cookson, 2009). LRRK2 kinase substrates include ezrin/radixin/moesin (ERM) proteins (Jaleel et al., 2007; Parisiadou et al., 2009), extracellular signal-regulated kinase (ERK) (Reinhardt et al., 2013), translation initiation factor binding partner (4E-BP) (Imai et al., 2008), Futsch (Lee et al., 2010b) and ribosomal protein 15 (Martin et al., 2014b) thereby implicating LRRK2 in the regulation of cytoskeleton dynamics, transcription and translation. However, other pathogenic *LRRK2* mutations do not alter kinase activity, therefore there might be an alternative pathogenic output, possibly from its ROC GTPase domain. As LRRK2 autophosphorylates at many sites in its ROC domain kinase activity may actually serve to regulate LRRK2 GTPase activity (Taymans, 2012). Incidentally, pathogenic mutations in the ROC domain modulate interactions between LRRK2 and DVL proteins of the Wnt signalling pathway (Sancho et al., 2009). DVL proteins lie upstream of all Wnt signalling pathways including that which leads to increases in intracellular  $\text{Ca}^{2+}$  (Wallingford and Habas, 2005).

As discussed, the PD-related genes *GBA1* and *ATP13A2* build a case for the involvement of lysosomes and  $\text{Ca}^{2+}$  in PD. This is supported by evidence that deregulated  $\text{Ca}^{2+}$  and lysosomal TPC  $\text{Ca}^{2+}$  channels are implicated in LRRK2-PD. In addition, the influence of LRRK2 appears to be widespread in processes such as autophagy, autophagy of mitochondria (mitophagy), endocytosis and retrograde transport, which all converge on the lysosome. The majority of other PD-related genes are also associated with such lysosome-centric pathways. Furthermore, *SNCA*, *PINK1*, *PRKN* and *PARK7* all have established links to familial PD and are associated with  $\text{Ca}^{2+}$  dysregulation (Kalinderi et al., 2016).

#### 1.4.2.1.4 SNCA

*SNCA* encodes the protein  $\alpha$ -synuclein ( $\alpha$ -syn) which is a major component of Lewy deposits that form in the neuronal soma (Lewy bodies) or neurites (Lewy neurites) (Spillantini et al., 1997). In its native form  $\alpha$ -syn has a role in neurotransmission (Bendor et al., 2013; Lashuel et al., 2013). It has been shown to act as a chaperone for SNARE complexes on pre-synaptic vesicles (Burré et al., 2010) and interacts with Rab3a, which regulates its cycling between membrane-bound and -unbound states (Chen et al., 2013). Importantly, mutations or multiplications of *SNCA* can cause

dominantly inherited PD that is clinically similar to sporadic PD (Chartier-Harlin et al., 2004; Krüger et al., 1998; Polymeropoulos et al., 1997; Zarranz et al., 2004). Furthermore,  $\alpha$ -syn-containing Lewy deposits are present in sporadic PD brains.

The damaging consequences of accumulating  $\alpha$ -syn are plenty. Overexpressed WT or mutant *SNCA* colocalises with mitochondrial membranes and has been associated with reduced mitochondrial complex 1 activity, increased mitophagy, and the release of cytochrome C and nitric oxide (Chinta et al., 2010; Parihar et al., 2008). Another prominent issue with  $\alpha$ -syn is the difficulty of its degradation, which may be exemplified by the presence of ubiquitin in Lewy deposits (Spillantini et al., 1998). Some of this ubiquitin is likely attached to  $\alpha$ -syn, which should be degraded by the proteasome, CMA or autophagy (Cuervo et al., 2004; Rott et al., 2011). However, Cuervo and colleagues reported that the uptake of mutant  $\alpha$ -syn into lysosomes is inhibited, and crucially, this may block the degradation of other substrates by CMA. Mutant  $\alpha$ -syn also appears to block the proteasome, induce an increase in autophagic structures, and disrupt lysosome-mediated degradation (Stefanis et al., 2001). Whether such inhibition of the degradative pathways precedes  $\alpha$ -syn aggregation or is a consequence is unclear. What is known is that mutations in  $\alpha$ -syn, as well as oxidative stress, phosphorylation, nitrative stress, iron, ubiquitination, cross-linking and truncation, are all thought to promote its aggregation (Oueslati et al., 2010).

So what is the problem with  $\alpha$ -syn aggregation? As an aggregate  $\alpha$ -syn forms fibrils with  $\beta$ -strand secondary structure (Comellas et al., 2012; Giasson et al., 2001). Before forming  $\beta$ -strand fibrils however, it can form smaller ring-shaped oligomers that insert into membranes (Danzer et al., 2007). Such  $\alpha$ -syn pores may form in synaptic vesicle membranes and release DA into the cytosol (Mosharov et al., 2006). Free DA is a potential problem as it contributes to the production of ROS and reactive quinones (Bisaglia et al., 2014).

Besides permitting DA into the cytosol,  $\alpha$ -syn pores likely open the membranes to unusual  $\text{Ca}^{2+}$  fluxes. Indeed, ring-oligomers have been linked to raised cytosolic  $\text{Ca}^{2+}$  concentrations, and cell death (Danzer et al., 2007). A year earlier it was reported that cells stably expressing mutant A53T  $\alpha$ -syn also exhibited higher basal  $\text{Ca}^{2+}$  levels, and that depolarisation-induced  $\text{Ca}^{2+}$  signals were larger (Furukawa et al., 2006). The latter has since been reported for cells overexpressing  $\alpha$ -syn WT, as well as depleted ER  $\text{Ca}^{2+}$  and inhibited SOCE (Hettiarachchi et al., 2009). More recently both monomeric and oligomeric  $\alpha$ -syn has been reported to induce  $\text{Ca}^{2+}$  influx in neurons, but only the oligomers were associated with apoptosis (Angelova et al., 2016).

#### 1.4.2.1.5 PINK1, PRKN and PARK7

The presence of mitochondrial dysfunction in PD is well-recognised. This is in part due to the mutations in *PINK1*, *PRKN* and *PARK7* that can cause early-onset PD with autosomal recessive inheritance (Kalinderi et al., 2016; Kitada et al., 1998; Pickrell and Youle, 2015; Valente et al., 2004). These three genes may be considered as guardians of the mitochondria with their roles in  $\text{Ca}^{2+}$  dynamics also coming to light.

PINK1 is a ubiquitin kinase, Parkin (encoded by *PRKN*) is a ubiquitin ligase, and together they regulate the degradation of compromised mitochondria via mitophagy (Pickrell and Youle, 2015). PINK1 deficiency has also been associated with de-regulated mitochondrial  $\text{Ca}^{2+}$ , ATP synthesis and permeability transition (PT) (Gandhi et al., 2009; Gautier et al., 2012; Heeman et al., 2011). For example, in response to rising cytosolic  $\text{Ca}^{2+}$  induced by extracellular stimuli, *PINK1*<sup>-/-</sup> cells are sensitised to PT pore opening (Gandhi et al., 2009). Therefore, dysfunctional PINK1 may pre-dispose neurons to  $\text{Ca}^{2+}$ -induced cell death. In another study *PINK1*-deficient cells exhibited reduced mitochondrial  $\text{Ca}^{2+}$  uptake in response to physiological stimuli, which was associated with impaired ATP synthesis (Heeman et al., 2011). Parkin has also been associated with  $\text{Ca}^{2+}$  as it promotes ER-mitochondria  $\text{Ca}^{2+}$  coupling, and ATP synthesis in response to histamine (Cali et al., 2013).

DJ-1 (encoded by *PARK7*) has been implicated in maintaining a healthy mitochondria population as a protector against oxidative stress in various guises. It may act as a sponge for ROS as it becomes oxidised on its cysteine residues (Blackinton et al., 2009), upregulate synthesis of the antioxidant glutathione (Zhou and Freed, 2005), down-regulate DA synthesis (Jeong et al., 2006), sequester death protein Daxx in the nucleus (Junn et al., 2009) and repress production of nitric oxide during neuroinflammation (Kahle et al., 2009). In *DJ-1*<sup>-/-</sup> MEFs damaged mitochondria and disrupted autophagy has been reported (Krebiehl et al., 2010; Thomas et al., 2011). DJ-1 is also thought to regulate the expression of uncoupling proteins (*UCP*) which modestly depolarise the mitochondrial membrane potential to slow down ATP synthesis and reduce associated ROS production (Guzman et al., 2010). These UCPs may protect against  $\text{Ca}^{2+}$ -induced mitochondrial oxidation and consequential cell death in the SNc (see Age and PD section).

Other PD-related genes that are less well-established in the causality of PD are listed overleaf and brief descriptions are appended (Table 1.3; Appendix A). As for the genes previously discussed, many of them are associated with cellular processes that converge upon the

lysosomes such as lysosome-mediated degradation and vesicular trafficking. Safe-guarding of mitochondrial health, combatting oxidative stress and links to Ca<sup>2+</sup> have also been reported.

**Table 1.3. Additional genes implicated in PD or parkinsonism**

<b>Gene</b>	<b>Product Function</b>	<b>Reference(s) regarding a PD/parkinsonism association</b>
<i>PLA2G6</i>	Ca <sup>2+</sup> Oxidative stress Mitochondrial health	(Paisan-Ruiz et al., 2009)
<i>SYNJ1</i>	Ca <sup>2+</sup> Vesicular trafficking	(Krebs et al., 2013; Quadri et al., 2013)
<i>HTRA2</i>	Degradation Mitochondria health	(Strauss et al., 2005)
<i>FBX07</i>	Degradation Mitochondrial health	(Fonzo et al., 2009)
<i>UCHL1</i>	Degradation	(Leroy et al., 1998)
<i>VPS13C</i>	Mitochondrial health	(Lesage et al., 2016)
<i>CHCHD2</i>	Oxidative stress Mitochondrial health	(Funayama et al., 2015)
<i>EIF4G1</i>	Translation	(Chartier-Harlin et al., 2011)
<i>DNAJC13</i>	Vesicular trafficking	(Vilariño-Güell et al., 2014)
<i>DNAJC6</i>	Vesicular trafficking	(Edvardson et al., 2012)
<i>TMEM230</i>	Vesicular trafficking	(Deng et al., 2016)

Whilst this genetic information is no doubt useful for deciphering the aetiology of familial PD a general hope is that these genes are stepping stones to understanding the pathogenesis of sporadic PD. However, there remain unanswered questions that may be relevant to both familial and sporadic PD. First, not all mutations in the aforementioned genes are fully penetrant. The *LRK2* G2019S mutation is one such example (Goldwurm et al., 2011). Therefore, what are the additional mechanisms involved in PD pathogenesis? Perhaps environmental factors contribute. Second, PD is a disease associated with ageing, so what are the underlying age-dependent processes that are involved? And third, why are the neurons of the SNc particularly vulnerable to degeneration? As research begins to answer some of these questions the lysosomes and Ca<sup>2+</sup> once again make an appearance under the spotlight.

#### **1.4.2.2 Environmental Factors and PD**

Exposure to pesticides, solvents, coolants, metals or air pollutants has been linked to an increased risk of developing PD (Goldman, 2014). Whilst such risks are often disputed there are some biochemical insights about these compounds which may be relevant to PD pathogenesis.



The link between environmental toxins and PD was strengthened in the 1970s when an opioid contaminant caused acute parkinsonism in young adults (Ballard et al., 1985; Davis et al., 1979a). The active contaminant derivative, MPP<sup>+</sup>, is thought to elicit its parkinsonian effect by inhibiting mitochondrial complex I (Goldman, 2014). It is also similar in structure to the pesticide Paraquat which has been associated with increased PD risk. Other pesticides have been shown to promote ROS production (Cicchetti et al., 2005; McCarthy et al., 2004; McCormack et al., 2002), inhibit mitochondrial complex I (Betarbet et al., 2000), inhibit ubiquitin pathways (Chou et al., 2008) and cause selective loss of SNc neurons (Betarbet et al., 2000; McCormack et al., 2002). Furthermore, pesticide exposure has been associated with altered autophagic flux which may serve as a protective or destructive mechanism (González-Polo et al., 2007; Wu et al., 2015a).

In addition to pesticide exposure, iron is another environmental toxin that has been associated with PD. Higher iron levels in PD patients have been reported, which may catalyse the production of damaging free radicals or quinones from DA (Dexter et al., 1991; Paris et al., 2005; Ward et al., 2014). Head injury may also be associated with an increased risk of developing PD (Jafari et al., 2013; Marras et al., 2014). This might compromise the blood brain barrier and expose the brain to more toxins, or the associated neuroinflammation may stress neurons. Viral infections have also been proposed as a possible contributing factor to parkinsonism and PD (Jang et al., 2009; Tsai et al., 2016; Wu et al., 2015b). Perhaps relevant to PD is the presence of anti-viral protein MxA in Lewy bodies (Haller et al., 2015; Wakabayashi et al., 2013). MxA has been shown to inhibit early stages of Influenza A infection by retaining its genome in perinuclear vesicles, some of them Rab7-positive (Xiao et al., 2013). For some viruses, the endolysosomal system is a favoured conduit to reach the nucleus (Grove and Marsh, 2011). For example, influenza has adapted so that it is released into the cytosol only when it encounters the low pH of late endosomes (Lakadamyali et al., 2004). Ebola virus activation also appears to be pH-dependent but this is due to its requirement of cathepsins which are active in the acidic lysosome (Chandran et al., 2005; Kaletsky et al., 2007). Recently molecular inhibition of TPCs was shown to inhibit Ebola infectivity (Sakurai et al., 2015). Supporting a role for TPC-mediated Ca<sup>2+</sup> release in Ebola infection, infectivity was also blocked by compounds which inhibited TPC currents and NAADP-induced Ca<sup>2+</sup> signals.

#### **1.4.2.3 Age and PD**

Assaults from toxins, head injuries and viruses may aggravate cellular stress. Over a lifetime events such as these add up and may cause a fair amount of wear and tear on the brain. With or without these events ageing is associated with a decline or remodelling of numerous

biological processes. As a consequence it is likely that with age cells are more sensitive to additional stressors and less able to survive them. Mutated DNA, impaired mitochondrial function and impaired proteostasis are generally accepted as ageing phenomena that affect the whole body (López-Otín et al., 2013). Examples of this in the substantia nigra (SN) include increased deletions of mitochondrial DNA (mtDNA) or reduced levels of cytochrome c oxidase (COX) (Bender et al., 2006; Kraytsberg et al., 2006). In the rodent SN, proteasomal activity declines with age, and in rhesus monkeys, deposits of ubiquitinated proteins increase with age (Kanaan et al., 2007; Zeng et al., 2005). Although interesting these reports do not consistently study other brain structures so it is not known whether these ageing characteristics are highly specific to the SNc. Indeed, the SNc does share characteristics with other brain regions but it is believed that its particular set of specialisms places it on the precipice of neuronal death in PD (Reeve et al., 2014). First, the SNc neurons are dopaminergic. When broken down DA can be converted to ROS or other harmful free radicals (Bisaglia et al., 2014; Paris et al., 2005; Ward et al., 2014). Consequent cumulative damage to lipids, proteins and nucleic acids may whorl the descent to cell death. In addition, expression of the dopamine transporter (DAT), which is important for uptake of free DA into vesicles, decreases with age (Ma et al., 1999). Increased iron levels in the SNc with age have been reported which may exacerbate oxidative stress (Bilgic et al., 2012; Daugherty and Raz, 2013). Both iron and DA can bind to, and accumulate with, neuromelanin - the dark pigment that affords the substantia nigra its name. As with other aggregates or deposits it is unclear whether these neuromelanin complexes are protective by sequestering harmful species, are dangerous hubs of toxicity, or both depending on size and content (Fedorow et al., 2006; Zecca et al., 2002).

The SNc is also specialised in terms of its  $\text{Ca}^{2+}$  signalling network. Intriguingly, although the splice variant SERCA2b is widespread in the brain, it is at low levels in the SN (Baba-Aissa et al., 1996). In addition, the more vulnerable ventral section of SNc has lower levels of  $\text{Ca}^{2+}$  buffer calbindin-D28K (Foehring et al., 2009). These differences may have substantial consequences in SNc neurons that exhibit changes in  $\text{Ca}^{2+}$  handling as they age.

The SNc is an autonomous pacemaker generating action potentials at a frequency of 2-10 Hz (Surmeier et al., 2017b). In adult neurons this activity is accompanied by intracellular  $\text{Ca}^{2+}$  oscillations mediated by L-type VOCCs Cav1.2 and Cav1.3. The consistent influx of  $\text{Ca}^{2+}$  through these channels may be energetically expensive for the neurons as they require more ATP to pump  $\text{Ca}^{2+}$  back out of the cytosol via P-type ATPases. Furthermore, the increases in intracellular  $\text{Ca}^{2+}$  may overload the mitochondria, disrupt the mitochondrial membrane potential, open the PT pore and lead to cell death. The many other  $\text{Ca}^{2+}$ -dependent cellular processes may also be

especially vulnerable in this environment. Cav1.3 is of particular interest because its mRNA levels are greater than that of Cav1.2 in the SNc (Chan et al., 2007). In addition, Cav1.3 is open at relatively polarising membrane potentials and therefore never fully closes (Surmeier et al., 2017a). Compounding this issue is the fact that the longer C-terminal Cav1.3 splice variant is less sensitive to Ca<sup>2+</sup>-dependent inactivation, whilst the shorter variant is active at even more negative potentials (Singh et al., 2008). Intriguingly though, these L-type Ca<sup>2+</sup> channels are not absolutely necessary for SNc pacemaking, which in juvenile neurons is driven by VONC, and hyperpolarisation and cyclic nucleotide gated cation (HCN) channels (Chan et al., 2007; Guzman et al., 2010). Chan et al “rejuvenated” mouse neurons with isradipine – a dihydropyridine (DHP) drug that inhibits L-type Ca<sup>2+</sup> channels. This treatment induced a switch back to dependence on VONC and HCN channels for pacemaking activity, and reduced mitochondrial oxidative stress in DJ-1<sup>-/-</sup> neurons (Chan et al., 2007; Guzman et al., 2010). This could be a potentially viable therapeutic approach to easing stress on the SNc. In fact there is some evidence that DHPs reduce the risk of developing PD (Pasternak et al., 2012). However, the Ca<sup>2+</sup> influx permitted by Cav1 channels may be required to promote ATP synthesis and keep up with energy expenditure (Denton, 2009; Glancy and Balaban, 2012). Ca<sup>2+</sup> transients are also linked to the expression of tyrosine hydroxylase – the enzyme required for DA synthesis (Aumann and Horne, 2012). Therefore, blocking these channels could cause problems of its own. Indeed, in the MitoPark mouse model of PD Cav1.3 expression in the SN increases with age and this increase is more pronounced compared to the SN of control mice (Branch et al., 2016). Therefore, upregulated Cav1.3 expression may be intended as a compensatory mechanism. In humans Cav1.2 and Cav1.3 are found in a smaller percentage of neurons in the PD SNc compared to controls but the intensity of Cav1.2 and Cav1.3 staining is greater suggesting that overall expression is unchanged (Hurley et al., 2013).

Importantly, the SNc is not alone in being an autonomous pacemaker or having Cav1.3 currents. For example, the locus coeruleus (LC) is also an autonomous pacemaker with Cav1.3-mediated Ca<sup>2+</sup> oscillations, and LC neurons are also lost in PD (Sulzer and Surmeier, 2013). However, the LC is differentiated from the SNc as it is not dopaminergic and Cav1.2 mRNA levels are greater in mouse LC neurons compared to Cav1.3 (Sanchez–Padilla et al., 2014). Ventral tegmental area (VTA) neurons are however dopaminergic autonomous pacemakers that express Cav1.3 but this region also has other properties to distinguish it from the SNc. First, Ca<sup>2+</sup> currents in the VTA are not as reliant upon L-type Ca<sup>2+</sup> channels compared to the SNc (Philippart et al., 2016). Second, basal oxidative phosphorylation is lower in the VTA, and third, VTA neurons are less branched than the SNc which may correlate to relatively lower energetic demands (Pacelli et al., 2015). Fourth, VTA neurons experience less mitochondrial oxidative stress mediated by L-type Ca<sup>2+</sup>

channels (Guzman et al., 2010). These distinguishing factors may favour VTA neuron survival when the brain is exposed to other stressors. The increased mitochondrial oxidative stress in the SNc is further worsened in DJ-1<sup>-/-</sup> neurons (Guzman et al., 2010). This may be attributed to reduced expression of uncoupling proteins (UCP) with the DJ-1 knockout, which are thought to ease mitochondrial stress by modestly depolarising the mitochondrial membrane. When comparing WT neurons the expression of *UCPs* 4 and 5 is lower in the VTA compared to the SNc which might support the idea that *UCP* expression is a compensatory mechanism for Ca<sup>2+</sup>-induced mitochondrial stress.

## 1.5 SUMMARY

Local lysosomal Ca<sup>2+</sup> release has emerged as an important component of lysosomal membrane fusion and trafficking. The generation of global Ca<sup>2+</sup> signals by lysosomal Ca<sup>2+</sup> release is also becoming better understood. Together, local and global Ca<sup>2+</sup> signals mediated by the lysosomes have the potential to affect numerous parts of cellular life including lysosome-mediated degradation, mitochondrial well-being and correct protein folding in the ER. In neurodegenerative diseases associated with the accumulation of pathogenic molecules, mitochondrial dysfunction and impaired protein folding it is plausible that disrupted lysosome Ca<sup>2+</sup> signalling lies upstream of these phenotypic changes or is an exacerbating factor (Fig. 1.5).

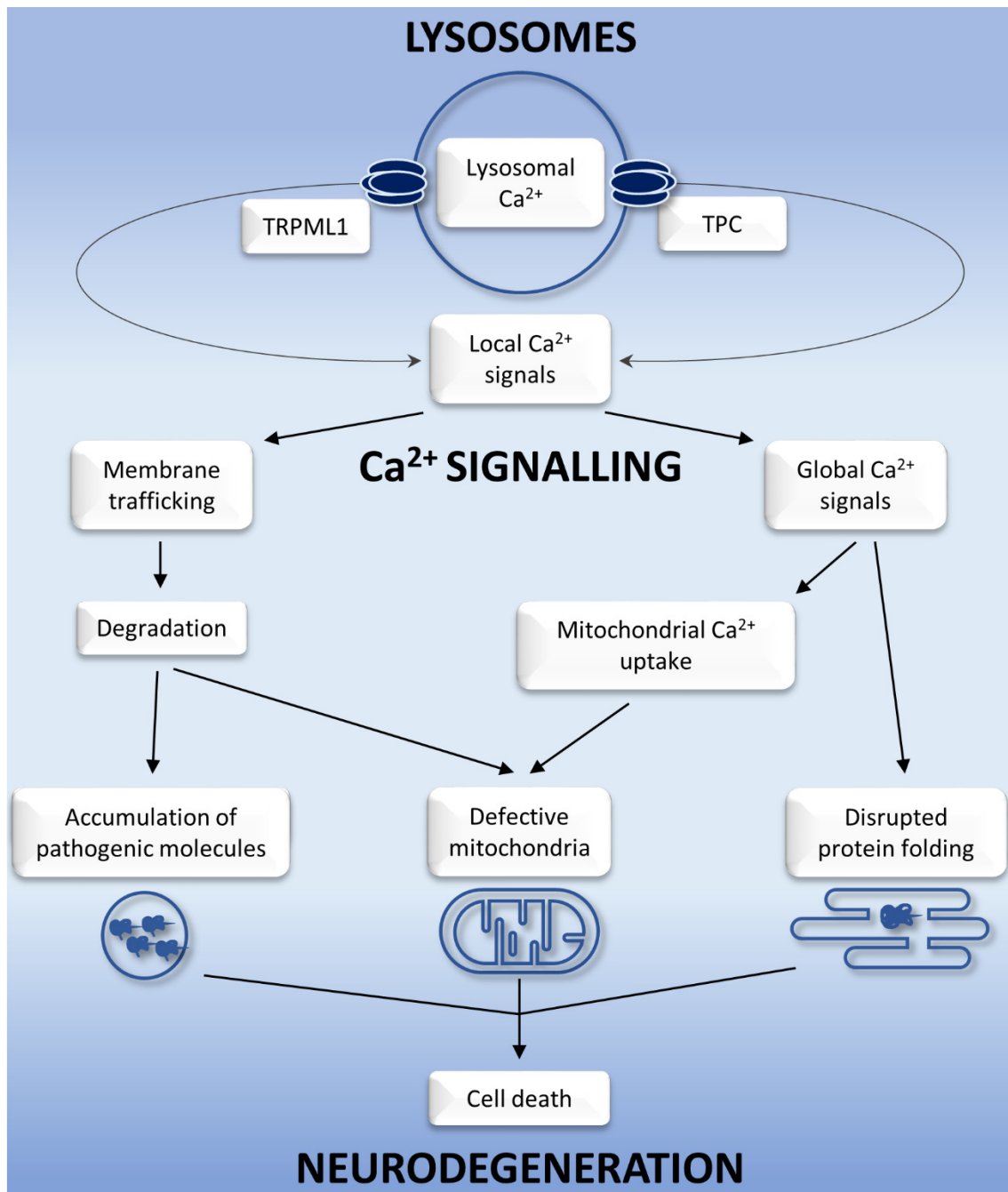


**Figure 1.5 Lysosomes, Ca<sup>2+</sup> and neurodegeneration**

As Ca<sup>2+</sup> stores lysosomes have the potential to influence multiple cellular processes. By releasing Ca<sup>2+</sup> through channels such as TRPML1 and TPCs into their local environment they may regulate their fusion with other organelles. This fusion is important for membrane trafficking and lysosome-mediated degradation. If it is disturbed this might lead to the accumulation of pathogenic molecules or dysfunctional organelles such as mitochondria. In addition to generating local Ca<sup>2+</sup> signals lysosomal Ca<sup>2+</sup> release can initiate global Ca<sup>2+</sup> signals by communicating with the ER. These signals may have considerable cell-wide impact upon Ca<sup>2+</sup>-sensitive processes. Under or over-loading the mitochondria with Ca<sup>2+</sup> may cause damage to these organelles. Altered global Ca<sup>2+</sup> signals may also disturb correct protein folding in the ER. The consequences of deregulated lysosomal Ca<sup>2+</sup> signalling may contribute to neuronal stress and eventual degeneration.

## 1.6 AIMS

Lysosomal membrane fusion and trafficking underpins numerous cellular processes including the degradation of pathogenic molecules and defective mitochondria - two entities that are often present in neurodegenerative diseases such as MLIV and PD. Altered activities of the lysosomal  $\text{Ca}^{2+}$  release channels, TRPML1 and TPC2, have been implicated in these diseases and lysosomal  $\text{Ca}^{2+}$  release is an integral part of lysosomal fusion and trafficking. Therefore, these channels present themselves as targets for pharmacological interventions which may improve membrane trafficking and downstream phenotypes that precede neurodegeneration. However, the consequences of altered TRPML1 and TPC activity on physiological global  $\text{Ca}^{2+}$  signalling is unclear. This is true both in the context of neurodegenerative disease or pharmacological manipulation. Understanding the impact of these channels on global  $\text{Ca}^{2+}$  signalling is important for generating a rounded view of how they might be linked to pathogenicity. For instance, as well as affecting lysosome-mediated degradation, disturbed TRPML1 or TPC activity may cause damage by modulating global  $\text{Ca}^{2+}$  levels and instigating cell-wide disruption to  $\text{Ca}^{2+}$ -sensitive processes. By extrapolation the pharmacological modulation of these channels may also have wide-spread effects that need to be avoided in a clinical setting.

In this thesis I explore the importance of TRPML1 and TPCs in global  $\text{Ca}^{2+}$  signalling, and the potential relevance of the latter to inherited and sporadic PD. My aims are as described below:

1. **Determine whether TRPML1 activation causes global  $\text{Ca}^{2+}$  signals.** TRPML1 has been reported to mediate local  $\text{Ca}^{2+}$  signals and is implicated in neurodegenerative diseases such as MLIV. However, whether TRPML1 can also generate global  $\text{Ca}^{2+}$  signals, and the potential impact of this in disease has not been addressed. Using novel synthetic compounds and molecular interventions I investigate whether TRPML1 activation can initiate global  $\text{Ca}^{2+}$  signals.
2. **In patient-derived fibroblasts determine whether lysosome morphology is disturbed in sporadic PD, and if TPC-dependent global  $\text{Ca}^{2+}$  signalling is altered in familial or sporadic PD.** Disturbed lysosome morphology and upregulated TPC activity has been associated with the *LRK2* G2019S mutation in fibroblasts from patients with familial PD. However, whether disturbed lysosome morphology is a feature of sporadic PD is unknown, as is the relevance of upregulated TPC activity to global  $\text{Ca}^{2+}$  signalling in PD.

Therefore, using *in silico* methods, I characterise lysosome morphology in sporadic PD patient fibroblasts, and by using pharmacological and molecular interventions, I assess the possible influence of TPCs on physiological global  $\text{Ca}^{2+}$  signals in PD patient fibroblasts.

- 3. In a neuronal model of PD determine whether TPC-dependent global  $\text{Ca}^{2+}$  signalling is altered.** Upregulated TPC activity in the presence of LRRK2 G2019S has been reported in fibroblasts and HEK293T cells. However, this and the relevance to global  $\text{Ca}^{2+}$  signalling in PD has not been explored in a neuronal setting. Using a neuronal model of LRRK2 G2019S PD I investigate whether physiological global  $\text{Ca}^{2+}$  signalling is disturbed as a consequence of altered TPC activity. The assessment of TPC contribution to  $\text{Ca}^{2+}$  signalling is impeded by the lack of selective TPC inhibitors. As part of my investigation I therefore examine the efficacy of putative novel TPC blockers in these neuronal cells, which may inform the development of selective compounds.

# CHAPTER 2: TRPML1 and Global Ca<sup>2+</sup> Signalling

## 2.1 INTRODUCTION

Mutations in the lysosomal Ca<sup>2+</sup> channel TRPML1 are known to cause mucopolidosis type IV (MLIV). This lysosomal storage disorder (LSD) affects people at a very young age causing severe psychomotor problems, ophthalmic degeneration and aberrant secretion of hydrochloric acid in the stomach (achlorhydria) (Bach, 2005; Frei et al., 1998; Kohn et al., 1977). Reduced TRPML1 activity has been linked to another early-onset LSD – Niemann-Pick type C disease (NPC) (Shen et al., 2012). This disease is caused by mutations in *NPC1* or *NPC2* which are thought to be involved in cholesterol efflux from the endolysosomes (Rosenbaum and Maxfield, 2011).

Despite different genetic causes these neurodegenerative diseases both exhibit defective lysosomal fusion and trafficking (Morgan et al., 2011). The defect in MLIV cells can be recapitulated by treating healthy cells with the fast-acting Ca<sup>2+</sup> chelator BAPTA (LaPlante et al., 2004). This supports the idea that Ca<sup>2+</sup> released through TRPML1 into the local vicinity of the lysosomes is important for normal lysosome fusion and trafficking but is impaired in MLIV (LaPlante et al., 2004; Luzio et al., 2007b; Pryor et al., 2000). However, the measurement and verification of such local Ca<sup>2+</sup> signals mediated by TRPML1 is not trivial.

One tool that reportedly records local lysosomal Ca<sup>2+</sup> signals is overexpressed TRPML1 fused to genetically-encoded Ca<sup>2+</sup> indicators GCaMP3 (Bae et al., 2014; Medina et al., 2015; Shen et al., 2012) or GECO (Cao et al., 2015b). These probes, together with the contemporary development of synthetic TRPML1 agonists and antagonists, have paved the way for modern TRPML1 research (Chen et al., 2014; Grimm et al., 2010; Samie et al., 2013; Shen et al., 2012). Indeed, it was by using the GCaMP3-TRPML1 fusion protein with the TRPML1 agonist ML-SA1 that TRPML1-mediated local Ca<sup>2+</sup> signals were shown to be reduced in NPC cells (Shen et al., 2012). Importantly these indicators, agonists and antagonists have also progressed the understanding of MLIV, HIV-related cognition impairments, autophagy and Alzheimer's disease (Bae et al., 2014; Chen et al., 2014; Lee et al., 2015; Medina et al., 2015).

Despite establishing TRPML1 as a mediator of local lysosomal Ca<sup>2+</sup> release there has been little investigation into whether activation of this channel also generates global Ca<sup>2+</sup> signals. There is precedent for exploring this as lysosomal Ca<sup>2+</sup> release stimulated by the mobilising messenger NAADP, or the lysosomotropic GPN, can trigger global Ca<sup>2+</sup> signals (Kilpatrick et al., 2013;



Morgan, 2016). Furthermore, there is a smattering of data that indicates TRPML1-activated global  $\text{Ca}^{2+}$  signalling is possible: Obscured in the 2012 study by Shen and colleagues ML-SA1 caused modest  $\text{Ca}^{2+}$  signals in Chinese hamster ovary (CHO) cells and mouse macrophages (Shen et al., 2012). In addition, this signal was inhibited in TRPML1 (and NPC1) knockout mouse macrophages. HEK239T cells overexpressing TRPML1 have also responded globally to ML-SA1 (Onyenwoke et al., 2015) and in mouse blastocysts very small average  $\text{Ca}^{2+}$  signals were stimulated by ML-SA1 (Lee et al., 2015).

If disturbed, global  $\text{Ca}^{2+}$  signals have the potential to cause cell-wide disruption to a myriad of  $\text{Ca}^{2+}$ -sensitive processes. Therefore, if global  $\text{Ca}^{2+}$  signals are regulated by TRPML1 their deregulation caused by TRPML1 dysfunction may contribute to neurodegeneration. Furthermore, as TRPML1 activation is pursued as a way to improve trafficking defects and possibly modify neurodegenerative disease any effect of TRPML1 activation on global  $\text{Ca}^{2+}$  signalling should be carefully considered (Cao et al., 2015b; Chen et al., 2014; Shen et al., 2012). The aim of this chapter is to investigate whether TRPML1 activation causes global  $\text{Ca}^{2+}$  signals (Fig. 2.1).

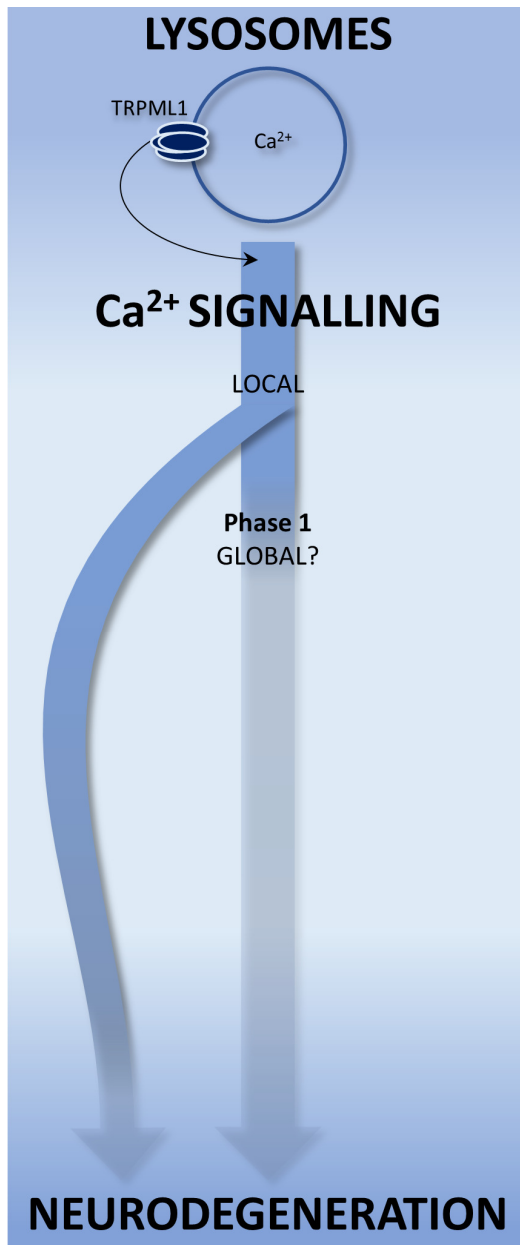


### Figure 2.1 Introduction

Dysfunction of the lysosomal Ca<sup>2+</sup> channel TRPML1 has been linked to neurodegeneration.

There is evidence that dysfunctional TRPML1 disturbs local Ca<sup>2+</sup> signals that emanate from the lysosomes. This may be a route by which TRPML1 contributes to neurodegeneration (curved left-hand arrow).

However, it is unclear whether dysfunctional TRPML1 also disturbs global Ca<sup>2+</sup> signals and contributes to neurodegeneration via this global route (straight right-hand arrow).

A first step to exploring this global possibility is to determine whether TRPML1 mediates global Ca<sup>2+</sup> signals (Phase 1).

## **2.2 METHODS and ANALYSIS**

### **2.2.1 Cell culture**

#### **2.2.1.1 HeLa**

HeLa cells were maintained in Dulbecco's Modified Eagle Medium (DMEM), supplemented with 10% v/v fetal bovine serum, 100 units/ml penicillin and 100 µg/ml streptomycin (all Gibco) at 37°C in a humidified atmosphere with 5% CO<sub>2</sub>. Cells were given fresh media every 3-4 days, passaged using trypsin (Gibco), and plated at 50,000 or 100,000 cells/ml onto 13 mm glass coverslips coated with poly-L-lysine (Sigma) (in a 24-well plate, 0.5 ml/coverslip) 1-4 days prior to imaging.

#### **2.2.1.2 Fibroblast**

Primary human skin fibroblast cultures were generated from biopsies and obtained from Drs Michelle Beavan, Alisdair McNeill, Jan-Willem Taanman and Tatiana Papkovskaia (Department of Clinical Neuroscience, UCL). Fibroblasts were maintained in Dulbecco's Modified Eagle Medium (DMEM), supplemented with 10% v/v fetal bovine serum, 100 units/ml penicillin and 100 µg/ml streptomycin (all Gibco) at 37°C in a humidified atmosphere with 5% CO<sub>2</sub>. Cells were given fresh media every 3-4 days, passaged by scraping, and plated onto a 25 mm glass coverslip (in a 6-well plate, 2ml/coverslip) 6 days prior to imaging. On the day of imaging cells were ~80-90% confluent.

#### **2.2.1.3 SH-SY5Y**

SH-SY5Y cells were maintained in 1:1 mixture of DMEM and Ham's F12 media, supplemented with 10% v/v fetal bovine serum, 100 units/ml penicillin and 100 µg/ml streptomycin and 1% (v/v) nonessential amino acids (all Gibco) at 37°C in a humidified atmosphere with 5% CO<sub>2</sub>. Cells were given fresh media every 2-3 days, passaged using trypsin (Gibco) and plated at 75,000 cells/ml onto 13 mm glass coverslips coated with poly-L-lysine (Sigma) (in a 24-well plate, 0.5ml/coverslip) 2 days prior to imaging.

#### **2.2.1.4 Neuronal**

Murine neuronal cultures were prepared by Dr Stephen Mullin (Institute of Neurology, UCL) as described (Magalhaes et al., 2016). Briefly, day 15 embryonic cortexes were dissected, and homogenised after removing meninges. Following centrifugation at 1000 rpm for 5 minutes, pellets were resuspended in neurobasal media (Invitrogen) supplemented with B27 (Invitrogen), glutamax (Sigma) and antimycotic/antibiotic solution (Sigma). Neurons were seeded onto 25

mm glass coverslips coated with poly-ornithine (Sigma) 6 days prior to imaging. Cells were maintained at 37°C in a humidified atmosphere with 5% CO<sub>2</sub> and fed with fresh media every 4 days.

## 2.2.2 Transfection

HeLa cells were transfected with plasmids the day before imaging/fixing using Lipofectamine 2000 (Invitrogen) according to the manufacturer's instructions. Plasmids used are listed below:

<b>ID</b>	<b>Protein</b>	<b>Tag</b>	<b>Position of tag: Amino (N) /Carboxyl(C)</b>	<b>Reference</b>
GCaMP3- ML1	TRPML1 WT	GCaMP3	N	(Shen et al 2012)
ML1 WT	TRPML1 WT	GFP	N	(Yamaguchi et al., 2011)
ML1 mutant	TRPML1 mutant (D471K)	GFP	N	(Yamaguchi et al., 2011)
LAMP1	LAMP1	GFP	C	(Falcon-Perez et al., 2005)
RFP-LAMP1	LAMP1	mRFP	C	(Sherer et al., 2003)

## 2.2.3 Cell labelling

For live cell imaging cells were immersed at room temperature in HEPES-buffered saline (HBS; pH 7.4) containing (from Sigma) 1.25 mM KH<sub>2</sub>PO<sub>4</sub>, 2 mM CaCl<sub>2</sub>, 2 mM MgSO<sub>4</sub>, 3 mM KCl, 156 mM NaCl, 10 mM glucose, and 10 mM HEPES. To measure changes in cytosolic Ca<sup>2+</sup> and Fe<sup>2+</sup> cells were incubated in HBS with Fura-2 AM (2.5µM) and 0.005% v/v pluronic acid (both Invitrogen) at room temperature for 1 hour. To detect lysosome distribution cells were incubated in HBS with LysoTracker® red (100 nM) (Invitrogen) for 15 minutes. After labelling cells were washed quickly 3 times with HBS and mounted in an imaging chamber (1 ml chamber for 13 mm coverslips; 2 ml chamber for 25 mm coverslips; Biosciences Tools). For fixed cell imaging cells were fixed for 10 minutes with 4% (w/v) paraformaldehyde (VWR) in phosphate buffered saline (PBS) (Sigma). Nuclei were labelled by incubation for 5 minutes with 1 µg/ml 4',6-diamidino-2-phenylindole (DAPI) (Sigma). Cells were washed three times in PBS before being mounted on microscope slides with 1,4 diazabicyclo[2,2,2]octane (DABCO) (Sigma) and sealed with colourless, transparent nail varnish.

## 2.2.4 Microscopy: Confocal

Images were captured using an LSM510 confocal scanner (Zeiss) attached to a Zeiss Axiovert 200M inverted microscope fitted with a 63x Plan Apochromat water-immersion objective. Excitation and emission wavelengths for fluorescent markers are detailed below:

<b>Probe</b>	<b>Excitation wavelength (nm)</b>	<b>Emission filter wavelength (nm)</b>
DAPI	364	385-470
GFP	488	505-550
mRFP	543	560-615
Lysotracker Red	543	560-615

12-bit images were taken at a 3x optical zoom. For colocalisation analysis, z-stacks (8-12 slices per stack) were obtained at 1  $\mu\text{m}$  intervals.

Colocalisation analysis was conducted on confocal images using the Fiji software package for ImageJ. Negative controls comprised the same images but with the red channel rotated 90° to the right. Each plot point represents one cell.

### 2.2.4.1 Pearson's correlation coefficient

Pearson's correlation coefficients were obtained from complete z-stacks using the ImageJ plugin Coloc2. Before execution, regions of interest (ROI) were manually drawn around each cell in the green channel to exclude extracellular pixels from the calculations.

### 2.2.4.2 Percentage of colocalised vesicles

For each z-stack the percentage of colocalised vesicles was calculated from the middle slice or from the two middle slices, which was then averaged (mean). This was done using the ImageJ plugin SQUASSH (Rizk et al., 2014). Before execution, ROIs were manually drawn around each cell to exclude extracellular pixels from the calculations. Calculation for the complete z-stack was not possible due to excessive computing time required. The parameters that were adjusted in SQUASSH are detailed on the next page.

**Table 2.3 SQUASSH Parameters**

<b>Background subtraction</b>	20 pixels / 1.86 $\mu$ M
<b>Regularization</b>	0.1
<b>Minimum object intensity</b>	0.2
<b>Local intensity estimation</b>	automatic
<b>Noise model</b>	Poisson
<b>PSF</b>	Computed for GFP
<b>Region filter</b>	Remove region with intensities <0.1

All parameters except PSF (point spread function) were chosen experimentally or as advised by Rizk et al (Rizk et al., 2014).

## 2.2.5 Microscopy: Epifluorescence

Epifluorescence images were captured every 3 seconds at room temperature with a cooled coupled device camera (TILL photonics) attached to an Olympus IX71 inverted fluorescence microscope that was fitted with a 20x objective and a monochromatic light source. Cells transfected with GCaMP3 or GFP proteins were identified before imaging commenced by taking snapshots of their fluorescence as follows:

**Table 2.4 Epifluorescence Microscopy Excitation/Emission wavelengths**

<b>Probe</b>	<b>Excitation wavelength (nm)</b>	<b>Emission filter wavelength (nm)</b>
GCaMP3	470	515 long pass
GFP	488	515 long pass

Excitation and emission wavelengths for probes tracking cytosolic  $\text{Ca}^{2+}$ ,  $\text{Fe}^{2+}$  and acidic organelles are detailed below:

**Table 2.5 Epifluorescence Microscopy Excitation/Emission wavelengths**

<b>Probe</b>	<b>Recording</b>	<b>Excitation wavelength (nm)</b>	<b>Emission filter wavelength (nm)</b>
GCaMP3	$\text{Ca}^{2+}$	470	515 long pass
Fura-2 (for simultaneous GCaMP3 plus Fura-2 imaging)	$\text{Ca}^{2+}$ (High noise/signal)	340/380	515 long pass
Fura-2	$\text{Ca}^{2+}$	340/380	440 long pass

Fura-2	Fe <sup>2+</sup>	360	440 long pass
Lysotracker Red	Acidic Organelles	560	590

Cells were challenged with ML-SA1 (20  $\mu$ M; Merck), MK6-83 (20  $\mu$ M; a kind gift from Professor Christian Grimm, Ludwig-Maximilian University of Munich), GW405833 hydrochloride (aka ML-SI1; 100  $\mu$ M; Sigma), ML-SI3 (100/10  $\mu$ M; a kind gift from Dr Haoxing Xu, University of Michigan), GPN (200  $\mu$ M; Santa Cruz Biotechnology), histamine (10  $\mu$ M; Sigma) BTP2 (20  $\mu$ M; Sigma), thapsigargin (1  $\mu$ M; Merck), FeCl<sub>2</sub> (100  $\mu$ M; Sigma) and FeCl<sub>3</sub> (100  $\mu$ M; Sigma). All compounds except histamine, FeCl<sub>2</sub> and FeCl<sub>3</sub> were dissolved in DMSO (Sigma). The exceptions were dissolved in H<sub>2</sub>O. The maximal volume of vehicle added in any experiment was 1% (v/v).

All Fe<sup>2+</sup> experiments were conducted in the absence of extracellular Ca<sup>2+</sup>. For all other experiments the absence of extracellular Ca<sup>2+</sup> is indicated where appropriate in the figures. Where displayed, Ca<sup>2+</sup> was replaced with 1 mM EGTA (Sigma).

One coverslip was used per experiment and fluorescence was recorded from all cells in the field of view. Each plot point corresponds to the mean response in an individual experiment.

#### 2.2.5.1 Ca<sup>2+</sup> - GCaMP3

To track changes in Ca<sup>2+</sup> concentration as indicated by GCaMP3 fluorescence ROIs were manually drawn around each cell, plus one for background subtraction. Fluorescence was calculated using TILLVISION software and averaged over a 60 second period before stimulus addition to acquire a basal value (F<sub>0</sub>). GCaMP3 fluorescence change ( $\Delta F$ ) is normalised to basal ( $\Delta F/F_0$ ) for the final data presentation.

#### 2.2.5.2 Ca<sup>2+</sup> - Fura-2

To track changes in cytosolic Ca<sup>2+</sup> concentration ROIs were manually drawn around each cell, plus one for background subtraction. The ratio of Fura-2 bound by Ca<sup>2+</sup> (ex: 340 nm) and unbound (ex: 380 nm) was calculated using TILLVISION software. The Fura-2 ratio was averaged over a 60 second period before stimulus addition to acquire a basal value. The change of the Fura-2 ratio between this basal value and the value at the peak of the signal ( $\Delta [Ca^{2+}]$  (ratio)) was calculated to quantify the magnitude of response. Cells were assigned responding status if this magnitude was  $\geq 0.1$ . Time to peak was measured from the point of stimulus addition.

### **2.2.5.3 Fe<sup>2+</sup> - Fura-2**

To track Fe<sup>2+</sup> entry ROIs were drawn around each cell, plus one for background subtraction. Fura-2 fluorescence (ex: 360 nm) was calculated using TILLvision software. For a 60 second period immediately after cells were immersed in Ca<sup>2+</sup> free HBS Fura-2 fluorescence was averaged to acquire a basal value (F<sub>0</sub>). Fluorescence was normalised to basal (F/F<sub>0</sub>) and the fluorescence value 144 seconds after Fe addition was tabulated to quantify Fe<sup>2+</sup> entry.

### **2.2.5.4 Acidic Organelles - Lyotracker Red**

To track acidic organelles for each cell one ROI was drawn around the cell plus one adjacent to it for cell-unique background subtraction. Lyotracker fluorescence was averaged over a 60 second period before stimulus addition to acquire a basal value (F<sub>0</sub>). Fluorescence was normalised to basal (F/F<sub>0</sub>).

## **2.2.6 Data Presentation**

The presented data combines representative results from single experiments and averaged results from multiple experiments. Where data is represented by plot points the mean is displayed as a superimposed horizontal black bar.



## 2.3 RESULTS

### 2.3.1 The TRPML1 agonist ML-SA1 evokes global Ca<sup>2+</sup> signals in cells overexpressing GCaMP3-ML1

A fusion protein comprising the lysosomal Ca<sup>2+</sup> channel TRPML1 and the Ca<sup>2+</sup> indicator GCaMP3 (GCaMP3-ML1) has been used to report Ca<sup>2+</sup> signals emanating from the lysosomes (Bae et al., 2014; Medina et al., 2015; Shen et al., 2012). Shen and colleagues demonstrated that in cells expressing GCaMP3-ML1 the TRPML1 agonist ML-SA1 caused localised lysosomal Ca<sup>2+</sup> release. Using HeLa cells I tested this fusion probe, also in conjunction with ML-SA1 stimulation. As shown in Figure 2.1A ML-SA1 induced robust increases in GCaMP3 fluorescence, consistent with previous studies (Medina et al., 2015; Shen et al., 2012). In these experiments HeLa cells were also loaded with the cytosolic Ca<sup>2+</sup> indicator Fura-2 to measure bulk changes in Ca<sup>2+</sup>, and therefore global Ca<sup>2+</sup> signals (Grynkiewicz et al., 1985). The simultaneous recording of GCaMP3 and Fura-2 fluorescence was conducted using the same emission filter (515 long pass) for both indicators. This was optimal for GCaMP3 but not for Fura-2, which resulted in high noise-to-signal data (Fig. 2.1B). Surprisingly though, activation of GCaMP3-ML1 with ML-SA1 appeared to induce Fura-2 responses, indicative of global Ca<sup>2+</sup> signals (Fig. 2.1B). To verify this result the experiment was repeated, this time omitting GCaMP3 recordings in favour of an appropriate Fura-2 emission filter (440 long pass). Before imaging commenced a snapshot of GCaMP3 fluorescence was captured to identify the cells expressing the ML1 construct. With the 440 nm long pass filter Fura-2 signals in cells expressing GCaMP3-ML1 were even more clear upon ML-SA1 stimulation (Fig. 2.1C and D). The Fura-2 trace shows a clear rise of cytosolic Ca<sup>2+</sup> in a digital manner (Fig. 2.1D), with 75% of cells responding. In untransfected cells from the same field of view cytosolic Ca<sup>2+</sup> increases were also observed (Fig. 2.1E), with 25% of cells responding. Notably, of these responding untransfected cells, some exhibited the same digital signature as the transfected GCaMP3-ML1 cells (Fig. 2.1F cf. Fig. 2.1D). This indicated possible mis-identification of transfected vs non-transfected HeLa. In a second category of responding untransfected cells the signal was not digital but complex and of low magnitude (Fig. 2.1G). This posed the possibility that endogenous TRPML1 was also mediating global Ca<sup>2+</sup> signals induced by ML-SA1. For all subsequent measurements of intracellular Ca<sup>2+</sup> cytosolic Fura-2 and the 440 nm long pass filter were used to record global Ca<sup>2+</sup> signals.

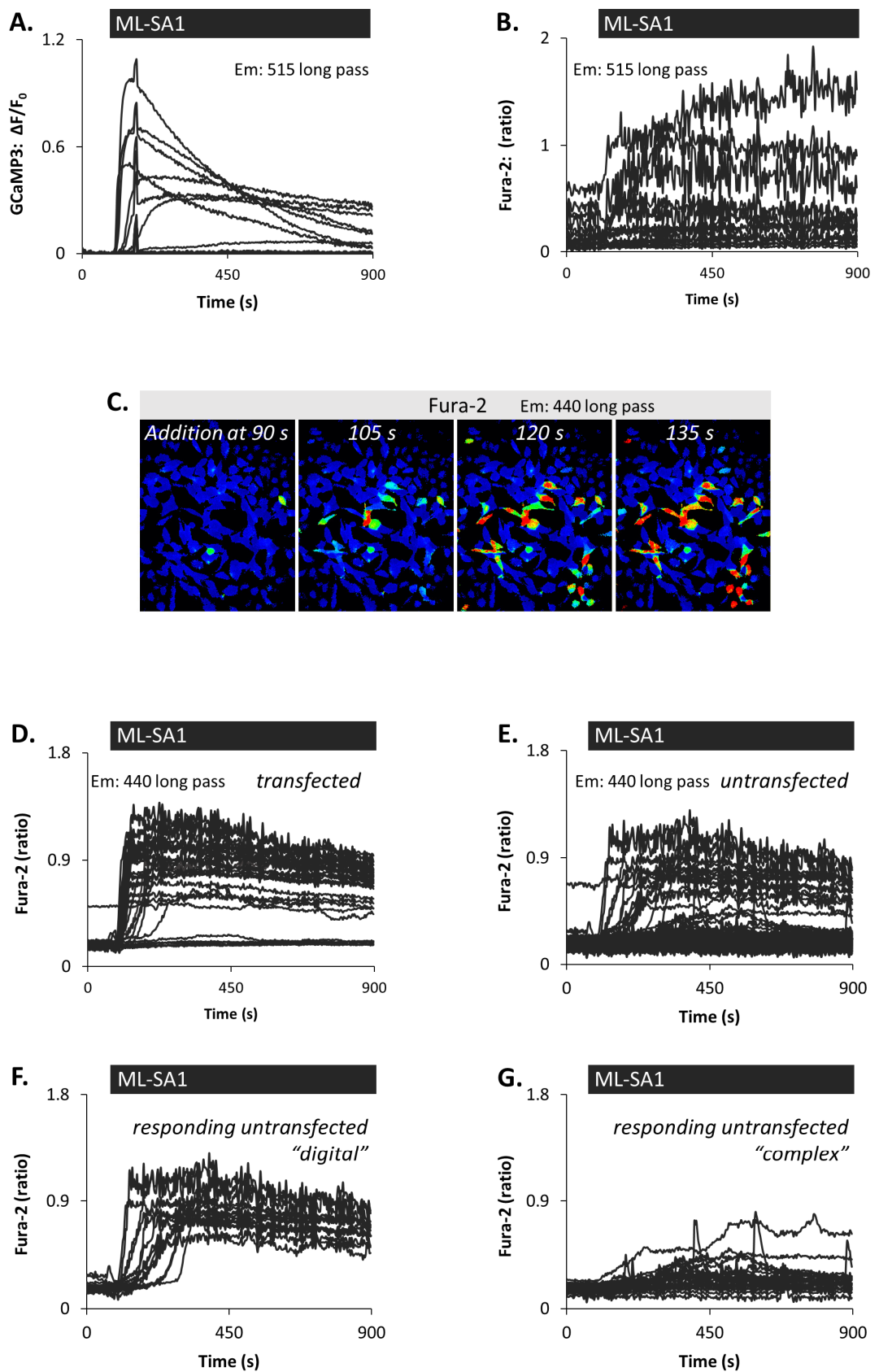


**Figure 2.1** The TRPML1 agonist ML-SA1 evokes global  $\text{Ca}^{2+}$  signals in cells overexpressing GCaMP3-TRPML1 (legend on next page)

**(A-B)** HeLa cells overexpressing GCaMP3-ML1 were stimulated with ML-SA1 (20  $\mu$ M). **(A)** GCaMP3 fluorescence traces of individual cells (n=16). Data presented as change in fluorescence from basal ( $\Delta F/F_0$ ). GCaMP3 fluorescence was recorded using a 515 nm long pass emission (Em) filter. **(B)** Fura-2 fluorescence traces of the same cells represented in **A**. Data presented is the ratio of Fura-2 fluorescence when excited at 340 nm and Fura-2 fluorescence when excited at 380 nm (Fura-2: (ratio)). Fura-2 fluorescence was recorded using a sub-optimal 515 nm long pass emission (Em) filter. **(C)** Pseudo-coloured images representing the Fura-2 ratio in HeLa following transfection of GCaMP3-ML1 and ML-SA1 (20  $\mu$ M) stimulation. Time series shows Fura-2 ratio at the point of ML-SA1 addition (90 s into imaging) and at subsequent 15 s intervals. Blue equates to a low Fura-2 ratio and red equates to a high ratio. Fura-2 fluorescence was recorded using a 440 nm long pass emission filter (Em). **(D-E)** Fura-2 traces of HeLa cells **(D)** expressing (*transfected*) (n=34) or **(E)** not expressing (*untransfected*) (n=161) GCaMP3-ML1, that correspond to the field of view in **C**. Fura-2 fluorescence was recorded using a 440 nm long pass emission (Em) filter. **(F and G)** The *responding untransfected* cells in **E** categorised according to **(F)** “*digital*” (n=14) and **(G)** “*complex*” (n=26) responses.

### 2.3.2 The TRPML1 agonist ML-SA1 evokes global $Ca^{2+}$ signals in untransfected cells

To probe whether endogenous TRPML1 could mediate global  $Ca^{2+}$  signals untransfected HeLa were stimulated with ML-SA1. Indeed, global  $Ca^{2+}$  signals were evoked in a concentration-dependent manner (Fig. 2.2A and B). However, the magnitudes of signal were highly variable and the percentage of cells responding was low, with only 21% at 20  $\mu$ M and 28% at the higher concentration of 80  $\mu$ M. To verify the specificity of these signals the cells were challenged with TRPML1 inhibitor ML-SI3 (Samie et al., 2013). The inhibitor ML-SI1 could not be used as it caused its own complex Fura-2  $Ca^{2+}$  signals that would complicate analysis of the subsequent ML-SA1 response (Fig. 2.2C). ML-SI3 did not elicit its own  $Ca^{2+}$  signals, and did inhibit ML-SA1-evoked endogenous global  $Ca^{2+}$  signals (Fig. 2.2D). However, on one occasion there was no clear ML-SA1 signal to be inhibited, attesting to the variability of the response (Fig.2.2E).

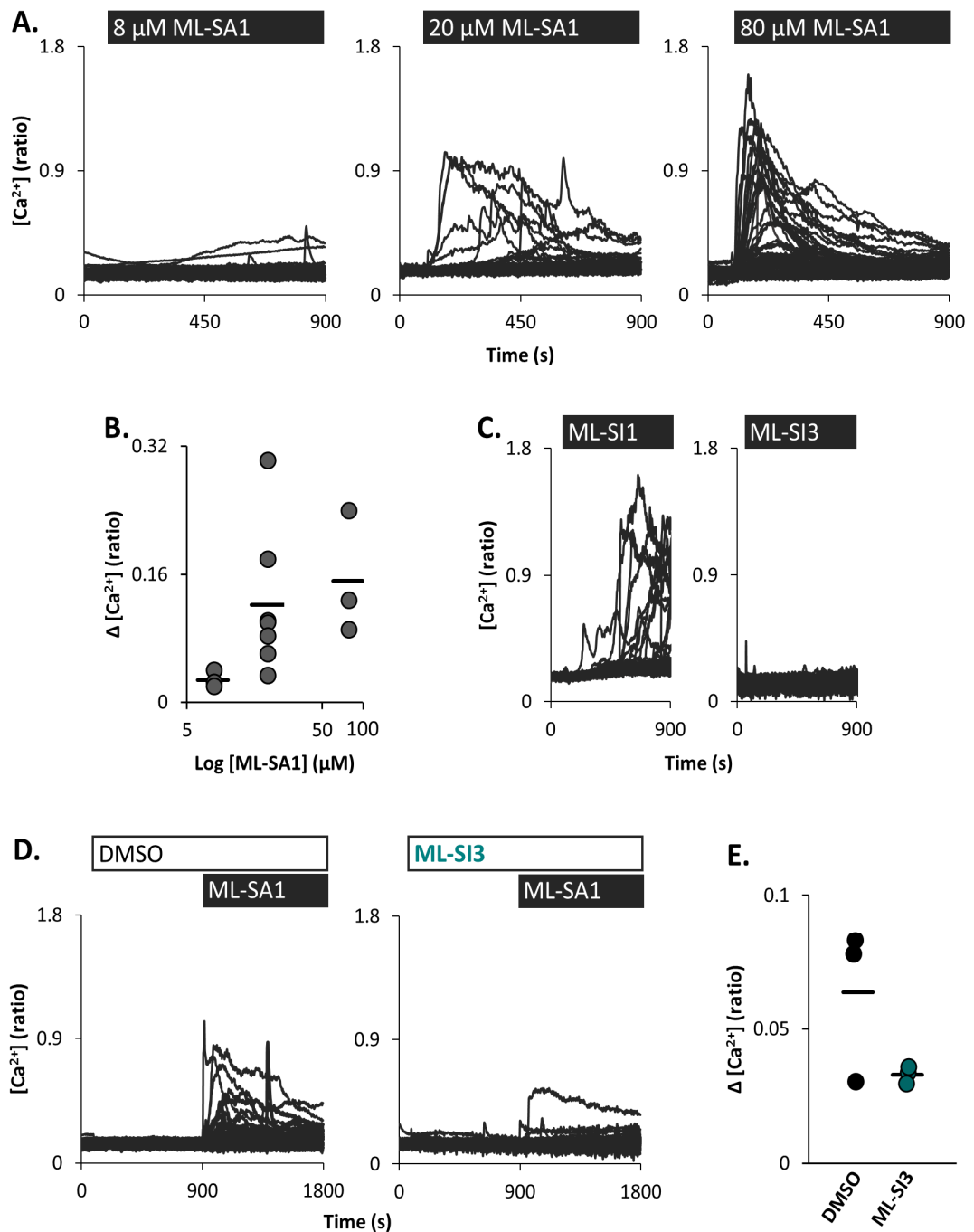


**Figure 2.2 The TRPML1 agonist ML-SA1 evokes global  $\text{Ca}^{2+}$  signals in untransfected cells**

**(A)** Cytosolic  $\text{Ca}^{2+}$  traces of individual untransfected HeLa cells stimulated with ML-SA1 at a range of concentrations. Each panel displays one representative experiment. **(B)** Data quantifying magnitude of responses exemplified in **A**. Each plot point represents one experiment,  $n=3/7/3$  (8  $\mu\text{M}$  /20  $\mu\text{M}$ / 80  $\mu\text{M}$ ). A total of 251/576/262 (8  $\mu\text{M}$ /20  $\mu\text{M}$ /80  $\mu\text{M}$ ) cells from 6 independent platings were analysed. **(C)** Cytosolic  $\text{Ca}^{2+}$  traces of HeLa cells upon addition of ML-SI1 or ML-SI3 (both 100  $\mu\text{M}$ ),  $n=74/116$  (ML-SI1/ML-SI3). **(D)** Traces of HeLa cells stimulated with ML-SA1 (20  $\mu\text{M}$ ) following addition of DMSO or ML-SI3 (10  $\mu\text{M}$ ). **(E)** Data quantifying magnitude of the ML-SA1 responses exemplified in **D**,  $n=3/3$  (DMSO/ML-SI3). A total of 283/302 (DMSO/ ML-SI3) cells from 3 independent platings were analysed.

### **2.3.3 Overexpressed TRPML1 and mutant TRPML1 colocalise with lysosomes**

Due to the variability of endogenous ML-SA1-evoked  $\text{Ca}^{2+}$  signals the investigation returned to TRPML1 overexpression in order to dissect the make-up of these signals. HeLa were transfected with GFP fused to the N-terminus of TRPML1 (ML1 WT), or inactive pore mutant TRPML1 (D471K) (ML1 mutant). Compared to  $\text{Ca}^{2+}$ -sensitive GCaMP3, GFP fluorescence was brighter at basal  $\text{Ca}^{2+}$  levels (data not shown). This facilitated the identification of transfected cells vs non-transfected cells for  $\text{Ca}^{2+}$  imaging. When examined by confocal microscopy ML1 WT or ML1 mutant displayed punctate distributions similar to that of lysosome-associated membrane protein 1 (LAMP1) in fixed cells (Fig. 2.3A). In live cells loaded with LysoTracker Red (LTR; a fluorescent dye used for labelling acidic organelles such as the lysosomes) both ML1 WT and ML1 mutant displayed some degree of colocalisation, suggestive of lysosomal localisation (Fig. 2.3B). However, false positive or negative colocalisation is a possible caveat when using multi-channel imaging to capture a dynamic system such as the endolysosomal system. Therefore, multi-channel imaging was also conducted in fixed cells co-expressing ML1 WT or ML1 mutant, with mRFP fused to the C-terminus of LAMP1 (Fig. 2.3C). Under these conditions colocalisation was also observed and quantified by Pearson's correlation coefficient and the percentage of colocalising vesicles (Fig. 2.3D and E). Collectively, these data indicate localisation of GFP-fused ML WT and ML1 mutant at the lysosomes.

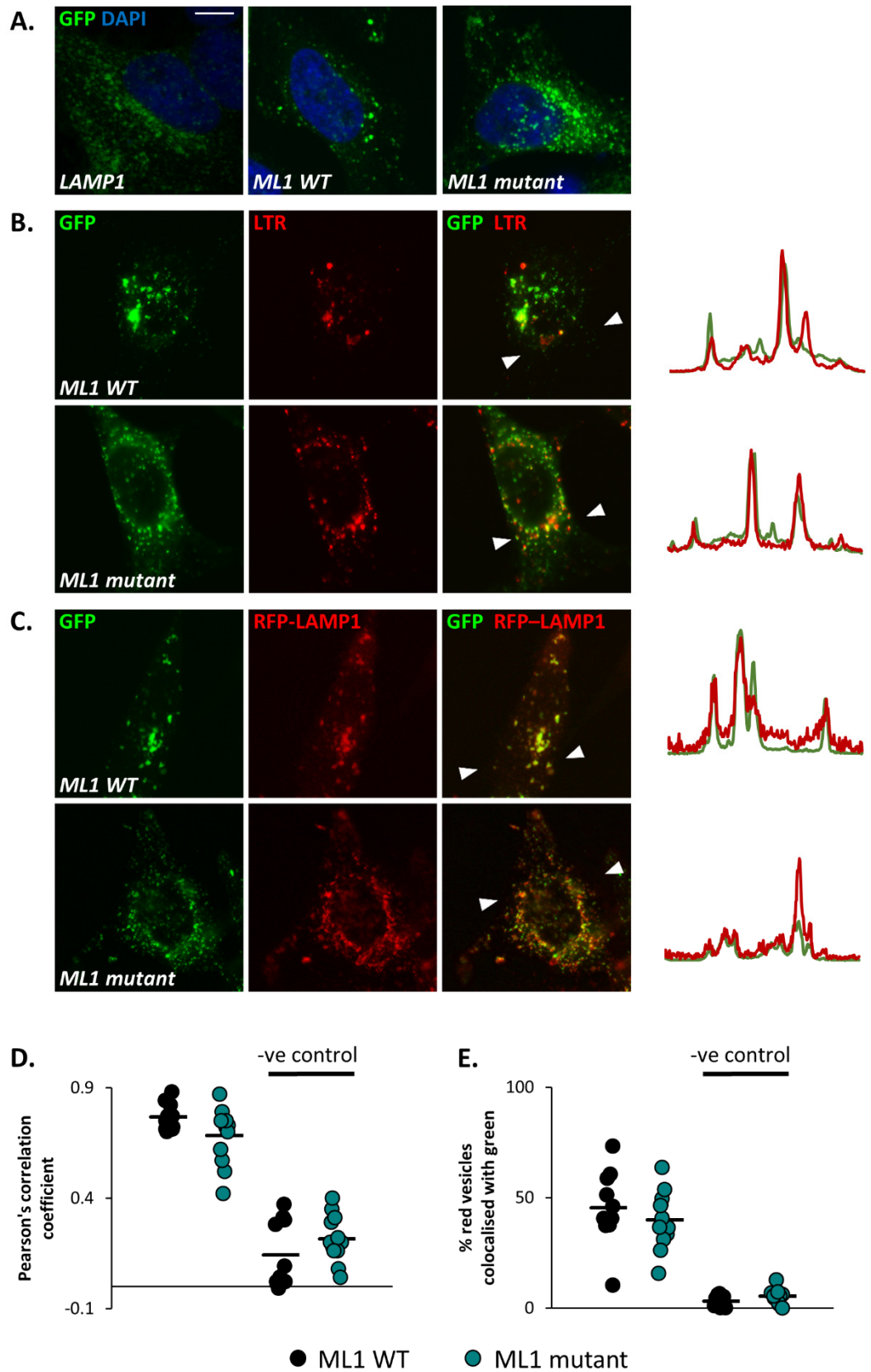


**Figure 2.3 Overexpressed TRPML1 and mutant TRPML1 colocalise with lysosomes**

(Legend on next page)

**(A)** Confocal images of fixed cells overexpressing GFP-LAMP1 (*LAMP1*), GFP-TRPML1 WT (*ML1 WT*) or GFP-TRPML1 mutant (*ML1 mutant*) (all green). Nuclei stained blue (DAPI). Scale bar = 10  $\mu$ m. **(B-C)** TRPML1 colocalisation with lysosomal markers. Images are accompanied by red and green fluorescence intensity plots which represent the paths indicated between the white triangles. **(B)** Images of live cells expressing ML1 WT or ML1 mutant (green) and labelled with Lysotracker Red (LTR) (red). **(C)** Middle images from representative z-stacks of fixed cells co-expressing ML1 WT or ML1 mutant (green) with mRFP-LAMP1 (red). **(D-E)** Data quantifying colocalisation in **C** with **(D)** Pearson's correlation coefficients and **(E)** the percentage of red vesicles colocalising with green vesicles. Each plot point represents one cell, with a total of 10/12 (ML1 WT/ML1 mutant) cells from 2 independent platings. The negative controls (-ve control) were generated from the same images but with the red channel rotated 90° to the right.

### **2.3.4 Overexpressed TRPML1 WT potentiates agonist-evoked global Ca<sup>2+</sup> signals but TRPML1 mutant does not**

As a control for cells overexpressing GFP-ML1 WT or GFP-ML1 mutant some cells were transfected with putatively inert GFP-LAMP1. When stimulated with TRPML1 agonist ML-SA1 a small fraction of LAMP1 cells responded (9%) (Fig. 2.4A and B) in a manner akin to untransfected cells (Fig. 2.2A and B). In ML1 WT cells ML-SA1-induced signals were hugely potentiated (Fig. 2.4A and B), displaying a similar digital signal to those in GCaMP3-ML1-expressing cells (Fig. 2.1D). Requirement of TRPML1 for these signals was indicated by a complete lack of response in cells overexpressing the ML1 mutant (Fig. 2.4A and B). Comparable results were obtained when using a structurally distinct TRPML1 agonist, MK6-83 (Chen et al., 2014) (Fig. 2.4C and D). Specificity of ML-SA1 and MK6-83-evoked signals in ML1 WT cells was demonstrated by the blocking effect of TRPML1 inhibitor ML-SI3 (Fig. 2.4E-H).

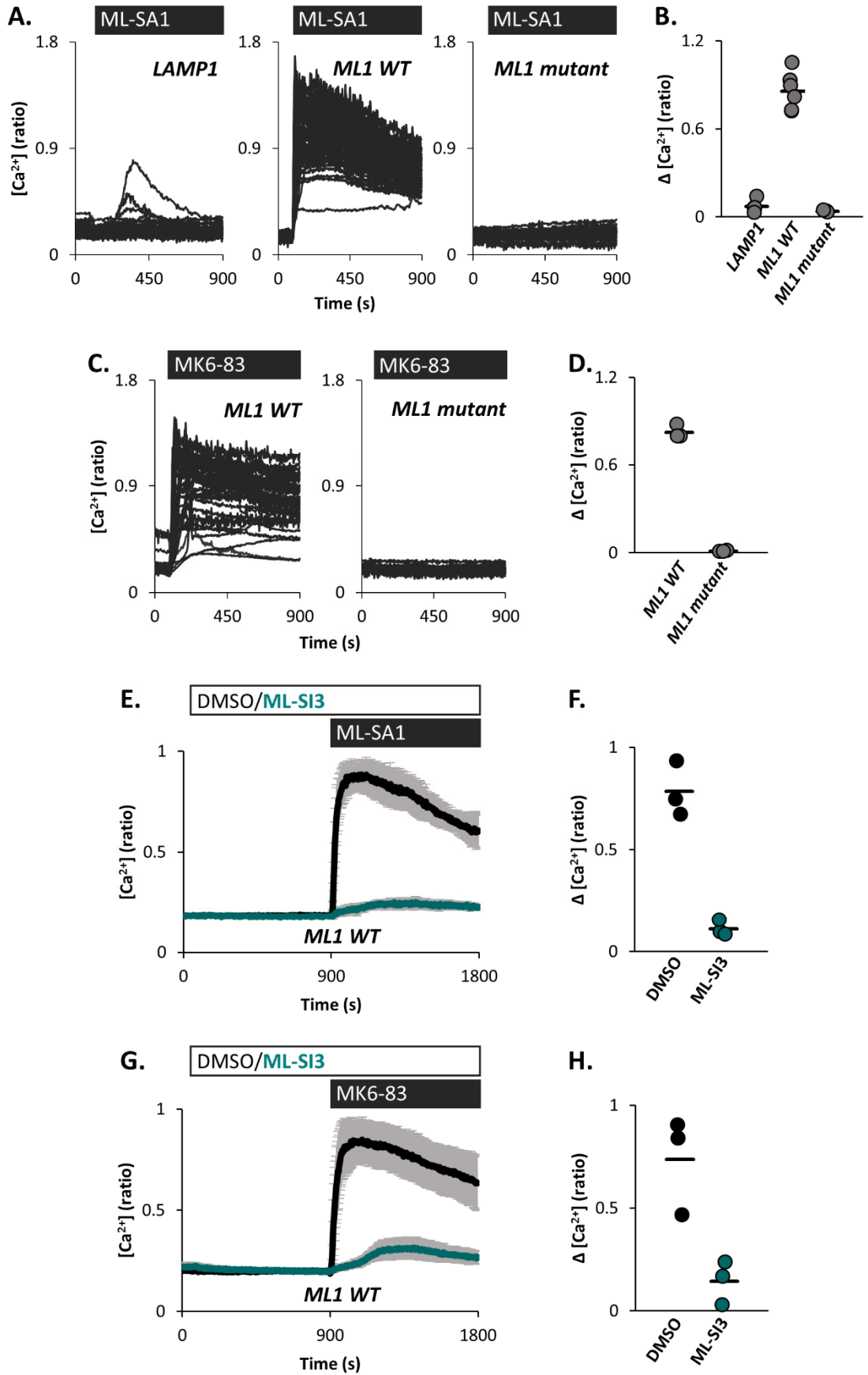


**Figure 2.4 Overexpressed TRPML1 WT potentiates agonist-evoked global  $Ca^{2+}$  signals but TRPML1 mutant does not (legend on next page)**



**(A)** Cytosolic  $\text{Ca}^{2+}$  traces of individual HeLa cells overexpressing GFP-fused *LAMP1*, *ML1* WT or *ML1* mutant, stimulated with ML-SA1 (20  $\mu\text{M}$ ). Each panel displays one representative experiment. **(B)** Data quantifying magnitude of responses exemplified in **A**. Each plot point represents one experiment,  $n=4/6/3$  (*LAMP1/ML1* WT/*ML1* mutant). A total of 134/264/99 (*LAMP1/ML1* WT/*ML1* mutant) cells from 5 independent platings were analysed. **(C)** Cytosolic  $\text{Ca}^{2+}$  traces of HeLa cells overexpressing *ML1* WT or *ML1* mutant, stimulated with MK6-83 (20  $\mu\text{M}$ ). **(D)** Data quantifying magnitude of responses exemplified in **C**,  $n=3/3$  (*ML1* WT/*ML1* mutant). A total of 111/94 (*ML1* WT/*ML1* mutant) cells from 2 independent platings were analysed. **(E and G)** Average cytosolic  $\text{Ca}^{2+}$  traces (mean of experiments  $\pm$  S.E.M) of HeLa cells overexpressing *ML1* WT, stimulated with **(E)** ML-SA1 (20  $\mu\text{M}$ ) or **(G)** MK6-83 (20  $\mu\text{M}$ ), following DMSO or ML-SI3 (10  $\mu\text{M}$ ). **(F and H)** Data quantifying magnitude of the ML-SA1 responses. **(F)** Data for **E**,  $n=3/3$  (DMSO/ML-SI3). A total of 99/85 (DMSO/ML-SI3) cells from 2 independent platings were analysed. **(H)** Data for **G**,  $n=3/3$  (DMSO/ML-SI3). A total of 107/101 (DMSO/ML-SI3) cells from 3 independent platings were analysed.

### 2.3.5 Extracellular $\text{Ca}^{2+}$ contributes to TRPML1-mediated global $\text{Ca}^{2+}$ signals

An initial step to dissect the components of these TRPML1-mediated global  $\text{Ca}^{2+}$  signals was to ascertain the contributions of intracellular  $\text{Ca}^{2+}$  release and extracellular  $\text{Ca}^{2+}$  entry. As usual, ML-SA1-evoked  $\text{Ca}^{2+}$  signals in *ML1* WT cells were large and digital in the presence of extracellular  $\text{Ca}^{2+}$  (Fig. 2.5A and B). However, in the absence of extracellular  $\text{Ca}^{2+}$ , the response was much smaller and more transient. This finding suggests only a small proportion of the TRPML1-mediated  $\text{Ca}^{2+}$  signal comes from release of intracellular  $\text{Ca}^{2+}$  stores.

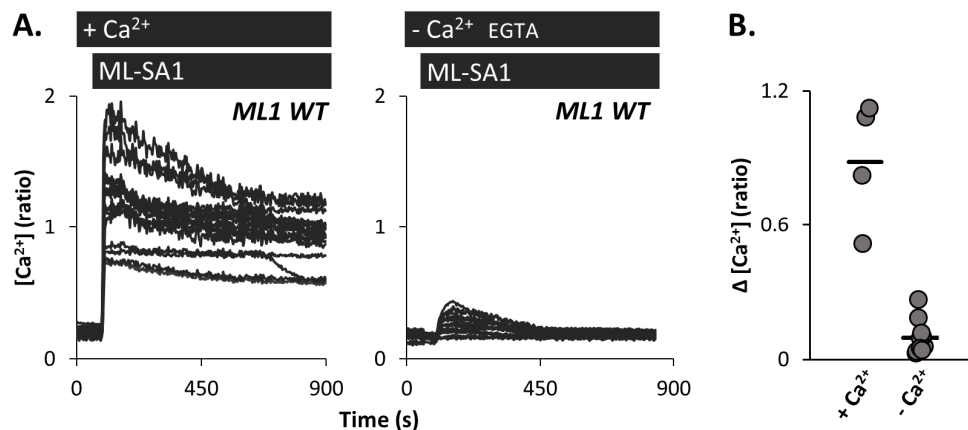


**Figure 2.5 Extracellular  $\text{Ca}^{2+}$  contributes to TRPML1-mediated global  $\text{Ca}^{2+}$  signals**

**(A)** Cytosolic  $\text{Ca}^{2+}$  traces of individual HeLa cells overexpressing *ML1* WT, stimulated with ML-SA1 (20  $\mu\text{M}$ ), either in the presence (+  $\text{Ca}^{2+}$ ) or absence (-  $\text{Ca}^{2+}$ ) of extracellular  $\text{Ca}^{2+}$  ( $\text{Ca}^{2+}$  was replaced with 1mM EGTA). Each panel displays one representative experiment. **(B)** Data quantifying magnitude of

responses exemplified in **A**. Each plot point represents one experiment,  $n=4/10$  (+ Ca<sup>2+</sup>/- Ca<sup>2+</sup>). A total of 70/231 (+ Ca<sup>2+</sup>/- Ca<sup>2+</sup>) cells from 10 independent platings were analysed.

### 2.3.6 Lysomotropic GPN inhibits TRPML1-mediated global Ca<sup>2+</sup> signals

To investigate the relatively small intracellular Ca<sup>2+</sup> release during TRPML1-mediated Ca<sup>2+</sup> signals experiments shown in Figures 2.6A and C were conducted in the absence of extracellular Ca<sup>2+</sup>. Following the vehicle DMSO, ML-SA1 induced a small Ca<sup>2+</sup> signal in cells overexpressing ML1 WT (Fig. 2.6A). However, when ML-SA1 stimulation followed the TRPML1 inhibitor ML-SI3 this signal was blocked. Furthermore, ML-SA1 stimulation failed to induce a response in cells expressing the inactive ML1 mutant, thus attesting to the specificity of the signal. Given the lysosomal localisation of ML1 WT and ML1 mutant (Fig. 2.3) it was suspected that the lysosomes would be required for the ML-SA1-evoked Ca<sup>2+</sup> release. To assess this the peptide GPN was used to compromise the lysosomes. GPN is a lysosomotrope which is cleaved by cathepsin C to generate products that cause lysosomal membrane disruption and leakage of luminal content (Jadot et al., 1984). As shown in Figure 2. 6B GPN caused a marked loss of LTR fluorescence, consistent with an effect on the lysosomes. Following GPN addition the ML-SA1 Ca<sup>2+</sup> signal was inhibited indicating that lysosomes are involved in TRPML1-mediated Ca<sup>2+</sup> release (Fig. 2.6C). Notably though, it appeared that post-GPN ML-SA1 responses were not blocked to the same degree as post-ML-SI3 responses or signals in the ML1 mutant cells (Fig. 2.6D). This suggested there may be some effect of ML-SA1 on Ca<sup>2+</sup> release channels other than TRPML1. To investigate whether ML-SA1 or ML-SI3 might affect Ca<sup>2+</sup> signals mediated by other channels Ca<sup>2+</sup> signals induced by IP<sub>3</sub>-forming histamine were examined in their presence (Bristow et al, 1991; Ishida et al 2014; Soares et al, 2007; Johnson et al, 1990). As shown in Figures 2.6E and F there was no major change to the magnitude of histamine Ca<sup>2+</sup> signals following ML-SA1 or ML-SI3.

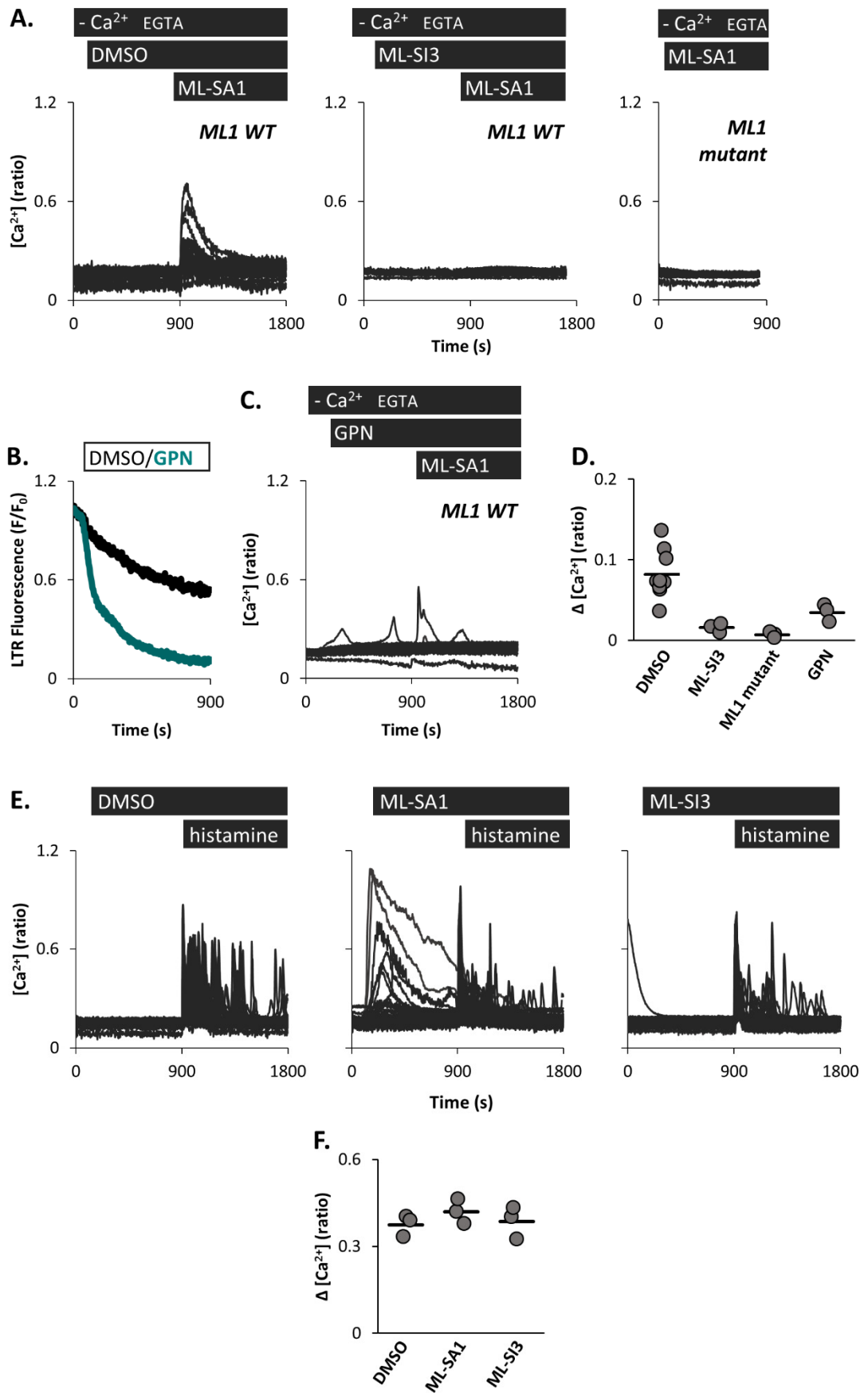


**Figure 2.6** Lysototropic GPN inhibits TRPML1-mediated global  $Ca^{2+}$  signals

(legend on next page)

**(A)** Cytosolic  $\text{Ca}^{2+}$  traces of individual HeLa cells, stimulated with ML-SA1 (20  $\mu\text{M}$ ) in the absence of extracellular  $\text{Ca}^{2+}$  ( $\text{Ca}^{2+}$  was replaced with 1mM EGTA). Left: ML-SA1 response following DMSO in cells overexpressing ML1 WT. Centre: ML-SA1 response following ML-SI3 (10  $\mu\text{M}$ ) in cells overexpressing ML1 WT. Right: ML-SA1 response in cells overexpressing ML1 mutant. Each panel displays one representative experiment. **(B)** Average LysoTracker Red (LTR) fluorescence traces (mean of 2 experiments) of untransfected HeLa cells upon addition of DMSO or GPN (200  $\mu\text{M}$ ). Data presented as ratio of fluorescence compared to basal fluorescence ( $F/F_0$ ). A total of 67/88 (DMSO/GPN) cells from 2 independent platings were analysed. **(C)** Cytosolic  $\text{Ca}^{2+}$  traces of individual HeLa cells overexpressing ML1 WT, stimulated with ML-SA1 (20  $\mu\text{M}$ ) following GPN (200  $\mu\text{M}$ ), in the absence of extracellular  $\text{Ca}^{2+}$  ( $\text{Ca}^{2+}$  was replaced with 1mM EGTA). **(D)** Data quantifying magnitude of ML-SA1 responses exemplified in **A** and **C**. Each plot point represents one experiment,  $n=9/3/3/3$  (DMSO/ML-SI3/ML1 mutant/GPN). A total of 315/60/71/91 cells (DMSO/ML-SI3/ML1 mutant/GPN) from 10 independent platings were analysed. **(E)** Cytosolic  $\text{Ca}^{2+}$  traces of untransfected HeLa cells, stimulated with histamine (10  $\mu\text{M}$ ), following DMSO, ML-SA1 (20  $\mu\text{M}$ ) or ML-SI3 (10  $\mu\text{M}$ ). **(F)** Data quantifying magnitude of histamine responses exemplified in **E**,  $n=3/3/3$  (DMSO/ML-SA1/ML-SI3). A total of 228/283/235 (DMSO/ML-SA1/ML-SI3) cells from 3 independent platings were analysed.

### 2.3.7 SOCE blocker BTP2 does not inhibit TRPML1-mediated global $\text{Ca}^{2+}$ signals

As  $\text{Ca}^{2+}$  entry appeared to be the major component of TRPML1-mediated global  $\text{Ca}^{2+}$  signals experiments were conducted to decipher the route. To assess whether store-operated  $\text{Ca}^{2+}$  entry (SOCE) contributed, the SOCE blocker BTP2 was employed (Ishikawa et al., 2003). In the first instance the ability of BTP2 to block SOCE was tested: In the absence of extracellular  $\text{Ca}^{2+}$  the SERCA inhibitor thapsigargin was used to deplete ER  $\text{Ca}^{2+}$  (Fig. 2.7A).  $\text{Ca}^{2+}$  was subsequently returned to the extracellular medium, inducing a second increase in Fura-2 fluorescence, indicative of SOCE. As expected SOCE was inhibited in the presence of BTP2 (Fig. 2.7.A and B). However, the magnitude of ML-SA1-evoked  $\text{Ca}^{2+}$  signals in ML1 WT cells was not reduced in the presence of BTP2 (Fig. 2.7C and D). This suggested that SOCE was not a major contributor to TRPML1-mediated  $\text{Ca}^{2+}$  signals. It was noted though that the rate of cytosolic  $\text{Ca}^{2+}$  increase in response to ML-SA1 was slowed by BTP2 (Fig. 2.7E and F).

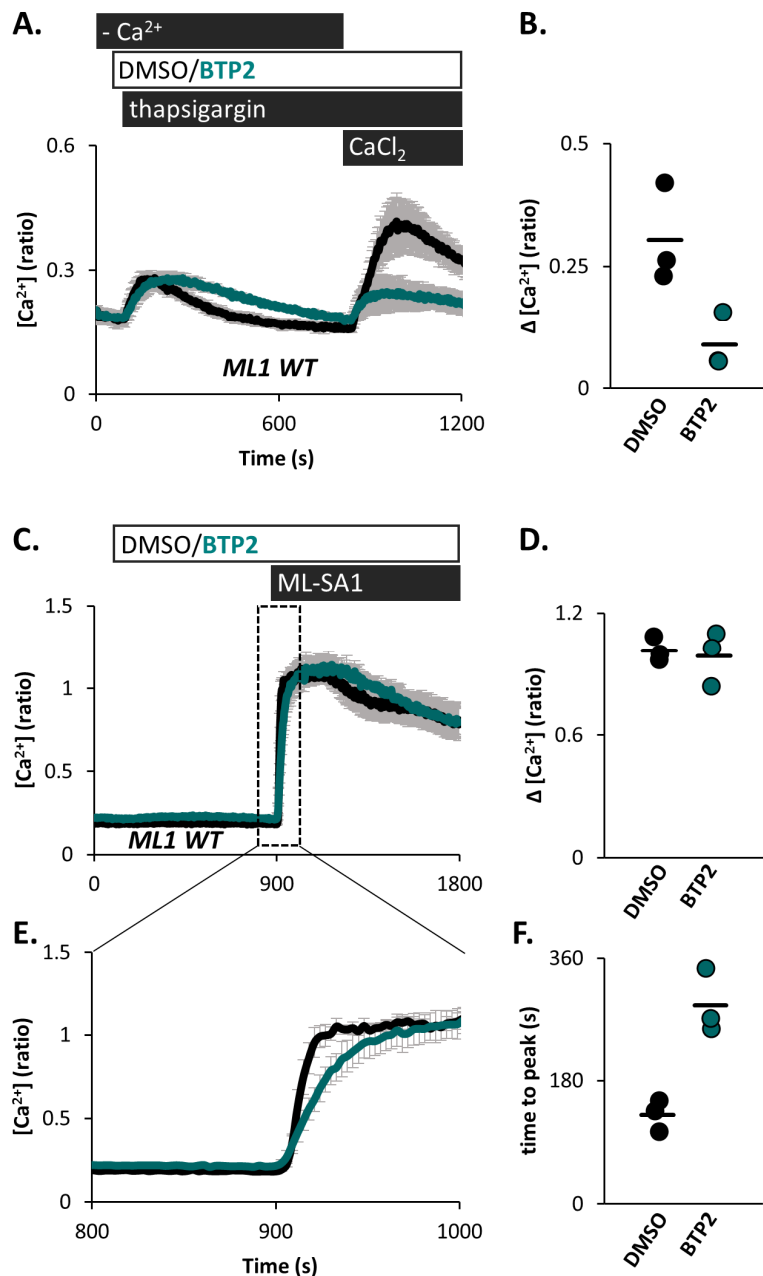


**Figure 2.7 The SOCE blocker BTP2 does not inhibit TRPML1-mediated global Ca<sup>2+</sup> signals**

**(A)** Average cytosolic Ca<sup>2+</sup> traces (mean of experiments ± S.E.M) of HeLa cells overexpressing ML1 WT. In the absence of extracellular Ca<sup>2+</sup> cells were challenged with DMSO or BTP2 (20 μM) followed by thapsigargin (1 μM). Subsequently, Ca<sup>2+</sup> was returned to the extracellular medium by addition of CaCl<sub>2</sub> (2 mM). **(B)** Data quantifying magnitude of the CaCl<sub>2</sub> response in **A**. Each plot point represents one experiment, n=3/3 (DMSO/BTP2). A total of 76 cells per condition from 3 independent platings were analysed. **(C)** Average cytosolic Ca<sup>2+</sup> traces (mean of experiments ± S.E.M) of HeLa cells overexpressing ML1 WT, stimulated with ML-SA1 (20 μM) in the presence of DMSO or BTP2 (20 μM). **(D)** Data quantifying magnitude of the ML-SA1 response in **C**, n=3/3 (DMSO/BTP2). A total of 139/112 (DMSO/BTP2) cells from 3 independent platings were analysed. **(E)** Section of **C**, expanded on the x axis to show rate of increasing cytosolic Ca<sup>2+</sup>. **(F)** Data quantifying time taken to reach peak ML-SA1 signal in **C**, n=3/3 (DMSO/BTP2).

### 2.3.8 TRPML1 agonists permit divalent cation entry

In light of the large  $\text{Ca}^{2+}$  entry component of ML-SA1-evoked  $\text{Ca}^{2+}$  signals, but the small contribution of SOCE, the possibility that TRPML1 directly mediates divalent cation entry was explored. This was done by exploiting the permeability of TRPML1 to  $\text{Fe}^{2+}$ , and the ability of  $\text{Fe}^{2+}$  to quench Fura-2 fluorescence. Briefly, Fura-2 has a stronger affinity for heavy metal ions compared to  $\text{Ca}^{2+}$  (Grynkiewicz et al., 1985) and when bound to  $\text{Fe}^{2+}$  Fura-2 emits negligible fluorescence (Kress et al., 2002). Therefore, if there is a rise in cytosolic  $\text{Fe}^{2+}$ , this can be recorded as a diminishing Fura-2 signal (quench). This technique was used in cells expressing plasma membrane-targeted TRPML1 to confirm the channel's permeability to  $\text{Fe}^{2+}$  (Dong et al., 2008). Here, to measure Fura-2 quench and associated  $\text{Fe}^{2+}$  entry, all experiments were conducted in the absence of extracellular  $\text{Ca}^{2+}$ , and Fura-2 was excited at its isosbestic wavelength (360 nm). This was to ensure that any changes to Fura-2 fluorescence were independent of  $\text{Ca}^{2+}$ . HeLa expressing ML1 WT were first stimulated with ML-SA1 to activate TRPML1, before addition of  $\text{FeCl}_2$  to the extracellular medium. Fura-2 fluorescence dropped sharply upon  $\text{FeCl}_2$  addition (Fig. 2.8A.1). When the cells were challenged with  $\text{FeCl}_3$  instead of  $\text{FeCl}_2$  there was no such drop (Fig. 2.8A2). Quench was also inhibited in the presence of TRPML1 inhibitor ML-SI3 (Fig. 2.8.A3) or in cells expressing the inactive ML1 mutant (Fig. 2.8A4; summary data in Fig. 2.8B and C). Fura-2 quench induced by MK6-83 was less pronounced (Fig. 2.8D and E) but was also blocked in the presence of ML-SI3 or in the ML1 mutant cells. These results provide evidence that active TRPML1 permits entry of divalent cations through the plasma membrane.

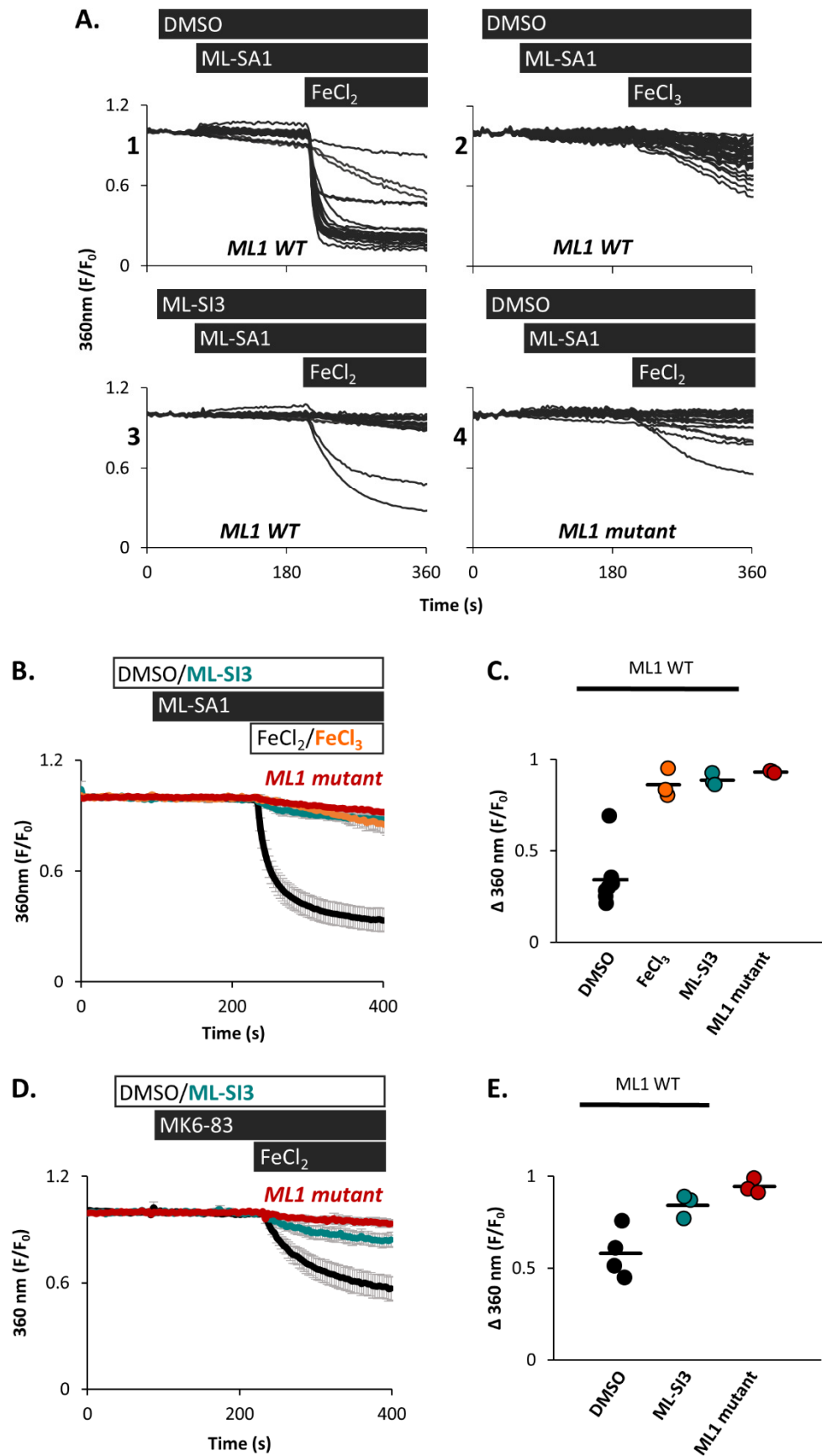


Figure 2.8 TRPML1 agonists permit divalent cation entry (legend on next page)

**(A)** Fura-2 quench traces of individual HeLa cells overexpressing **(1-3)** ML1 WT or **(4)** ML1 mutant. Stimulation with ML-SA1 (20  $\mu$ M) was followed by addition of **(1,3 and 4)** FeCl<sub>2</sub> or **(2)** FeCl<sub>3</sub> (both 1 mM), in the presence of **(1,2 and 4)** DMSO or **(3)** ML-SI3 (10  $\mu$ M). Each panel displays one representative experiment. **(B)** Average Fura-2 quench traces (mean of experiments  $\pm$  S.E.M) corresponding to **A**. **(C)** Data quantifying quench in **A** and **B**. Each plot point represents one experiment, n=7/3/3/3 (DMSO/FeCl<sub>3</sub>/ML-SI3/ML1 mutant). A total of 158/134/80/56 (DMSO/FeCl<sub>3</sub>/ML-SI3/ML1 mutant) cells from 6 independent platings were analysed. **(D)** Average Fura-2 quench traces (mean of experiments  $\pm$  S.E.M) of cells stimulated with alternative TRPML1 agonist MK6-83. **(E)** Data quantifying quench in **D**, n=4/3/3 (DMSO/ML-SI3/ML1 mutant). A total of 87/59/72 (DMSO/ML-SI3/ML1 mutant) cells from 4 independent platings were analysed.



### 2.3.9 Divalent cation entry is inhibited by SOCE blocker BTP2, but is not induced by ER Ca<sup>2+</sup> depletion

TRPML1-mediated Fe<sup>2+</sup> entry, as detected by Fura-2 quench, may be considered as a proxy for TRPML1-mediated Ca<sup>2+</sup> entry (Fig. 2.8). To probe such a comparison the effect of SOCE blocker BTP2 on ML-SA1-evoked Fura-2 quench was tested. In ML1 WT cells BTP2 had a modest effect on ML-SA1-evoked Ca<sup>2+</sup> signals (Fig. 2.7). In contrast though, BTP2 clearly blocked ML-SA1-evoked Fura-2 quench (Fig. 2.9A and B). However, the idea that Fe<sup>2+</sup> entry was store-operated was refuted by a lack of quench following ER Ca<sup>2+</sup> depletion by thapsigargin (Fig. 2.9C and D).

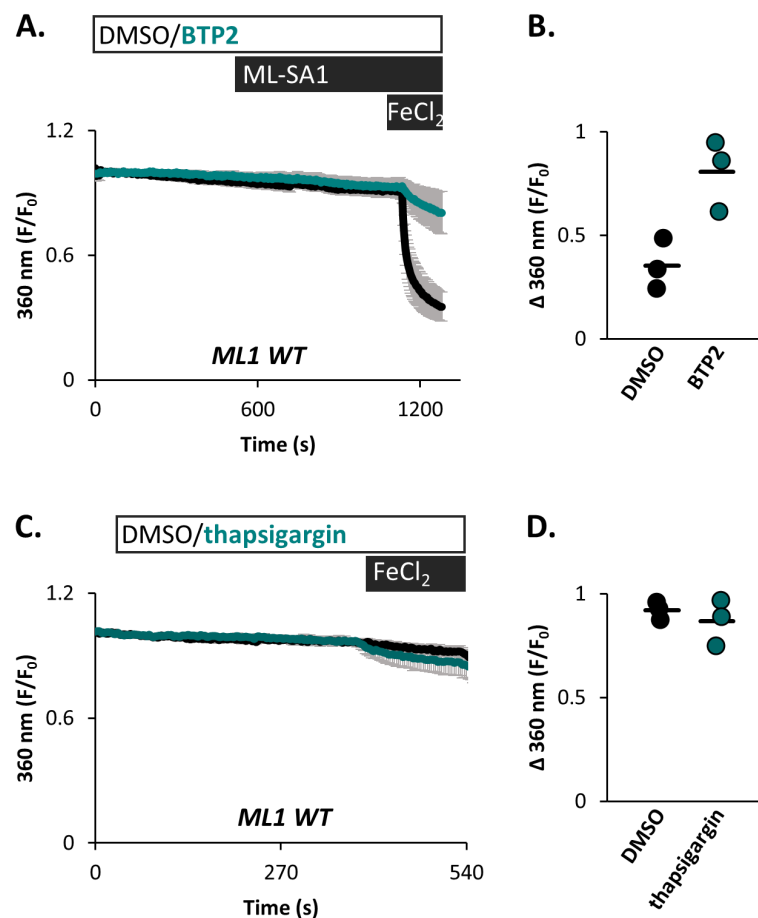


**Figure 2.9 Divalent cation entry is inhibited by SOCE blocker BTP2, but is not induced by ER Ca<sup>2+</sup> depletion**

**(A and C)** Average Fura-2 quench traces (mean of experiments ± S.E.M) of HeLa cells overexpressing ML1 WT. **(A)** Addition of ML-SA1 (20 μM) was followed by FeCl<sub>2</sub> (1 mM), in the presence of DMSO or BTP2 (20 μM). **(B)** Data quantifying Fura-2 quench in **A**. Each plot point represents one experiment, n=3/3 (DMSO/BTP2). A total of 63/64 (DMSO/BTP2) cells from 2 independent platings were analysed. **(C)** Cells were challenged with FeCl<sub>2</sub> (1 mM), following DMSO or thapsigargin (1 μM). **(D)** Data quantifying quench in **C**, n=3/3 (DMSO/thapsigargin). A total of 86/59 (DMSO/thapsigargin) cells from 3 independent platings were analysed.

### 2.3.10 The TRPML1 agonist ML-SA1 evokes global $\text{Ca}^{2+}$ signals in multiple untransfected cell types

Having uncovered the ability of TRPML1 to mediate global  $\text{Ca}^{2+}$  signals in HeLa cells the effect of agonist ML-SA1 was explored in other cell types. ML-SA1-evoked increases in cytosolic  $\text{Ca}^{2+}$  were observed in fibroblasts, SH-SY5Y cells and mouse neurons (Fig. 2.10).

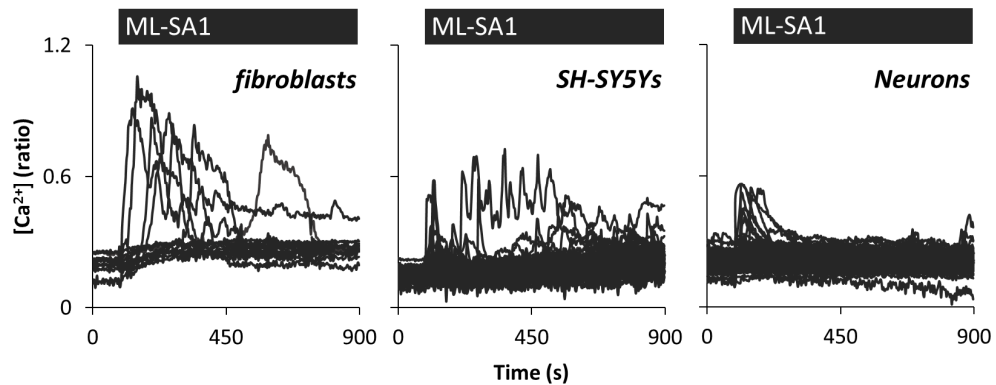


**Figure 2.10 The TRPML1 agonist ML-SA1 evokes global  $\text{Ca}^{2+}$  signals in multiple untransfected cell types**

**(A)** Cytosolic  $\text{Ca}^{2+}$  traces of individual fibroblasts ( $n=14$ ), SH-SY5Ys ( $n=90$ ) or mouse neurons ( $n=90$ ), stimulated with ML-SA1 ( $300\mu\text{M}$ ).

## 2.4 DISCUSSION

Activation of the lysosomal  $\text{Ca}^{2+}$  release channel TRPML1 has been reported to generate local lysosomal  $\text{Ca}^{2+}$  signals, and its dysfunction has been implicated in neurodegenerative diseases such as MLIV and NPC (Bae et al., 2014; LaPlante et al., 2004; Medina et al., 2015; Shen et al., 2012). Here I show that TRPML1 activation can also cause global  $\text{Ca}^{2+}$  signals. Moreover, it is  $\text{Ca}^{2+}$  influx that is the major contributor to these signals despite TRPML1's predominantly intracellular and lysosomal localisation.

To preferentially measure lysosomal  $\text{Ca}^{2+}$  release in intact cells the genetically-encoded  $\text{Ca}^{2+}$  indicator, GCaMP3, has been fused to the lysosomal  $\text{Ca}^{2+}$  release channel TRPML1 (GCaMP3-ML1) (Shen et al., 2012). In cells overexpressing this construct the TRPML1 agonist ML-SA1 evokes an increase in GCaMP3 fluorescence, suggesting that TRPML1 mediates local lysosomal  $\text{Ca}^{2+}$  signals (Bae et al., 2014; Medina et al., 2015; Shen et al., 2012). Using the same probe in HeLa cells I also observed rising GCaMP3 fluorescence in response to ML-SA1 (Fig. 2.1A). However, by measuring the fluorescence of Fura-2 in these cells, global rises in cytosolic  $\text{Ca}^{2+}$  were also apparent (Fig. 2.1B-D). These data raise the possibility that GCaMP3-ML1 does not only detect local lysosomal  $\text{Ca}^{2+}$  signals but global  $\text{Ca}^{2+}$  signals originating from other compartments. In fact, in the data (albeit limited) demonstrating the preferential detection of lysosomal  $\text{Ca}^{2+}$  by GCaMP3-ML1, ER  $\text{Ca}^{2+}$  release could also be recorded by the probe (Shen et al., 2012). In addition, large  $\text{Ca}^{2+}$  signals induced by the  $\text{Ca}^{2+}$  ionophore ionomycin were detected by the probe. These ionomycin signals are unlikely to represent lysosomal  $\text{Ca}^{2+}$  alone as their magnitude is ~8-fold greater than signals induced by lysosomotrope GPN (Shen et al., 2012). Notably, detection of  $\text{Ca}^{2+}$  entry by GCaMP3-ML1 was not assessed by Shen and colleagues as the experiments were conducted in low external  $\text{Ca}^{2+}$ . In this chapter (except where indicated),  $\text{Ca}^{2+}$  signals mediated by endogenous or overexpressed TRPML1 were recorded in the presence of extracellular  $\text{Ca}^{2+}$ , thus providing a more physiologically-relevant backdrop. Indeed, the manifestation of endogenous global TRPML1  $\text{Ca}^{2+}$  signals in the presence of extracellular  $\text{Ca}^{2+}$  may be relevant to TRPML1's role in neurodegenerative disease (Fig. 2.2).

TRPML1 reportedly localises to the lysosomes which is dependent upon its dileucine motifs (Falardeau et al., 2002; Thompson et al., 2007; Vergarajauregui and Puertollano, 2006; Zeevi et al., 2009). Consistent with this I found that GFP-fused ML1 WT and ML1 mutant co-localised with the acidic organelle probe LysoTracker red (LTR) and overexpressed mRFP-LAMP1 (Fig. 2.3B-E). To control for the GFP-ML1 transfection GFP fused to putatively inert LAMP1 was also

overexpressed. In HeLa transfected with LAMP1, ML-SA1-induced  $\text{Ca}^{2+}$  signals were similar to the endogenous signals (Fig. 2.4A cf. Fig. 2.2). This implies that in this context LAMP1 is indeed an inactive protein. In cells overexpressing ML1 WT, TRPML1 agonists ML-SA1 and MK6-83 evoked the same large digital  $\text{Ca}^{2+}$  signals that were seen in cells expressing GCaMP3-ML1 (Fig. 2.4A cf. Fig. 2.1D). Unfortunately, the TRPML1 inhibitor ML-SI1 was unsuitable for confirming the specificity of these signals as it elicited its own  $\text{Ca}^{2+}$  signals (Fig. 2.2C). This may be due to its partial agonist activity at cannabinoid receptor type 2 ( $\text{CB}_2$ ) - a receptor that can elicit global  $\text{Ca}^{2+}$  signals when activated (ML-SI1 is also known as GW405833 hydrochloride; Clayton et al., 2002; Valenzano et al., 2005; Zoratti et al., 2003).

Despite the prevalent lysosomal localisation of ML1 WT intracellular  $\text{Ca}^{2+}$  release made a relatively small contribution to the ML-SA1-induced global  $\text{Ca}^{2+}$  signals (Fig. 2.5). Rather, it was  $\text{Ca}^{2+}$  entry that constituted the major portion of the response. Lysosome involvement was however indicated when the intracellular  $\text{Ca}^{2+}$  release was inhibited by the lysosomotrope GPN (Fig. 2.6A-D). It was noted though that GPN did not block ML-SA1-induced  $\text{Ca}^{2+}$  release to the same degree as ML-SI3 nor the ML1 mutant. This may indicate that ML-SA1 stimulates  $\text{Ca}^{2+}$  release from channels other than TRPML1. To probe this the effect of ML-SA1 or ML-SI3 on  $\text{Ca}^{2+}$  signals induced by  $\text{IP}_3$ -forming histamine was assessed (Bristow et al., 1991; Ishida et al., 2014; Johnson et al., 1990). The magnitude of the histamine signal was slightly greater in the presence of ML-SA1 but unaffected by ML-SI3 (Fig. 2.6E and D). This suggests that ML-SI3 does not inhibit  $\text{Ca}^{2+}$  signals mediated by  $\text{IP}_3$  receptors. To extrapolate, the residual ML-SA1-evoked  $\text{Ca}^{2+}$  signal that is left in the wake of lysosome disruption, but blocked by ML-SI3, is not likely due to ML-SA1 activation of the  $\text{IP}_3$  receptor. This may be clarified by assessing the effect of ML-SA1 or ML-SI3 on  $\text{Ca}^{2+}$  signals evoked by membrane-permeable  $\text{IP}_3$  derivatives. Similar experiments centred on ryanodine receptors may also be informative.

That ML-SA1 does not directly activate  $\text{IP}_3$  receptors does not however discount their involvement in ML-SA1-evoked  $\text{Ca}^{2+}$  signals. Indeed, acute treatment of HeLa with 2-APB to block the  $\text{IP}_3$  receptors does reduce the magnitude of subsequent ML-SA1-evoked  $\text{Ca}^{2+}$  signals (Kilpatrick et al., 2016a). Depletion of ER  $\text{Ca}^{2+}$  by thapsigargin also inhibits the response. This indicates that activation of this lysosomal  $\text{Ca}^{2+}$  channel (TRPML1) induces ER  $\text{Ca}^{2+}$  release, perhaps in a similar mode to  $\text{Ca}^{2+}$  signals triggered by NAADP (Morgan, 2016).

In regard to the extensive  $\text{Ca}^{2+}$  entry caused by ML-SA1 in ML1 WT cells SOCE was considered as a possible entry route. As part of the investigation the pyrazole BTP2 was used. BTP2 can block

thapsigargin-induced SOCE (Ishikawa et al., 2003) which was also demonstrated here (Fig. 2.7A and B). Intriguingly, BTP2 also modulated the  $\text{Ca}^{2+}$  signal evoked by thapsigargin which appeared slightly potentiated. This raises the possibility that BTP2 inhibits a route of cytosolic  $\text{Ca}^{2+}$  extrusion besides SERCA or inhibits another mechanism of  $\text{Ca}^{2+}$  signal silencing. Nevertheless, although BTP2 inhibited SOCE, its inhibitory effect on the large ML-SA1-evoked  $\text{Ca}^{2+}$  signals in ML1 WT cells was very modest (Fig. 2.7C-F). This suggests that whilst SOCE may have a small role in TRPML1-mediated  $\text{Ca}^{2+}$  entry it is not the principle route.  $\text{Ca}^{2+}$  entry mediated directly by TRPML1 at the plasma membrane was also explored. TRPML1 activation and addition of  $\text{Fe}^{2+}$  into the extracellular medium resulted in a quench of Fura-2 fluorescence. This is indicative of  $\text{Fe}^{2+}$  entry through TRPML1 at the plasma membrane, into the cytosol (Dong et al., 2008; Kress et al., 2002). To surmise, if divalent  $\text{Fe}^{2+}$  can enter the cell directly through TRPML1 at the plasma membrane, so may  $\text{Ca}^{2+}$ .

Adding a layer of complexity to TRPML1-mediated cation entry are two results regarding the  $\text{Fe}^{2+}$  entry/Fura-2 quench. First, SOCE blocker BTP2 substantially inhibited Fura-2 quench following ML-SA1 stimulation (Fig. 2.9A and B). This result may be interpreted to mean that Fura-2 quench represents store-operated cation entry. Discounting this notion however was the result that ER  $\text{Ca}^{2+}$  depletion by thapsigargin did not induce Fura-2 quench (Fig. 2.9D). Therefore, Fura-2 quench was not likely representative of store-operated cation entry. A possible explanation for these contradictory results is that BTP2 directly inhibits TRPML1 in a similar manner to its inhibitory effect on TRPCs, and that the principle SOCE channels are not  $\text{Fe}^{2+}$ -permeable (He et al., 2005). Why though BTP2 blocks TRPML1-mediated  $\text{Fe}^{2+}$  entry but not TRPML1-mediated  $\text{Ca}^{2+}$  signals, which are largely composed of  $\text{Ca}^{2+}$  entry, is unknown. It is possible that TRPML1-mediated entry of  $\text{Ca}^{2+}$  or  $\text{Fe}^{2+}$  is differentially regulated by the TRPML1-mediated intracellular  $\text{Ca}^{2+}$  release. Perhaps the coordination between  $\text{Ca}^{2+}$  release and  $\text{Ca}^{2+}$  entry somehow overrides BTP2's inhibitory effect on TRPML1 at the plasma membrane. By inhibiting the intracellular  $\text{Ca}^{2+}$  release with GPN its differential regulation of TRPML1-mediated  $\text{Ca}^{2+}$  and  $\text{Fe}^{2+}$  entry may be uncovered.

That TRPML1 at the plasma membrane mediates considerable  $\text{Ca}^{2+}$  or  $\text{Fe}^{2+}$  entry, is at odds with the largely lysosomal habitation of ML1 WT and ML1 mutant (Fig. 2.3). It may also challenge the report that PM-targeted TRPML1 is inactive in the context of rescuing trafficking defects (Pryor et al., 2006). However, TRPML1 expression at the plasma membrane has been reported (Kiselyov et al., 2005). Moreover, this expression is more pronounced with the constitutively active form of the channel and may be a result of upregulated lysosomal exocytosis (Dong et al.,

2009; LaPlante et al., 2006). Perhaps then, by activating lysosomal TRPML1 with ML-SA1 or MK6-83, lysosomal exocytosis is triggered and TRPML1 is directed to the plasma membrane where it permits  $\text{Ca}^{2+}$  or  $\text{Fe}^{2+}$  entry. The possibility of such a change in TRPML1 localisation should be investigated using total internal reflection fluorescence (TIRF) microscopy (Brailoiu et al., 2010a; Sreetama et al., 2016). In the argument against TRPML1 activity at the plasma membrane, TRPML1 currents are greater in acidic environments (such as the lysosomes) compared to neutral ones (such as the plasma membrane) (Chen et al., 2014; Dong et al., 2008; Feng et al., 2014a; Xu et al., 2007). It should be noted however that acidic pH has been shown to inhibit TRPML1 activity and that elevated lysosomal pH has been linked to larger ML-SA1-evoked  $\text{Ca}^{2+}$  signals (Lee et al., 2015; Raychowdhury et al., 2004). Returning to the argument against plasma membrane TRPML1 activity, it has also been suggested that TRPML1 is less active here due to the presence of  $\text{PI}(4,5)\text{P}_2$  and high extracellular  $\text{Ca}^{2+}$  (Li et al., 2017; Zhang et al., 2012).

There is also a possibility that endogenous TRPML3 mediates the  $\text{Ca}^{2+}$  entry. Unlike TRPML1 and 2, which predominantly localise to the lysosomes, TRPML3 has been reported to localise at the plasma membrane (Grimm et al., 2007; Kim et al., 2007, 2009). Furthermore, the predecessors of ML-SA1 and MK6-83 were identified using recombinant TRPML3, and ML-SA1 is capable of activating whole cell currents in cells overexpressing TRPML3 (Grimm et al., 2010; Shen et al., 2012). An argument to counter this is the requirement of a low  $\text{Na}^+$  medium for TRPML3 activity, which was not used here (Grimm et al., 2010; Kim et al., 2007). In addition, ML-SA1 and MK6-83 failed to evoke  $\text{Ca}^{2+}$  signals in cells overexpressing the ML1 mutant (Fig.2.4A-D). Yet, the complete lack of signal in ML1 mutant cells suggests it has a dominant negative effect on endogenous TRPML1. This effect may also inhibit endogenous TRPML3 through heterooligomerisation (Curcio-Morelli et al., 2010b; Venkatachalam et al., 2006). Finally, in the case against TRPML3 involvement, this isoform is not permeable to  $\text{Fe}^{2+}$  (Dong et al., 2008). Therefore, the sharp entry of divalent cations in Figure 2.8 is presumed to be mediated by TRPML1 alone. However, to discount TRPML3 involvement in  $\text{Ca}^{2+}$  entry TRPML1-mediated  $\text{Ca}^{2+}$  signals must be examined in cells with reduced TRPML3 expression.

Here, global  $\text{Ca}^{2+}$  signals mediated by TRPML1 have been generated using synthetic TRPML1 agonists. The physiological relevance of these global  $\text{Ca}^{2+}$  signals is dependent upon the identification of endogenous TRPML1 agonists that generate similar signals. Currently, one prominent candidate is phosphatidylinositol 3,5-bisphosphate ( $\text{PI}(3,5)\text{P}_2$ ) (Dong et al., 2010). However, although  $\text{PI}(3,5)\text{P}_2$  activates TRPML1 currents, it has not been shown to initiate its own  $\text{Ca}^{2+}$  signals. The  $\text{Ca}^{2+}$  mobilising messenger NAADP has also been shown to elicit TRPML1-

dependent global  $\text{Ca}^{2+}$  signals, although this has been contended (Yamaguchi et al., 2011; Zhang et al., 2009, 2011). Another approach to determine the relevance of TRPML1 to global  $\text{Ca}^{2+}$  signalling is to assess the channel's contribution to physiological signals elicited by extracellular stimuli. A handful of studies have done this by knocking out TRPML1, or using MLIV mutants. For example, in TRPML1-deficient cells,  $\text{Ca}^{2+}$  signals induced by cholecystokinin and endothelin-1 (ET-1) are inhibited (Park et al., 2016; Zhang et al., 2009), and in F408 $\Delta$  MLIV fibroblasts  $\text{Ca}^{2+}$  signals were inhibited in response to thrombin (LaPlante et al., 2004). LaPlante and colleagues acknowledged that this could be due to impaired  $\text{Ca}^{2+}$  mobilisation from late endosomes/lysosomes, sub-optimal targeting of mutant TRPML1 to these compartments, or a more indirect effect via a remodelled  $\text{Ca}^{2+}$  signalling network. Elsewhere, bradykinin-evoked  $\text{Ca}^{2+}$  signals were no smaller in MLIV cells but were slightly delayed (Soyombo et al., 2006). Besides reducing TRPML1 expression or using TRPML1 mutants such studies may benefit from the use of TRPML1 inhibitor ML-SI3, which as shown here can robustly block TRPML1-mediated global  $\text{Ca}^{2+}$  signals.

As a final point, the use of GCaMP3-ML1 or GECO-ML1 to measure  $\text{Ca}^{2+}$  signals emanating from TRPML1 in disease models may not be wholly appropriate. This is because overexpression of TRPML1 or activation of TRPML1 has been shown to alter disease phenotypes (Cao et al., 2015b; Chen et al., 2014; Shen et al., 2012). Similarly overexpression of GCaMP3- or GECO-ML1 might be expected to cause phenotypic changes and conceivably remodel the  $\text{Ca}^{2+}$  signalling network. Therefore,  $\text{Ca}^{2+}$  release as measured by these constructs may be influenced by their own overexpression and not represent a pure read-out of TRPML1  $\text{Ca}^{2+}$  signalling in disease. Here, ML-SA1-evoked  $\text{Ca}^{2+}$  signals in cells overexpressing lysosomal LAMP1 were comparable to endogenous responses (Fig. 2.4A cf. 2.2A and B). Therefore, LAMP1 may be a more appropriate protein to fuse to GCaMP3 or GECO to compare TRPML1-mediated  $\text{Ca}^{2+}$  signals in health and disease (McCue et al., 2013).

To summarise, the lysosomal  $\text{Ca}^{2+}$  channel TRPML1 has previously been associated with local lysosomal  $\text{Ca}^{2+}$  release and is relevant to neurodegenerative diseases such as MLIV and NPC. In this chapter I demonstrated that TRPML1 activation can also cause global  $\text{Ca}^{2+}$  signals. Furthermore, these signals are largely composed of  $\text{Ca}^{2+}$  entry across the plasma membrane despite the predominant lysosomal localisation of the channel. These new aspects of TRPML1 signalling may shed new light upon the channel's role in neurodegenerative disease and should be considered in the development of TRPML1-targeting therapeutics.

# CHAPTER 3: TPCs and Global Ca<sup>2+</sup> Signalling

## - in Familial and Sporadic PD Fibroblasts

### 3.1 INTRODUCTION

The *LRRK2* G2019S (*LRRK2*-GS) mutation accounts for ~5% of familial PD and ~1% of sporadic PD cases (Bardien et al., 2011; Healy et al., 2008). Furthermore, the symptoms of familial *LRRK2*-GS PD are indistinguishable from those of sporadic PD. Therefore, *LRRK2* is a rational focus of PD research both to delineate the aetiology of familial PD and as a possible bridge to uncovering the pathogenic mechanisms of sporadic PD.

Mutant *LRRK2*'s mode of pathogenicity is unclear as the *LRRK2* enzyme has been linked to a plethora of cellular processes (Manzoni et al., 2015; Porras et al., 2015). Reports though of a functional association with Rab GTPases have implicated *LRRK2* in the regulation of lysosomal trafficking and morphology (Dodson et al., 2012; Gómez-Suaga et al., 2014; MacLeod et al., 2013; Shin et al., 2008; Steger et al., 2016). For example, in flies, the overexpression of pathogenic *LRRK2*-GS and Rab7 promotes perinuclear lysosome clustering which is thought to promote autophagy (Dodson et al., 2012; Korolchuk and Rubinsztein, 2011). In addition, lysosomal morphology defects in *LRRK2*-GS PD patient fibroblasts can be improved by inhibiting Rab7 (Hockey et al., 2015).

Recently, data has surfaced to implicate the lysosomal Ca<sup>2+</sup> channel TPC2 in *LRRK2* PD. First, there is evidence that TPCs interact with Rab7 (Lin-Moshier et al., 2014). Moreover, defective lysosome morphology in *LRRK2*-GS PD fibroblasts could be improved by reducing TPC2 expression as an alternative to Rab7 inhibition (Hockey et al., 2015). This defect could also be improved by chelating local Ca<sup>2+</sup> with cell-permeable BAPTA. These findings suggest that upregulated local Ca<sup>2+</sup> release through TPC2 is a feature of *LRRK2*-GS PD. As part of the endolysosomal system lysosomes are interconnected with numerous cellular processes. Therefore, lysosome morphology disturbances may signify poor lysosomal health that might impact the cell globally. Indeed, TPC2 and local Ca<sup>2+</sup> have been implicated in *LRRK2*-dependent autophagy defects (Gómez-Suaga et al., 2012). Such defects may contribute to neurodegeneration by permitting the accumulation of pathogenic molecules, or the survival of defective mitochondria that are less able to buffer Ca<sup>2+</sup> or synthesise ATP (Cherra et al., 2013; Heeman et al., 2011; Rott et al., 2011). In fact, in the study by Gómez-Suaga and colleagues, the



LRRK2-dependent autophagy defect sensitised cells to death when under further proteostatic stress (Gómez-Suaga et al., 2012). Therefore, TPC2 over-activity and local  $\text{Ca}^{2+}$  signalling may be particularly relevant in the context of PD and the vulnerable SNc.

One question arising from the observation of disturbed lysosome morphology in familial LRRK2-GS PD fibroblasts, is whether it is also disturbed in sporadic PD. Indeed, a coveted outcome of PD research is to identify unifying mechanisms of disease across all patients regardless of genotypes. Sporadic PD constitutes ~90% of PD cases and therefore the identification of appropriate therapeutic targets in these patients has the potential to improve quality of life for millions (Gandhi and Wood, 2010).

The lysosome morphology defects in LRRK2-GS PD fibroblasts were ascribed to upregulated TPC2 activity and local  $\text{Ca}^{2+}$  signals (Hockey et al., 2015; Pryor et al., 2000). In addition, these cells exhibited augmented global  $\text{Ca}^{2+}$  signals in response to the mobilising messenger NAADP (Hockey et al., 2015). Although there has been some controversy around TPC activation there is evidence that NAADP causes TPC-dependent global  $\text{Ca}^{2+}$  signals (Brailoiu et al., 2009; Calcraft et al., 2009; Jha et al., 2014). Taken together this may indicate that upregulated TPC activity in LRRK2-GS PD fibroblasts is responsible for augmented global  $\text{Ca}^{2+}$  signals as well as local ones. However, whether physiological global  $\text{Ca}^{2+}$  signals evoked by extracellular stimuli are also augmented is unknown, and is a focus of this chapter.

Although various extracellular stimuli have been associated with NAADP synthesis (Table 1.1) there is very little data about those which require TPCs to evoke their global  $\text{Ca}^{2+}$  signals. Therefore, an intermediate aim of this chapter is to identify an extracellular agonist that requires TPCs to elicit physiological global  $\text{Ca}^{2+}$  signals. The final aim is to determine whether such TPC-dependent, physiological global  $\text{Ca}^{2+}$  signals are augmented in familial and sporadic PD fibroblasts. If so this would support the notion that TPC activity is upregulated in PD. Furthermore, augmented global  $\text{Ca}^{2+}$  signals may cause cell-wide disruption to  $\text{Ca}^{2+}$ -dependent processes such as protein folding or ATP synthesis (Glancy and Balaban, 2012; Wang and Kaufman, 2016). Such signals may also cause mitochondrial  $\text{Ca}^{2+}$  overload and promote cell death (Rizzuto et al., 2012). Therefore, upregulated TPC activity may contribute to neurodegeneration by augmenting global  $\text{Ca}^{2+}$  signals as well as local ones (Fig. 3.1).

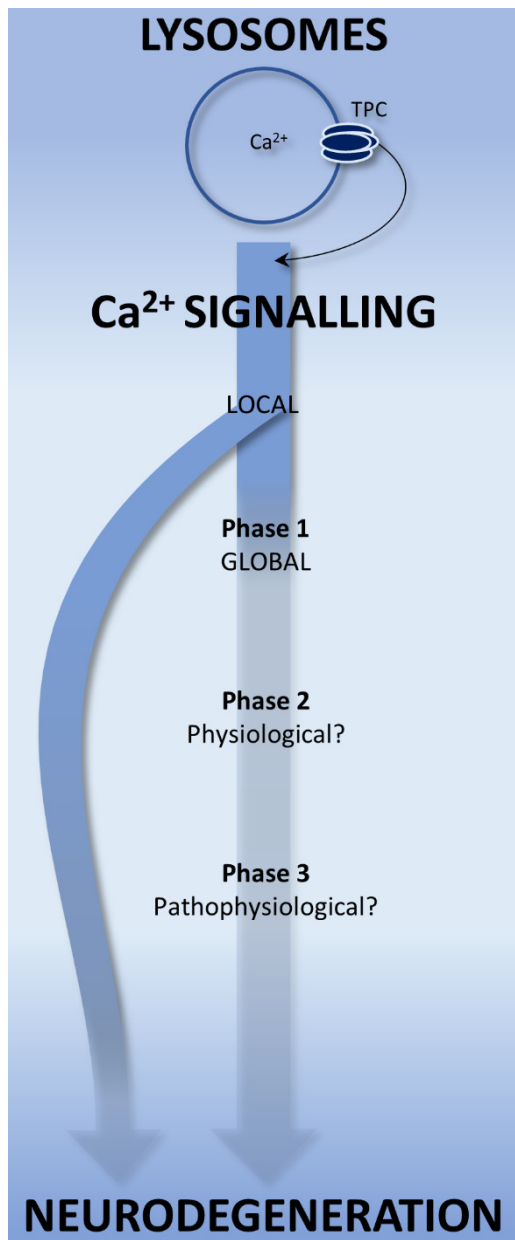


### Figure 3.1 Introduction

The lysosomal Ca<sup>2+</sup> channel TPC2 has been implicated in PD that is linked to dysfunction of the enzyme LRRK2.

There is some evidence that upregulated TPC activity disturbs local Ca<sup>2+</sup> signalling, which may contribute to neurodegeneration (curved left-hand arrow). Upregulated TPC activity may also contribute to neurodegeneration by disturbing global Ca<sup>2+</sup> signals (straight right-hand arrow).

This global route to neurodegeneration is a possibility as it has been reported that TPCs are required for global Ca<sup>2+</sup> signals stimulated by NAADP (Phase 1). However, there is very little information on whether TPCs are important for physiological global Ca<sup>2+</sup> signals evoked by extracellular stimuli (Phase 2). Furthermore, it is not known whether TPC-dependent, physiological global Ca<sup>2+</sup> signals are augmented in PD and thus are of pathophysiological importance (Phase 3). In this chapter these two phases are addressed.

## 3.2 METHODS and ANALYSIS

### 3.2.1 Recurrent methods

Fura-2 labelling and data presentation are as described in Chapter 2.

### 3.2.2 Cell culture

#### 3.2.2.1 Fibroblast

Fibroblasts were maintained and passaged as described in Chapter 2. Primary human skin fibroblast cultures were generated from biopsies and obtained from Drs Michelle Beavan, Alisdair McNeill, Jan-Willem Taanman and Tatiana Papkovskaia (Department of Clinical Neuroscience, UCL). Data from affected fibroblasts were compared to that of age-matched controls never more than 2 passages apart. Sporadic PD patients were not genotyped as there was no family history of the disease. Details of the patient fibroblasts are listed in the table below:

**Table 3.1 Patient-derived fibroblasts**

ID	Status	Age	Sex
Ctrl1	Healthy Control	52	F
Ctrl2 #	Healthy Control	50	F
Ctrl3	Healthy Control	55	F
LRRK2-GS PD1 #	Familial LRRK2 G2019S PD	52	F
LRRK2-GS PD2 #	Familial LRRK2 G2019S PD	48	F
Ctrl4	Healthy Control	82	F
Ctrl5	Healthy Control	78	M
sp PD1	Sporadic PD	81	F
sp PD2	Sporadic PD	79	M

#=sisters; F=female; M=male

Cells were plated onto 13 mm glass coverslips (in a 24-well plate, 0.5 ml/coverslip) 5-7 days prior to imaging or fixation. Cells were ~80-90% confluent on the day of imaging or fixation. Some Ctrl fibroblasts were treated with vacuolin (5 $\mu$ M; VWR) or vehicle (DMSO; Sigma) for 5 hours prior to fixation.

### 3.2.3 Immunocytochemistry

Fibroblasts were fixed for 10 minutes with 4% w/v paraformaldehyde, washed three times in phosphate-buffered saline (PBS) and then permeabilised for 10 minutes with 40  $\mu$ M  $\beta$ -escin.

Cells were washed again (x3 in PBS) and blocked for 1 hour with PBS supplemented with 1% (w/v) bovine serum albumin (BSA) and 10% (v/v) foetal bovine serum (FBS). Fibroblasts were sequentially incubated for 1 hour at 37°C with anti-LAMP1 antibody (mouse, Developmental Hybridoma Bank H4A3 clone supernatant; 1/10 dilution) and anti-mouse Alexa Fluor® 647 dye (donkey, Invitrogen; 1/1000 dilution) in blocking solution. Nuclei were labelled by incubation for 5 minutes with 1 µg/ml 4',6-diamidino-2-phenylindole (DAPI) (Sigma). Cells were washed three times in PBS containing 0.1% (v/v) Tween in between incubations. Coverslips were mounted onto microscope slides with DABCO (1,4 diazabicyclo[2,2,2]octane) and sealed with colourless, transparent nail varnish.

### 3.2.4 Microscopy: Confocal

Images were captured using an LSM510 confocal scanner (Zeiss) attached to a Zeiss Axiovert 200M inverted microscope fitted with a 63x Plan Apochromat water-immersion objective. Excitation and emission wavelengths for fluorescent markers are detailed below:

<b>Probe</b>	<b>Excitation wavelength (nm)</b>	<b>Emission filter wavelength (nm)</b>
DAPI	364	LP 385
AlexaFluor 647	633	LP 650 or BP 655-719

Microscope settings (including master gain, detectors, filters and pinhole) were kept constant on a given day to compare affected and control groups. Zoomed images were taken at a 4x optical zoom.

The pairings between data from control and affected/treated groups are determined by the day of image acquisition. Paired groups were also simultaneously passaged, plated, treated, fixed, and subjected to immunocytochemistry. Each data point corresponds to mean values from all cells in a group that were imaged on a single day. Where two fibroblast lines were used for one group the mean of the two cell line means was calculated for the result.

#### 3.2.4.1 Automated image analysis for LAMP1 intensity

12-bit immunofluorescence images were analysed using the Fiji software package of ImageJ. For each cell a region of interest (ROI) was manually drawn to contain its lysosome population. One background ROI per image was also drawn. The channel displaying LAMP1 immunofluorescence was saved with ROIs overlaid as a TIFF file. These files were processed by the Multiple Image

Processor plugin, and a macro (Fig. 3.M.1) was employed with mean grey value set as the output in results. Results were compiled and analysed in Microsoft Excel.

```
1 id = getImageID();
2 run("To ROI Manager");
3 roiManager("Measure");
```

**Figure 3.M.1 Macro commands for LAMP1 intensity analysis**

### 3.2.4.2 Automated image analysis for lysosome size and frequency

Briefly, TIFF files were created as for LAMP1 intensity analysis but with background ROIs omitted. These images were converted from 12 to 8-bit to enable processing by the Auto Local Threshold plugin which binarised them into white objects and black background. Average object size per cell and object frequency per cell were measured from these binary images using the “Analyse Particle” function. The method is described in detail below.

#### 3.2.4.2.1 Generating binary images by local thresholding

To ensure this image processing and analysis could identify changes in lysosome size fibroblasts were treated with vacuolin before fixation, immunocytochemistry and microscopy, as described in METHODS and ANALYSIS sections 3.2.2-3.2.4 (Fig. 3.M.2). Vacuolin enlarges LAMP1-positive structures therefore any viable mode of image processing and analysis should report this in the results (Cerny et al., 2004; Huynh and Andrews, 2005).

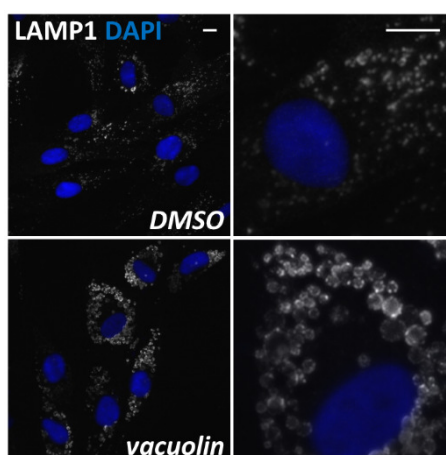


**Figure 3.M.2 LAMP1-positive structures are enlarged in fibroblasts treated with vacuolin**

Representative immunofluorescence images of LAMP1 staining (white) in Ctrl fibroblasts treated with *DMSO* or *vacuolin* (5  $\mu$ M) for 5 hours before fixing. Nuclei are stained blue (DAPI). Right-hand images are 4x optical zooms of individual cells in left-hand images. Scale bar = 10  $\mu$ m.

Binary images were generated according to local contrasts. This has advantages over global thresholding which employs a single grey value cut-off to define structures. When the ImageJ thresholder (accessed by: Image>Adjust>Threshold) is in default mode the intensity chosen is based on an iterative intermeans algorithm (Li, 1998; T.W Ridler and Calvard, 1978). Source code can be viewed here:

<https://imagej.nih.gov/ij/source/ij/plugin/Thresholder.java>;

<https://imagej.nih.gov/ij/source/ij/process/AutoThresholder.java>

Initially a low threshold is chosen by the algorithm. The image pixels are then defined as objects if their grey level values are above this threshold or as background if their grey level values are below. A calculation based on the average grey values of object and background pixels is then executed.

If:  $(\text{Av. OBJECT GREY VALUE} + \text{Av. BACKGROUND GREY VALUE}) / 2 < \text{THRESHOLD}$

the threshold is incremented by 1 grey value and the process is iterated.

If however:  $(\text{Av. OBJECT GREY VALUE} + \text{Av. BACKGROUND GREY VALUE}) / 2 = \text{THRESHOLD}$

the process stops here and that threshold is the implemented global threshold that appears in the ImageJ console. The user can use the unique automated threshold that is generated for each image or chose a threshold experimentally. Using a simplified representation of a 16x16 pixel 8-bit image (Fig. 3.M.3A) this global thresholding can be readily visualised. The global threshold set by the iterative algorithm for this image would be 112. Consequently all pixels with a grey value of 112 and above are transformed into an object and appear white in the generated binary image (Fig. 3.M.3B and C). All pixels with a grey value less than 112 are transformed into black background. Two issues with this method that are illustrated in Figure 3.M.3C are that objects of low fluorescence intensity are ignored and objects of high intensity can be artificially aggregated. Although by eye there appears to be a dim object in the top left (circled, red) it is assigned as background. At the bottom of the image there appears to be two distinct brighter objects (arrows, red). However, some of the pixels in between are assigned as object, therefore they appear as one object in the binary image. An additional problem is that only the brighter apices of particles may be defined as object, which can then skew size data (Fassina et al., 2012).

**A.**

80	80	80	80	96	96	96	96	48	48	48	48	240	240	240	240
80	80	80	80	96	96	96	96	48	48	48	48	240	240	240	240
80	80	80	80	96	96	96	96	48	48	48	48	240	240	240	240
80	80	80	80	96	96	96	96	48	48	48	48	240	240	240	240
0	0	0	0	32	32	32	32	16	16	16	16	144	144	144	144
0	0	0	8	32	32	32	32	16	16	16	16	144	144	144	144
0	0	0	0	32	32	32	32	16	16	16	16	144	144	144	144
0	0	0	0	32	32	32	32	16	16	16	16	144	144	144	144
128	128	128	128	112	112	112	112	160	160	160	160	176	176	176	176
128	128	128	128	112	112	112	112	160	160	160	160	176	176	176	176
128	128	128	128	112	112	112	112	160	160	160	160	176	176	176	176
128	128	128	128	112	112	112	112	160	160	160	160	176	176	176	176
192	192	192	192	64	64	64	64	224	224	224	224	208	208	208	208
192	192	192	192	64	64	64	64	224	224	224	224	208	208	208	208
192	192	192	192	64	64	64	64	224	224	224	224	208	208	208	208
192	192	192	192	64	64	64	64	224	224	224	224	208	208	208	208

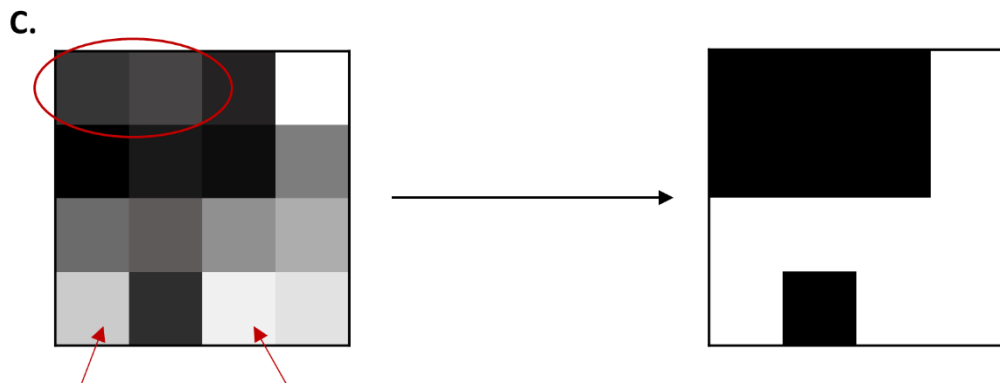
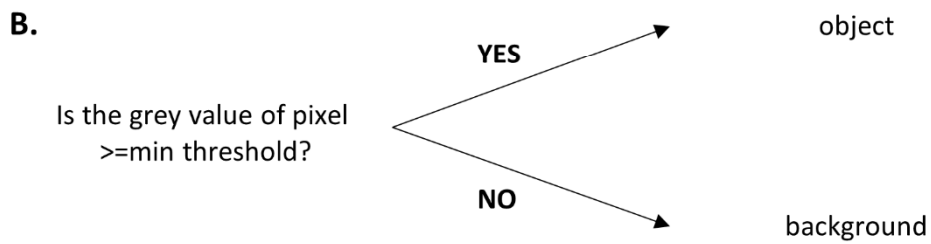


**Figure 3.M.3 Schematic of global thresholding in ImageJ**

(A) A simplified representation of a 16x16 pixel 8-bit image. Grey level values for each pixel are indicated. (B) Workflow of binary image generation by global thresholding in ImageJ. (C) Shrunk version of A and binary image generated by following schematic in B with the minimum grey threshold set at 112. Red circle surrounds a simplified representation of a dim object. Red arrows indicate a simplified representation of two bright objects close together.

Binary images of the vacuolin-treated fibroblasts generated by global thresholding are displayed in Figure 3.M.4B. These images provide an impression of the originals but are not true to the objects and background seen by eye. Therefore, subsequent analysis may result in morphometric data that are artefacts of image processing and highly dependent on LAMP1 immunofluorescence intensity. Where this type of thresholding is used further processing is often required. For example, artificial clusters that are not resolved must be manually eliminated (Kukic et al., 2013) or can be filtered out by high circularity values (Seo et al., 2014). These methods are likely time consuming and may exclude many important structures that do not fulfil the “perfect” criteria.

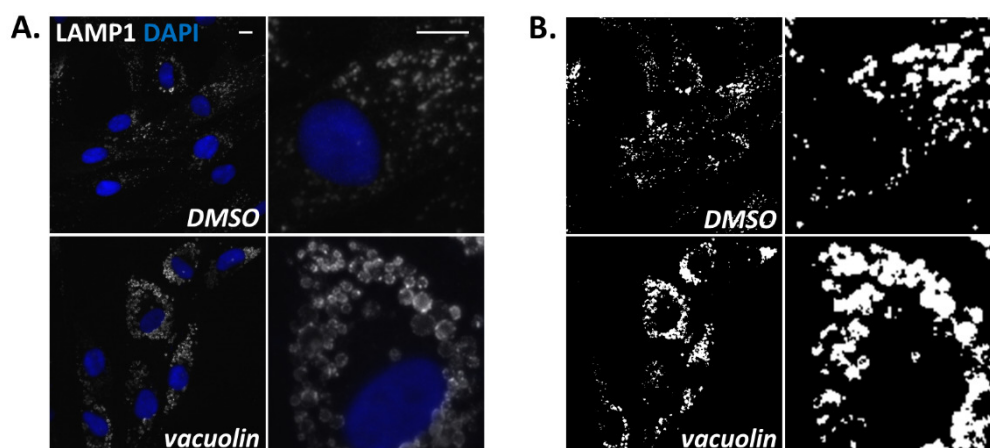


**Figure 3.M.4 Immunofluorescence images converted to binary by global thresholding**  
**(A)** As for Fig. 3.M.2. **(B)** Binary images of **A** generated by auto global thresholding in ImageJ.

Local thresholding (accessed by: Image>Adjust>Auto Local Threshold) accounts for variability of fluorescence intensity in the environment surrounding each pixel. Therefore, it can avoid the issues with global thresholding described here. It was determined experimentally that the Bernsen algorithm for local thresholding generated the truest binary representations of lysosome morphology in fibroblasts (Sezgin and Sankur, 2004). Source code can be viewed here: [https://github.com/fiji/Auto\\_Threshold/blob/master/src/main/java/fiji/threshold/Auto\\_Local\\_Threshold.java](https://github.com/fiji/Auto_Threshold/blob/master/src/main/java/fiji/threshold/Auto_Local_Threshold.java)

The Bernsen algorithm in ImageJ works by creating a circular “window” around each pixel (“X”) (Fig. 3.M.5A). For analysis in this chapter a window with a 5-pixel radius was chosen experimentally. This equates to a radius of  $1.43 \mu\text{m}^2$  and an area of  $6.42 \mu\text{m}^2$ . As a rule of thumb, the radius of the window should be set so that the objects being analysed can just fit inside it. Using too large a window can increase processing time and overlook small dim objects (Bieniecki and Grabowski, 2005). Too small a window can incorrectly segment an object that is larger than the window.



**A.**

80	80	80	80	96	96	96	96	48	48	48	48	240	240	240	240
80	80	80	80	96	96	96	96	48	48	48	48	240	240	240	240
80	80	80	80	96	96	96	96	48	48	48	48	240	240	240	240
80	80	80	80	96	96	96	96	48	48	48	48	240	240	240	240
0	0	0	0	32	32	32	32	16	16	16	16	144	144	144	144
0	0	0	8	32	32	32	32	16	16	16	16	144	144	144	144
0	0	0	0	32	32	32	32	16	16	16	16	144	144	144	144
0	0	0	0	32	32	32	32	16	16	16	16	144	144	144	144
128	128	128	128	112	112	112	112	112	160	160	160	160	176	176	176
128	128	128	128	112	112	112	112	112	160	160	160	160	176	176	176
128	128	128	128	112	112	112	112	112	160	160	160	160	176	176	176
128	128	128	128	112	112	112	112	112	160	160	160	160	176	176	176
192	192	192	192	64	64	64	64	64	224	224	224	224	208	208	208
192	192	192	192	64	64	64	64	64	224	224	224	224	208	208	208
192	192	192	192	64	64	64	64	64	224	224	224	224	208	208	208
192	192	192	192	64	64	64	64	64	224	224	224	224	208	208	208

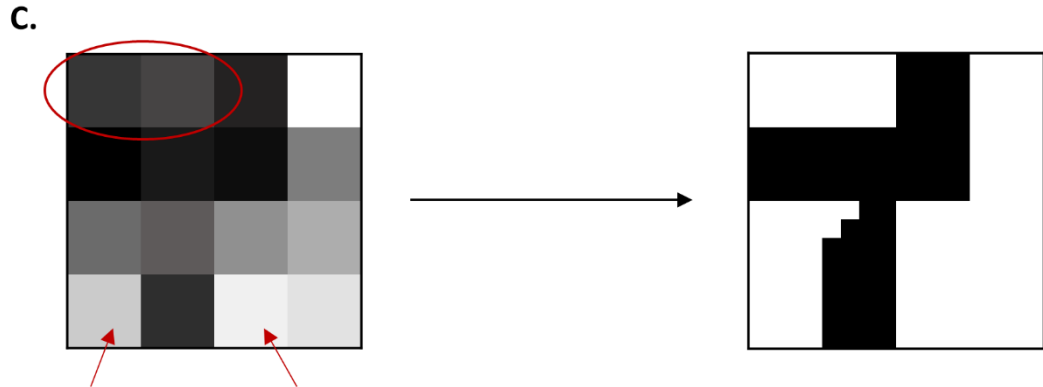
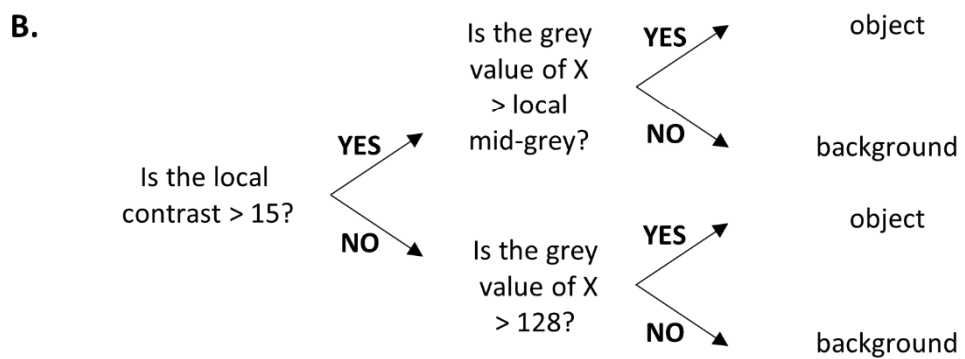


**Figure 3.M.5 Schematic of Bernsen local thresholding in ImageJ**

**(A)** A simplified representation of a 16x16 pixel 8-bit image as appears in Fig. 3.M.3A. To define a pixel “X” as object or background calculations about grey values within a circular window (pink; radius = 5 pixels) are executed. **(B)** Workflow of binary image generation by Bernsen local thresholding in ImageJ. **(C)** Shrunk version of A as appears in Fig.3.M.3C, and binary image generated by following schematic in A with a 5-pixel radius and the default local contrast threshold set at 15.

Within each window the minimum (MIN) and maximum (MAX) grey values are identified. The local contrast is then calculated:

$$\text{LOCAL CONTRAST} = \text{MAX} - \text{MIN}$$

The local mid-grey for this window is also calculated:

$$\text{LOCAL MID-GREY} = (\text{MAX} + \text{MIN}) / 2$$

To determine whether pixel “X” should be set as an object or background the algorithm runs through conditional statements about the local contrast and local mid-grey values, as depicted in Figure 3.M.5B. Note the default contrast threshold in ImageJ is 15. By running through these statements to set each pixel as an object or background the image is binarised as shown in Figure 3.M.5C. Notably, by using this method on the simplified 8-bit image the dim particle in the top left is assigned as an object in the binary image and the two particles in the bottom of the image are also separated.

#### 3.2.4.2.2 Watershed segmentation

Watershed segmentation is used to separate particles in close proximity and was implemented here to separate any residual object aggregates following the local thresholding. In ImageJ the watershed function implements the EDM (Euclidean Distance Map) and Maximum Finder plugins. Source code can be viewed here:

<https://imagej.nih.gov/ij/source/ij/plugin/filter/EDM.java>

<https://imagej.nih.gov/ij/developer/source/ij/plugin/filter/MaximumFinder.java.html>

This segmentation involves 2 sequential functions (Fig. 3.M.6A):

- 1) An EDM is created in which each object pixel is assigned a value that equates to its distance from the nearest background pixel.
- 2) The maxima of the EDM are known as Ultimate Eroded Points (UEP) which are identified. The algorithm then descends from the UEPs through sequential EDM levels in a “dilation”. At each EDM level it determines whether it has encountered a dilation from another UEP. If so, a line is marked between the dilating UEPs and the pixels in this line are set to background. An example of the outcome of this watershedding is shown in Figure 3.M.6B.

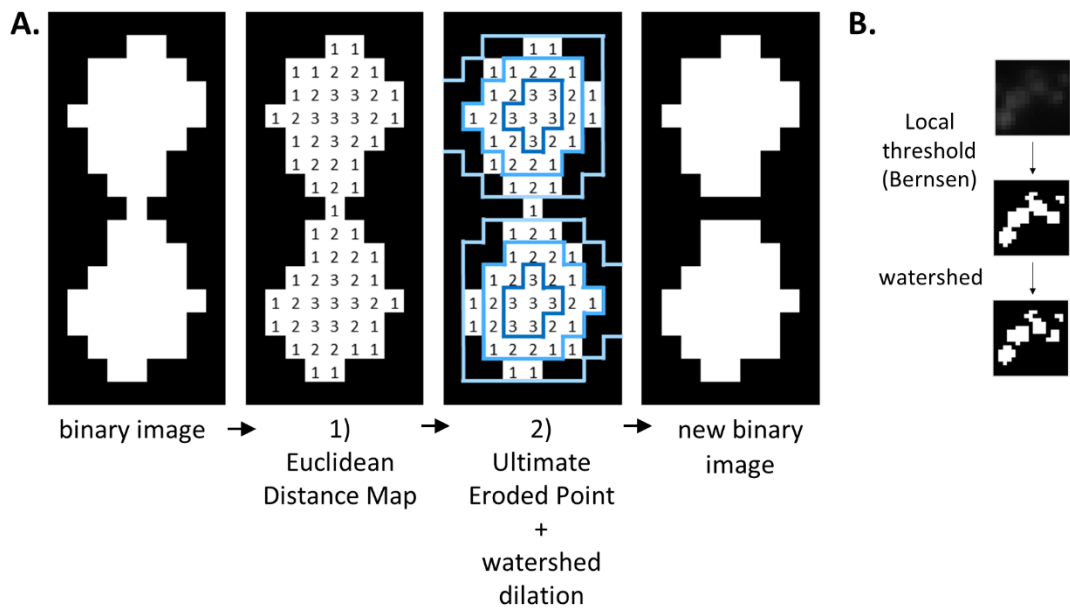


**Figure 3.M.6 Schematic of watershed segmentation in ImageJ**

**(A)** Workflow of watershed segmentation in ImageJ. From a binary image that displays conjoined objects (far left panel) an Euclidean Distance Map (EDM) is generated. Subsequently the Ultimate Eroded Points (UEP) are identified and dilated. Blue polygons represent sequential dilations, starting from the UEP (dark blue) to the edge of the objects (light blue). At the point where dilations from 2 UEPs meet pixels are assigned to background and the objects are separated (far right panel). **(B)** A digital zoom of LAMP1 staining in vacuolin-treated Ctrl fibroblasts to show transformation by Bernsen auto local thresholding and successful object separation by watershed segmentation.

Local thresholding with the Bernsen algorithm plus watershed segmentation generates binary images that include both dim and bright objects and avoid artificial object aggregation (Fig. 3.M.7). The Multiple Image Processor and the macro in Figure 3.M.8 were used to generate these binary images and analyse them, with area set as the output in results. The binary images were compared to their immunofluorescence counterparts periodically to check for likeness. Example binary images for each experiment are available in Appendix B. Results were compiled and analysed in Microsoft Excel.

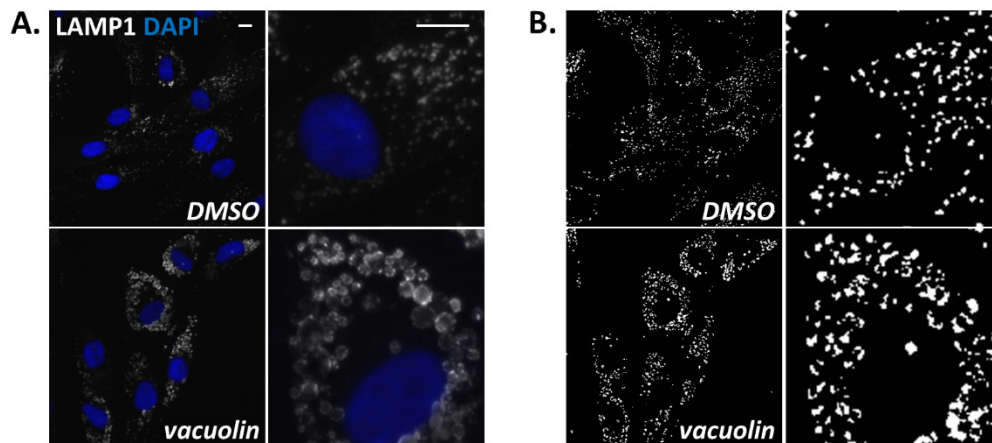


**Figure 3.M.7 Immunofluorescence images converted to binary by Bernsen local thresholding and watershed segmentation**

(A) As for Fig. 3.M.2. (B) Binary images of A generated by auto local thresholding using the Bernsen algorithm (5-pixel radius with the default contrast threshold) and watershed segmentation in ImageJ.

```

1 id = getImageID();
2 run("To ROI Manager");
3 run("8-bit");
4 run("Auto Local Threshold", "method=Bernsen radius=5 parameter_1=0 parameter_2=0 white");
5 run("Watershed");
6 for (i=0 ; i<roiManager("count"); i++) {
7   selectImage(id);
8   roiManager("select", i);
9   run("Analyze Particles...", "size=0-infinity show=Masks display include summarize");
10 }

```

**Figure 3.M.8 Macro commands for lysosome size and frequency analysis**

The data identified enlarged objects in vacuolin-treated fibroblasts compared to controls (Fig. 3.M.9A). As well as average data for each cell, ImageJ outputs area data for each object. This large dataset was used to gain better insight into the type of objects that caused the increase in average object size.

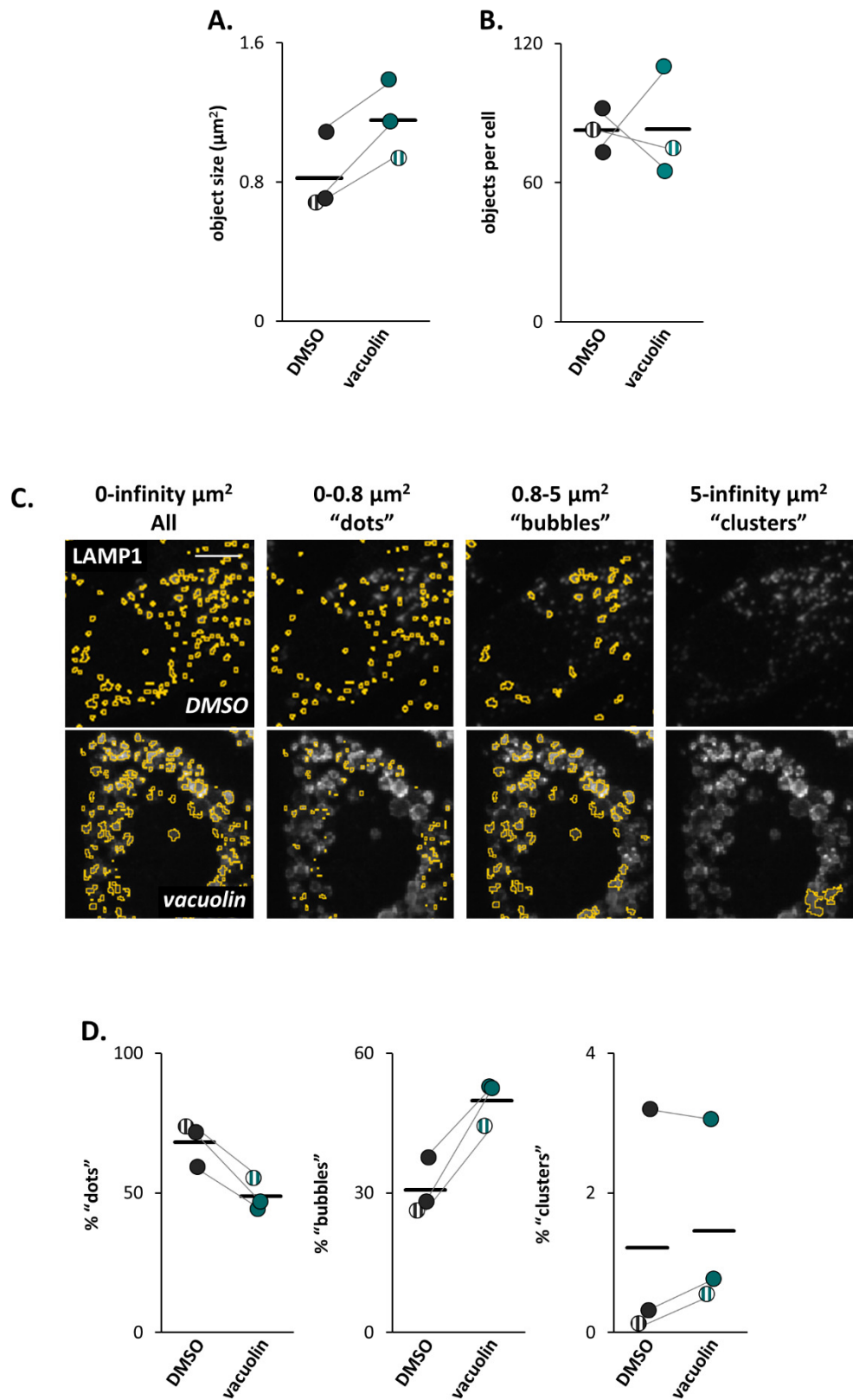


Figure 3.M.9 Automated image processing and analysis confirms enlarged lysosomes in vacuolin-treated fibroblasts (legend on next page)

**(A and B)** Data quantifying LAMP1-positive objects in DMSO or vacuolin-treated Ctrl fibroblasts from images exemplified in Fig. 3.M.2. For details on data pairings please refer to METHODS and ANALYSIS section 3.2.4. Striped plot points represent the use of two different fibroblast lines to provide the result. A total of 233/242 (DMSO/vacuolin) cells from 3 experiments and 3 independent platings were analysed. **(A)** Average object size per cell. **(B)** Average object frequency per cell. **(C)** Digital zooms of LAMP1-positive objects in images exemplified in Fig.3.M.2. Nuclei staining omitted. In the far left panel masks representing the binary images generated from Bernsen local thresholding and watershed segmentation are superimposed in yellow (0-infinity  $\mu\text{m}^2$  All). In the remaining panels the same masks are filtered to display only the objects within the indicated size range. Each size range is assigned a morphotype descriptive (“dots”, “bubbles” or “clusters”). Scale bar = 10  $\mu\text{m}$ . **(D)** Data quantifying the relative frequency of lysosome morphotypes. A total of 19,833/18,079 (DMSO/vacuolin) objects from the same 3 experiments represented in **A** and **B** were analysed.

#### 3.2.4.2.3 Distinguishing between lysosome morphotypes

LAMP1-positive objects can be categorised per appearance. For instance, a sub-population appear as small dots each with apparently homogenous immunofluorescence intensity (Fig.3.9C). These “dots” are 0-0.8  $\mu\text{m}^2$ . Other structures are bubble-like with a dimmer core and brighter periphery. These “bubbles” are within the 0.8-5  $\mu\text{m}^2$  range. Finally, clusters of LAMP1-positive objects generally have an area of more than 5  $\mu\text{m}^2$ . By categorising the object data within these size bins it is possible to determine whether the average object size increase in vacuolin-treated fibroblasts is due to enlargement of individual lysosomes or a greater number of clusters formed. In vacuolin-treated fibroblasts the relative frequency of lysosome “dots” is reduced compared to controls, whereas the frequency of “bubbles” increases (Fig. 3.9D). This data therefore closely corresponds to what can be seen by eye.

#### **3.2.5 siRNA transfection**

Fibroblasts were plated at 100,000 cells/ml (For epifluorescence microscopy: 13 mm glass coverslips in 24-well plates, 0.4 ml/well; For quantitative PCR analysis: no coverslips, 6-well plates, 1.5ml/well) and transfected with siRNAs using Lipofectamine® RNAiMAX (Invitrogen) for 24h. Fibroblasts were re-transfected in fresh media for a further 24 hours and cultured for 48 hours in the absence of siRNA before experimentation. A control siRNA duplex (AllStars Neg.Control) was purchased from Qiagen. Details of targeting siRNAs on the next page.

**Table 3.3 TPC-targeting siRNAs**

ID	Brand	Product Name	Target gene	Target exon	Target sequence (5'-3')
TPC1 siRNA	Qiagen	Hs_TPCN1_5	<i>TPC1</i>	10	CGAGCTGTATTTTCATCATGAA
TPC2 siRNA	Qiagen	Hs_TPCN2_6	<i>TPC2</i>	2	CAGGTGGGACCTCTGCATTGA

### 3.2.6 Quantitative PCR

siRNA-transfected fibroblasts were harvested by scraping and pipet transfer to Maxymum Recovery tubes (Axygen). Cells were centrifuged at RCF=300 for 5 minutes, supernatant was discarded and pellets stored at -80°C. Upon thawing RNA was extracted using the RNeasy Mini Kit and RNase-Free DNase Set (both Qiagen) as per the manufacturer's instructions but omitting the homogenisation steps and repeating the final elution step. cDNA was synthesised using Superscript III RT kit (Invitrogen), Random Primers (Promega) and Oligo dT (12-18) primers (Invitrogen). cDNA was amplified using SYBR® Green JumpStart™ *Taq* ReadyMix™ (Sigma) and primers for human *TPC1*, *TPC2* and housekeepers *UBC* and *GAPDH* (Sigma) as detailed below (Brailoiu et al., 2009):

**Table 3.4 Quantitative PCR primers**

Gene	Forward Primer (5'-3')	Reverse Primer (5'-3')
Hsa <i>TPC1</i>	TTCTGTGTTTTGCTTTAGGG	ATTCCGCTTCCATTAGATCC
Hsa <i>TPC2</i>	GTTTGACATGGAGAGAACCTTGAC	GATGAAAATAACTGGCAATCAGAACC
Hsa <i>UBC</i>	GAAGATGGACGCACCCTGTC	CCTTGTCTTGGATCTTTGCCTT
Hsa <i>GAPDH</i>	TGTGAACCATGAGAAGTATGAC	ATGAGTCCTTCCACGATACC

Samples were denatured at 94°C for 2 minutes followed by 39 cycles of denaturation (94°C, 15 s), annealing (60°C, 30 s) and extension (72°C, 30 s). The reaction was replicated three times for each sample.

Amplification thresholds for each run were set automatically by Bio-Rad CFX Manager software. Anomalous reaction replicates were excluded from analysis. Threshold cycles (Ct) were used to calculate transcript levels via exponential expression transform ( $\text{Expression} = 2^{-\text{Ct}}$ ). Expression was corrected for any amplification occurring in samples that had not been treated with reverse transcriptase (-RT) and should not contain any cDNA. *TPC1* and 2 expression was normalised to *UBC* expression.

## 3.2.7 Microscopy: Epifluorescence

### 3.2.7.1 Ca<sup>2+</sup> - Fura-2

Cytosolic Ca<sup>2+</sup> was measured using Fura-2 and analysed as described in Chapter 2. Cells were challenged with GPN (200 µM; SantaCruz Biotech), NH<sub>4</sub>Cl (100mM; Sigma), ML-SA1 (200µM; Merck), thapsigargin (1 µM; Merck), and bradykinin (10nM; Sigma). All compounds except NH<sub>4</sub>Cl and bradykinin were dissolved in DMSO (Sigma). NH<sub>4</sub>Cl and bradykinin were dissolved in H<sub>2</sub>O. The maximal volume of vehicle added in any experiment was 1% (v/v). The absence of extracellular Ca<sup>2+</sup> is indicated where appropriate in the figures. Where displayed, Ca<sup>2+</sup> was replaced with 1 mM EGTA (Sigma). Excitation and emission wavelengths for Fura-2 detailed below:

**Table 3.5 Epifluorescence microscopy excitation/emission wavelengths**

Probe	Recording	Excitation wavelength (nm)	Emission filter wavelength (nm)
Fura-2	Ca <sup>2+</sup>	340/380	440 long pass

Time to peak and percentage of oscillating cells were analysed only from cells displaying a magnitude  $\geq 0.1$ . Cells were deemed oscillatory if more than one peak was recorded during imaging. For this, a peak was defined as an increase in Fura-2 ratio of  $\geq 0.1$ , followed by a decrease of  $\geq 0.1$ .

## 3.2.8 Statistical Analysis

Analysis was performed using IBM SPSS Statistics 22. Tests to determine statistical significance were performed on datasets in which more than three experiments had been conducted per group/condition and experimental means were clearly different between groups, but where values from individual experiments in one group shared the range of another. Paired-Samples T tests were performed on confocal microscopy data where the differences between the paired values were normally distributed. Where the differences were not normally distributed, statistical significance was determined by a Wilcoxon Signed Ranks test. A One-Way ANOVA was performed to determine the statistical significance of data from more than two groups that exhibited normal distribution and equal variance. For data from more than two groups that were not normally distributed statistical significance was determined by a Kruskal-Wallis H test followed by Mann-Whitney U post-hoc tests.



## 3.3 RESULTS

### 3.3.1 Disturbed lysosome morphology is associated with increased LAMP1 immunofluorescence in LRRK2-GS but not sporadic PD patient fibroblasts

Fibroblasts are an amenable cell type for investigating organelle morphology as they are relatively flat and large which simplifies imaging. Furthermore, primary human fibroblasts can be cultured from living patients by taking a skin biopsy. Together this makes fibroblasts an attractive, physiologically relevant model of human disease. In recently published work disturbed lysosome morphology was reported in familial PD patient fibroblasts harbouring the *LRRK2*-GS mutation (Hockey et al., 2015). To assess this fibroblasts were fixed and stained with an antibody raised to LAMP1 (lysosome-associated membrane protein 1). This disturbed morphology was associated with increased LAMP1 fluorescence intensity compared to age-matched healthy controls. Using the same methods I independently examined lysosome morphology in these cells. Representative images of *LRRK2*-GS PD fibroblasts exhibit greater lysosome populations and a higher occurrence of larger lysosomes and lysosome clustering compared to controls (Fig. 3.1A). This was associated with an increase in LAMP1 intensity (Fig. 3.1C). Whilst the finding of disturbed morphology in familial PD fibroblasts is important the *LRRK2*-GS mutation is responsible for only a small fraction of PD cases. A general hope in PD research is that clues provided by familial PD lead to the discovery of pathogenic pathways that are also common to sporadic PD, which accounts for ~90% of cases (Gandhi and Wood, 2010). Interestingly the *LRRK2*-GS mutation is found in ~1% of sporadic cases and the symptoms of familial *LRRK2*-GS PD patients are indistinguishable from those of sporadic PD (Bardien et al., 2011; Healy et al., 2008). It is possible therefore that disturbed lysosome morphology is a shared point of pathology in familial *LRRK2*-GS and sporadic PD. To examine lysosome morphology in sporadic PD (sp PD) the same LAMP1-staining method was used. Representative images of sp PD fibroblasts in Figure. 3.1B show some larger clusters and subtle changes to lysosome size compared to age-matched controls. However, there was no clear increase in LAMP1 intensity, which was reflected in the quantification (Fig. 3.1D).

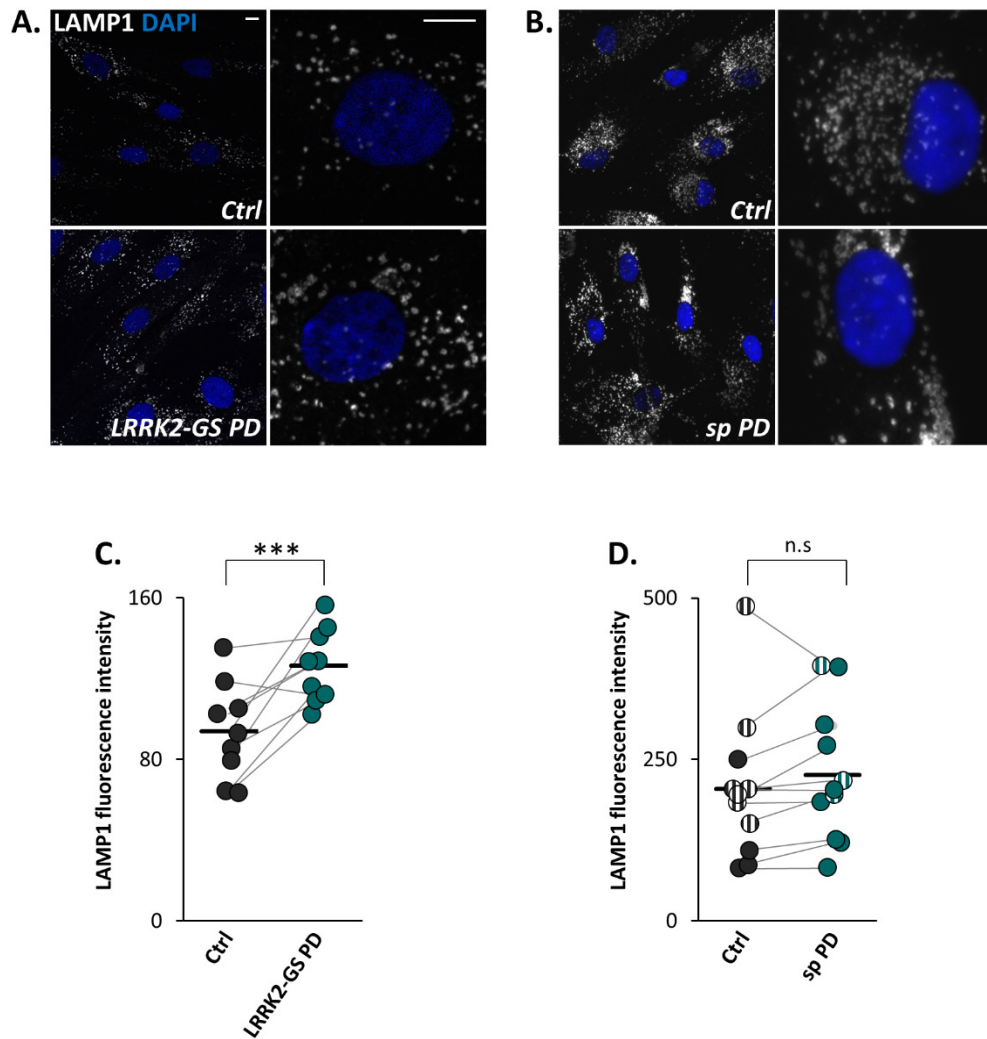


**Figure 3.1 Disturbed lysosome morphology is associated with increased LAMP1 immunofluorescence in LRRK2-GS but not sporadic PD patient fibroblasts**

**(A and B)** Representative immunofluorescence images of LAMP1 staining (white) in **(A)** *LRRK2-GS PD* or **(B)** *sp PD* and age-matched *Ctrl* fibroblasts (*LRRK2-GS PD* fibroblasts paired with *Ctrl*1, *Ctrl*2 and *Ctrl*3; *sp PD* fibroblasts paired with *Ctrl*4 and *Ctrl*5). Nuclei stained blue (DAPI). Right-hand images are 4x optical zooms of individual cells in left-hand images. Scale bar = 10  $\mu$ m. **(C and D)** Average LAMP1 intensity of cells exemplified by **A** and **B** respectively. For details on data pairings please refer to METHODS and ANALYSIS section 3.2.4. Striped plot points represent the use of two different fibroblast lines to provide the result. **(C)** A total of 634/566 (*Ctrl*/*LRRK2-GS PD*) cells from 9 experiments and 7 independent platings were analysed. 2 *LRRK2-GS PD* lines and 3 *Ctrl* lines were used. \*\*\* $p < 0.005$  as determined by a Paired-Samples T test. **(D)** A total of 692/617 (*Ctrl*/*sp PD*) cells from 11 experiments and 8 independent platings were analysed. 2 *sp PD* lines and 2 *Ctrl* lines were used. Results were not statistically significant (n.s) as determined by a Paired Samples T test.

### **3.3.2 Automated lysosome analysis confirms enlarged lysosomes in sporadic PD fibroblasts**

As the sp PD fibroblasts did not exhibit high LAMP1 fluorescence intensity compared to age-matched controls the immunofluorescence images were subjected to automated binarisation to quantify the LAMP1-positive objects. As described in depth in METHODS and ANALYSIS section 3.2.4.2 automated local thresholding was implemented in ImageJ (Bernsen algorithm, 5-pixel radius, default contrast threshold) followed by watershed segmentation. Measurements of average object size and object frequency in each cell were then taken from the resultant binary images. Examples of the binary images generated in this process are shown in Figure 3.2B. This analysis revealed that in control fibroblasts the average size of LAMP1-positive objects was  $0.553 \mu\text{m}^2$  (Fig.3.2C). In sp PD fibroblasts the average size was consistently larger, with an average of  $0.692 \mu\text{m}^2$ . There was however no consistent difference in regard to object frequency per cell (Fig. 3.2D). As described in METHODS and ANALYSIS section 3.2.4.2.3, size data for each individual object in all cells was analysed to provide more information about the size increase of LAMP1 objects in sp PD fibroblasts. Briefly, objects were binned according to morphotype (“dots”:  $0-0.8\mu\text{m}^2$ ; “bubbles”:  $0.8-5 \mu\text{m}^2$ ; “clusters”:  $>5 \mu\text{m}^2$ ) and their relative frequency was tabulated. In sp PD cells a smaller proportion of structures fell into the “dots” category of small punctate lysosomes compared to controls (Fig. 3.2E). This was concomitant with a higher proportion of LAMP1-positive objects that belonged to the “bubbles” category of large, individual lysosomes. A higher proportion of LAMP1 objects also fell into the “clusters” category.

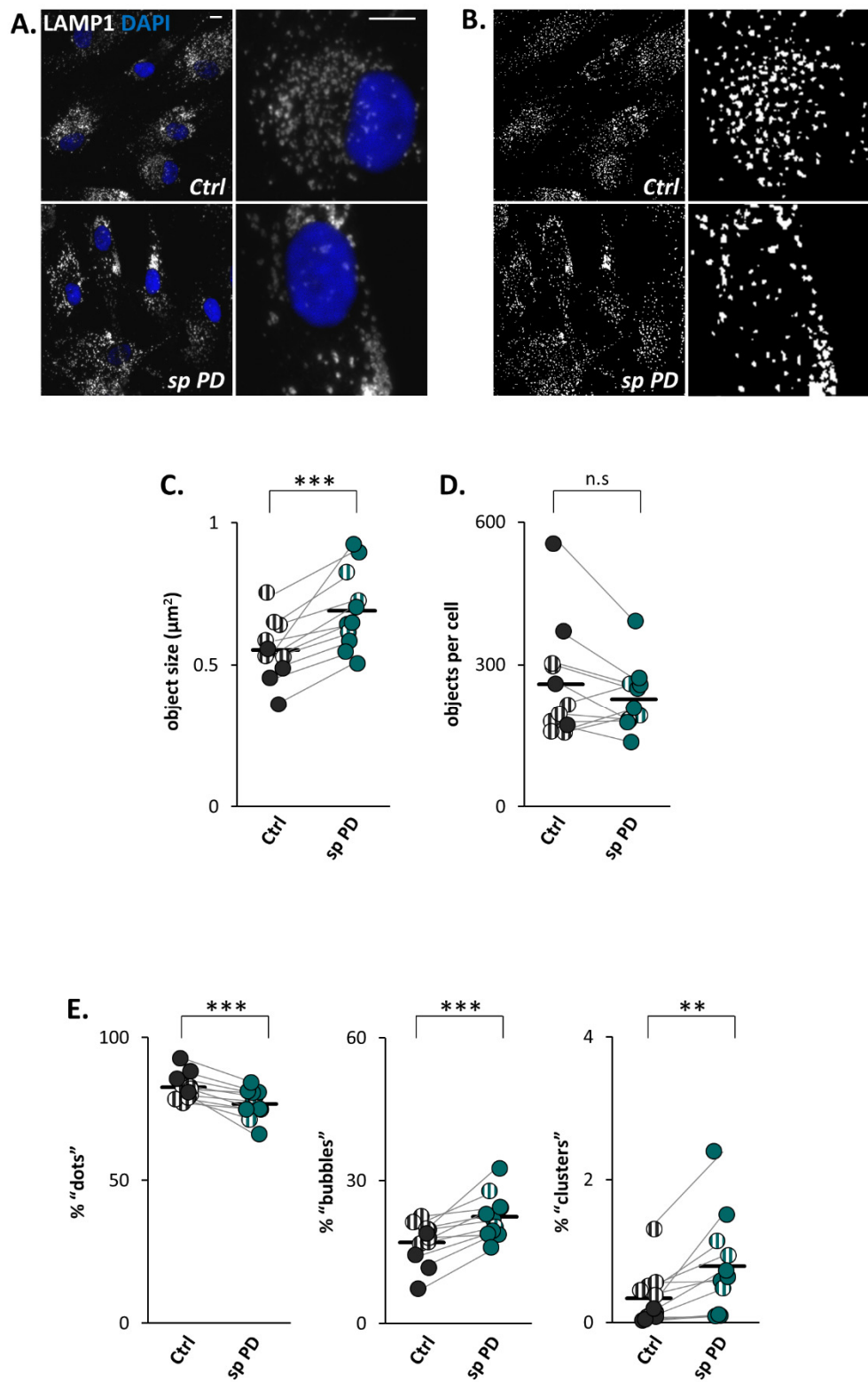


**Figure 3.2. Automated lysosome analysis confirms enlarged lysosomes in sporadic PD fibroblasts** (legend on next page)

**(A)** As for Fig.3.1.B. **(B)** Binary images corresponding to **A**, generated by Bernsen local thresholding and watershed segmentation. **(C-D)** Data quantifying LAMP1-positive objects in *Ctrl* and *sp PD* fibroblasts from binary images exemplified in **B**. For details on data pairings please refer to METHODS and ANALYSIS section 3.2.4. Striped plot points represent the use of two different fibroblast lines to provide the result. A total of 692/617 (*Ctrl*/*sp PD*) cells from 11 experiments and 8 independent platings were analysed. 2 *sp PD* lines and 2 *Ctrl* lines were used. **(C)** Average object size per cell. \*\*\*  $p < 0.005$  as determined by a Wilcoxon signed ranks test. **(D)** Average object frequency per cell. Not statistically significant (n.s.) as determined by a Paired-Samples T test. **(E)** Relative frequency of lysosome morphotypes. A total of 153,230/121,779 (*Ctrl*/*spPD*) objects from the 11 experiments represented in **C** and **D** were analysed. \*\*\* $p < 0.005$ , \*\* $p < 0.01$  as determined by Paired-Samples T tests.

### 3.3.3 NH<sub>4</sub>Cl as a tool to deplete lysosomal Ca<sup>2+</sup>

Lysosome morphology appears to be disturbed in familial LRRK2-GS PD and sp PD fibroblasts. In LRRK2-GS PD cells this has been attributed to upregulation of TPC2 activity and increased local Ca<sup>2+</sup> fluxes (Hockey et al., 2015). These cells also exhibit augmented global Ca<sup>2+</sup> signals in response to NAADP. This may indicate that lysosomal Ca<sup>2+</sup> channel TPC2 contributes to potentiated global Ca<sup>2+</sup> signals in LRRK2-GS PD too (Calcraft et al., 2009). However, whether such TPC upregulation potentiates physiological global Ca<sup>2+</sup> signals elicited by extracellular agonists is unknown. To investigate this I set out to identify an extracellular agonist that requires TPCs to elicit global Ca<sup>2+</sup> signals, with the intention of comparing the agonist-evoked signals in PD and control fibroblasts. As a first step I sought an extracellular agonist that elicits Ca<sup>2+</sup> signals through the lysosomes. To compromise the lysosomes and determine their contribution to various events cells can be stimulated with GPN to permeabilise the lysosomal membrane and cause leakage of luminal content (Haller et al., 1996; Jadot et al., 1984). However, in fibroblasts GPN gives rise to complex oscillatory Ca<sup>2+</sup> signals that are long-lasting (Fig. 3.3A), as reported previously (Kilpatrick et al., 2013). This would complicate the examination of subsequent signals evoked by other stimuli. Furthermore, these complex GPN-evoked Ca<sup>2+</sup> signals are generated from lysosomal Ca<sup>2+</sup> release but also coupled Ca<sup>2+</sup> release from the ER (Kilpatrick et al., 2013). An alternative, ammonium chloride (NH<sub>4</sub>Cl), can also be used to disrupt the lysosomes by increasing lysosomal pH and causing a concurrent reduction of lysosomal Ca<sup>2+</sup> (Christensen et al., 2002). When fibroblasts were stimulated with NH<sub>4</sub>Cl simple and relatively transient Ca<sup>2+</sup> signals were generated (Fig. 3.3A). Therefore NH<sub>4</sub>Cl would allow simple analysis of Ca<sup>2+</sup> signals caused by subsequent stimuli. To probe the lysosomal nature of the NH<sub>4</sub>Cl-evoked Ca<sup>2+</sup> signals cells were subsequently challenged with lysosomotrope GPN. As shown in Figure 3.3B and C GPN-evoked Ca<sup>2+</sup> signals were present following addition of the vehicle, H<sub>2</sub>O. However, following NH<sub>4</sub>Cl addition, the GPN-evoked Ca<sup>2+</sup> signals were blocked. Similar results were obtained with ML-SA1, an agonist of the lysosomal Ca<sup>2+</sup> channel TRPML1 (Fig. 3.3D and E). The effect of NH<sub>4</sub>Cl on ER Ca<sup>2+</sup> was also assessed. This was done by using the SERCA inhibitor, thapsigargin, to stimulate ER Ca<sup>2+</sup> release after the NH<sub>4</sub>Cl transient. Although a subtle change in the thapsigargin-evoked Ca<sup>2+</sup> signal was observed following NH<sub>4</sub>Cl the response was not blocked (Fig. 3.3F and G).

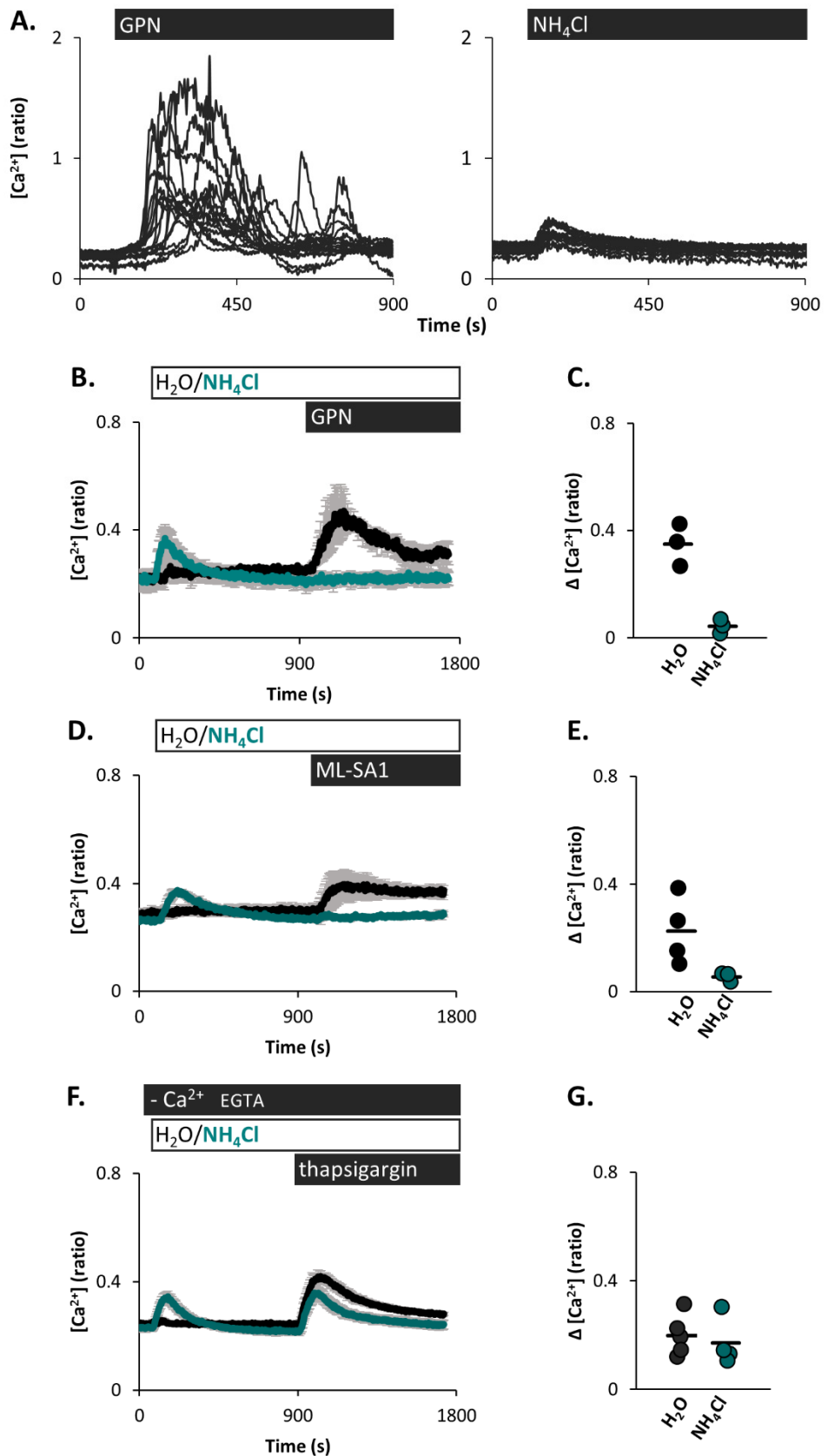


Figure 3.3 NH<sub>4</sub>Cl as a tool to deplete lysosomal Ca<sup>2+</sup> (legend on next page)

**(A)** Cytosolic  $\text{Ca}^{2+}$  traces of individual Ctrl fibroblasts stimulated with GPN (200  $\mu\text{M}$ ) ( $n=17$ ) or  $\text{NH}_4\text{Cl}$  (100 mM) ( $n=18$ ). **(B, D and F)** Average cytosolic  $\text{Ca}^{2+}$  traces (mean of experiments  $\pm$  S.E.M) of Ctrl fibroblasts stimulated with **(B)** GPN (200  $\mu\text{M}$ ), **(D)** ML-SA1 (200  $\mu\text{M}$ ) or **(F)** thapsigargin (1  $\mu\text{M}$ ), following addition of  $\text{H}_2\text{O}$  or  $\text{NH}_4\text{Cl}$  (100 mM). **(F)** Conducted in the absence of extracellular  $\text{Ca}^{2+}$  ( $\text{Ca}^{2+}$  in was replaced with 1mM EGTA). **(C, E and G)** Each plot point represents one experiment. **(C)** Data quantifying magnitude of GPN responses in **B**,  $n=3/3$  ( $\text{H}_2\text{O}/\text{NH}_4\text{Cl}$ ). A total of 72 cells per condition from 3 independent platings were analysed. **(E)** Data quantifying magnitude of ML-SA1 responses in **D**,  $n= 4/3$  ( $\text{H}_2\text{O}/\text{NH}_4\text{Cl}$ ). A total of 78/63 ( $\text{H}_2\text{O}/\text{NH}_4\text{Cl}$ ) cells from 3 independent platings were analysed. **(G)** Data quantifying magnitude of thapsigargin responses in **F**,  $n= 5/4$  ( $\text{H}_2\text{O}/\text{NH}_4\text{Cl}$ ). A total of 81/64 ( $\text{H}_2\text{O}/\text{NH}_4\text{Cl}$ ) cells from 2 independent platings were analysed.



### **3.3.4 Inflammatory mediator bradykinin evokes concentration-dependent global Ca<sup>2+</sup> signals which are blocked by NH<sub>4</sub>Cl**

A candidate extracellular agonist for the investigation of physiological global Ca<sup>2+</sup> signalling in PD fibroblasts was bradykinin. This short, naturally occurring peptide mediates inflammation through activation of B<sub>1</sub>R and B<sub>2</sub>R GPCRs (Marceau and Regoli, 2004). In fibroblasts it elicits robust Ca<sup>2+</sup> signals within the nanomolar range in a concentration-dependent manner (Fig. 3.4A and B). A sub-maximal dose of 10 nM was chosen for subsequent experiments to facilitate observations of inhibited or augmented signals. To investigate the contribution of the lysosomes to bradykinin-evoked Ca<sup>2+</sup> signals fibroblasts were first stimulated with NH<sub>4</sub>Cl to compromise these organelles. Following the vehicle alone (H<sub>2</sub>O), robust bradykinin-evoked Ca<sup>2+</sup> signals were observed (Fig. 3.4C and D). However, after NH<sub>4</sub>Cl addition, the bradykinin-evoked Ca<sup>2+</sup> signals were inhibited.

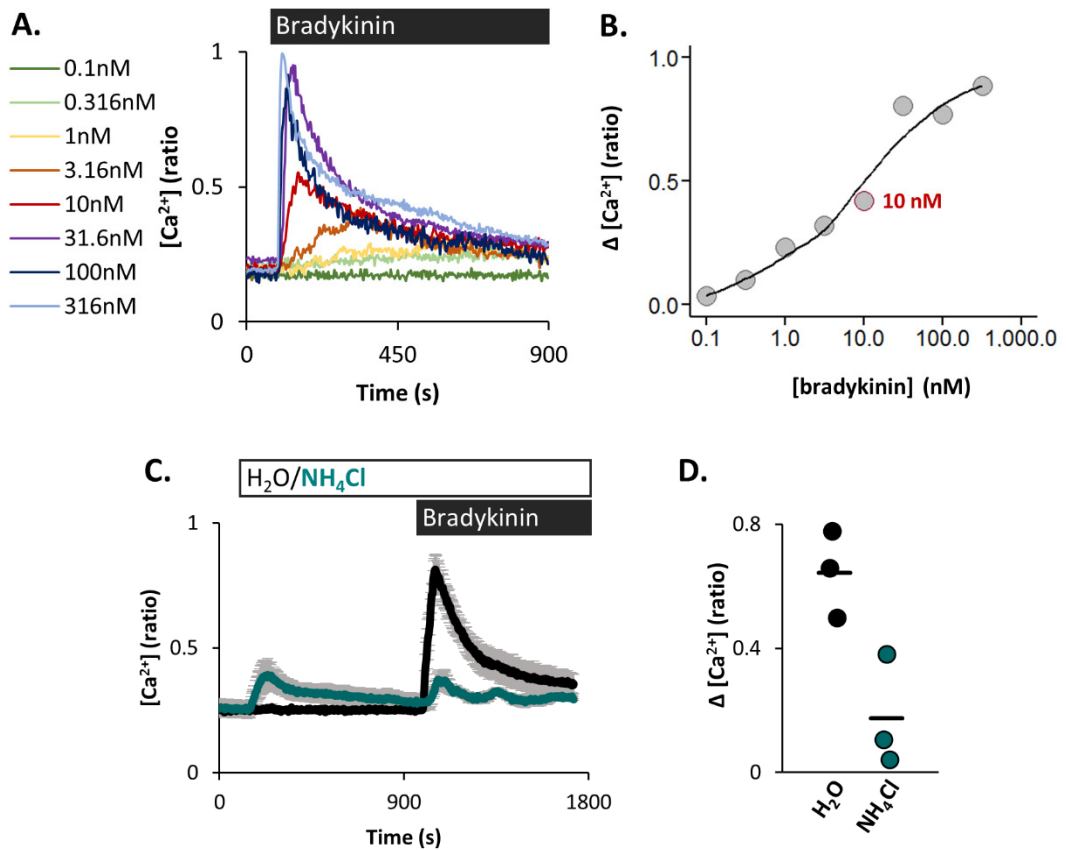


**Figure 3.4 Inflammatory mediator bradykinin evokes concentration-dependent global  $Ca^{2+}$  signals which are blocked by  $NH_4Cl$**

(A) Average cytosolic  $Ca^{2+}$  traces (mean of cells in a single experiment) of Ctrl fibroblasts stimulated with bradykinin at a range of concentrations. (B) Data quantifying magnitude of responses in A. Each plot point represents one experiment. The bradykinin concentration used in subsequent experiments (10 nM) is outlined in red. Data from 28-32 cells per experiment from 1 plating. (C) Average cytosolic  $Ca^{2+}$  traces (mean of experiments  $\pm$  S.E.M) of Ctrl fibroblasts stimulated with bradykinin (10 nM), following addition of  $H_2O$  or  $NH_4Cl$  (100 mM). (D) Data quantifying magnitude of bradykinin responses in A. Each plot point represents one experiment,  $n=3/3$  ( $H_2O/NH_4Cl$ ). A total of 65/52 ( $H_2O/NH_4Cl$ ) cells from 2 independent platings were analysed.

### 3.3.5 Validation of TPC knockdown in fibroblasts by quantitative PCR

As bradykinin-evoked global  $\text{Ca}^{2+}$  signals were inhibited by  $\text{NH}_4\text{Cl}$  the next step was to assess the contribution of TPCs to the signals. To do this, fibroblasts transfected with siRNAs targeted to TPC1 and TPC2 were stimulated by bradykinin. cDNA was generated from the mRNA in these cells and measured by quantitative PCR (QPCR). An example of one analysis shows amplification curves for *TPC1* and *TPC2* and house-keeping genes ubiquitin C (*UBC*) and glyceraldehyde 3-phosphate dehydrogenase (*GAPDH*) (Fig. 3.5A). TPC transcript levels were normalised to UBC as is displayed in Figure 3.5B. Noticeably, TPC1 levels were higher than TPC2. In the final presentation (Fig. 3.5C and D) the data is expressed as a percentage of the TPC transcripts in cells treated with control siRNA, and as a ratio of *TPC1* and *TPC2* expression. QPCR confirmed selective knockdown of TPC1 and TPC2 by respective siRNAs.

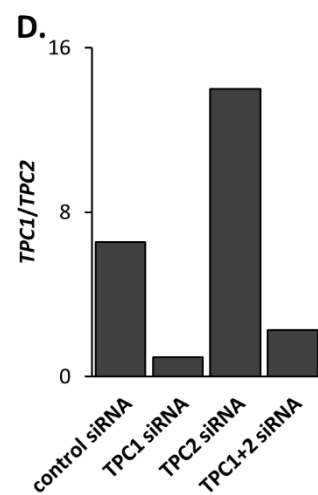
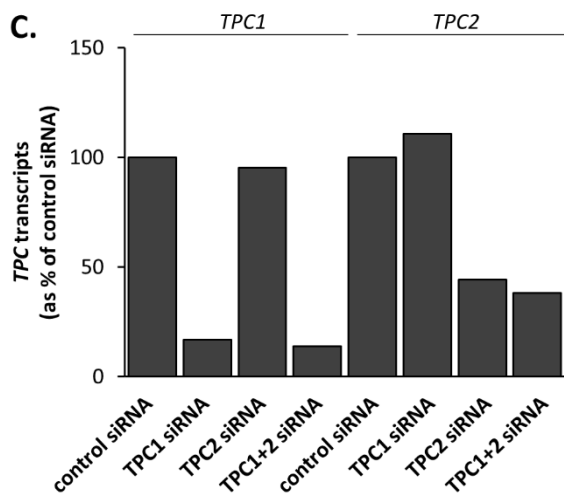
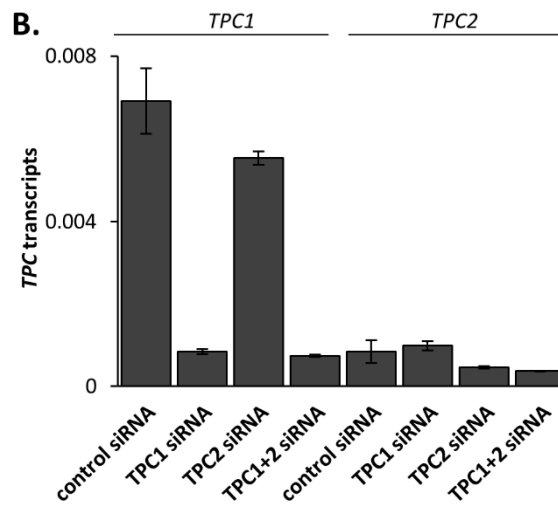
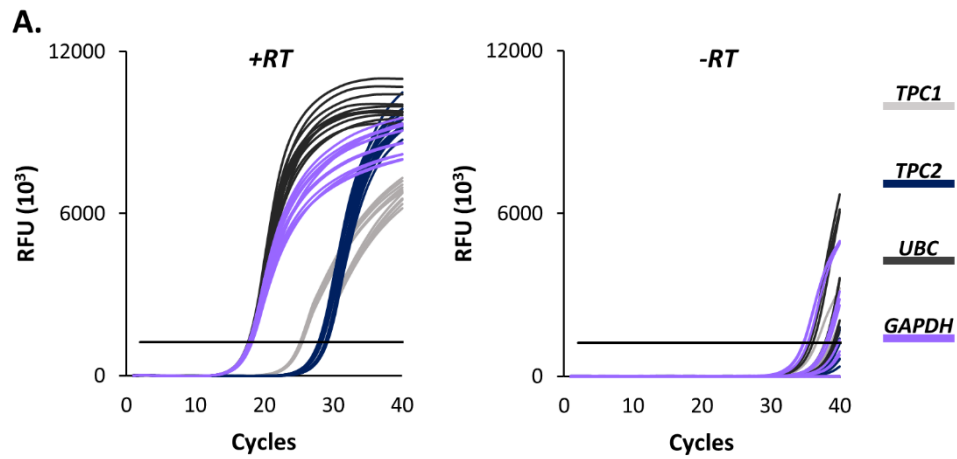


**Figure 3.5 Validation of TPC knockdown in fibroblasts by quantitative PCR**

(A) Representative QPCR amplification curves generated from samples of Ctrl fibroblasts transfected with control or TPC siRNA. Prior to amplification RNA samples were incubated with reverse transcriptase (+RT) to synthesise cDNA, or without (-RT) as a negative control. Black horizontal line shows position of automatically set amplification threshold. (B) Data quantifying TPC transcripts

(mean  $\pm$  S.D) in **A**, corrected for amplification in -RT samples, and normalised to *UBC*. **(C and D)** Summary data quantifying TPC transcripts in 2 experiments from 2 independent platings. **(C)** Data are normalised to *TPC* levels in fibroblasts transfected with control siRNA. **(D)** Ratio comparing transcript levels of *TPC1* and *TPC2*.

### 3.3.6 TPC knockdown inhibits bradykinin-evoked Ca<sup>2+</sup> signals

Having successfully knocked down *TPC* levels I examined bradykinin-evoked Ca<sup>2+</sup> signals in these cells (Fig. 3.6A and B). Average signal magnitude was reduced in cells treated with *TPC1* siRNA or *TPC2* siRNA (Fig. 3.6C). Co-transfection of *TPC1* and *TPC2* siRNA also inhibited the magnitude although the effect was not additive. Time to reach the peak of the bradykinin-evoked signal was extended in cells transfected with *TPC2* siRNA or co-transfected with *TPC1* and *TPC2* siRNAs (Fig. 3.6D). Quantification of the percentage of cells exhibiting oscillatory responses revealed an upward trend in *TPC* siRNA conditions, however it did not reach statistical significance (Fig. 3.6E).

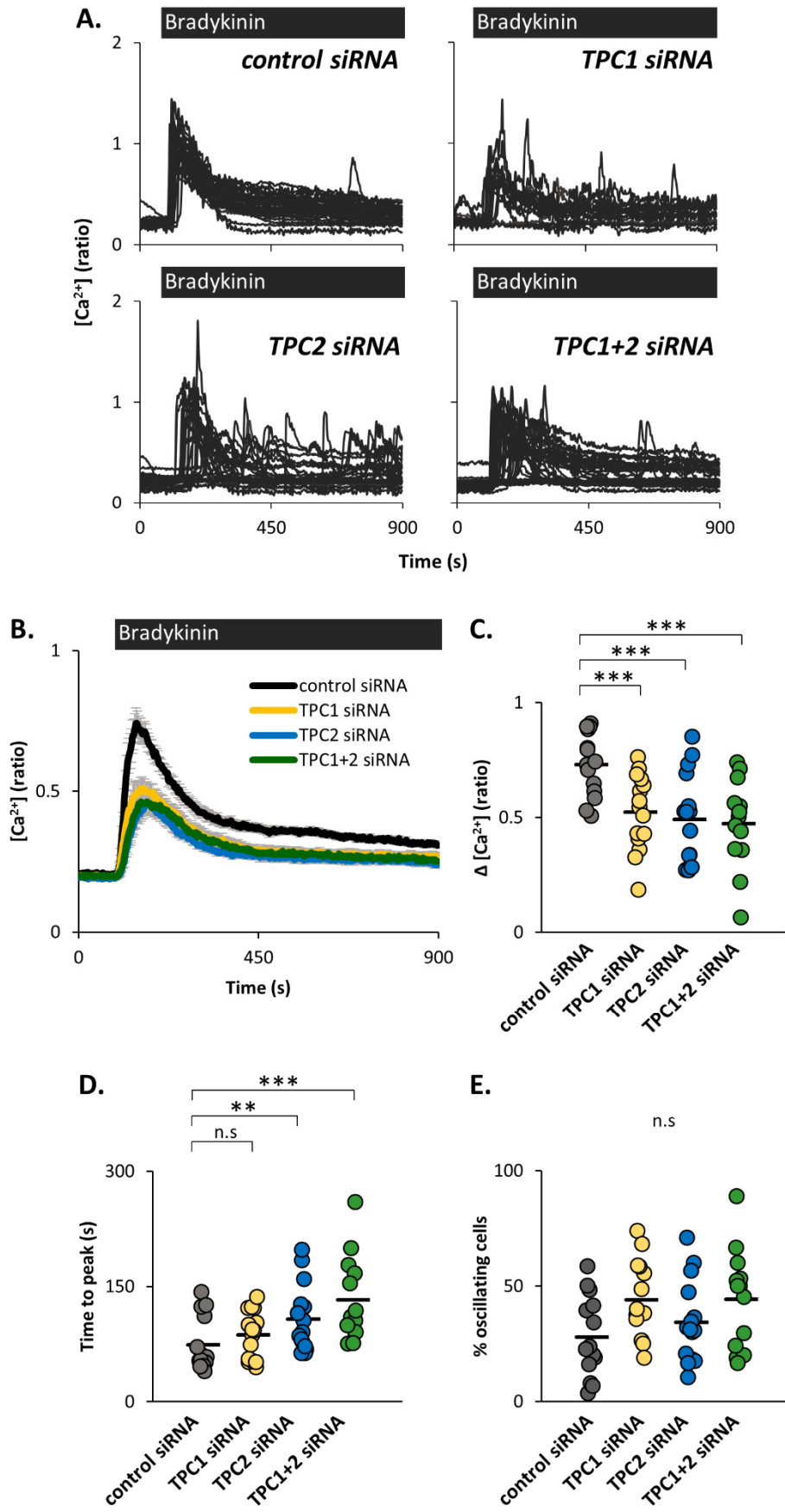
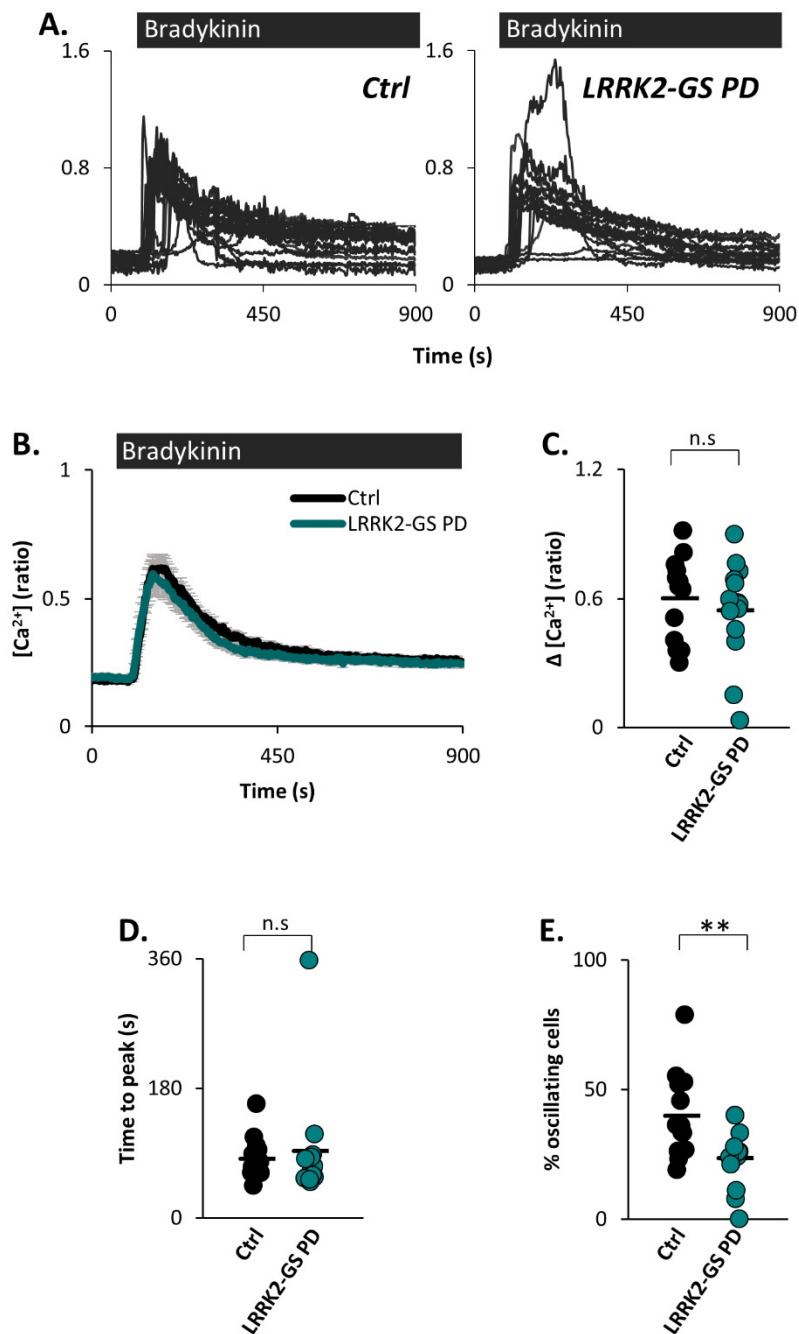


Figure 3.6 TPC knockdown inhibits bradykinin-evoked  $\text{Ca}^{2+}$  signals (legend on next page)

**(A and B)** Cytosolic Ca<sup>2+</sup> traces of Ctrl fibroblasts transfected with control or TPC siRNA and stimulated with bradykinin (10 nM). **(A)** Representative cytosolic Ca<sup>2+</sup> traces of individual fibroblasts. **(B)** Average cytosolic Ca<sup>2+</sup> traces (mean of experiments ± S.E.M). **(C-E)** Data quantifying bradykinin responses in **B**. Each plot point represents one experiment, n=14/15/15/13 (control/TPC1/TPC2/TPC1+2 siRNA). A total of 504/418/520/478 (control/TPC1/TPC2/TPC1+2 siRNA) cells from 5 independent platings were analysed. **(C)** Magnitude of bradykinin responses. **(D)** Time to reach signal peak, analysed from fibroblasts with magnitude ≥0.1. **(C and D)** \*\*p<0.01, \*\*\*p<0.005, or data that were not statistically significant (n.s) as determined by Kruskal-Wallis H tests followed by post hoc Mann-Whitney U tests. P values fell below a Bonferroni-corrected alpha of 0.0167. **(E)** Percentage of cells with oscillatory responses, analysed from fibroblasts with magnitude ≥0.1. Data that were not statistically significant (n.s) as determined by a one-way ANOVA.

### **3.3.7 Bradykinin-evoked Ca<sup>2+</sup> signals are similar in LRRK2-GS PD and control fibroblasts**

The inhibition of bradykinin-evoked Ca<sup>2+</sup> signals by reducing TPC expression suggests that TPCs are involved in such signalling. As disturbed lysosome morphology in LRRK2-GS PD fibroblasts is associated with upregulated TPC2 activity I investigated the possibility that TPC-dependent, bradykinin-evoked Ca<sup>2+</sup> signals would be potentiated in these cells (Hockey et al., 2015). Bradykinin-evoked Ca<sup>2+</sup> signals were largely unchanged in LRRK2-GS PD fibroblasts compared to controls (Fig. 3.7.A-D). Magnitude was inhibited in two experiments but the average was only marginally reduced compared to controls (Fig. 3.7C). In one experiment time to reach the signal peak was drastically delayed but there was very little difference when comparing the average (Fig. 3.7D). A reduction in the percentage of cells exhibiting oscillatory responses was the only result to reach statistical significance (Fig. 3.7E).



**Figure 3.7 Bradykinin-evoked  $Ca^{2+}$  signals are similar in LRRK2-GS PD and control fibroblasts**

**(A and B)** Cytosolic  $Ca^{2+}$  traces of *Ctrl* or *LRRK2-GS PD* fibroblasts stimulated with bradykinin (10 nM). **(A)** Representative cytosolic  $Ca^{2+}$  traces of individual fibroblasts. **(B)** Average cytosolic  $Ca^{2+}$  traces (mean of experiments  $\pm$  S.E.M). **(C-E)** Data quantifying bradykinin responses in **B**,  $n=13/14$  (*Ctrl*/*LRRK2-GS PD*). A total of 276/282 (*Ctrl*/*LRRK2-GS PD*) cells from 6 independent platings were analysed. Each plot point represents one experiment. **(C)** Magnitude of bradykinin responses. Data that were not statistically significant (n.s) as determined by an Independent-Samples T test. **(D)** Time to reach signal peak, analysed from fibroblasts with magnitude  $\geq 0.1$ . Data that were not statistically significant (n.s) as determined by a Mann Whitney U test. **(E)** Percentage of cells with oscillatory



responses, analysed from fibroblasts with magnitude  $\geq 0.1$ .  $**p < 0.01$  as determined by an Independent-Samples T test.

### **3.3.8 Bradykinin-evoked $\text{Ca}^{2+}$ signals are similar in sporadic PD and control fibroblasts**

In addition to LRRK2-GS PD I assessed bradykinin-evoked  $\text{Ca}^{2+}$  signals in sp PD fibroblasts which also exhibit disturbed lysosome morphology (Fig. 3.2). Magnitude of response in these cells was slightly reduced but was not statistically different compared to controls (Fig. 3.8A-C). There was also no difference between sp PD fibroblasts and controls in time taken to reach the signal peak nor the percentage of oscillating cells (Fig. 3.8D and E).

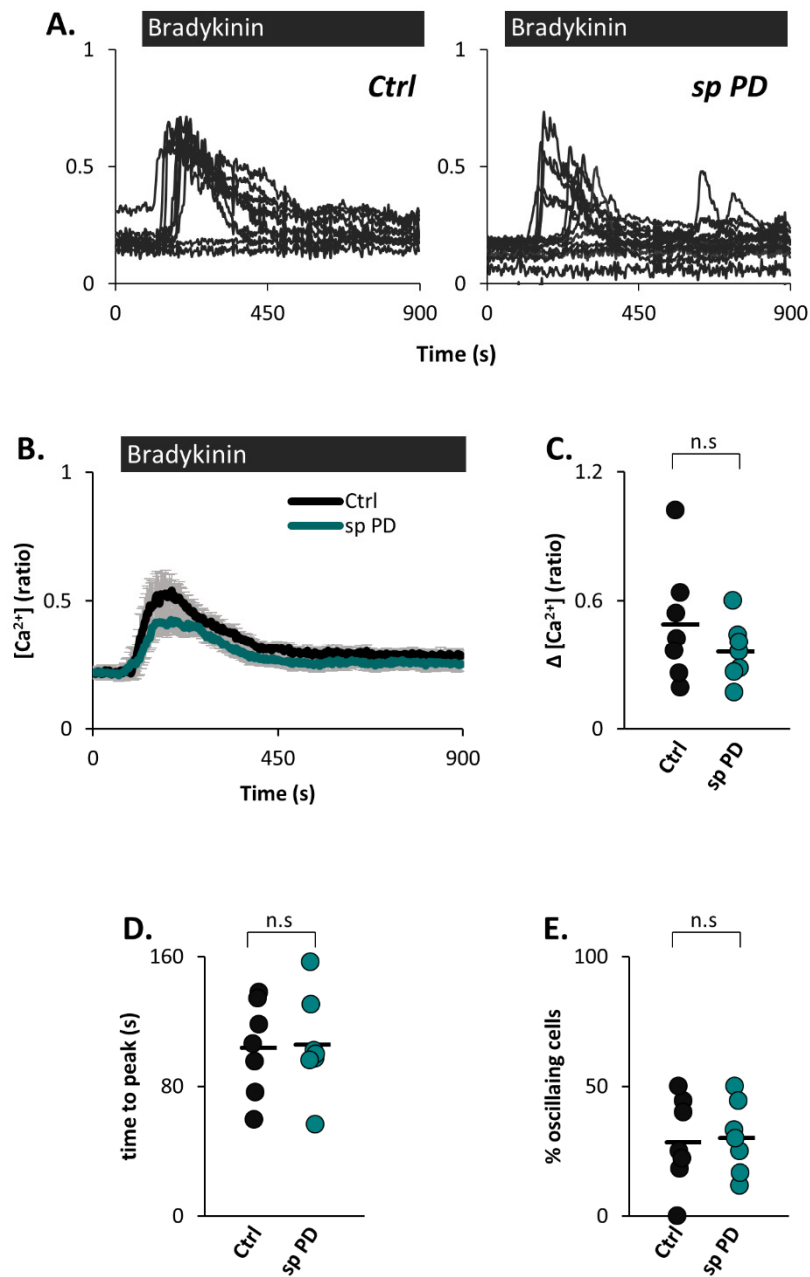


**Figure 3.8 Bradykinin-evoked  $Ca^{2+}$  signals are similar in sporadic PD and control fibroblasts** (A and B) Cytosolic  $Ca^{2+}$  traces of *Ctrl* or *sp PD* fibroblasts stimulated with bradykinin (10 nM). (A) Representative cytosolic  $Ca^{2+}$  traces of individual fibroblasts. (B) Average cytosolic  $Ca^{2+}$  traces (mean of experiments  $\pm$  S.E.M). (C-E) Data quantifying bradykinin responses in B. Each plot point represents one experiment, n=7/7 (Ctrl/sp PD). A total of 87/88 (Ctrl/sp PD) cells from 5 independent platings were analysed. (B) Magnitude of bradykinin responses. (C) Time to reach signal peak, analysed from fibroblasts with magnitude  $\geq 0.1$ . (D) Percentage of cells with oscillatory responses, analysed from fibroblasts with magnitude  $\geq 0.1$ . (D-E) Results were not statistically significant (n.s) as determined by Independent-Samples T tests.

### 3.4 DISCUSSION

In familial LRRK2-GS PD patient fibroblasts upregulated TPC2 activity has been associated with disturbed lysosome morphology and augmented global  $\text{Ca}^{2+}$  signals in response to NAADP (Hockey et al., 2015). Here, I independently report disturbed lysosome morphology in these LRRK2-GS PD cells. In addition, I show that lysosome morphology is altered in sporadic PD fibroblasts compared to age-matched controls. To investigate the connection between upregulated TPC2 activity and global  $\text{Ca}^{2+}$  signaling in LRRK2-GS PD fibroblasts, and to probe the physiological relevance of this, I stimulated the cells with inflammatory peptide bradykinin. Compromising the lysosomes and reducing *TPC* expression in control fibroblasts inhibited bradykinin-evoked global  $\text{Ca}^{2+}$  signals indicating their reliance on both. Despite this, and the reported over-activity of TPC2 in LRRK2-GS PD fibroblasts, bradykinin-evoked  $\text{Ca}^{2+}$  signals were not augmented in these cells. Nor were they augmented in sporadic PD fibroblasts compared to age-matched controls.

Lysosomes are dynamically connected with other organelles, both physically and functionally (Luzio et al., 2007a). Therefore, monitoring of lysosome morphology may serve as useful readout of lysosomal health and the well-being of other allied organelles and processes. For example, lysosome swelling occurs as a result of defective retrograde transport, possibly due to disrupted lysosomal hydrolase delivery (Arighi et al., 2004). Fibroblasts lend themselves to the study of lysosome morphology due to their relatively large size and flat profile. More importantly, fibroblasts derived from living patients are a valuable first-look model of disease (Auburger et al., 2012). In fibroblasts from familial PD patients with the *LRRK2*-GS mutation, Hockey and colleagues associated disturbed lysosome morphology with increased fluorescence of a LAMP1-targeted antibody (Hockey et al., 2015). Here (Fig. 3.1A and C) I independently show that LAMP1 intensity is greater in these cells compared to age-matched controls. Importantly, the *LRRK2*-GS mutation is not just found in familial PD but also ~1% of sporadic cases. Furthermore, the symptoms of familial LRRK2-GS PD patients are indistinguishable from those of sporadic PD (Bardien et al., 2011; Healy et al., 2008). It is possible therefore that familial LRRK2-GS PD and sporadic PD share routes of pathogenesis which correlate with disturbed lysosome morphology. However, unlike the LRRK2-GS PD fibroblasts, lysosome morphology in sporadic PD cells was not associated with an increase in LAMP1 intensity compared to age-matched controls (Fig. 3.1B and D). PD status aside, this may in part be due to the age of these cells. Indeed, the LRRK2-GS PD cells were obtained from patients in their 50s (“young”) whereas the sporadic PD cells were obtained from patients around their 80<sup>th</sup> year (“aged”). In a recent study using the same assay

and fibroblasts that fall into the “young” category, LAMP1 intensity was considerably higher in PD cells harbouring the *GBA1* N370S mutation compared to age-matched controls (Kilpatrick et al., 2016b). However, when *GBA1* N370S PD fibroblasts from the “aged” category were assessed there was no such increase in LAMP1 intensity. Furthermore, enhanced ER Ca<sup>2+</sup> signalling was found in the “young” PD cells but also in the “aged” PD cells and control cells alike. Therefore, age-related changes to lysosome morphology or cellular Ca<sup>2+</sup> in healthy controls may mimic or mask pathogenic disturbances. Of course, ageing is accompanied by lysosomal changes including impaired degradative function and build-up of the indigestible pigment lipofuscin (Cuervo and Dice, 2000). Notably, although lysosome proliferation in fibroblasts has been reported during *in vitro* ageing, there is evidence that such proliferation is not related to age of the individual at which the biopsy is taken (Hwang et al., 2009; Robbins et al., 1970). This should be verified by using the techniques described in this chapter and control fibroblasts of different biopsy ages.

Despite no increased LAMP1 intensity in sporadic PD fibroblasts I did notice a subtle increase in lysosome size in these cells compared to controls. To quantify this I implemented automated *in silico* image processing using the Fiji package of ImageJ software. Often, a single fluorescence intensity threshold is used to segment objects for such analysis. However, this method is intrinsically dependent on pixel intensity and can cause artificial aggregation of bright objects, and overlook dimmer ones (Fassina et al., 2012; Kukic et al., 2013; Seo et al., 2014). Local thresholding considers local contrasts thereby allowing dimmer particles to be identified if the intensity of the local background is low enough. Furthermore, it can differentiate individual particles of high intensity. Whilst this type of thresholding is available on pay-for software such as MetaXpress, ImageJ is free and open-source. Therefore, development of image analysis methods in ImageJ has the scope to offer transparent and widely-available research tools. A limitation of this are the often-ambiguous descriptions of image analysis in published work. As *in silico* image analysis can be as central to generating results as experiments in the lab there is precedent for obtaining detailed explanations that may prove useful to other researchers.

The LAMP1-positive objects in fibroblasts here were identified by the Bernsen algorithm implementation in ImageJ. Use of this algorithm has been published, for example in the size analysis of Weibel Palade bodies (Ketteler et al., 2017). However, this and other local thresholding algorithms in ImageJ appear to be overlooked in the analysis of endolysosomes. For the analysis in this chapter the radius of the Bernsen algorithm circular window (5 pixels) was chosen experimentally. Although this renders the analysis quasi-automated this type of parameter modification is customary and necessary to allow adaptation of the algorithm to

various cell types, probes and organelles of interest. Watershed segmentation is a common method used to separate objects or cells in close proximity and here was implemented to counter any short-falls of the local thresholding. The results from this analysis showed that in sporadic PD fibroblasts LAMP1-positive objects were on average larger than those of age-matched controls (Fig. 3.2C). More specifically, there was a reduction in the relative frequency of small lysosomes ( $0-0.8 \mu\text{m}^2$ ) and an increase in larger individual lysosomes ( $0.8-5 \mu\text{m}^2$ ) and of lysosome clusters ( $>5 \mu\text{m}^2$ ) (Fig. 3.2E). In some experiments this shift was accompanied by a decrease in the number of LAMP1-positive objects per cell (Fig. 3.2D) which could be interpreted as upregulated lysosome fusion and impaired fission. However, in 3 out of 11 experiments there was an increase in the number of lysosomes suggesting there was a subtle proliferation. This proliferation may represent a compensatory mechanism to cope with lysosome dysfunction as is induced by cathepsin inhibitors (Dickinson et al., 2010).

The mechanism responsible for enlarged lysosomes in sporadic PD fibroblasts is unknown and requires further investigation. Although the lysosomal disturbance in sporadic PD fibroblasts manifests differently to that of younger LRRK2-GS PD cells, experiments using similar assays centred on Rab7 and TPC2 function would be informative (Hockey et al., 2015). Lysosome enlargement may be a consequence of reduced lysosomal protease activity (Dickinson et al., 2010; Yu et al., 2010). Enlarged lysosomes have also been attributed to impaired fission, changes in osmolarity, or the accumulation of proteins, lipids or glycosaminoglycans (Bandyopadhyay et al., 2014; Durchfort et al., 2012; Parkinson-Lawrence et al., 2010). Vacuolin similarly enlarges lysosomes (Fig. 3.M9). Despite this, the mechanism by which it induces this effect has not been clear. Vacuolin has been shown to inhibit  $\text{Ca}^{2+}$ -dependent lysosomal exocytosis (Cerny et al., 2004). However, it has also been shown not to (Huynh and Andrews, 2005). Lysosome enlargement by vacuolin may be caused by impaired fusion to lysosomes and endosomes, or to autophagosomes (Cerny et al., 2004; Lu et al., 2014). One study attributed the latter to increases in lysosomal pH and activation of Rab5a (Lu et al., 2014). Interestingly, the same group has reported that overexpressed TPC2 inhibits lysosome fusion to autophagosomes, also by increasing lysosomal pH (Lu et al., 2013). In addition, they found that this TPC2-dependent autophagy defect was regulated by  $\text{Ca}^{2+}$ , and not mTOR, which supported findings published a year earlier (Gómez-Suaga et al., 2012). Last year it was reported that vacuolin is an inhibitor of PIKfyve (Sano et al., 2016). This enzyme synthesises  $\text{PI}(3,5)\text{P}_2$ , the phosphoinositide that can activate TRPML1 and TPCs (Dong et al., 2010; Jha et al., 2014; McCartney et al., 2014). Sano and colleagues demonstrated that both vacuolin and PIKfyve inhibitor YM-201636 inhibit autophagic flux and impair trafficking of lysosomal enzymes (Jefferies et al., 2008; Sano et al., 2016). Taken together the above publications imply that lysosome enlargement may be a

consequence of modulated lysosomal  $\text{Ca}^{2+}$  channel activity. Intriguingly YM-201636, which can enlarge lysosomes, appears to improve lysosome morphology in LRRK2-GS PD fibroblasts as reported by a reduction in LAMP1 intensity (Hockey et al., 2015; Sano et al., 2016). The effect on lysosome size in this context has not yet been determined.

The relevance of enlarged lysosomes in regards to PD aetiology is unclear. The functional properties of larger lysosomes have been shown to differ from their smaller counterparts. For example, lysosome size has been inversely correlated to lysosome diffusion rates (Bandyopadhyay et al., 2014), and increased lysosome proliferation and size has been correlated to enhanced lysosomal  $\text{Ca}^{2+}$  signals (Dickinson et al., 2010).

Besides lysosomes, the enlarged LAMP1-positive objects in sporadic PD fibroblasts may represent late endosomes (Kilpatrick et al., 2017) or hybrid organelles such as endolysosomes and autolysosomes. Indeed, fusion between late endosomes and lysosomes gives rise to larger hybrid organelles (Mullock et al., 1998). In addition, enlarged LAMP1-positive objects colocalise with autophagosome marker LC3, and shrink with its disappearance (Yu et al., 2010). Therefore, examination of these PD fibroblasts with autophagosome and endosome markers is warranted to dissect the true identity of these enlarged species, and shed light on areas of dysfunction. Notably, disturbed autophagy in sporadic PD fibroblasts has recently been reported (Zhou et al., 2016).

In addition to lysosome morphology defects in LRRK2-GS PD fibroblasts, which have been ascribed to upregulated TPC2 activity and increased local  $\text{Ca}^{2+}$  fluxes, global  $\text{Ca}^{2+}$  signals induced by NAADP are augmented in these cells (Hockey et al., 2015; Pryor et al., 2000). Although there has been some controversy surrounding TPC activators NAADP can activate TPCs to drive such global  $\text{Ca}^{2+}$  signals (Brailoiu et al., 2009; Calcraft et al., 2009; Jha et al., 2014). Therefore it is plausible that upregulated TPC activity is responsible for the augmented NAADP-evoked  $\text{Ca}^{2+}$  signals. If a similar potentiation is caused in a physiological context these larger  $\text{Ca}^{2+}$  signals may disturb a careful  $\text{Ca}^{2+}$  balance and disturb  $\text{Ca}^{2+}$ -dependent protein folding, ATP synthesis, or even cause to apoptosis (Glancy and Balaban, 2012; Rizzuto et al., 2012; Wang and Kaufman, 2016). To investigate this possibility I used the naturally occurring peptide bradykinin. This extracellular agonist is involved in the inflammatory response and activates GPCRs (Marceau and Regoli, 2004). Bradykinin can induce  $\text{IP}_3$  and cADPR synthesis but NAADP synthesis has not been reported (Ataei et al., 2013; Johnson et al., 1990; Kip et al., 2006). As such, it is often considered as a typical stimulant of ER  $\text{Ca}^{2+}$  release (Shi et al., 1999). To find out whether lysosomes

contribute to the bradykinin-evoked global  $\text{Ca}^{2+}$  signal  $\text{NH}_4\text{Cl}$  was used in light of its ability to deplete lysosomal  $\text{Ca}^{2+}$  (Christensen et al., 2002). The use of GPN in these cells was not practicable as it elicits long-lasting oscillatory  $\text{Ca}^{2+}$  signals even in the absence of extracellular  $\text{Ca}^{2+}$  (Kilpatrick et al., 2013).  $\text{NH}_4\text{Cl}$  did inhibit bradykinin-evoked  $\text{Ca}^{2+}$  signals and also those of GPN (Fig. 3.4.C and D; Fig. 3.3B and C). This may indicate that  $\text{NH}_4\text{Cl}$  successfully depletes lysosomal  $\text{Ca}^{2+}$  and that lysosomal  $\text{Ca}^{2+}$  is required for bradykinin signalling. However, GPN-evoked  $\text{Ca}^{2+}$  signals depend upon its cleavage by the lysosomal enzyme cathepsin C (Haller et al., 1996; Jadot et al., 1984; Kilpatrick et al., 2013). This enzyme is pH-dependent and elsewhere inhibition of GPN-evoked  $\text{Ca}^{2+}$  signals has been attributed to changes in pH caused by  $\text{NH}_4\text{Cl}$  and not changes to lysosomal  $\text{Ca}^{2+}$  content (Haller et al., 1996; Jadot et al., 1984). The synthetic TRPML1 agonist, ML-SA1, is believed to induce  $\text{Ca}^{2+}$  release from the lysosome and therefore was also used to test the effects of  $\text{NH}_4\text{Cl}$  (Chapter 2; Shen et al., 2012). As shown in Figures 3.3D and E  $\text{NH}_4\text{Cl}$  inhibited ML-SA1-evoked  $\text{Ca}^{2+}$  signals supporting the use of  $\text{NH}_4\text{Cl}$  to deplete lysosomal  $\text{Ca}^{2+}$ . It should be noted however that the relationship between pH and TRPML1 is contentious with studies demonstrating that TRPML1 is inhibited at acidic pH, is optimally active at acidic pH and regulates lysosomal pH itself (Dong et al., 2008; Feng et al., 2014a; Kiselyov et al., 2005; Raychowdhury et al., 2004; Soyombo et al., 2006; Xu et al., 2007). More recently it has been reported that TRPML1 currents are enhanced at a slightly alkaline cytosolic pH and that ML-SA1-induced  $\text{Ca}^{2+}$  signals are greater in cells with a higher lysosomal pH (Lee et al., 2015; Li et al., 2016). Without unequivocal data regarding TRPML1 and pH it cannot be ruled out that  $\text{NH}_4\text{Cl}$  causes pH-dependent inhibition of ML-SA1-evoked  $\text{Ca}^{2+}$  signals, regardless of lysosomal  $\text{Ca}^{2+}$  content. An alternative to using  $\text{NH}_4\text{Cl}$  and GPN to deplete lysosomal  $\text{Ca}^{2+}$  is bafilomycin A. However, this inhibitor of the vacuolar  $\text{H}^+$ -ATPase is thought to indirectly deplete lysosomal  $\text{Ca}^{2+}$  by reducing the proton content of lysosomes (Morgan et al., 2011). Therefore, its effects are also inextricably linked to lysosomal pH. The sterol U18666a does reportedly deplete lysosomal  $\text{Ca}^{2+}$  without affecting lysosomal pH (Lloyd-Evans et al., 2008). Therefore its effect on bradykinin-evoked  $\text{Ca}^{2+}$  signals should be tested in future work to verify their dependence on lysosomal  $\text{Ca}^{2+}$ .

As a high concentration (100 mM) of  $\text{NH}_4\text{Cl}$  was used to compromise the lysosomes the possibility that it had off-target effects elsewhere in the cell was considered. Therefore, as a control experiment, the impact of  $\text{NH}_4\text{Cl}$  on thapsigargin-evoked  $\text{Ca}^{2+}$  signals was assessed (Fig. 3.3F and G). Thapsigargin inhibits  $\text{Ca}^{2+}$  uptake by SERCA into the ER thereby exposing any ER  $\text{Ca}^{2+}$  efflux (Brini and Carafoli, 2009; Chen et al., 2017; Thastrup et al., 1990). Although there was a small inhibition of the thapsigargin-evoked  $\text{Ca}^{2+}$  signal by  $\text{NH}_4\text{Cl}$  it was minor compared to the

inhibition of the GPN or ML-SA1-evoked  $\text{Ca}^{2+}$  signals. This suggests that ER  $\text{Ca}^{2+}$  was minimally affected compared to lysosomal  $\text{Ca}^{2+}$ .

With some evidence that bradykinin-evoked global  $\text{Ca}^{2+}$  signals are reliant on the lysosomes I investigated the contribution of the TPC lysosomal  $\text{Ca}^{2+}$  channels. Quantification of *TPC* transcripts in fibroblasts transfected with TPC1 or TPC2 siRNA revealed selective knockdown (Fig. 3.5C). It was noted that knockdown of TPC2 was less efficient than that of TPC1, which has been reported elsewhere (García-Rúa et al., 2016; Sakurai et al., 2015). To mimic the physiological environment fibroblasts were stimulated with bradykinin in the presence of extracellular  $\text{Ca}^{2+}$ . Therefore, the results from these TPC knockdown experiments may encompass changes to  $\text{Ca}^{2+}$  entry as well as  $\text{Ca}^{2+}$  release (Mcallister et al., 1993). Despite the discrete localisation, functions and reported channel regulation of TPC1 and TPC2 (please refer to TPC section in Chapter 1: Introduction) reduced expression of either isoform inhibited the magnitude of bradykinin-evoked  $\text{Ca}^{2+}$  signals (Fig. 3.6C). Interestingly, knockdown of both isoforms simultaneously did not worsen this inhibition. This may be due to a compensatory  $\text{Ca}^{2+}$  release pathway coming into play or because knockdown of one isoform impacts the activity of the other, or because knockdown of one isoform is sufficiently disruptive to the  $\text{Ca}^{2+}$  signalling network. In fibroblasts transfected with TPC2 siRNA in particular it was also observed that it took longer for the bradykinin-evoked  $\text{Ca}^{2+}$  signals to reach their peak (Fig. 3.6A and D). During these responses there is a slow, shallow rise in cytosolic  $\text{Ca}^{2+}$  immediately before the initial sharp increase. This may represent the “pacemaker” transition phase between the generation of local  $\text{Ca}^{2+}$  signals and the propagation of a global one (Bootman et al., 1997). Perhaps it is this transition which is impaired in cells with reduced *TPC2* expression. It was also observed that cells displaying oscillatory responses to bradykinin were slightly more frequent in cells transfected with TPC siRNA, particularly with TPC1 siRNA (Fig. 3.7A and E). These oscillations may be a product of lysosome-ER cross-talk as has been demonstrated for GPN, or extracellular  $\text{Ca}^{2+}$  may be involved (Dupont et al., 2011; Kilpatrick et al., 2013). The segregation of delayed signal peak with TPC2 knockdown, and increased oscillating cell frequency with TPC1 knockdown, may be indicative of discrete isoform roles in the generation of bradykinin-evoked  $\text{Ca}^{2+}$  signals. Perhaps TPC2 is the true trigger isoform whereas TPC1 maintains smooth dialogue between the endolysosomes and the ER once the signal has been initiated.



The inhibitory effects of TPC knockdown on bradykinin signalling may work through various modes:

1)  $\text{Ca}^{2+}$  release from the lysosome is known to trigger further  $\text{Ca}^{2+}$  release from the ER, to which it is functionally and physically coupled (Kilpatrick et al., 2013; Morgan, 2016). Therefore, if lysosomal  $\text{Ca}^{2+}$  release through TPCs is the initial trigger for bradykinin-evoked  $\text{Ca}^{2+}$  signals their knockdown would explain an inhibition of the signal.

2) The coupling of  $\text{Ca}^{2+}$  release from the lysosomes and the ER is believed to be maintained by membrane contact sites (MCS) between the two organelles, which keep them within 30 nm of each other (Kilpatrick et al., 2013, 2017). Very recently it has been demonstrated that TPC knockdown disrupts MCS. Specifically, TPC1 knockdown disrupts late endosome-ER MCS, and TPC2 knockdown disrupts lysosome-ER MCS (Kilpatrick et al., 2017). Therefore, TPC knockdown may inhibit bradykinin-evoked  $\text{Ca}^{2+}$  signals by breaking down the lysosome-ER MCS regardless of the lysosomal  $\text{Ca}^{2+}$  channel that might trigger the signal.

3) Although much attention is given to the “trigger” hypothesis of lysosomal  $\text{Ca}^{2+}$  signals being amplified by the ER the inverse scenario has also been reported. By using measurements of lysosomal pH as a proxy for NAADP-induced  $\text{Ca}^{2+}$  release Morgan and colleagues demonstrated that  $\text{Ca}^{2+}$  release from the ER is followed by NAADP-induced lysosomal  $\text{Ca}^{2+}$  release (Morgan, 2016; Morgan et al., 2013). Therefore, what we may be seeing in the inhibited bradykinin-evoked  $\text{Ca}^{2+}$  signals is an intact ER  $\text{Ca}^{2+}$  signal but an inhibited lysosomal counterpart through the TPCs. Indeed, the bradykinin signal may be composed of multiple reciprocal  $\text{Ca}^{2+}$  release events between the ER and the lysosomes.

4) Finally, TPC knockdown by siRNA transfection is a relatively severe intervention that may have unforeseen effects upon the cell. Currently there are no selective TPC blockers which could reveal the effects of acute TPC inhibition.

Whatever the mode of inhibition caused by TPC knockdown, the results suggest that bradykinin requires the TPCs to elicit a global  $\text{Ca}^{2+}$  signal. Bradykinin is thus an addition to a very limited list of physiological stimuli that evoke TPC-dependent global  $\text{Ca}^{2+}$  signals (Table 3.1). One of the other stimuli is glucose (Arredouani et al., 2015). However, this has been contended by a previous study and a more recent publication (Cane et al., 2016; Wang et al., 2012).

**Table 3.6 TPC-dependent, stimulus-evoked Ca<sup>2+</sup> signals**

Stimulus	Concentration	Isoform	Method	Cell type	Species	Reference
Anti-CD3 Ab	10 µg/ml	1 & 2	Knockdown (siRNA)	Jurkat 1G4	Human	(Davis et al., 2012)
Glucose	10 mM	1 & 2	Knockout	Pancreatic β cells	mouse	(Arredouani et al., 2015)
Isoprenaline plus electrical stimulation	3 nM 1 Hz	2	Knockout	Myocytes	Mouse	(Capel et al., 2015)
RANKL	1 nM	2	Knockdown (miRNA)	RAW BMM	Mouse	(Notomi et al., 2012)
VEGF	100 µg/L	2	Knockdown (shRNA)	HUVEC	Human	(Favia et al., 2014)

As bradykinin-evoked global Ca<sup>2+</sup> signals appeared to be TPC-dependent, the hypothesis was that the signals would be enhanced in LRRK2-GS PD fibroblasts which have been associated with upregulated TPC2 activity. However, there was no such potentiation when compared to the signals in age-matched control fibroblasts (Fig. 3.7C). This may be because other parts of the Ca<sup>2+</sup> signalling network recruited by bradykinin are altered in LRRK2-GS PD fibroblasts so that the effect of TPC over-activity is hidden.

The time taken to reach the peak of the bradykinin-evoked Ca<sup>2+</sup> signal was unchanged in LRRK2-GS PD fibroblasts (Fig. 3.7D). Interestingly however, the frequency of cells displaying oscillatory responses was reduced (Fig. 3.7E). Knockdown of both TPC isoforms increased the percentage of oscillating cells in control fibroblasts although it was more pronounced by TPC1 knockdown (Fig. 3.6E). These two sets of data could therefore indicate that TPC1 activity is upregulated in LRRK2-GS PD fibroblasts. Upregulated TPC2 activity in these cells has already been reported as its knockdown improves their disturbed lysosome morphology (Hockey et al., 2015). However, the reduced bradykinin-evoked Ca<sup>2+</sup> oscillations in LRRK2-GS PD cells may be caused by other unknown factors in this disease context. To probe the possibility of upregulated TPC1 activity in LRRK2-GS PD the effect of TPC1 knockdown on bradykinin-evoked Ca<sup>2+</sup> oscillations should be assessed in these disease model cells. Importantly, Ca<sup>2+</sup> oscillations encode vital information for various processes and effectors (Smedler and Uhlén, 2014; Uhlén and Fritz, 2010). For example,

Ca<sup>2+</sup> oscillations drive sustained activation of mitochondrial dehydrogenases (Hajnóczky et al., 1995). Therefore, the reduction of oscillatory responses in LRRK2-GS PD fibroblasts could represent a loss of important data which might impair ATP synthesis and place the cell under energetic stress. Alternatively, reduced oscillations may represent a compensatory mechanism to spare the mitochondria from the oxidative stress that can accompany ATP synthesis (Denton, 2009; Glancy and Balaban, 2012; Turrens, 2003).

Bradykinin-evoked Ca<sup>2+</sup> signals in sporadic PD fibroblasts were also not enhanced. In fact, there was a small reduction in signal magnitude (Fig. 3.8A-C). Recently, reduced ER Ca<sup>2+</sup> content and impaired SOCE was reported in sporadic PD fibroblasts which may be responsible for the reduced bradykinin-evoked Ca<sup>2+</sup> signals here (Zhou et al., 2016). Moreover, the reduced ER Ca<sup>2+</sup> reported by Zhou et al. was linked to impaired autophagy in these cells. As discussed above, impaired autophagy could be the cause of the enlarged LAMP1-positive structures identified in the sporadic PD fibroblasts (Fig. 3.2C). As well as aberrant autophagy reduced bradykinin-evoked Ca<sup>2+</sup> signals may be relevant to PD aetiology via regulation of tyrosine hydroxylase. Elevated cytosolic Ca<sup>2+</sup>, and bradykinin Ca<sup>2+</sup> signals in particular, have been linked to expression of the DA-synthesising enzyme (Aumann and Horne, 2012; Menezes et al., 1996). Given that DA depletion is the cause of motor symptoms in PD a reduced bradykinin response may exacerbate the problem (Brichta et al., 2013). Despite a small reduction in the magnitude of the signal there was no difference in the time taken to reach the signal peak nor the frequency of oscillatory cells (Fig. 3.8D and E). The bradykinin-evoked Ca<sup>2+</sup> signals in LRRK2-GS and sporadic PD fibroblasts here are subtly different which may suggest their Ca<sup>2+</sup> networks are modelled differently. However, the age difference between groups may also influence their Ca<sup>2+</sup> signalling (Kilpatrick et al., 2016b).

In this chapter, experiments have been conducted solely in fibroblasts. These cells, derived from live patients, are an attractive model of disease as they are physiologically relevant and robust (Auburger et al., 2012). One drawback encountered here however is that GPN-evoked Ca<sup>2+</sup> signals in fibroblasts are complex and prolonged and therefore do not lend themselves to experiments involving subsequent Ca<sup>2+</sup> signals. Furthermore, there are obvious questions about the relevance of fibroblasts when modelling a neurodegenerative disease. For instance, changes in neurons that may be relevant to PD aetiology are not always seen in fibroblasts (Ordonez et al., 2012). Therefore, other more neuronal models may prove more effective for the identification of perturbed Ca<sup>2+</sup> signalling that is relevant to PD.

To summarise, changes to lysosome morphology were detected in fibroblasts from patients with familial LRRK2-GS or sporadic PD thereby supporting a role for lysosomes in PD pathology. In addition, the extracellular agonist bradykinin was identified as requiring TPCs to elicit its full, physiological global  $\text{Ca}^{2+}$  signal. However despite this, and the report of upregulated TPC2 activity in LRRK2-GS PD fibroblasts, bradykinin-evoked  $\text{Ca}^{2+}$  signals were not potentiated in these cells. Nor were bradykinin-evoked  $\text{Ca}^{2+}$  signals larger in sporadic PD fibroblasts.

# CHAPTER 4: TPCs and Global Ca<sup>2+</sup> Signalling

## - In a Neuronal PD Model

### 4.1 INTRODUCTION

The lysosomal Ca<sup>2+</sup> channel TPC2 has been implicated in Parkinson's disease (PD) that is associated with dysfunction of the enzyme LRRK2. First, in HEK293T cells overexpressing LRRK2, TPC2 activity and increased local Ca<sup>2+</sup> fluxes have been associated with autophagy defects (Gómez-Suaga et al., 2012). Second, in fibroblasts from familial PD patients, who harbour the *LRRK2*-GS mutation, upregulated TPC2 activity and local Ca<sup>2+</sup> fluxes have been associated with disturbed lysosome morphology (Hockey et al., 2015). In addition, these fibroblasts exhibit augmented global Ca<sup>2+</sup> signals in response to the Ca<sup>2+</sup>-mobilising messenger NAADP. Although there has been some debate upon the subject there is evidence that global Ca<sup>2+</sup> signals evoked by NAADP are TPC-dependent (Brailoiu et al., 2009; Calcraft et al., 2009). Therefore, the potentiated NAADP signals in LRRK2-GS PD may also be a consequence of upregulated TPC activity. However, whether such activity augments physiological global Ca<sup>2+</sup> signals in response to extracellular stimuli is unclear. In Chapter 3 I investigated this by first identifying an extracellular agonist that required the lysosomes and TPCs to elicit its global Ca<sup>2+</sup> signal. I then examined these agonist-evoked Ca<sup>2+</sup> signals in the LRRK2-GS PD fibroblasts. There was a small reduction in the proportion of cells displaying oscillatory Ca<sup>2+</sup> signals compared to age-matched controls. However, there was no clear potentiation.

Whilst fibroblasts derived from live PD patients are an attractive model of disease their relevance to neurodegeneration is often questioned (Auburger et al., 2012). Indeed, use of a neuronal cell type may uncover important aspects of pathogenicity that are not observed in fibroblasts (Ordonez et al., 2012). To this end a neuronal cell line, SH-SY5Y, is commonly used for PD research (Xicoy et al., 2017). SH-SY5Ys have been sub-cloned from human metastatic neuroblastoma tissue and possess dopaminergic (DAergic) activity (Biedler et al., 1973, 1978). This activity may make SH-SY5Ys an appropriate model of the DAergic SNC - the brain region which undergoes extensive neurodegeneration in PD (Braak et al., 2003). In this chapter I use SH-SY5Y cells that stably express the LRRK2 mutant, LRRK2-GS, as a neuronal model of LRRK2-GS PD. As for Chapter 3, one aim is to identify an extracellular agonist that requires TPCs to elicit its global Ca<sup>2+</sup> signals in this cell line. The second aim is to determine whether such signals are

potentiated in the neuronal LRRK2-GS cells, which may be indicative of upregulated TPC activity, and be of potential significance to PD aetiology as previously discussed (Fig. 4.1).

In addition, pharmacological inhibition of TPCs is investigated. Recently the alkaloid tetrandrine has been identified as a TPC inhibitor (Sakurai et al., 2015). Sakurai et al. demonstrated that tetrandrine inhibits TPC currents, NAADP-evoked  $\text{Ca}^{2+}$  signals and Ebola infectivity; the latter of which was also reduced by TPC knockdown. This compound may therefore be a useful tool for probing the contribution of TPC activity to physiological global  $\text{Ca}^{2+}$  signals. However, tetrandrine is not a selective TPC blocker and there are currently none that are known. As part of my investigation I assay putative TPC blockers that may inform the development of selective compounds.

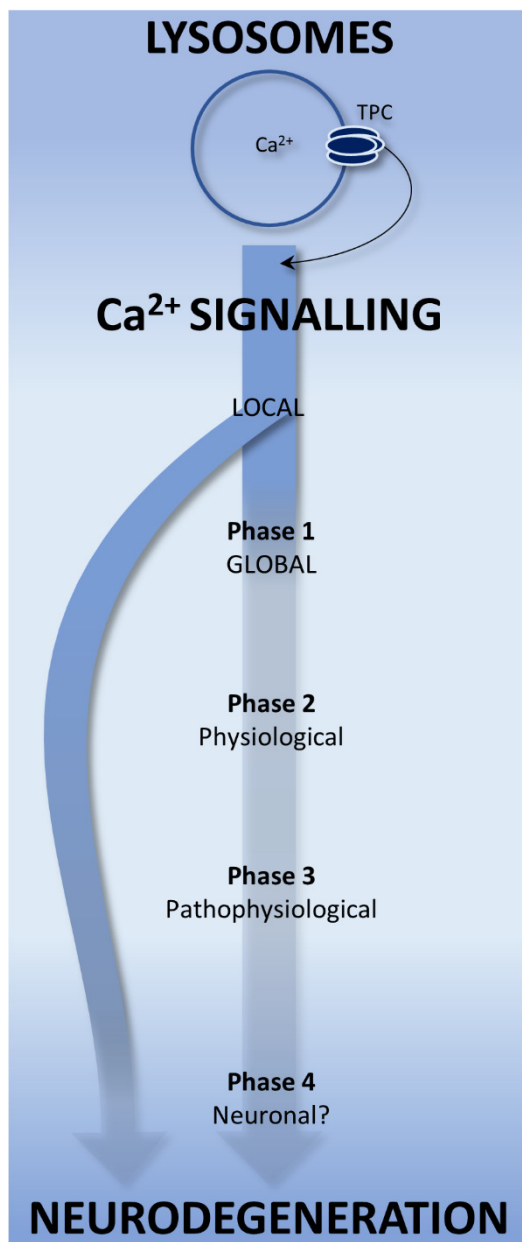


#### Figure 4.1 Introduction

Upregulation of the lysosomal  $\text{Ca}^{2+}$  channel TPC2 has been linked to LRRK2-GS PD. It may be through potentiated local  $\text{Ca}^{2+}$  signalling that this contributes to neurodegeneration (curved left-hand arrow). In LRRK2-GS PD fibroblasts global  $\text{Ca}^{2+}$  signals are also potentiated, which may contribute to neurodegeneration too (straight right-hand arrow).

This global route from TPC2 dysfunction to neurodegeneration is feasible as it has been reported that TPCs are required for global  $\text{Ca}^{2+}$  signals stimulated by NAADP (Phase 1). However, there is very little information about extracellular stimuli that require TPCs to elicit physiological global  $\text{Ca}^{2+}$  signals (Phase 2) or whether such signals are augmented in LRRK2-GS PD and thus are of pathophysiological importance (Phase 3). To further explore the link between TPCs, global  $\text{Ca}^{2+}$  signalling and neurodegeneration in PD the investigation was moved from patient-derived fibroblasts in Chapter 3 into a neuronal model of PD in this chapter (Phase 4).

## **4.2 METHODS and ANALYSIS**

### **4.2.1 Recurrent methods**

Fibroblast culture, quantitative PCR, Fura-2 labelling, lysotracker (LTR) labelling, LTR imaging and data presentation are as described in Chapters 2 and 3.

### **4.2.2 Cell culture**

#### **4.2.2.1 SH-SY5Y**

SH-SY5Y cells were maintained in 1:1 mixture of DMEM and Ham's F12 media supplemented with 10% v/v fetal bovine serum, 100 units/ml penicillin and 100 µg/ml streptomycin and 1% (v/v) nonessential amino acids (all GIBCO) at 37°C in a humidified atmosphere with 5% CO<sub>2</sub>. SH-SY5Ys were given fresh media every 2-3 days and passaged using trypsin (Gibco). SH-SY5Y cell lines with the stable expression of wildtype and G2019S mutated LRRK2 (LRRK2 WT and LRRK2-GS, respectively) were developed by Drs Kai-Yin Chau and Mark Cooper (Department of Clinical Neuroscience, UCL). These cells were accompanied by a control untransfected line and were plated at 100,000 cells/ml (T25 flasks, 5ml/flask) 2 days prior to harvesting for analysis by quantitative PCR. Details of platings for alternative experiments are described below.

### **4.2.3 siRNA transfection**

#### **4.2.3.1 Standard protocol**

For the siRNA transfection analysed by western blot the following protocol was adhered to, except for a 200,000 cells/ml plating density. For all other standard siRNA transfections: SH-SY5Y cells were plated at 350,000 cells/ml (For epifluorescence microscopy: 13 mm glass coverslips coated in poly-L-lysine (Sigma), in 24-well plates, 0.3 ml/well; for western blot/quantitative PCR analysis: no coverslips, 6-well plates, 1.5ml/well) and transfected with siRNAs using Lipofectamine® RNAiMAX (Invitrogen) overnight. The following morning SH-SY5Ys were re-transfected in fresh media for a further 8 hours and cultured overnight in the absence of siRNA before experimentation. A control siRNA duplex (AllStars Neg.Control) was purchased from Qiagen. Details of targeting siRNAs on the next page.

**Table 4.1 TPC-targeting siRNAs**

ID	Brand	Product Name	Target gene	Target exon	Target sequence (5'-3')
TPC1 siRNA	Qiagen	Hs_TPCN1_5	<i>TPC1</i>	10	CGAGCTGTATTTTCATCATGAA
TPC2 siRNA	Qiagen	Hs_TPCN2_6	<i>TPC2</i>	2	CAGGTGGGACCTCTGCATTGA
TPC2 siRNA #2	Thermo Fisher	s47773	<i>TPC2</i>	3	CGGTATTACTCGAACGTAT
TPC2 siRNA #3	Thermo Fisher	s47774	<i>TPC2</i>	13	ACAGAAGTGTGGTTAAAGA

#### 4.2.3.2 Extended protocol

SH-SY5Y cells were plated at 200,000 cells/ml (no coverslips, 6-well plates, 1.5ml/well) and cultured overnight in the absence of siRNA. The following day SH-SY5Ys were transfected with siRNAs using Lipofectamine® RNAiMAX (Invitrogen) for 72 hours. SH-SY5Ys were transfected with the same TPC2-targeted siRNAs used in the standard protocol.

### 4.2.4 Microscopy: Epifluorescence

#### 4.2.4.1 Ca<sup>2+</sup> - Fura-2

SH-SY5Y were plated 2 days prior to imaging at 100,000 cells/ml (13 mm glass coverslips coated in poly-L-lysine (Sigma), in 24-well plates, 0.5 ml/well), except for those subjected to siRNA transfection. Ca<sup>2+</sup> was measured using Fura-2 and analysed as described in Chapters 2 and 3. Cells were challenged with GPN (200 µM; Santa Cruz Biotechnology), carbachol (3.16 µM; 100 µM; Sigma), bradykinin (100 nM; 10 µM; Sigma), thapsigargin (1 µM; Merck) and CaCl<sub>2</sub> (2 mM; Sigma). Some cells were incubated with tetrandrine (10 µM; Santa Cruz Biotechnology), L-deprenyl (1 mM; Sigma), sunitinib (10 µM; Sigma) or pimozone (10 µM; Sigma) during imaging and for 1 hour prior to imaging during Fura-2 loading. Some cells were treated acutely with these drugs or fluphenazine (10 µM; Sigma). All compounds except L-deprenyl and fluphenazine were dissolved in DMSO (Sigma). L-deprenyl and fluphenazine were dissolved in H<sub>2</sub>O. The maximal volume of vehicle added in any experiment was 1% (v/v). Where indicated Ca<sup>2+</sup> was omitted from the HBS or replaced with 1 mM EGTA (Sigma).

The change of the Fura-2 ratio between the basal value and the value at 250 seconds into imaging ( $\Delta$  [Ca<sup>2+</sup>] (ratio) at 250 s) was calculated to quantify the magnitude of response at 250 seconds.



#### **4.2.5 Western blotting**

Cells were harvested by scraping, lysed in RIPA buffer (pH 7.4) containing 150 mM NaCl, 0.5% (w/v) sodium dodecyl sulphate (SDS), 0.1% (v/v) sodium dodecyl sulphate (SDS), 1% (v/v) Triton X-100, 50 mM Tris, and treated with EDTA-free protease inhibitor (Roche) and Halt Phosphatase Inhibitor Cocktail (Thermo Scientific) for 30 minutes on ice. Samples were centrifuged at 15,000 g for 15 minutes at 4°C and supernatant was stored at -20°C. Protein concentration of the supernatant was determined using bicinchoninic acid and bovine albumin serum standards. 13 µg of protein per sample was incubated with NuPAGE LDS sample buffer (Invitrogen) and 100 mM dithiothreitol (Sigma) for 45 minutes at room temperature. Along with PageRuler Plus protein ladder (Thermo Scientific) samples were separated on a NuPAGE 4-12% Bis-Tris gel (Invitrogen) and transferred to a PVDF filter (Bio-Rad) in buffer (48 mM Tris, 40 mM glycine, 0.04% (v/v) SDS, 20% (v/v) methanol). The blot was blocked with Tris-buffered saline plus Tween (TBS-T; pH 7.4) containing 25 mM Tris-HCl, 137 mM NaCl and 2.7 mM KCl, 0.1% (v/v) Tween 20, plus 5% (w/v) dried skimmed milk, overnight at 4°C. The blot was sequentially incubated with rabbit anti-TPC1 (Abcam ab80961; 1/200 dilution) and HRP-conjugated anti-rabbit (Santa Cruz Biotechnology; Sc-2005; 1/2000 dilution) in TBS-T containing 2.5% (w/v) milk for 1 hour at room temperature. Between and after incubations the blot was washed with TBS-T with no milk. The blot was developed using Amersham ECL Prime Western Blotting Detection Reagent (GE Healthcare) and imaged using the Bio-Rad ChemiDoc MP imaging system. To control for protein loading the blot was stripped with boiling acidic glycine and re-probed using goat anti-actin (Santa Cruz Biotechnology; Sc-1615; 1/500 dilution) and HRP-conjugated rabbit anti-goat (Santa Cruz Biotechnology; sc-2768; 1/2000 dilution).

Intensity of antibody staining was analysed in ImageJ. Boxes of equal size were manually plotted over each lane and intensity was visualised using Analyze>Gels>Plot Lanes. Background intensity was excluded using the \*straight\* tool and area under the peak was measured using the wand tool. Expression of TPC1 was normalised to that of actin.

#### **4.2.6 Statistical analysis**

Analysis was performed using IBM SPSS Statistics 22. Tests to determine statistical significance were performed on datasets in which more than three experiments had been conducted per group/condition, experimental means were clearly different between groups, but where values from individual experiments in one group shared the range of another. Independent-Samples T tests were performed to determine the statistical significance of data from two groups exhibiting normal distribution. Where data were not normally distributed significance was determined by

a Mann-Whitney U test. A Kruskal-Wallis H test followed by post-hoc Mann-Whitney U tests was performed to determine the statistical significance of data from more than two groups that exhibited normal distribution but unequal variance.

## 4.3 RESULTS

### 4.3.1 Lysomotropic agent GPN evokes simple Ca<sup>2+</sup> signals in SH-SY5Y cells

In fibroblasts from people with familial LRRK2-GS PD upregulated TPC2 activity is associated with augmented global Ca<sup>2+</sup> signals in response to NAADP (Hockey et al., 2015). However, whether LRRK2-GS-dependent TPC upregulation potentiates physiological global Ca<sup>2+</sup> signals is unclear. To probe this in the neuronal cell line SH-SY5Y I sought an extracellular agonist that required the TPCs to elicit its full global Ca<sup>2+</sup> signal with the intention of examining such signals in cells that stably express the LRRK2-GS mutant. The first port of call was to identify extracellular agonists that evoked their signals through the lysosomes. To do this the lysosomes were first compromised by addition of GPN, which permeabilises the lysosomal membrane, and causes leakage of luminal content (Haller et al., 1996; Jadot et al., 1984). In fibroblasts GPN evoked complex, long-lasting Ca<sup>2+</sup> signals that would complicate the examination of subsequent signals evoked by extracellular agonists (Fig. 4.1A). In SH-SY5Ys though, the Ca<sup>2+</sup> signal induced by GPN was simple and monotonic (Fig. 4.1A). Therefore, in this cell line, GPN was a viable tool with which to identify extracellular agonists that recruit the lysosomes. The reason for the different GPN-evoked Ca<sup>2+</sup> signals in fibroblasts and SH-SY5Ys is unknown. GPN reduces lysotracker (LTR) fluorescence and thus acidic organelles at comparable rates in both cell types (Fig. 4.1B).

### 4.3.2 Carbachol and bradykinin evoke concentration-dependent Ca<sup>2+</sup> signals

The cholinergic agonist carbachol was one candidate stimulus of TPC-dependent, physiological global Ca<sup>2+</sup> signals. The agonist bradykinin was also considered as its signals in fibroblasts were inhibited by NH<sub>4</sub>Cl, and TPC knockdown in Chapter 3. Both carbachol and bradykinin are known to stimulate IP<sub>3</sub> synthesis (Ataei et al., 2013; Chen and Hsu, 1994; Johnson et al., 1990; Piiper et al., 1994; Shin et al., 2003), and carbachol has been shown to stimulate NAADP synthesis too (Aley et al., 2013). In untransfected SH-SY5Y cells these two agonists evoked concentration-dependent Ca<sup>2+</sup> signals of quite different kinetics (Fig. 4.2). Carbachol elicits a biphasic response (initial single peak followed by a plateau phase; Fig. 4.2A) whereas bradykinin produces a single peak response (Fig. 4.2C). Notably, bradykinin induces a slightly different signal in SH-SY5Ys compared to fibroblasts: Whereas cytosolic Ca<sup>2+</sup> promptly returns to basal levels in SH-SY5Ys (<450s; Fig. 4.2C) it remains elevated for more than 800s in fibroblasts (Fig. 3.4A). The sub-maximal concentrations of 3.16 μM and 100 nM were chosen for subsequent experiments

involving carbachol and bradykinin respectively (Fig. 4.2B and D). This was to facilitate observations of any inhibitory or potentiating effects upon their signals.

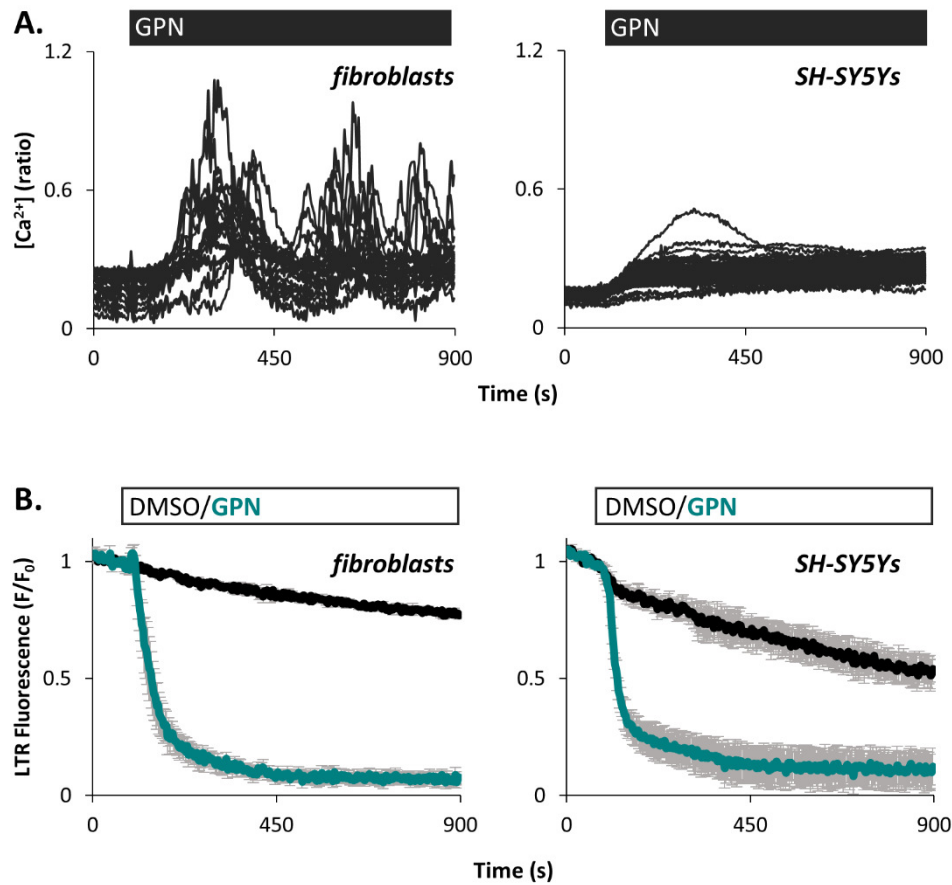


**Figure 4.1** Lysototropic agent GPN evokes simple  $Ca^{2+}$  signals in SH-SY5Y cells

**(A)** Cytosolic  $Ca^{2+}$  traces of individual *fibroblasts* ( $n=23$ ) or *SH-SY5Ys* ( $n=23$ ) stimulated with GPN ( $200 \mu M$ ). **(B)** Average Lysotracker Red fluorescence (LTR) traces (mean of experiments  $\pm$  S.E.M) of *fibroblasts* or *SH-SY5Ys* upon addition of DMSO or GPN ( $200 \mu M$ ). Data presented as ratio of fluorescence compared to basal fluorescence ( $F/F_0$ ). A total of 101/153 (DMSO/GPN) fibroblasts from 4 independent platings were analysed over 3/5 experiments (DMSO/GPN) to generate the data in **B**. A total of 122/124 (DMSO/GPN) SH-SY5Ys from 1 plating were analysed over 3 experiments per condition to generate the data in **B**.

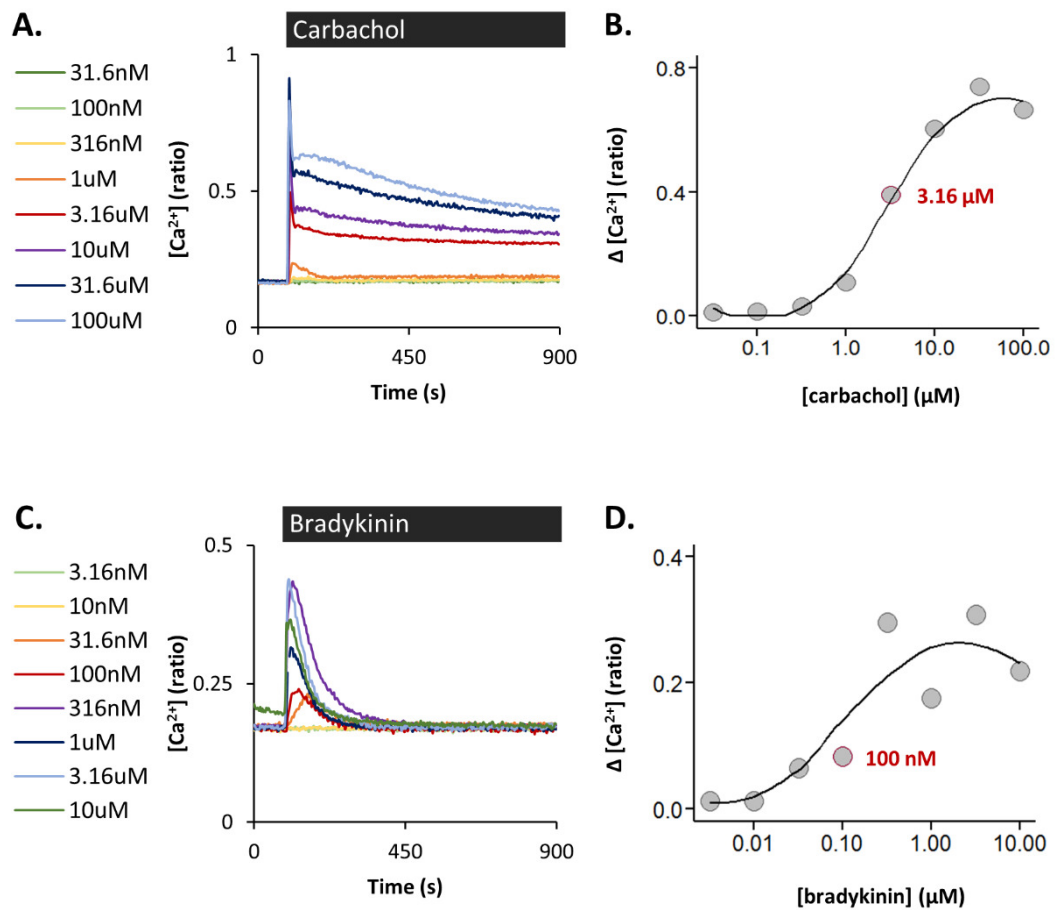


**Figure 4.2 Carbachol and bradykinin evoke concentration-dependent  $Ca^{2+}$  signals**

(A) Average cytosolic  $Ca^{2+}$  traces (mean of individual cells in a single experiment) of SH-SY5Ys stimulated with carbachol at a range of concentrations. (B) Data quantifying magnitude of responses in A. Each plot point represents one experiment. The carbachol concentration used in subsequent experiments (3.16  $\mu M$ ) is outlined in red. 39-68 SH-SY5Ys from 1 plating were analysed per carbachol concentration. (C and D) Same format as for A and B, upon stimulation with bradykinin. 51-127 SH-SY5Ys from 1 plating were analysed per concentration.

### 4.3.3 GPN inhibits carbachol but not bradykinin-evoked Ca<sup>2+</sup> signals

As shown in Figures 4.3A and C global Ca<sup>2+</sup> signals were evoked by both carbachol and bradykinin in the presence of the vehicle, DMSO. To investigate the contribution of the lysosomes to carbachol and bradykinin-evoked Ca<sup>2+</sup> signals SH-SY5Y cells were first stimulated with GPN. Following this GPN challenge carbachol-evoked Ca<sup>2+</sup> signals were inhibited (Fig. 4.3A and B). Interestingly however, the bradykinin-evoked Ca<sup>2+</sup> signals remained intact (Fig. 4.3C and D).

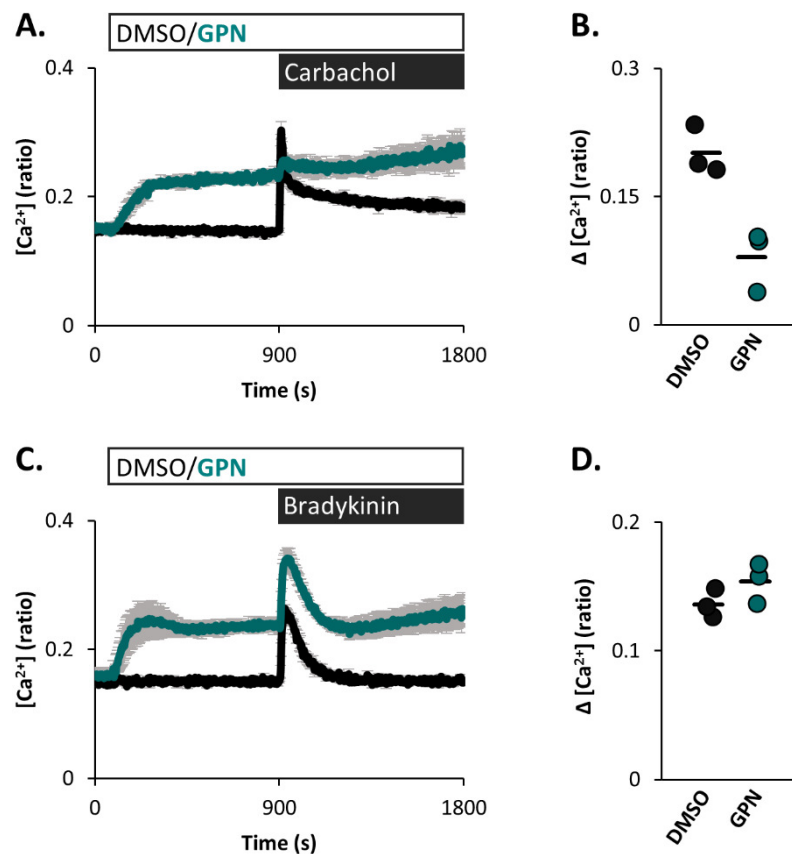


**Figure 4.3 GPN inhibits carbachol but not bradykinin-evoked Ca<sup>2+</sup> signals**

**(A)** Average cytosolic Ca<sup>2+</sup> traces (mean of experiments ± S.E.M.) of SH-SY5Ys stimulated with carbachol (3.16 μM), following DMSO or GPN (200 μM). **(B)** Data quantifying magnitude of carbachol responses in A. Each plot point represents one experiment, n=3/3 (DMSO/GPN). A total of 260/297 (DMSO/GPN) SH-SY5Ys from 3 independent platings were analysed. **(C and D)** Same format as for A and B, upon stimulation with bradykinin (100 nM), n=3/3 (DMSO/GPN). A total of 329/280 (DMSO/GPN) SH-SY5Ys from 2 independent platings were analysed.

#### **4.3.4 Carbachol but not bradykinin blocks GPN-evoked Ca<sup>2+</sup> signals**

Having seen that carbachol-evoked Ca<sup>2+</sup> signals were selectively blocked by GPN, the inverse experiment was carried out. That is, SH-SY5Ys were first stimulated with carbachol or bradykinin before examining a subsequent GPN-evoked Ca<sup>2+</sup> signal. This was conducted in the absence of extracellular Ca<sup>2+</sup> to isolate the cells from Ca<sup>2+</sup> entry, and to ensure the termination of agonist-evoked Ca<sup>2+</sup> signals before the GPN addition. To maximally deplete the intracellular Ca<sup>2+</sup> stores in this experiment only, the highest agonist concentrations from the concentration-response curves were used (Fig. 4.2). As the control experiment an addition of the agonist vehicle (HEPES-buffered saline (HBS)) was made before an addition of GPN, which generated a small but clear Ca<sup>2+</sup> signal (Fig. 4.4). In contrast, no GPN-evoked Ca<sup>2+</sup> signal was detected after carbachol stimulation. Following bradykinin however, the GPN-evoked Ca<sup>2+</sup> signal remained intact. This result, together with the result displayed in Figure 4.3, indicates that carbachol-evoked Ca<sup>2+</sup> signals work through the lysosomes but that bradykinin-evoked Ca<sup>2+</sup> signals do not.

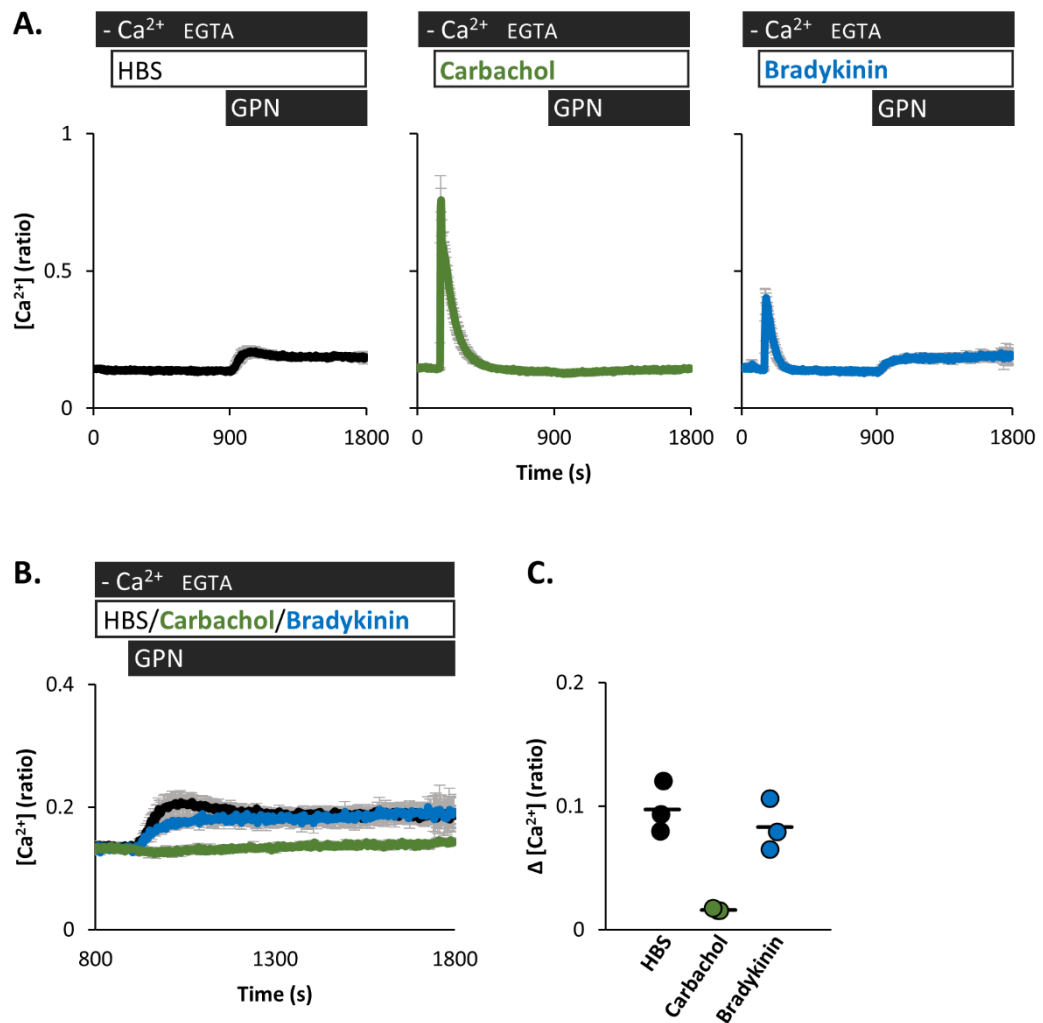


**Figure 4.4 Carbachol but not bradykinin blocks GPN-evoked  $Ca^{2+}$  signals**

**(A)** Average cytosolic  $Ca^{2+}$  traces (mean of experiments  $\pm$  S.E.M) of SH-SY5Ys stimulated with GPN (200  $\mu$ M) following HBS, carbachol (100  $\mu$ M) or bradykinin (10  $\mu$ M) in the absence of extracellular  $Ca^{2+}$  ( $Ca^{2+}$  was replaced with 1mM EGTA). **(B)** Graphs from **A** overlaid and x axis expanded to show the GPN  $Ca^{2+}$  signals. **(C)** Data quantifying magnitude of GPN responses in **A** and **B**. Each plot point represents one experiment,  $n=3/3/3$  (HBS/Carbachol/Bradykinin). A total of 261/290/276 (HBS/Carbachol/Bradykinin) SH-SY5Ys from 3 independent platings were analysed.

### 4.3.5 Thapsigargin inhibits both carbachol and bradykinin-evoked $Ca^{2+}$ signals

Both carbachol and bradykinin have been associated with  $IP_3$  synthesis and ER  $Ca^{2+}$  release (Ataei et al., 2013; Chen and Hsu, 1994; Johnson et al., 1990; Kip et al., 2006; Luciani et al., 2009; Piiper et al., 1994; Shin et al., 2003; Suzuki et al., 2014). To assess whether ER  $Ca^{2+}$  was a component of their signals in SH-SY5Ys I depleted ER  $Ca^{2+}$  using the SERCA inhibitor thapsigargin. These experiments were conducted in the absence of extracellular  $Ca^{2+}$  to isolate the cells from  $Ca^{2+}$



entry, and specifically store-operated  $\text{Ca}^{2+}$  entry (SOCE) which occurs as a consequence of ER  $\text{Ca}^{2+}$  depletion (Shen et al., 2011). As shown in Figures 4.5A and C both carbachol and bradykinin generated global  $\text{Ca}^{2+}$  signals in the absence of extracellular  $\text{Ca}^{2+}$  following the thapsigargin vehicle, DMSO. However, following thapsigargin stimulation, both agonist-evoked  $\text{Ca}^{2+}$  signals were inhibited (Fig. 4.5). This indicates that both carbachol and bradykinin-evoked  $\text{Ca}^{2+}$  signals require ER  $\text{Ca}^{2+}$ .

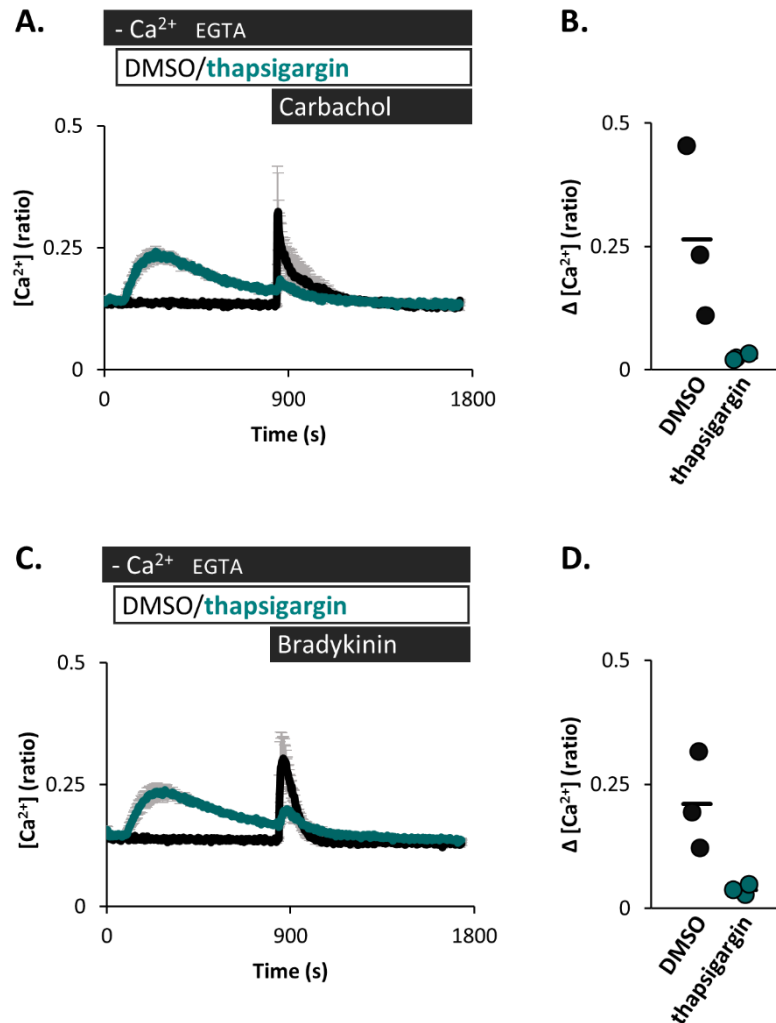


**Figure 4.5 Thapsigargin inhibits both carbachol and bradykinin-evoked  $\text{Ca}^{2+}$  signals**

**(A)** Average cytosolic  $\text{Ca}^{2+}$  traces (mean of experiments  $\pm$  S.E.M) of SH-SY5Ys stimulated with carbachol ( $3.16 \mu\text{M}$ ) following DMSO or thapsigargin ( $1 \mu\text{M}$ ), in the absence of extracellular  $\text{Ca}^{2+}$  ( $\text{Ca}^{2+}$  was replaced with  $1\text{mM}$  EGTA). **(B)** Data quantifying magnitude of carbachol responses in **A**. Each plot point represents one experiment,  $n=3/3$  (DMSO/thapsigargin). A total of 269/322 (DMSO/thapsigargin) SH-SY5Ys from 3 independent platings were analysed. **(C and D)** Same format as for **A** and **B**, upon stimulation with bradykinin ( $100 \text{ nM}$ ),  $n=3/3$  (DMSO/thapsigargin). A total of 279/219 (DMSO/thapsigargin) SH-SY5Ys from 3 independent platings were analysed.

### 4.3.6 Validating TPC knockdown in SH-SY5Ys

Having observed that carbachol-evoked global  $\text{Ca}^{2+}$  signals were inhibited by GPN I went on to investigate the contribution of TPCs to these responses. To do this SH-SY5Y cells were transfected with siRNAs targeted to TPC1 or TPC2, and stimulated with carbachol. In the first instance, the viability of TPC knockdown in this cell line was assessed by western blot. As shown in Figures 4.6A and B, TPC1 expression was reduced by TPC1 siRNA but not TPC2 siRNA. Subsequently, the knockdown protocol was adjusted to optimise cell density for  $\text{Ca}^{2+}$  imaging and mRNA was extracted from these cells to be analysed by quantitative PCR. Results from this analysis showed selective knockdown of each TPC isoform by ~50% (Fig. 4.6C). Interestingly, both siRNAs increased the transcript levels of the non-targeted TPC. The upregulation of TPC1 by TPC2 siRNA was variable but large, and this contributed to a considerable change in *TPC1/TPC2* expression ratio (Fig. 4.6D).

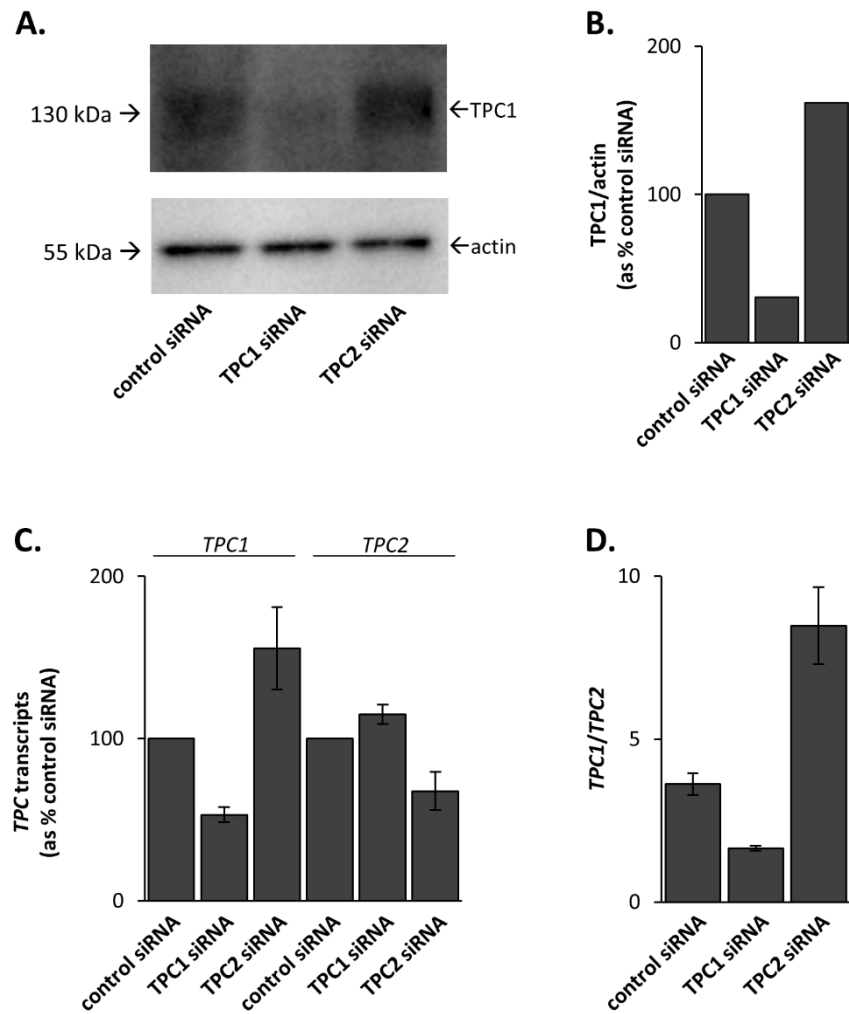


**Figure 4.6 Validating TPC knockdown in SH-SY5Ys**

**(A)** Western blot of samples from SH-SY5Ys transfected with control or TPC siRNA. Blot stained with antibodies raised to TPC1 and actin. Position and size of accompanying protein ladder markers are indicated on the left. Data from one experiment. **(B)** Intensity analysis of **A** performed in ImageJ. TPC1 protein expression was normalised to that of actin and presented as a percentage of TPC1 protein expression in SH-SY5Ys transfected with control siRNA. **(C and D)** Data quantifying *TPC* transcripts in SH-SY5Ys that have been transfected with control or TPC siRNA. The mean ( $\pm$  S.E.M) of 3 experiments from 3 independent platings is displayed. **(C)** TPC transcripts were normalised to those of UBC and are presented as a percentage of the TPC transcript levels in SH-SY5Ys transfected with control siRNA. **(D)** Ratio comparing transcript levels of *TPC1* and *TPC2*.

### 4.3.7 TPC1 knockdown inhibits carbachol-evoked $\text{Ca}^{2+}$ signals

In SH-SY5Ys transfected with TPC siRNA global  $\text{Ca}^{2+}$  signals induced by carbachol were inhibited (Fig. 4.7A and B). Notably, this inhibitory effect was clearer in cells transfected with TPC1 siRNA. In those transfected with TPC2 siRNA the magnitude of the signal was modestly reduced compared to controls but this did not reach statistical significance. Analysis of time taken to reach the signal peak revealed that there was no change between conditions (Fig. 4.7C).

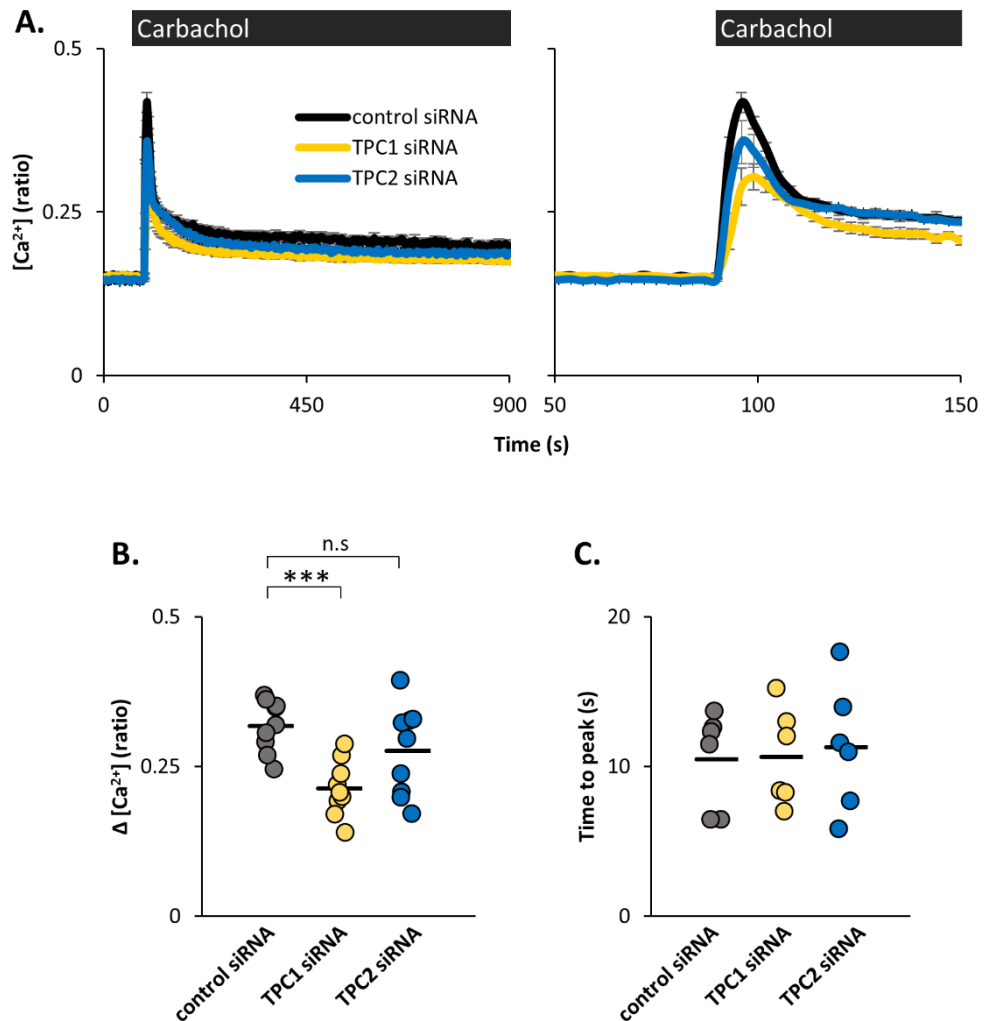


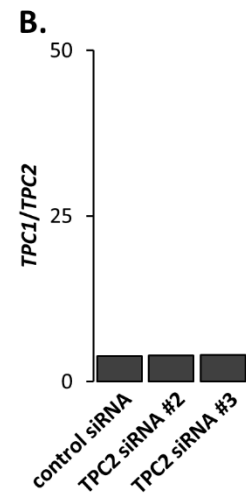
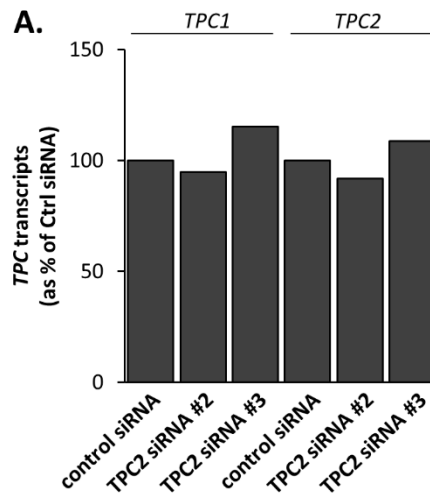
**Figure 4.7 TPC1 knockdown inhibits carbachol-evoked  $\text{Ca}^{2+}$  signals**

**(A)** Average cytosolic  $\text{Ca}^{2+}$  traces (mean of experiments  $\pm$  S.E.M) of SH-SY5Ys transfected with control or TPC siRNA, and stimulated with carbachol ( $3.16 \mu\text{M}$ ). Left panel shows entire imaging time course. The same dataset is shown in right-hand panel, with an expanded x axis. **(B and C)** Data quantifying carbachol responses in **A**. Each plot point represents one experiment,  $n=9/9/9$  (control siRNA/TPC1 siRNA/TPC2 siRNA). A total of 1187/1168/1058 (control siRNA/TPC1 siRNA/TPC2 siRNA) SH-SY5Ys from 3 independent platings were analysed. **(B)** Magnitude of responses. **(C)** Time to reach peak magnitude, analysed from SH-SY5Ys with magnitude  $\geq 0.1$ . \*\*\* $p < 0.005$  as determined by a Kruskal-Wallis H test followed by a post hoc Mann-Whitney U test.

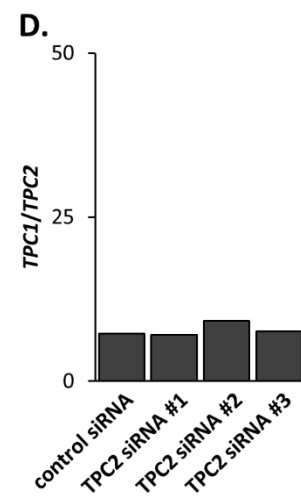
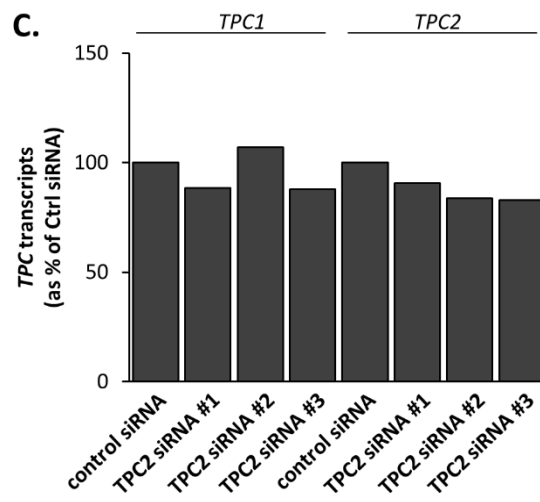
#### **4.3.8 TPC2 siRNAs reduce *TPC2* transcript levels in fibroblasts but not SH-SY5Ys**

In SH-SY5Y cells transfected with TPC1 or TPC2 siRNA the inhibition of carbachol-evoked Ca<sup>2+</sup> signals (Fig. 4.7A and B) appeared to correlate with TPC knockdown efficiency (Fig. 4.6A). That is, the inhibition of signal magnitude in cells transfected with TPC1 siRNA was more pronounced compared to those transfected with TPC2 siRNA. This reflected a greater knockdown of TPC1 compared to that of TPC2. To see if TPC2 knockdown efficiency could be improved two alternative TPC2 siRNAs were tested using the same standard transfection protocol. Analysis by quantitative PCR showed that neither of the alternative TPC2 siRNAs reduced TPC2 expression (Fig. 4.8A and B). These two new siRNAs, and the original, were then tested using a prolonged protocol in which SH-SY5Ys were cultured for five days instead of three. Unfortunately, this protocol also failed to induce reasonable knockdown (Fig. 4.8C and D). To ensure the two new TPC2 siRNAs were functional they were transfected into fibroblasts using the protocol described in Chapter 3. Indeed, the data in Figures 4.8E and F show that in fibroblasts these siRNAs are capable of considerable knockdown. Of note, TPC2 siRNA #3 also induced a ~25% knockdown of TPC1. These results confirm that the TPC2 siRNAs tested here were functional in fibroblasts but demonstrate poor efficiency under the SH-SY5Y protocols.

SH-SY5Ys – standard protocol



SH-SY5Ys – extended protocol



fibroblasts

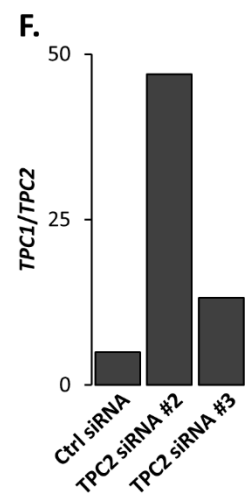
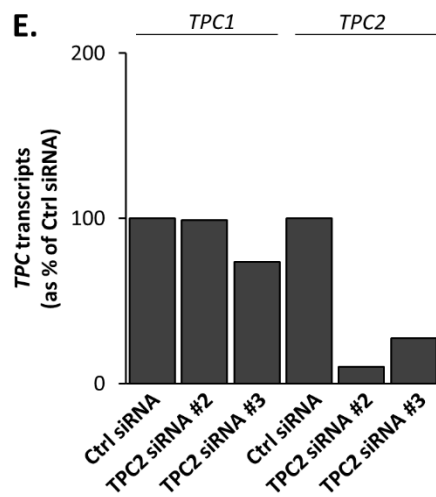


**Figure 4.8** TPC2 siRNAs reduce TPC2 transcript levels in fibroblasts but not SH-SY5Ys  
(legend on next page)

(A-D) Data quantifying *TPC* transcripts in *SH-SY5Y*s that have been transfected with control or *TPC2* siRNA, according to the (A and B) *standard protocol* or (C and D) *extended protocol*. (E and F) Data quantifying *TPC* transcripts in Ctrl *fibroblasts* that have been transfected with control or *TPC2* siRNA according to the protocol described in Chapter 3. (A, C and E) *TPC* transcripts normalised to those of *UBC* and presented as a percentage of the *TPC* transcript levels in cells transfected with control siRNA. (B, D and F) Ratios comparing *TPC1* and *TPC2* transcript levels. (A-F) The mean of technical replicates from one experiment is displayed.

#### 4.3.9 Recently identified *TPC* inhibitor tetrandrine blocks carbachol but not bradykinin-evoked $\text{Ca}^{2+}$ signals

In addition to *TPC* knockdown a pharmacological approach was explored to investigate the contribution of *TPCs* to carbachol-evoked  $\text{Ca}^{2+}$  signals. In a recent study an L-type voltage-operated  $\text{Ca}^{2+}$  channel (VOCC) antagonist was reported to block Ebola infectivity as well as *TPC* currents and NAADP-induced  $\text{Ca}^{2+}$  signals (Sakurai et al., 2015). This *TPC* inhibitor, tetrandrine (Fig. 4.9A), was therefore used as a tool to assess the importance of *TPCs* in carbachol-evoked  $\text{Ca}^{2+}$  signalling. *SH-SY5Y* cells were incubated with DMSO or tetrandrine during imaging and for 1 hour before, during Fura-2 labelling. As shown in Figures 4.9B and C the carbachol-evoked  $\text{Ca}^{2+}$  signal was intact in the presence of DMSO but completely blocked in the presence of *TPC* inhibitor tetrandrine. In contrast, bradykinin-evoked  $\text{Ca}^{2+}$  signals were unaffected by tetrandrine (Fig. 4.9D and E). It was noted that tetrandrine incubation was associated with a small increase in basal  $\text{Ca}^{2+}$  (mean  $\pm$  S.E.M [ $\text{Ca}^{2+}$ ] (ratio): DMSO =  $0.152 \pm 0.0038$ , n=8 experiments; tetrandrine =  $0.161 \pm 0.0021$ , n=8 experiments)

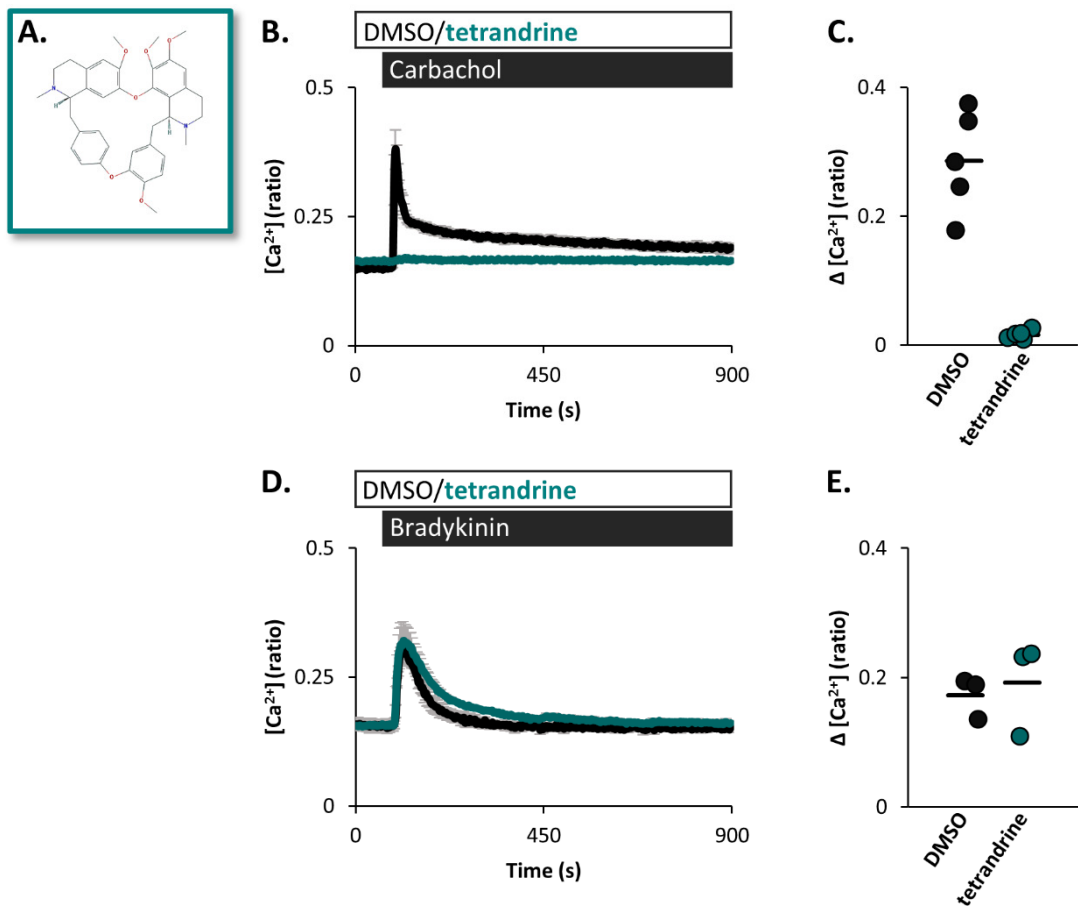


**Figure 4.9** Recently identified TPC inhibitor tetrandrine blocks carbachol but not bradykinin-evoked  $Ca^{2+}$  signals

**(A)** Chemical structure of tetrandrine. **(B)** Average cytosolic  $Ca^{2+}$  traces (mean of experiments  $\pm$  S.E.M) of SH-SY5Ys stimulated with carbachol (3.16  $\mu$ M) in the presence of DMSO or tetrandrine (10  $\mu$ M). **(C)** Data quantifying magnitude of responses in B. Each plot point represents one experiment,  $n=5/5$  (DMSO/tetrandrine). A total of 407/634 (DMSO/tetrandrine) SH-SY5Ys from 5 independent platings were analysed. **(D and E)** Same format as for B and C, upon stimulation with bradykinin (100 nM),  $n=3/3$  (DMSO/tetrandrine). A total of 268/264 (DMSO/tetrandrine) SH-SY5Ys from 3 independent platings were analysed.



#### **4.3.10 Putative TPC blocker and MAO inhibitor L-deprenyl blocks carbachol but not bradykinin-evoked Ca<sup>2+</sup> signals**

Whilst tetrandrine may be a useful TPC inhibitor in the lab it is not approved for clinical use by the US Food and Drug Administration (FDA) nor the European Medicines Agency (EMA). Therefore, any potential benefits of TPC inhibition such as modification of PD or preventing Ebola infection cannot be realised in humans. Furthermore, tetrandrine is not a selective TPC blocker nor are there currently any available. Indeed, tetrandrine's ability to block TPCs may not be surprising given it is classed as an antagonist of L-Type VOCCs, which along with voltage-operated Na<sup>+</sup> channels (VONC), are thought to be evolutionarily linked to TPCs and to share a common pharmacological binding site (Ishibashi et al., 2000; Rahman et al., 2014). To tackle these issues of drug approval and TPC selectivity FDA-approved drugs have been subjected to *in silico* screens conducted by Dr Taufiq Rahman (University of Cambridge) and Dr Christopher Penny (UCL) in the hope that they can be re-purposed as TPC inhibitors. To find selective TPC inhibitors, drugs that are not classed as channel blockers, have been the focus of these screens. Top candidates have also been tested against NAADP-induced Ca<sup>2+</sup> signals in sea urchin egg homogenate by Dr Christopher Penny and Professor Sandip Patel (UCL) but not against Ca<sup>2+</sup> signals in intact human cells. L-deprenyl was identified as a putative TPC blocker through a ligand-based screen (details of screen in Appendix C) (Fig. 4.10A). This drug, also known as Selegiline, is a monoamine oxidase (MAO) inhibitor and is administered to PD patients to inhibit dopamine (DA) metabolism (Youdim and Bakhle, 2006). To test the effect of L-deprenyl on carbachol or bradykinin-evoked Ca<sup>2+</sup> signals in SH-SY5Ys, cells were incubated with H<sub>2</sub>O or L-deprenyl during imaging, and for 1 hour prior, during Fura-2 labelling. In the presence of H<sub>2</sub>O both carbachol and bradykinin-evoked Ca<sup>2+</sup> signals in SH-SY5Ys were clear (Fig. 4.10B and D). In the presence of L-deprenyl however, carbachol-evoked Ca<sup>2+</sup> signals were blocked (Fig. 4.10B and C). In contrast, bradykinin-evoked Ca<sup>2+</sup> signals were not blocked but somewhat potentiated in the presence of L-deprenyl (Fig. 10.D and E).

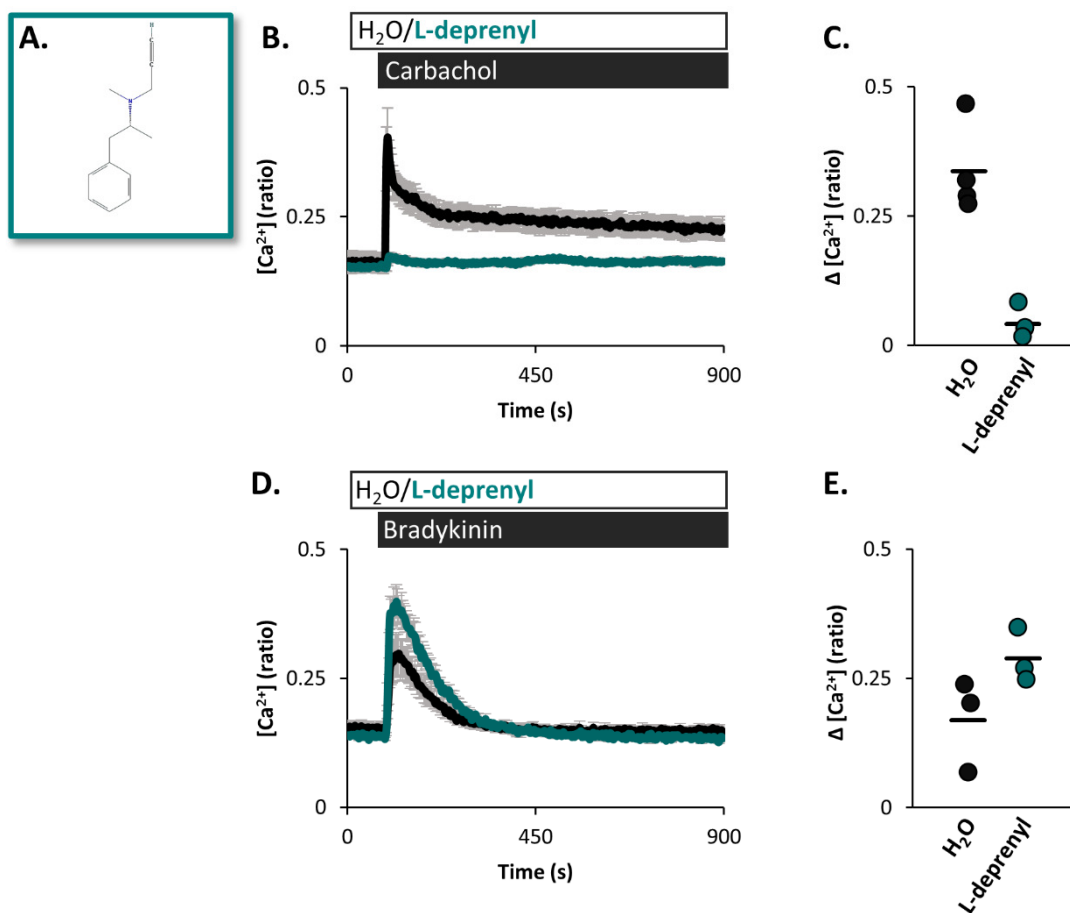


**Figure 4.10 Putative TPC blocker and MAO inhibitor L-deprenyl blocks carbachol but not bradykinin-evoked  $Ca^{2+}$  signals**

**(A)** Chemical structure of L-deprenyl. **(B)** Average cytosolic  $Ca^{2+}$  traces (mean of experiments  $\pm$  S.E.M) of SH-SY5Ys stimulated with carbachol (3.16  $\mu$ M) in the presence of H<sub>2</sub>O or L-deprenyl (1 mM). **(C)** Data quantifying magnitude of responses in B. Each plot point represents one experiment, n=4/4 (H<sub>2</sub>O/L-deprenyl). A total of 397/319 (H<sub>2</sub>O/L-deprenyl) SH-SY5Ys from 4 independent platings were analysed. **(D and E)** Same format as for B and C, upon stimulation with bradykinin (100 nM), n=3/3 (H<sub>2</sub>O/L-deprenyl). A total of 394/331 (H<sub>2</sub>O/L-deprenyl) SH-SY5Ys from 3 independent platings were analysed.

#### 4.3.11 Putative TPC blockers sunitinib and pimozone block carbachol but not bradykinin-evoked $Ca^{2+}$ signals

From an alternative screen sunitinib and pimozone were identified as putative TPC blockers (Fig. 4.11A and B) (details of screen in Appendix C). Briefly, this screen combined results from a virtual structure-based assay with data from *in vitro* Ebola infectivity assays that have been published by other groups (Johansen et al., 2015; Kouznetsova et al., 2014); the rationale being that if TPC activity is required for Ebola infectivity as has been reported, then inhibitors of Ebola infection may be TPC inhibitors (Sakurai et al., 2015). To test the effects of sunitinib or pimozone on

carbachol or bradykinin-evoked  $\text{Ca}^{2+}$  signals in SH-SY5Ys, cells were incubated with DMSO or the drugs as they had been with tetrandrine and L-deprenyl. As shown in Figures 4.11C and D sunitinib and pimoziide incubations both blocked carbachol-evoked  $\text{Ca}^{2+}$  signals. However, bradykinin-evoked  $\text{Ca}^{2+}$  signals were not inhibited by sunitinib but their return to basal  $\text{Ca}^{2+}$  did appear delayed (Fig. 4.11E and F). Although bradykinin-evoked  $\text{Ca}^{2+}$  signals were not completely blocked by pimoziide they were visibly reduced. It was noted that sunitinib incubation was associated with a small increase in basal  $\text{Ca}^{2+}$  (mean  $\pm$  S.E.M [ $\text{Ca}^{2+}$ ] (ratio): DMSO =  $0.142 \pm 0.0046$ , n=6 experiments; sunitinib =  $0.164 \pm 0.0033$ , n=6 experiments).

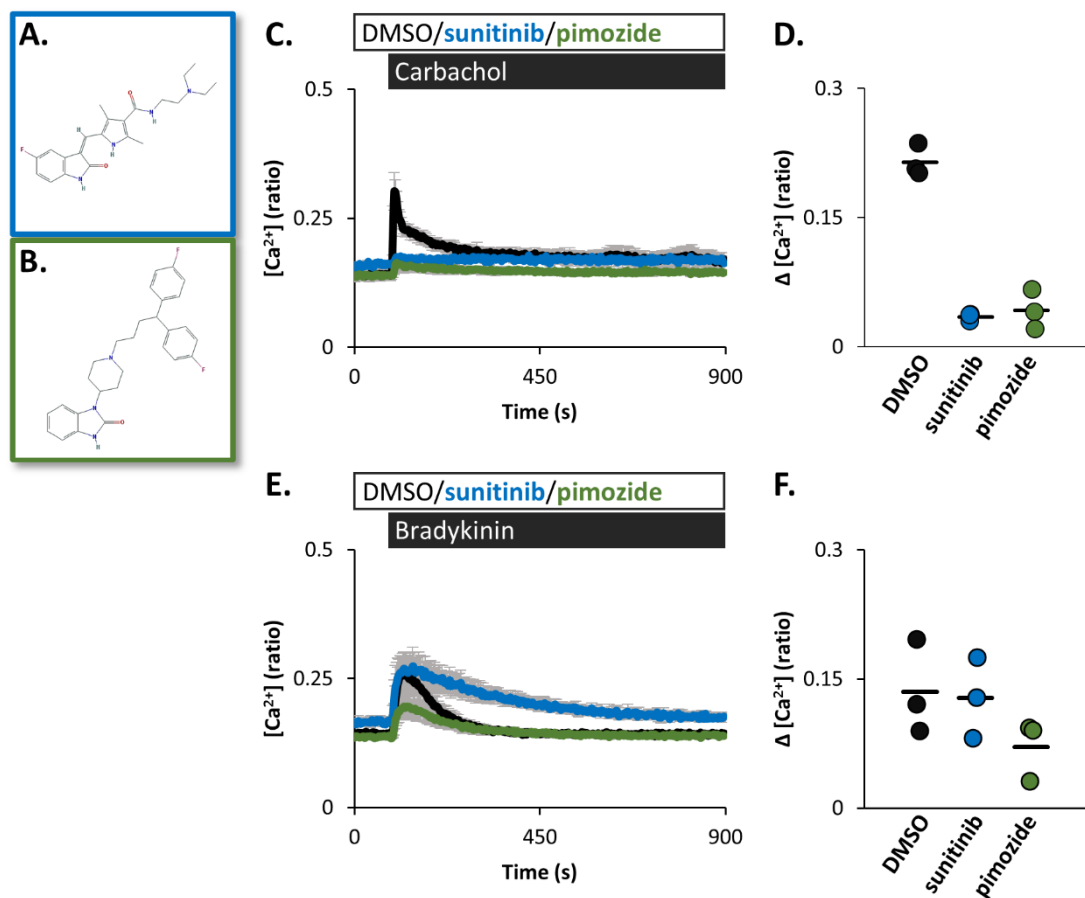


**Figure 4.11 Putative TPC blockers sunitinib and pimoziide block carbachol but not bradykinin-evoked  $\text{Ca}^{2+}$  signals**

**(A)** Chemical structure of sunitinib. **(B)** Chemical structure of pimoziide. **(C)** Average cytosolic  $\text{Ca}^{2+}$  traces (mean of experiments  $\pm$  S.E.M) of SH-SY5Ys stimulated with carbachol (3.16  $\mu\text{M}$ ) in the presence of DMSO, sunitinib (10  $\mu\text{M}$ ) or pimoziide (10  $\mu\text{M}$ ). **(D)** Data quantifying magnitude of responses in C. Each plot point represents one experiment, n=3/3/3 (DMSO/sunitinib/pimoziide). A total of 308/334/286 (DMSO/sunitinib/pimoziide) SH-SY5Ys from 3 independent platings were analysed. **(E and F)** Same format as for C and D, upon stimulation with bradykinin (100 nM), n=3/3/3 (DMSO/sunitinib/pimoziide). A total of 296/243/249 (DMSO/sunitinib/pimoziide) SH-SY5Ys from 3 independent platings were analysed.

#### **4.3.12 Putative TPC blocker fluphenazine blocks carbachol but not bradykinin-evoked Ca<sup>2+</sup> signals**

From the same screen that identified sunitinib and pimozide as putative TPC inhibitors fluphenazine was also highlighted as a candidate (Fig. 4.12A). However, fluphenazine caused large elevations of basal Ca<sup>2+</sup> and therefore was not suitable for a long incubation. Instead, fluphenazine was added to the cells whilst imaging, 2 minutes prior to stimulation with carbachol or bradykinin. As shown in Figures 4.12B and C fluphenazine blocked carbachol-evoked Ca<sup>2+</sup> signals in SH-SY5Ys. In contrast, the bradykinin-evoked Ca<sup>2+</sup> signals were not blocked but somewhat potentiated in the presence of fluphenazine (Fig. 4.12D and E). A preliminary dataset shows that tetrandrine, L-deprenyl and sunitinib can also block carbachol-evoked Ca<sup>2+</sup> signals after just a 2-minute treatment (Fig. 4.12.Supplement).

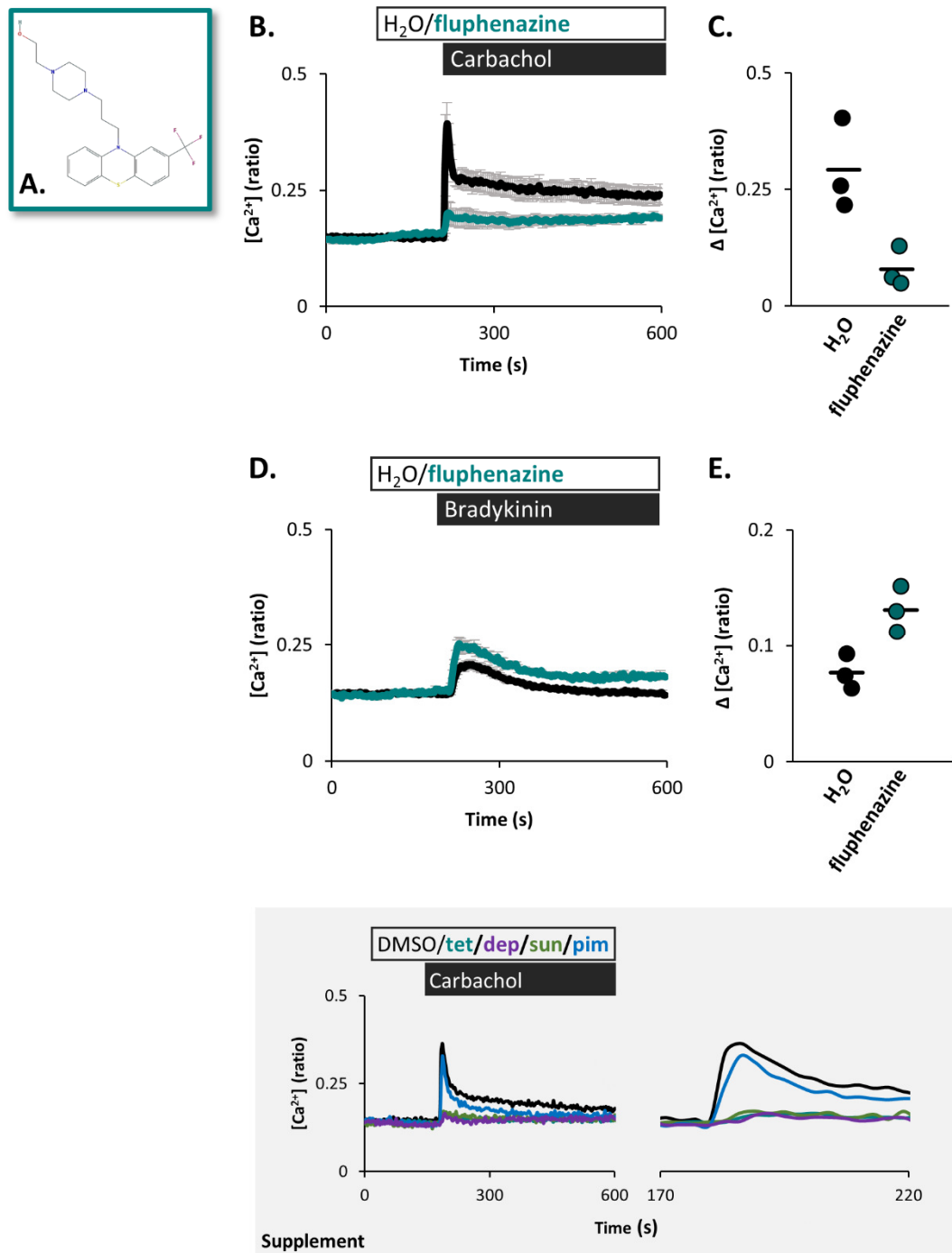


**Figure 4.12 Putative TPC blocker fluphenazine blocks carbachol but not bradykinin-evoked  $Ca^{2+}$  signals**

**(A)** Chemical structure of fluphenazine. **(B)** Average cytosolic  $Ca^{2+}$  traces (mean of experiments  $\pm$  S.E.M.) of SH-SY5Ys stimulated with carbachol (3.16  $\mu$ M) following H<sub>2</sub>O or fluphenazine (10  $\mu$ M). **(C)** Data quantifying magnitude of responses in B, n=3/3 (H<sub>2</sub>O/fluphenazine). A total of 331/317 (H<sub>2</sub>O/fluphenazine) SH-SY5Ys from 3 independent platings were analysed. **(D and E)** Same format as for B and C, upon stimulation with bradykinin (100 nM), n=3/3 (H<sub>2</sub>O/fluphenazine). A total of 365/308 (H<sub>2</sub>O/fluphenazine) SH-SY5Ys from 3 independent platings were analysed. **Supplement:** Average cytosolic  $Ca^{2+}$  traces (mean of individual cells in a single experiment) of SH-SY5Ys stimulated with

carbachol (3.16  $\mu\text{M}$ ) following DMSO, tetrandrine (tet; 10  $\mu\text{M}$ ), L-deprenyl (dep; 1 mM), sunitinib (sun; 10  $\mu\text{M}$ ) or pimozide (pim; 10  $\mu\text{M}$ ).

### 4.3.13 Carbachol but not bradykinin-evoked $\text{Ca}^{2+}$ signals are potentiated in LRRK2-GS cells

To recap, the above data demonstrates that carbachol-evoked  $\text{Ca}^{2+}$  signals in SH-SY5Y cells are inhibited by the lysosomotrope GPN, TPC1 knockdown, the novel TPC inhibitor tetrandrine, and four structurally distinct putative TPC blockers. Bradykinin signals however are not inhibited by GPN, and are relatively unaffected by the same TPC drugs. These two agonists therefore offer a prototype tool set with which to distinguish TPC-dependent and TPC-independent changes to physiological  $\text{Ca}^{2+}$  signals in these cells. In work on patient-derived fibroblasts, LRRK2-GS has been associated with augmented global  $\text{Ca}^{2+}$  signals in response to the  $\text{Ca}^{2+}$  mobilising messenger NAADP, which may be a consequence of upregulated TPC activity (Brailoiu et al., 2009; Calcraft et al., 2009; Hockey et al., 2015). Therefore, it was hypothesised that carbachol-evoked global  $\text{Ca}^{2+}$  signals (TPC-dependent) may be upregulated in SH-SY5Ys that stably express LRRK2-GS, but that bradykinin-evoked global  $\text{Ca}^{2+}$  signals (TPC-independent) would not be. Carbachol or bradykinin-evoked  $\text{Ca}^{2+}$  signals were compared in SH-SY5Y cells stably expressing LRRK2 wildtype (WT) or LRRK2-GS. Notably, although each cell line was plated at the same density, LRRK2-GS cells were more sparse on the day of experimentation compared to the LRRK2 WT controls or untransfected SH-SY5Ys (Fig. 4.13A). When stimulated with carbachol the untransfected cells, LRRK2 WT and LRRK2-GS cells all exhibited clear  $\text{Ca}^{2+}$  signals (Fig. 4.13B). Furthermore, the magnitude of the carbachol-evoked  $\text{Ca}^{2+}$  signals in the LRRK2 WT and LRRK2-GS cells were comparable (Fig. 4.13B and C). However, when comparing the plateau phase of the signal the response in the LRRK2-GS cells appeared potentiated compared to LRRK2 WT. This was quantified by calculating the magnitude of the signal at 250 seconds into imaging (Fig. 4.13D). When stimulated with bradykinin, the  $\text{Ca}^{2+}$  signals were also clear in all cell lines. However, the magnitude of response in LRRK2-GS cells was smaller compared to LRRK2 WT (Fig. 4.13E and F). Although bradykinin-evoked  $\text{Ca}^{2+}$  signals in SH-SY5Ys do not display a plateau phase, magnitude of the signal at 250 s was analysed for direct comparison with the carbachol signals. This analysis showed that bradykinin signals were not potentiated in the LRRK2-GS cells at 250 seconds into imaging (Fig. 4.13G).

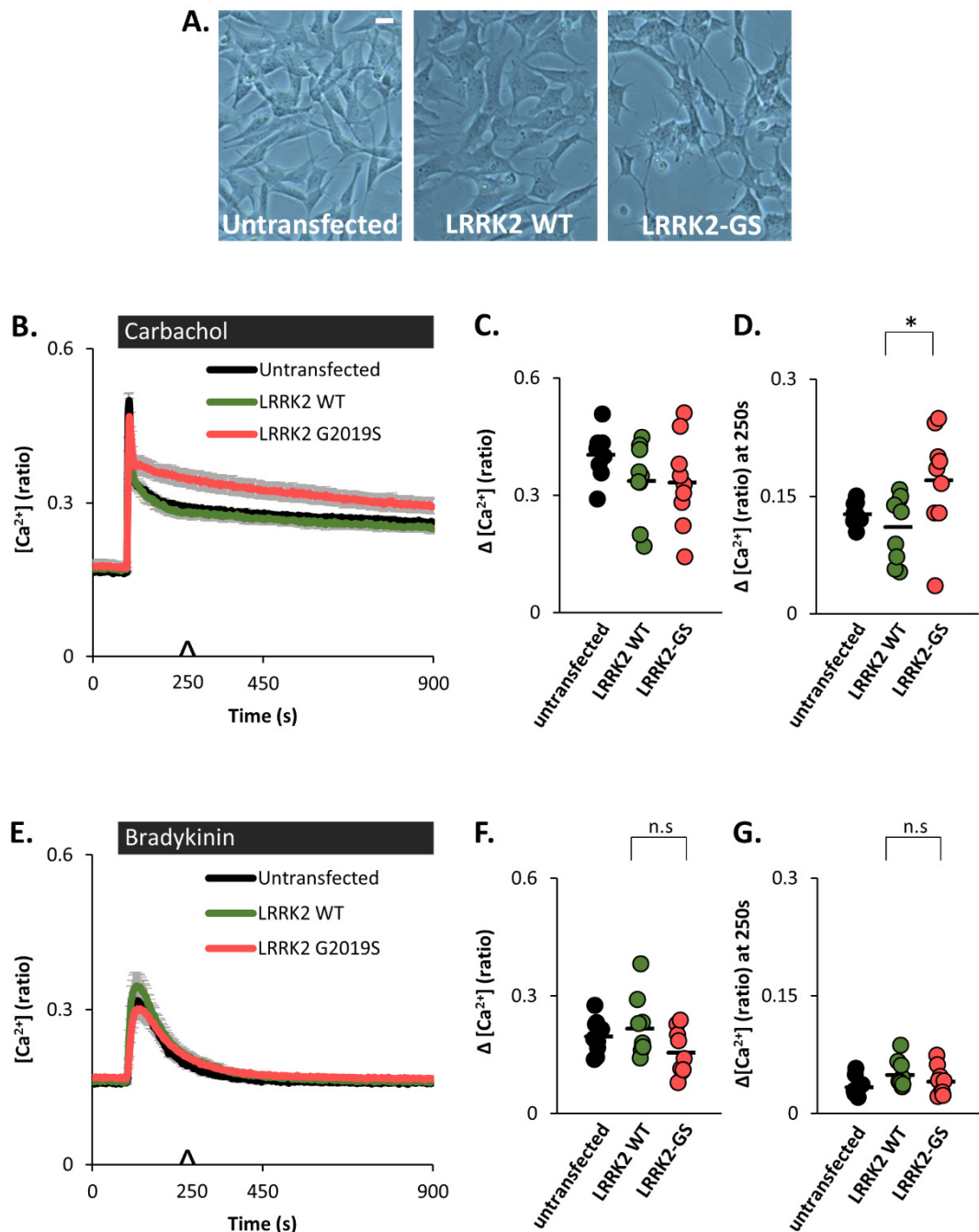


**Figure 4.13 Carbachol but not bradykinin-evoked  $\text{Ca}^{2+}$  signals are potentiated in LRRK2-GS cells**

(A) Light microscope images of SH-SY5Ys taken prior to imaging. SH-SY5Ys were untransfected, or stably transfected with *LRRK2* WT or *LRRK2*-GS. Scale bar = 20  $\mu\text{m}$ . (B) Average cytosolic  $\text{Ca}^{2+}$  traces (mean of experiments  $\pm$  S.E.M.) of SH-SY5Ys stimulated with carbachol (3.16  $\mu\text{M}$ ). (C and D) Data quantifying the responses in B. Each plot point represents one experiment, n=9/9/9 (untransfected/LRRK2 WT/LRRK2-GS). A total of 436/425/487 (untransfected/LRRK2 WT/LRRK2-GS) SH-SY5Ys from 3 independent platings were analysed. (C) Magnitude of carbachol response. (D) Magnitude of the carbachol signal at 250 s (250 s from imaging commencing, indicated by arrow head on x axis). \*p<0.05 as determined by an Independent Samples-T test. (E-G) Same format as B-D, upon stimulation with bradykinin (100 nM), n=9/9/9 (untransfected/LRRK2 WT/LRRK2-GS). A total of

495/576/528 (untransfected/LRRK2 WT/LRRK2-GS) SH-SY5Ys from 3 independent platings were analysed. Data that were not statistically significant (n.s) as determined by (F) Independent-Samples T test or (G) Mann-Whitney U test.

#### 4.3.14 TPC transcript levels are unaltered in LRRK2-GS cells

Having observed the potentiated plateau phase of carbachol-evoked  $\text{Ca}^{2+}$  signals in LRRK2-GS cells, but no such potentiation to bradykinin signals, the possible causes for this were considered. As described previously carbachol-evoked  $\text{Ca}^{2+}$  signals were inhibited by TPC knockdown, the novel TPC blocker tetrandrine and putative TPC blockers. In light of this, the possibility that TPC expression might be greater in LRRK2-GS cells was investigated using quantitative PCR. As shown in Figure 4.14A TPC expression appeared reduced in the SH-SY5Ys expressing either LRRK2 WT or LRRK2-GS compared to the untransfected cells. This reduction was more pronounced for TPC1 than TPC2, as exhibited by the smaller  $TPC1/TPC2$  ratios displayed in Figure 4.13B. However, there was no difference associated with the pathogenic LRRK2-GS mutation compared to LRRK2 WT.

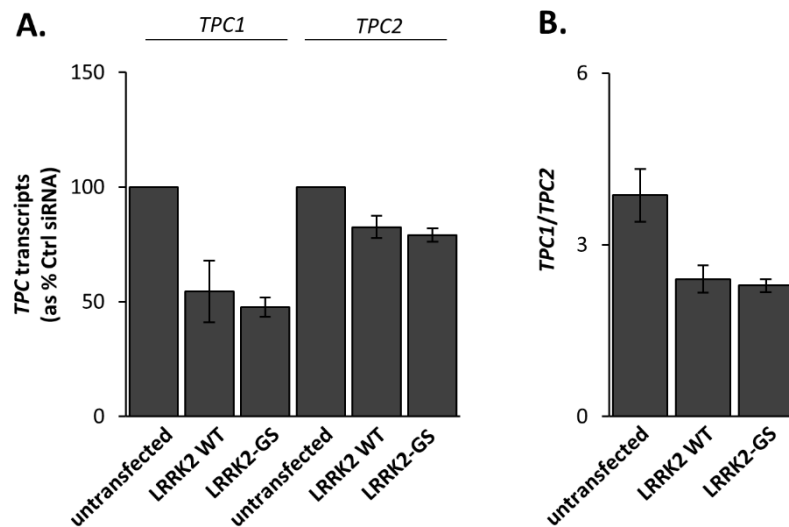


**Figure 4.14 TPC transcript levels are unaltered in LRRK2-GS cells**

(A and B) Data quantifying TPC transcripts in SH-SY5Ys which were untransfected, or stably transfected with LRRK2 WT or LRRK2-GS. Data shows mean  $\pm$  S.E.M of 3 experiments from 3 independent platings. (A) TPC transcripts normalised to those of UBC and presented as a percentage of the TPC transcript levels in untransfected SH-SY5Ys. (B) Ratio comparing transcript levels of TPC1 and TPC2.



### 4.3.15 GPN and thapsigargin-evoked $\text{Ca}^{2+}$ signals are unchanged in LRRK2-GS cells

As GPN and thapsigargin had inhibited carbachol-evoked  $\text{Ca}^{2+}$  signals (Fig. 4.3 and 4.5) it was reasoned that the pools of  $\text{Ca}^{2+}$  they mobilise contribute to carbachol-evoked signals. It was therefore considered that these pools might be greater in the LRRK-GS cells and be responsible for the potentiation of carbachol-evoked  $\text{Ca}^{2+}$  signals. To assess this GPN or thapsigargin-induced  $\text{Ca}^{2+}$  signals in LRRK2-GS SH-SY5Ys were compared to those in the LRRK2 WT counterparts. However, as shown in Figure 4.15A and B, GPN-induced  $\text{Ca}^{2+}$  signals were not potentiated in LRRK2-GS cells compared to LRRK2 WT. This was also the case for signals induced by thapsigargin (Fig. 4.15C and D).

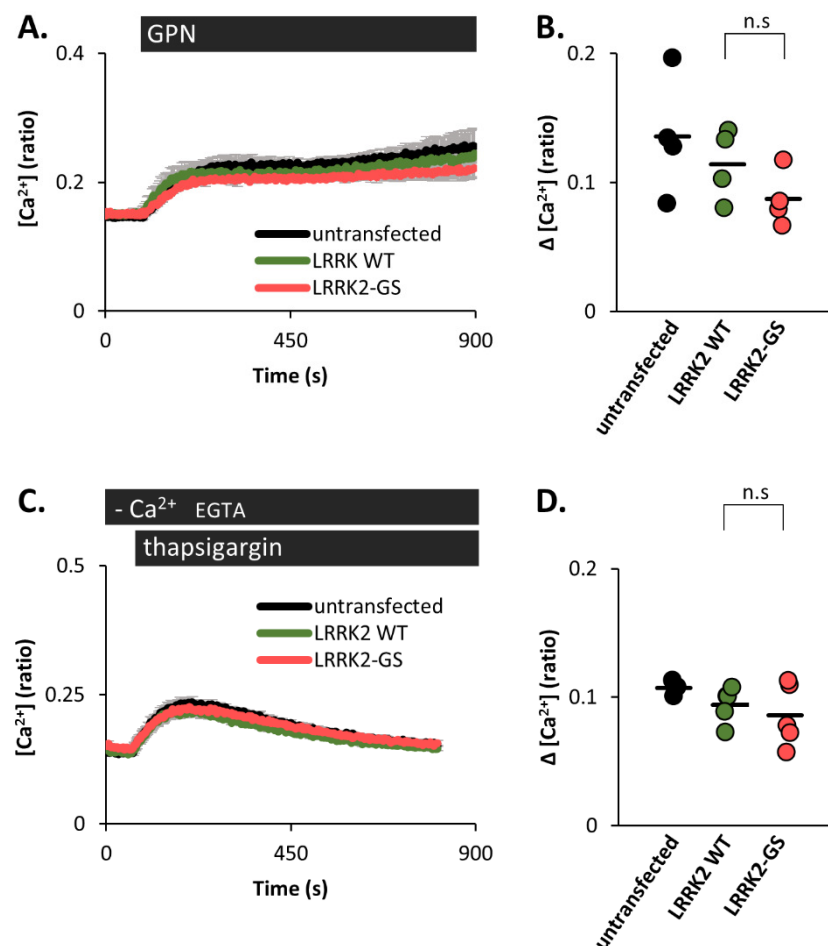


**Figure 4.15 GPN and thapsigargin-evoked  $\text{Ca}^{2+}$  signals are unchanged in LRRK2-GS cells**

(A) Average cytosolic  $\text{Ca}^{2+}$  traces (mean of experiments  $\pm$  S.E.M) of SH-SY5Ys stimulated with GPN (200  $\mu\text{M}$ ). SH-SY5Ys were untransfected or stably transfected with *LRRK2* WT or *LRRK2*-GS. (B) Data quantifying magnitude of responses in A. Each plot point represents one experiment,  $n=4/4/4$  (untransfected/LRRK2 WT/LRRK2-GS). A total of 451/422/450 (untransfected/LRRK2 WT/LRRK2-GS) SH-SY5Ys from 3 independent platings were analysed. (C and D) Same format as for A and B upon addition of thapsigargin, in the absence of extracellular  $\text{Ca}^{2+}$  ( $\text{Ca}^{2+}$  was replaced with 1mM EGTA),

n=3/5/5 (untransfected/LRRK2 WT/LRRK2-GS). A total of 378/535/525 (untransfected/LRRK2 WT/LRRK2-GS) SH-SY5Ys from 3 independent platings were analysed. Data that were not statistically significant (n.s) as determined by Independent-Samples T tests.

#### 4.3.16 SOCE is inhibited in LRRK2-GS cells

Finally, carbachol-evoked  $\text{Ca}^{2+}$  signals appear to require ER  $\text{Ca}^{2+}$ , which is depleted by thapsigargin (Fig. 4.5A and B). It was therefore considered that SOCE might be important to sustain the carbachol signals by replenishing ER  $\text{Ca}^{2+}$ . Furthermore, it was speculated that it might be the SOCE component of the carbachol-evoked  $\text{Ca}^{2+}$  signals that is potentiated in LRRK2-GS SH-SY5Ys. In the absence of extracellular  $\text{Ca}^{2+}$  SERCA was blocked using thapsigargin to deplete ER  $\text{Ca}^{2+}$  (Fig. 4.16A). As displayed in Fig. 4.15C and D the  $\text{Ca}^{2+}$  signals evoked by thapsigargin were once again no different in the LRRK2 WT and LRRK2-GS cells. Subsequently,  $\text{Ca}^{2+}$  was added back to the extracellular medium and cytosolic  $\text{Ca}^{2+}$  levels rose rapidly, indicative of SOCE. As shown in Figures 4.16A and B the magnitude of this SOCE response was not potentiated in LRRK2-GS cells compared to LRRK2 WT, but rather reduced.

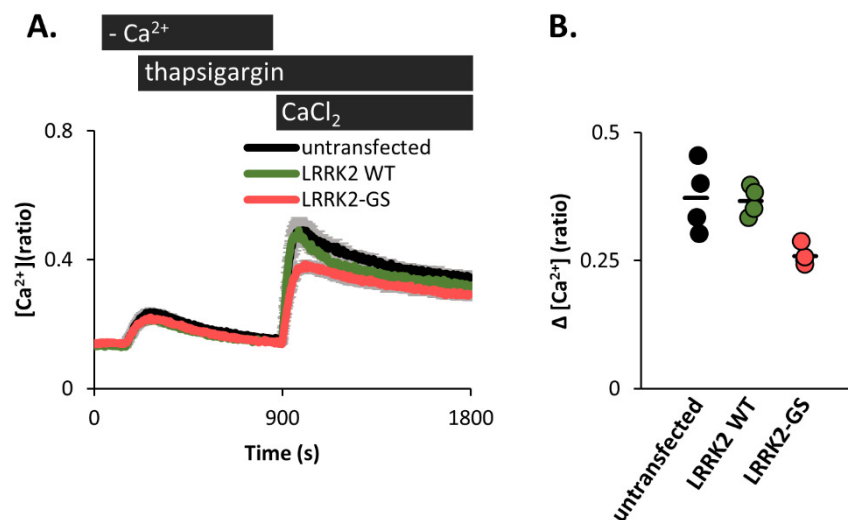


**Figure 4.16 SOCE is inhibited in LRRK2-GS cells**

(A) Average cytosolic  $\text{Ca}^{2+}$  traces (mean of experiments  $\pm$  S.E.M) of SH-SY5Ys upon addition of thapsigargin in the absence of extracellular  $\text{Ca}^{2+}$ , followed by return of  $\text{CaCl}_2$  (2 mM) to the extracellular medium. SH-SY5Ys were untransfected or stably transfected with *LRRK2* WT or *LRRK2*-GS. (B) Data quantifying magnitude of the  $\text{CaCl}_2$  response in A. Each plot point represents one experiment, n=4/4/4 (untransfected/LRRK2 WT/LRRK2-GS). A total of 385/355/435 (untransfected/LRRK2 WT/LRRK2-GS) SH-SY5Ys from 2 independent platings were analysed.

## 4.4 DISCUSSION

In Chapter 3 I investigated the relevance of upregulated TPC2 activity in LRRK2-GS PD patient fibroblasts, to physiological global  $\text{Ca}^{2+}$  signals. In this chapter I extended the study into a DAergic neuronal model of LRRK2-GS PD. I also used two different extracellular agonists, each with different target receptors and global  $\text{Ca}^{2+}$  signal kinetics. Both the cholinergic agonist carbachol and the inflammatory peptide bradykinin required ER  $\text{Ca}^{2+}$  to elicit their global signals in the neuronal SH-SY5Y cell line. However, disrupting the lysosomes with GPN inhibited carbachol-evoked  $\text{Ca}^{2+}$  signals but not those of bradykinin. In addition, the novel TPC blocker tetrandrine, and putative TPC blockers L-deprenyl, sunitinib, pimozide and fluphenazine blocked carbachol-evoked  $\text{Ca}^{2+}$  signals but not those of bradykinin. These findings may indicate that lysosomes and TPCs are required for the generation of physiological global  $\text{Ca}^{2+}$  signals evoked by carbachol but not those of bradykinin in SH-SY5Ys. Considering carbachol as a putative TPC-dependent agonist, and bradykinin as a TPC-independent agonist, their signals in SH-SY5Y cells stably expressing LRRK2-GS were assessed. Interestingly, carbachol but not bradykinin-evoked  $\text{Ca}^{2+}$  signals were potentiated in the LRRK2-GS cells compared to the LRRK2 WT controls. This may be indicative of upregulated TPC activity. In first steps toward elucidating the cause of carbachol signal potentiation in LRRK2-GS cells, I found that it could not be attributed to enhanced TPC expression, lysosomal  $\text{Ca}^{2+}$  content (as measured by its release with GPN), and neither ER  $\text{Ca}^{2+}$  content (as triggered by its release with thapsigargin) nor SOCE (which was inhibited). Overall, my data suggests that TPCs experience a gain of function in this neuronal model of LRRK2-GS PD. This may contribute to neurodegeneration by disturbing global  $\text{Ca}^{2+}$  signalling.

In fibroblast cultures derived from patients with familial LRRK2-GS PD, disturbed lysosome morphology is associated with upregulated TPC2 activity and disturbed local  $\text{Ca}^{2+}$  signals (Hockey et al., 2015). These cells also exhibit augmented global  $\text{Ca}^{2+}$  signals in response to the  $\text{Ca}^{2+}$ -mobilising messenger NAADP. Although there has been some controversy surrounding TPC activation, NAADP can cause global  $\text{Ca}^{2+}$  signals which require intact lysosomes and TPCs (Brailoiu et al., 2009; Calcraft et al., 2009; Churchill et al., 2002; Jha et al., 2014). Taken together, it is plausible that the upregulated TPC activity in LRRK2-GS PD is responsible for the augmented NAADP-evoked  $\text{Ca}^{2+}$  signals. Potentiated global  $\text{Ca}^{2+}$  signals such as these may cause wide-spread dysfunction in the cell by disrupting  $\text{Ca}^{2+}$ -dependent protein folding, causing mitochondrial  $\text{Ca}^{2+}$  overload and stress, or even promoting cell death (Rizzuto et al., 2012; Wang and Kaufman,

2016). If a similar TPC-dependent potentiation is observed with physiological  $\text{Ca}^{2+}$  signals it would merit the consideration of TPC-dependent global  $\text{Ca}^{2+}$  signalling as a contributing factor to PD neurodegeneration. Using fibroblasts in Chapter 3, I found that bradykinin-evoked global  $\text{Ca}^{2+}$  signals were inhibited when the lysosomes were compromised or when *TPC* expression was reduced. However, bradykinin signals were not augmented in the LRRK2-GS PD fibroblasts which have been associated with upregulated TPC2 activity (Hockey et al., 2015). In this chapter I used the neuronal SH-SY5Y cell line to ask the same questions as Chapter 3: First, are there extracellular agonists that require TPCs to elicit their global  $\text{Ca}^{2+}$  signals? Secondly, are these physiological signals potentiated in SH-SY5Ys expressing PD-associated, mutant LRRK2-GS?

The SH-SY5Y cell line is commonly used in PD research. This is due to its neuronal and DAergic properties which may help to recapitulate the environment of the DAergic SNc that undergoes extensive neurodegeneration in PD (Biedler et al., 1978; Braak et al., 2003; Brichta et al., 2013; Xicoy et al., 2017). In addition, SH-SY5Ys express Cav1.3, the L-type VOCC that is thought to mediate pathogenic  $\text{Ca}^{2+}$  entry in the SNc (Sousa et al., 2013; Surmeier et al., 2017a). As for the majority of PD studies the SH-SY5Ys in this chapter were undifferentiated (Xicoy et al., 2017). Currently there is much debate over the pros and cons of inducing differentiation in this cell line and likewise of the different methods used (Cheng et al., 2013; Filograna et al., 2015; Forster et al., 2016; Khwanraj et al., 2015; Korecka et al., 2013; Lopes et al., 2010). For example, differentiation may be important as it induces a more neuronal SH-SY5Y morphology with extended neurites (Filograna et al., 2015; Forster et al., 2016; Lopes et al., 2010). This may to some extent mirror the heightened energy demands of the SNc neurons due to their complex arborisation (Pacelli et al., 2015). Another cited reason for SH-SY5Y differentiation is that it enhances the DAergic properties of these cells (Khwanraj et al., 2015; Korecka et al., 2013; Lopes et al., 2010). This is important because although SH-SY5Ys are DAergic they may be better defined as catecholaminergic cells as they also produce noradrenaline (Filograna et al., 2015). However, conflicting reports demonstrate that SH-SY5Y differentiation can also down-regulate DA markers (Filograna et al., 2015) or does not cause any change (Forster et al., 2016). As the debate continues undifferentiated SH-SY5Ys present a DAergic neuronal system that requires relatively straightforward culturing and permits fast experiment turnover. The SH-SY5Y cells used in this chapter have been characterised previously, with the stable expression of LRRK2-GS being associated with increased oxygen consumption and decreased mitochondrial membrane potential (Papkovskaia et al., 2012).

In a similar vein to Chapter 3 the first step to identifying extracellular agonists that induce TPC-dependent global  $\text{Ca}^{2+}$  signals was to identify agonists that require the lysosomes. The lysosomotropic GPN permeabilises lysosomal membranes, permitting leakage of luminal content (Haller et al., 1996; Jadot et al., 1984). Therefore, GPN is a useful tool with which to disrupt these organelles. A practical advantage of the SH-SY5Y cell line in this context is that GPN does not elicit complex  $\text{Ca}^{2+}$  signals as it does in fibroblasts (Fig. 4.1A). Instead it caused a small, simple rise in cytosolic  $\text{Ca}^{2+}$  which could be easily distinguished from subsequent  $\text{Ca}^{2+}$  signals elicited by other stimuli. Therefore, it was used as a tool to probe the contribution of the lysosomes to agonist-induced global  $\text{Ca}^{2+}$  signals in this neuronal cell line. The cause for the very different GPN  $\text{Ca}^{2+}$  signals in fibroblasts and SH-SY5Ys is unknown. GPN-induced loss of LTR fluorescence occurred at a similar rate in both cell types (Fig. 4.1B). If this LTR loss is regarded as a measure of lysosome permeabilisation and thus leakage of lysosomal  $\text{Ca}^{2+}$ , these comparable rates rule out a simple correlation between speed of lysosomal  $\text{Ca}^{2+}$  release and the magnitude or nature of the signal. Previous research has demonstrated that the complex GPN signals generated in fibroblasts are dependent upon  $\text{Ca}^{2+}$  release from both the lysosomes and the ER which may rely on the membrane contact sites (MCS) between the two organelles (Kilpatrick et al., 2013). It is a possibility therefore that the MCS in SH-SY5Ys are modelled differently or regulated by different components to those in fibroblasts.

In this chapter two extracellular agonists were tested to see if their global  $\text{Ca}^{2+}$  signals required the lysosomes. The first candidate agonist was carbachol, a synthetic compound that can activate muscarinic and nicotinic acetylcholine receptors (mAChR and nAChR) (Williams and Kauer, 1997), and has been reported to induce both  $\text{IP}_3$  and NAADP synthesis (Aley et al., 2013; Chen and Hsu, 1994; Piiper et al., 1994; Shin et al., 2003). The other agonist tested was bradykinin, which was also used in Chapter 3 for fibroblast work. Although bradykinin has been linked to  $\text{IP}_3$  and cAPDR synthesis there has been no such link to NAADP (Ataei et al., 2013; Johnson et al., 1990; Kip et al., 2006). Crucially, there has been no report that  $\text{Ca}^{2+}$  signals induced by either agonist require TPCs.

Disruption of the lysosomes using GPN provided the first evidence that  $\text{Ca}^{2+}$  signals induced by carbachol and bradykinin were differentially generated. GPN markedly blocked subsequent carbachol-evoked  $\text{Ca}^{2+}$  signals, suggesting that the lysosomes were involved in initiating this signal (Fig. 4.3A and B). Considering the possibility that the disruptive effect of GPN may not be limited to the lysosomes, it was reassuring that bradykinin-evoked  $\text{Ca}^{2+}$  signals remained intact (Fig. 4.3C and D). This data indicated that carbachol-evoked  $\text{Ca}^{2+}$  signals may be lysosome-

dependent whereas bradykinin-evoked  $\text{Ca}^{2+}$  signals were lysosome-independent. This was supported by results from a second experiment using the inverse order of GPN and agonist stimulation. That is, agonist stimulation followed by GPN (Fig. 4.4). Although it was thought that lysosomal  $\text{Ca}^{2+}$  might contribute to carbachol-evoked  $\text{Ca}^{2+}$  signals the size of this contribution was unknown. If only a small amount of lysosomal  $\text{Ca}^{2+}$  contributed this might be difficult to observe as a reduction in GPN-evoked  $\text{Ca}^{2+}$  signal following carbachol stimulation. By evoking larger  $\text{Ca}^{2+}$  signals more  $\text{Ca}^{2+}$  may be released from the lysosomes and cause a clearer inhibition of the small GPN signals that follow (Tugba Durlu-Kandilci et al., 2010). For this reason agonist concentrations at the top of the concentration-response curves in Figure 4.2 were used for this experiment only. This experiment was also conducted in the absence of extracellular  $\text{Ca}^{2+}$ , thereby excluding any effects of  $\text{Ca}^{2+}$  entry. Following carbachol stimulation the subsequent GPN-evoked  $\text{Ca}^{2+}$  signal was completely blocked but following bradykinin it was largely unchanged (Fig. 4.4). This data supports that idea that carbachol-evoked  $\text{Ca}^{2+}$  signals require the lysosomes and possibly lysosomal  $\text{Ca}^{2+}$  whereas bradykinin-evoked  $\text{Ca}^{2+}$  signals do not. However, given that the effects of GPN requires its cleavage by pH-sensitive cathepsin C it cannot be ruled out that carbachol-evoked  $\text{Ca}^{2+}$  signals prevent GPN signals by disrupting lysosomal pH or enzyme activity (Haller et al., 1996; Lopez-Sanjurjo et al., 2013; Morgan et al., 2013). The sterol U18666a reportedly depletes lysosomal  $\text{Ca}^{2+}$  without affecting lysosomal pH and would therefore serve as a useful control to verify the agonist-selective contribution of lysosomal  $\text{Ca}^{2+}$  (Lloyd-Evans et al., 2008).

Association between carbachol-evoked  $\text{Ca}^{2+}$  signals and the lysosomes has been reported elsewhere but in two different modes. In agreement with the results presented here pre-incubation of GPN has been shown to inhibit carbachol-evoked  $\text{Ca}^{2+}$  signals (Melchionda et al., 2016). However, in a study by Lopez-Sanjurjo and colleagues, lysosomes were reported to act as important sites of  $\text{Ca}^{2+}$  uptake during carbachol  $\text{Ca}^{2+}$  signalling and not as sites of release (Lopez-Sanjurjo et al., 2013). This was exemplified by potentiated carbachol-evoked  $\text{Ca}^{2+}$  signals following the pre-incubation of cells with GPN. They also reported that carbachol-evoked  $\text{Ca}^{2+}$  signals were accompanied by a rise in lysosomal pH. Currently, lysosomal  $\text{Ca}^{2+}$  uptake is believed to be mediated by ATPase activity and  $\text{Ca}^{2+}/\text{H}^+$  exchange (Melchionda et al., 2016; Morgan et al., 2011; Patel and Docampo, 2010). For the latter,  $\text{Ca}^{2+}$  uptake into the lysosome requires the efflux of lysosomal protons. Therefore, an increase in lysosomal pH might be expected in lysosomes acting as  $\text{Ca}^{2+}$  buffers (Lopez-Sanjurjo et al., 2013). However, increases in lysosomal pH are also associated with NAADP-induced  $\text{Ca}^{2+}$  release (Morgan et al., 2013). Whilst there is clearly much to be understood, the contrasting GPN and carbachol data reported by Lopez-Sanjurjo and Melchionda may reflect in part the different cell types used and whether the experiments were

conducted in the absence or presence of extracellular  $\text{Ca}^{2+}$  (Lopez-Sanjurjo et al., 2013; Melchionda et al., 2016).

Although carbachol but not bradykinin appeared to require the lysosomes to generate its  $\text{Ca}^{2+}$  signal, both agonists have been associated with the synthesis of  $\text{IP}_3$ , and ER  $\text{Ca}^{2+}$  release (Ataei et al., 2013; Chen and Hsu, 1994; Johnson et al., 1990; Kip et al., 2006; Luciani et al., 2009; Piiper et al., 1994; Shin et al., 2003; Suzuki et al., 2014). Therefore, I assessed the effect of depleting ER  $\text{Ca}^{2+}$  on both agonist-evoked  $\text{Ca}^{2+}$  signals in SH-SY5Ys. As expected, both carbachol and bradykinin-evoked  $\text{Ca}^{2+}$  signals were blocked following the depletion of ER  $\text{Ca}^{2+}$  with SERCA inhibitor thapsigargin (Fig. 4.5). This result however, opens up a potential Pandora's box. The block of a  $\text{Ca}^{2+}$  signal by thapsigargin may sometimes be interpreted as the ER being the only essential intracellular organelle for said response. Consequently, further experiments designed to dissect the origin of the signal may be deemed futile. Here, the  $\text{Ca}^{2+}$  signals evoked by carbachol are clearly blocked following thapsigargin but are also completely abolished when the lysosomes are compromised. This indicates that both organelles are essential for the generation of carbachol-evoked  $\text{Ca}^{2+}$  signals. It is possible that in similar experiments the lysosome loses out on recognition for its signal contribution in the wake of its already established signalling partner – the ER. Another consideration is that thapsigargin and GPN may reciprocally effect the non-targeted  $\text{Ca}^{2+}$  store. For example, increases in cytosolic  $\text{Ca}^{2+}$  caused by ER  $\text{Ca}^{2+}$  release (stimulated by thapsigargin) may trigger further lysosomal  $\text{Ca}^{2+}$  release. Alternatively lysosomal  $\text{Ca}^{2+}$  release (stimulated by GPN) may trigger further ER  $\text{Ca}^{2+}$  release (Kilpatrick et al., 2013; Morgan, 2016). In these experiments the latter is controlled for by the intact bradykinin signals following GPN addition: As bradykinin signals require ER  $\text{Ca}^{2+}$  (Fig. 4.5C and D) this suggests that GPN leaves the ER  $\text{Ca}^{2+}$  store intact. To determine whether ER  $\text{Ca}^{2+}$  depletion impacts on lysosomal  $\text{Ca}^{2+}$  the measurement of GPN responses following thapsigargin is necessary.

Considering the data that indicated lysosome involvement in global  $\text{Ca}^{2+}$  signals evoked by carbachol, I investigated whether the lysosomal TPCs might also be involved. As for fibroblasts in Chapter 3, one strategy was to examine the carbachol response in SH-SY5Ys with reduced TPC expression. In a preliminary experiment in the SH-SY5Ys, TPC1 expression at the protein level was inhibited by TPC1 siRNA, but not TPC2 siRNA, as expected (Fig. 4.6A and B). In the main knockdown experiments, TPC1 expression at the transcript level was reduced by ~50%, but TPC2 was only reduced by ~30% when using isoform-specific siRNAs (Fig. 4.6C). This echoes the differential knockdown efficiency in the fibroblasts (Chapter 3, Fig. 3.5C) which has also been reported in other studies using different cell types (García-Rúa et al., 2016; Sakurai et al., 2015). However, this is not always the case (Davis et al., 2012). Interestingly, the preliminary western blot and the quantitative PCR data indicate that treatment of SH-SY5Ys with TPC2 siRNA results

in increased TPC1 expression (Fig. 4.6B and C). Knockdown of either TPC isoform inhibited carbachol-evoked  $\text{Ca}^{2+}$  signals but for TPC2 this was modest and did not reach statistical significance (Fig. 4.7A and B). Time to peak did not change with TPC knockdown but this could be due to a combination of the rapid increase of cytosolic  $\text{Ca}^{2+}$  evoked by carbachol and limited time resolution (images of Fura-2 fluorescence were taken every 3 seconds). With a shorter time resolution and a lower affinity  $\text{Ca}^{2+}$  indicator, local  $\text{Ca}^{2+}$  signals induced by carbachol in SH-SY5Ys can be visualised before the global one (Smith et al., 2009). Indeed, experiments using a similar set up may provide additional detail about the generation of these agonist-evoked  $\text{Ca}^{2+}$  signals and how they may differ in disease. As the relatively modest inhibitory effect of TPC2 knockdown on carbachol signals correlated with a relatively modest reduction in TPC2 expression, I sought to improve TPC2 knockdown efficiency. It is perhaps even more pertinent to improve TPC2 knockdown in SH-SY5Ys as it appears to be associated with compensatory upregulation of TPC1 (Fig. 4.6A and D). As TPC1 appears to be required for carbachol  $\text{Ca}^{2+}$  signals its upregulation may mask any inhibitory effect caused by TPC2 knockdown. That being the case, double knockdown of TPC1 and TPC2 may be important in these cells to avoid such reciprocal compensation, and to uncover the sum of their contributions to carbachol-evoked  $\text{Ca}^{2+}$  signals. The original 3-day TPC knockdown protocol for undifferentiated SH-SY5Ys was chosen so that experiments could be carried out in a timely manner, but more importantly, so that a balance was struck between having an adequate population to image, and a population not so confluent that identifying individual cells for analysis would be problematic. Using this 3-day protocol I tested two alternative siRNAs which were targeted to different exons in the *TPC2* transcript. However, neither improved the knockdown of TPC2 compared to the original TPC2 siRNA used (Fig. 4.8A and B). I then tested all three TPC2 siRNAs in a protocol with an extended period of siRNA incubation. This method did sacrifice optimal confluency for imaging but could potentially be modified if proven successful. Unfortunately however, this extended protocol did not improve TPC2 knockdown either (Fig. 4.8C and D). For reassurance that the two new siRNAs were functional and could selectively knockdown TPC2 I carried out the usual 5-day knockdown protocol in fibroblasts. Both siRNAs clearly reduced TPC2 expression although one (TPC2 siRNA #3) also reduced *TPC1* expression by ~25% (Fig. 4.8E and D). The upshot from this data is that TPC knockdown in SH-SY5Ys requires intensive optimisation for TPC2 knockdown to be a reliable, reproducible tool in this neuronal cell line. Evidence that such a knockdown can be achieved has very recently been published, but without a description of the method used for this cell type (Pereira et al., 2016).

In addition to reducing TPC activity by reducing their expression, pharmacological inhibition was explored. The NAADP antagonist Ned-19 is often used in conjunction with other interventions



to manipulate TPC activity (Naylor et al., 2009). However, there are some reasons for reservation about its use:

1) The exact mechanism of how NAADP (the Ned-19 target) activates TPCs is unclear and appears to require interaction with an accessory binding protein instead of binding to the TPCs directly (Lin-Moshier et al., 2012; Walseth et al., 2012a, 2012b).

2) Although NAADP induces TPC activity this is under regulation by multiple other factors (Jha et al., 2014).

3) At nanomolar concentrations Ned-19 can actually potentiate TPC2 activity (Pitt et al., 2010).

4) NAADP can activate TRPML1-dependent  $\text{Ca}^{2+}$  signals, and Ned-19 has been shown to inhibit  $\text{Ca}^{2+}$  signals induced by the TRPML1 agonist ML-SA1 (Lee et al., 2015; Zhang et al., 2009, 2011).

Therefore, NAADP antagonism is a somewhat convoluted way of inhibiting TPCs with possibly undesired or off-target effects. The development or identification of a molecule that can directly bind and selectively block TPCs might mean that off-target effects of NAADP antagonism can be avoided, that the influence of non-NAADP factors on TPC activity can be negated, and that the undesired effect of nanomolar Ned-19 on TPC2 can be averted. Such a molecule has the potential to greatly advance research that pivots upon TPC activity.

Although not selective for TPCs the recently identified TPC blocker, tetrandrine, is expected to bind TPCs directly as it does to the evolutionarily-linked L-type VOCCs (King et al., 1988; Rahman et al., 2014; Sakurai et al., 2015). Tetrandrine is also known to have inhibitory effects on T-type VOCCs,  $\text{Ca}^{2+}$ -dependent  $\text{K}^+$  channels and  $\text{Ca}^{2+}$ -dependent chloride channels in SH-SY5Ys (Bhagya and Chandrashekar, 2016; Fang et al., 2004). In this chapter carbachol-evoked global  $\text{Ca}^{2+}$  signals were completely blocked by tetrandrine but bradykinin-evoked  $\text{Ca}^{2+}$  signals were left intact (Fig. 4.9). This may indicate that TPCs are indeed involved in the generation of carbachol-evoked  $\text{Ca}^{2+}$  signals but not those of bradykinin. As the entire carbachol signal was wiped out by tetrandrine it suggests that tetrandrine inhibits the initiation of the signal. Furthermore, from the data in Figures 4.4A and 4.5A, we know that carbachol signals can initiate in the absence of extracellular  $\text{Ca}^{2+}$ . Taken together, the implication is that the block of carbachol-evoked  $\text{Ca}^{2+}$  signals by tetrandrine is not caused solely by tetrandrine's inhibitory effect at VOCCs. Therefore, it is reasonable to believe that tetrandrine inhibits the initiation of the carbachol-evoked  $\text{Ca}^{2+}$  signal by inhibiting intracellular  $\text{Ca}^{2+}$  release. Moreover, as bradykinin signals rely on ER  $\text{Ca}^{2+}$  (Fig. 4.5C and D) but are not inhibited by tetrandrine (Fig. 4.9D and E), it appears that tetrandrine does not inhibit ER  $\text{Ca}^{2+}$  release.

This agonist-specific inhibition of global  $\text{Ca}^{2+}$  signals by tetrandrine is a promising start to the development of a cell-based screening assay for novel selective TPC blockers. However, it also highlights the need to determine the contribution of the various  $\text{Ca}^{2+}$  channels expressed in SH-SY5Ys to carbachol-evoked  $\text{Ca}^{2+}$  signals. This has been investigated previously but with a higher dose of carbachol: In the 1990s one research group published multiple reports on this topic and demonstrated that carbachol-evoked  $\text{Ca}^{2+}$  signals were insensitive to L-type and N-type  $\text{Ca}^{2+}$  channel blockers, but that the plateau phase was sensitive to nickel, which can inhibit T-type  $\text{Ca}^{2+}$  channels (Lambert et al., 1990; Perez-Reyes, 2003). They also demonstrated that continued  $\text{Ca}^{2+}$  entry required the continued presence of carbachol at its receptor (Lambert and Nahorski, 1990). Besides  $\text{Ca}^{2+}$  entry via VOCCs, nicotinic acetylcholine receptors (nAChR) may have a role in carbachol-evoked  $\text{Ca}^{2+}$  signals (Williams and Kauer, 1997). This was however rebutted by Lambert and colleagues who suggested that SOCE may constitute the  $\text{Ca}^{2+}$  entry plateau phase of the carbachol signal (Forsythe et al., 1992; Lambert and Nahorski, 1992). To re-balance the argument in favour of nAChRs, nicotine through activation of nAChRs and VOCCs has been shown to induce  $\text{Ca}^{2+}$  signals in SH-SY5Ys (Dajas-Bailador et al., 2002; Ring et al., 2015). Interestingly, it has been reported that these signals require ER  $\text{Ca}^{2+}$  but that they only occur in the presence of extracellular  $\text{Ca}^{2+}$  (Dajas-Bailador et al., 2002). There is also a case for TRPC involvement in  $\text{Ca}^{2+}$  entry during carbachol-evoked  $\text{Ca}^{2+}$  signals. It has been reported that carbachol activates TRPC currents (Strübing et al., 2003; Zhang et al., 2012) and that carbachol-induced  $\text{Ca}^{2+}$  entry is potentiated with the overexpression of TRPC3 but not of  $\text{Ca}^{2+}$ -impermeant mutants (Poteser et al., 2011). In SH-SY5Ys which express TRPCs impaired carbachol-evoked  $\text{Ca}^{2+}$  signalling has also been linked to reduced TRPC1 expression (Bollimuntha et al., 2006; Liu et al., 2017).

In the search for novel TPC blockers that are not known to inhibit VOCCs as tetrandrine is, or any other  $\text{Ca}^{2+}$  channels, one course of virtual screening has led to L-deprenyl. L-deprenyl is a monoamine oxidase (MAO) inhibitor and is administered to PD patients to inhibit DA metabolism (Youdim and Bakhle, 2006). Here, in a similar manner as tetrandrine, L-deprenyl blocked carbachol-evoked  $\text{Ca}^{2+}$  signals in SH-SY5Ys (Fig. 4.10B and C). Despite using a high concentration of the drug (1 mM) bradykinin-evoked  $\text{Ca}^{2+}$  signals were not inhibited but in fact slightly potentiated. This result was encouraging and helped to refute the argument that tetrandrine was merely a fluke carbachol antagonist. L-deprenyl is not known to block VOCCs but has been implicated in mitochondrial function and  $\text{Ca}^{2+}$ : It inhibits  $\text{Ca}^{2+}$ -induced mitochondrial membrane depolarisation as well as mitochondrial  $\text{Ca}^{2+}$  efflux through the PT pore and associated superoxide release (Czerniczyniec et al., 2007; Wu et al., 2015c). L-deprenyl has also been reported to inhibit non-classical DA-induced  $\text{Ca}^{2+}$  release (Jennings et al., 2017;

Vaarmann et al., 2010). Vaarmann and colleagues propose a pathway of DA-evoked  $\text{Ca}^{2+}$  signals whereby DA metabolism by MAO produces reactive oxygen species (ROS) which in turn causes lipid peroxidation and stimulates the synthesis of  $\text{IP}_3$ . Crucially, these  $\text{Ca}^{2+}$  signals could be completely blocked by L-deprenyl or thapsigargin, suggestive of MAO and ER involvement in these signals. However, the contribution of lysosomal  $\text{Ca}^{2+}$  to this response was not assessed. As discussed previously, data in this chapter shows that complete block of a  $\text{Ca}^{2+}$  signal (induced by carbachol) by thapsigargin does not preclude lysosomal involvement (Fig. 4.3 and Fig. 4.5). It is possible therefore that DA/ROS-induced  $\text{Ca}^{2+}$  signals in astrocytes also require the lysosomes and perhaps TPCs. Indeed, L-deprenyl may not only be active in this context as an inhibitor of MAO activity but also as an inhibitor of lysosomal  $\text{Ca}^{2+}$  release. Incidentally, ROS has been implicated in the potentiation of lysosomal  $\text{Ca}^{2+}$  release recently (Zhang et al., 2016). It should be noted however that the concentration of L-deprenyl used to inhibit the DA/ROS-induced  $\text{Ca}^{2+}$  signalling is 50-fold lower than that which was used in this chapter.

From an alternative virtual screen, in combination with *in vitro* Ebola screen data, the drugs sunitinib, pimozone and fluphenazine were put forward as putative TPC blockers. Again encouragingly, all three drugs blocked carbachol-evoked  $\text{Ca}^{2+}$  signals in SH-SY5Ys (Fig. 4.11 and Fig. 4.12). As (by now) expected bradykinin-evoked  $\text{Ca}^{2+}$  signals were not inhibited by sunitinib or fluphenazine. However, antipsychotic pimozone did reduce the magnitude of the signal. The reason for this is unknown but report of pimozone as a SERCA inhibitor at resting  $\text{Ca}^{2+}$  levels is anticipated (Loulousis et al., 2016). This may explain reduced bradykinin-evoked  $\text{Ca}^{2+}$  signals via a reduction in ER  $\text{Ca}^{2+}$  content.

The first of these three drugs, sunitinib, is used as an anti-tumour drug. It inhibits multiple receptor tyrosine kinases (RTK) probably by binding to their ATP-binding sites (Johnson, 2009; Mendel et al., 2003; Roskoski Jr., 2007). One of sunitinib's RTK targets is vascular endothelial growth factor receptor (VEGFR). Intriguingly VEGFR's ligand, VEGF, has recently been shown to require TPC2 to elicit its  $\text{Ca}^{2+}$  signal (Favia et al., 2014). If TPCs regulate VEGFR-mediated  $\text{Ca}^{2+}$  signals perhaps it is sunitinib's effect on TPCs that in turn inhibits VEGFR. If carbachol does elicit its  $\text{Ca}^{2+}$  signals through TPCs a close functional connection between TPCs and RTKs may also underlie the finding that carbachol can activate the epidermal growth factor receptor (EGFR) RTK (Keely et al., 1998). This also poses the possibility that RTKs contribute to carbachol-evoked  $\text{Ca}^{2+}$  signals in SH-SY5Ys. Indeed, this cell line expresses VEGFR, therefore its contribution should be assessed by knockdown and a range of inhibitors (Meister et al., 1999).

The other two putative TPC blockers from the virtual structure-based/*in vitro* Ebola screen were pimozide and fluphenazine. These two drugs are antipsychotics which like sunitinib are believed to have multiple pharmacological targets, including DA receptors (Peters, 2013). Pimozide is reported to block L, T, P and N-type VOCCs (Bancila et al., 2011; Enyeart et al., 1990; Sah and Bean, 1994) and fluphenazine can block T, P and N-type VOCCs (Sah and Bean, 1994; Xie et al., 2007). Therefore, assessment of VOCC involvement in carbachol-evoked Ca<sup>2+</sup> signals is required by these results as well as those from the tetrandrine data. Intriguingly, fluphenazine has been shown to inhibit IP<sub>3</sub>-induced Ca<sup>2+</sup> release (IICR) although not completely block it (Khan et al., 2001). Although carbachol has been associated with IP<sub>3</sub> synthesis, which may be important for its Ca<sup>2+</sup> signal, fluphenazine's inhibitory effect upon IICR is not expected to be the reason for its inhibitory effect on the carbachol-evoked Ca<sup>2+</sup> signal (Chen and Hsu, 1994; Piiper et al., 1994; Shin et al., 2003). This is because bradykinin is also reported to induce IP<sub>3</sub> synthesis and bradykinin-evoked Ca<sup>2+</sup> signals were not inhibited by fluphenazine (Ataei et al., 2013; Johnson et al., 1990). However, this does highlight the need to confirm agonist-induced IP<sub>3</sub> production in these SH-SY5Ys. Also reported by Khan and colleagues was fluphenazine's ability to inhibit SERCA (Khan et al., 2000, 2001). Inhibited Ca<sup>2+</sup> uptake into the ER via SERCA could explain their finding that fluphenazine inhibited IICR. Noticeably here, fluphenazine caused a relatively rapid rise in basal Ca<sup>2+</sup> which may be due to this SERCA inhibition, and a consequent net efflux of ER Ca<sup>2+</sup> (Fig. 4.12B and D). Furthermore, this may have contributed to the potentiated bradykinin responses that were observed (Fig. 4.11.D and E). If fluphenazine is truly inhibiting SERCA it would be expected that after a longer treatment both carbachol and bradykinin-evoked Ca<sup>2+</sup> signals would be blocked due to ER Ca<sup>2+</sup> depletion. This can be examined by using the 1 hour pre-incubation method that was used for tetrandrine and the other putative TPC blockers.

The selective block of carbachol-evoked Ca<sup>2+</sup> signals by novel TPC blocker tetrandrine and putative TPC blockers is a promising start to identifying TPC-dependent global Ca<sup>2+</sup> signals in SH-SY5Ys that may be physiologically relevant. Furthermore, it may serve as a useful human cell screen for novel, selective TPC blockers in the future. However, at present, it is unclear whether these drugs truly work at the level of the TPCs. Indeed, in addition to blocking carbachol-evoked Ca<sup>2+</sup> signals which appear to rely on the lysosomes, tetrandrine, sunitinib, pimozide and fluphenazine have all been associated with lysosomes previously: In screens designed to find therapeutics for Gaucher Disease fluphenazine was identified as a chaperone for lysosomal enzyme glucocerebrosidase although it failed to enhance enzyme activity in cell culture (Maegawa et al., 2009). In addition, fluphenazine and pimozide have been shown to inhibit lysosomal enzyme acid sphingomyelinase (Kornhuber et al., 2011). Interestingly, tetrandrine, sunitinib, pimozide and fluphenazine have also all been linked to the regulation of autophagy.

Tetrandrine induces autophagy and disrupts autophagic flux which may be due to its effect on lysosomal pH or ROS production (Miyamae et al., 2016; Qiu et al., 2014; Wang et al., 2015a). Fluphenazine and pimozide have also been identified as autophagy inducers (Barmada et al., 2014), and sunitinib as an inhibitor of autophagic flux (Giuliano et al., 2015). It is possible of course that these compounds effect autophagy by modulating TPC activity (Gómez-Suaga et al., 2012).

Tetrandrine, pimozide and fluphenazine also inhibit infectivity of viruses and bacteria which are known to journey through the endolysosomal system. Tetrandrine inhibits NAADP-induced  $\text{Ca}^{2+}$  signals and Ebola infection which has been attributed to its inhibitory effect on TPCs (Sakurai et al., 2015). Fluphenazine inhibits Middle East respiratory syndrome coronavirus (MERS-CoV) and severe acute respiratory syndrome coronavirus (SARS-CoV) although there is currently no evidence that TPCs are involved (Dyall et al., 2014; Millet and Whittaker, 2015). Finally, pimozide inhibits bacterial infections, with its effect on *Listeria monocytogenes* notably independent of  $\text{Ca}^{2+}$  entry (Alvarez-Dominguez et al., 1997; Lieberman and Higgins, 2009).

Although the hope is that these drugs identified by *in silico* screens are genuine inhibitors of TPCs, they may affect the carbachol-evoked  $\text{Ca}^{2+}$  signals, autophagy or infection in intact cells by becoming sequestered inside the lysosomes. According to the phenomenon of ion trapping lipophilic weak bases can move through membranes and enter the acidic lysosome (Kaufmann and Krise, 2007). Here they obtain protons which causes the lysosomal pH to rise. As the protonated forms of these weak bases are impermeable to the lysosomal membrane they become trapped inside the lysosome and accumulate. An acid dissociation constant (pKa) of  $>7$  and a lipophilicity (logP) of  $>2$  are considered to promote such lysosomal ion trapping (Kaufmann and Krise, 2007; Nadanaciva et al., 2011; Seo et al., 2014). L-deprenyl, sunitinib, pimozide and fluphenazine are all predicted to have pKa values  $>7$  and logP values of  $>2$  (predicted by ChemAxon as listed by DrugBank). The pKa of tetrandrine is also predicted to fall within the parameters that favour ion trapping (Yang et al., 2007). If these compounds do become trapped in the lysosomes in the SH-SY5Ys, measurements of LTR fluorescence may reveal a concomitant reduction in acidic organelles. Furthermore, if we consider that  $\text{Ca}^{2+}$  uptake is dependent upon lysosomal pH, this trapping may reduce lysosomal  $\text{Ca}^{2+}$  (Morgan et al., 2011). This alone would be expected to inhibit carbachol-evoked  $\text{Ca}^{2+}$  signals irrespective of a compound's ability to bind and block the TPCs. As well as causing loss of lysosomal acidity and  $\text{Ca}^{2+}$  these drugs may rupture the lysosomes if they are trapped inside. Indeed, fluphenazine and pimozide have been shown to cause permeabilisation of the lysosomal membrane (Pagliero et al., 2016). However, only

fluphenazine induced a complete loss of LTR fluorescence, implying that retention of lysosomal acidity does not necessarily equate to an intact lysosomal membrane. Therefore, to establish whether lysosomal permeabilisation is caused by putative TPC blockers in SH-SY5Ys, the high-throughput assay described by Pagliero et al., or experiments to determine the size of leaked lysosomal molecules should also be carried out (Pagliero et al., 2016; Penny et al., 2014).

Lysosomal sequestration of the RTK inhibitor sunitinib has been studied in the context of drug-resistance (Giuliano et al., 2015; Zhitomirsky and Assaraf, 2014). If sunitinib “hides” inside the lysosome its therapeutic properties are effectively wasted. Moreover, sunitinib can promote lysosomal biogenesis which exacerbates the problem by generating a greater lysosome volume in which it can hide (Zhitomirsky and Assaraf, 2014). Lysosomal sequestration of sunitinib may be driven by ABCB1 (also known as MDR1 and P-glycoprotein) expression which is thought to pump the drug into the lysosomes and out of the cell. (Giuliano et al., 2015). In contrast, tetrandrine inhibits ABCB1 and can reverse drug resistance (Liu et al., 2016). Although the putative TPC blockers tested in this chapter may eventually become trapped inside the lysosomes it is important to consider that their rates of entrapment may differ (De Duve et al., 1974). If these rates are known, suitable temporal windows before sequestration could be used to re-examine the effects of these drugs upon TPC-mediated  $\text{Ca}^{2+}$  signals. Very preliminary work shows that tetrandrine, L-deprenyl and sunitinib all block carbachol-evoked  $\text{Ca}^{2+}$  signals in SH-SY5Ys after just a 2-minute incubation, but pimozone does not (Fig. 4.12.Supplement). If pimozone accumulates in the lysosomes at a slower rate than the others this may indicate that lysosome trapping is at play. Incidentally, neither tetrandrine, nor any of the putative TPC blockers induced global  $\text{Ca}^{2+}$  signals of their own in the 2 minutes (Fig. 4.12.Supplement). As a final point regarding the specificity of these drugs and ion trapping, it may be informative to also test compounds that were not hits from the virtual screens but that have similar pKa and logP values.

In the presence of tetrandrine and the putative TPC blockers global  $\text{Ca}^{2+}$  signals induced by carbachol were blocked in a similar manner. An intriguing and unexpected observation however, was that L-deprenyl, sunitinib and fluphenazine all potentiated bradykinin-evoked  $\text{Ca}^{2+}$  signals, but in subtly different modes. L-deprenyl potentiated the initial peak of the  $\text{Ca}^{2+}$  signal but  $\text{Ca}^{2+}$  levels returned to basal at much the same rate as the control group (Fig. 4.10D). Sunitinib on the other hand did not affect the size of the initial peak but prevented the return of  $\text{Ca}^{2+}$  levels to basal throughout imaging (Fig. 4.11E). Finally, fluphenazine appeared to uniformly potentiate the bradykinin signal (Fig. 4.12D). This indicates that whilst all three drugs may inhibit lysosomal

Ca<sup>2+</sup> release they differentially effect other components of the Ca<sup>2+</sup> signalling network. This may not be surprising as these three drugs are currently administered based on distinct mechanisms of action. As bradykinin-evoked Ca<sup>2+</sup> signals appear to be dependent upon ER Ca<sup>2+</sup> (Fig. 4.5) it is important to assess the impact of these potentiating drugs on ER Ca<sup>2+</sup> release. Likewise, repeating the experiments in Figures 4.10-12 in the absence of extracellular Ca<sup>2+</sup> may help to determine whether these drugs potentiate bradykinin-evoked Ca<sup>2+</sup> signals by promoting Ca<sup>2+</sup> entry.

The data presented in this chapter indicate that lysosomes, and possibly TPCs, are involved in carbachol-evoked global Ca<sup>2+</sup> signals in neuronal SH-SY5Ys. Supporting this, lysosomes and TPC2 have previously been implicated in carbachol-induced muscle contraction (Tugba Durlu-Kandilci et al., 2010). However, unlike the data presented here, lysosomal disruption (nor TPC2 knockout) did not result in complete contraction inhibition. Indeed, the severe block of carbachol-evoked Ca<sup>2+</sup> signals by GPN, tetrandrine and putative TPC blockers suggests that lysosomes, and possibly TPCs, are integral to the initiation of the signal. Initial lysosomal Ca<sup>2+</sup> release may trigger further Ca<sup>2+</sup> release from the ER as has been reported for NAADP (Morgan, 2016). However, this “trigger hypothesis” may be more controversial for “textbook” Ca<sup>2+</sup> signals that are thought to be mediated by IP<sub>3</sub>. Perhaps the reverse scenario is true where local ER Ca<sup>2+</sup> release acts as the initial trigger stimulating NAADP synthesis, and requiring lysosomal Ca<sup>2+</sup> to propagate the signal (Morgan, 2016; Morgan et al., 2013).

Reinforcing the idea that TPCs may be important for Ca<sup>2+</sup> signal initiation is the report that TPC2 is needed for the generation of Ca<sup>2+</sup> signals in muscle (Kellu et al., 2015). Notably, these signals could also be blocked by inhibiting IP<sub>3</sub>R, nAChR or L-type VOCCs (Cheung et al., 2011; Kellu et al., 2015). This once again reiterates the point that identification of one source of Ca<sup>2+</sup> release or one route of Ca<sup>2+</sup> entry, as an essential component for Ca<sup>2+</sup> signals, does not preclude others. Indeed, the idea that multiple Ca<sup>2+</sup> mobilising messengers work together to initiate global Ca<sup>2+</sup> signals is not new (Cancela et al., 2002).

From experiments conducted in untransfected SH-SY5Ys the data suggest that carbachol-evoked Ca<sup>2+</sup> signals are lysosome- and possibly TPC-dependent but that bradykinin-evoked Ca<sup>2+</sup> signals are not. (It should be noted that this dependence may be specific not only to the agonist used but also the agonist concentration (Tugba Durlu-Kandilci et al., 2010)). The purpose of identifying a TPC-dependent extracellular agonist was to examine its physiological global Ca<sup>2+</sup> signals in a neuronal model of LRRK2-GS PD which has been associated with upregulated TPC2

(Hockey et al., 2015). The hypothesis was that TPC-dependent global  $\text{Ca}^{2+}$  signals would be augmented in LRRK2-GS cells, which may contribute to TPC-mediated neurodegeneration in PD. When comparing untransfected SH-SY5Ys with those stably expressing LRRK2 WT or LRRK2-GS their appearance was noticeably different (Fig. 4.13.A). First, the bodies of the LRRK2 WT SH-SY5Ys appeared larger and flatter compared to the untransfected and LRRK2-GS cells. Neurites also appeared stunted. Second, LRRK2-GS SH-SY5Ys were consistently sparser on the day of imaging despite being plated at the same density as untransfected and LRRK2 WT cells. In an effort to control for such different densities, patches of similar confluency in each cell line were sought for imaging. The scarcity of LRRK2-GS cells may also be the reason why they appeared to have more, longer neurites compared to the LRRK2 WT cells. Notably, TPCs have been implicated in cell differentiation therefore differential TPC activities may be responsible for the varied SH-SY5Y morphology here (Aley et al., 2010a; Brailoiu et al., 2006; Zhang et al., 2013). Experiments to examine the differentiation state of these cells, and those transfected with TPC siRNAs, may prove affirmative. Importantly, LRRK2 is also associated with differentiation (Bahnassawy et al., 2013; Schulz et al., 2011). Paradoxically though, neurite length in differentiated LRRK2-GS SH-SY5Ys is shorter compared to WT controls (Plowey et al., 2008). As this result reported by Plowey and colleagues is in line with data from neurons it supports the transfer of the experiments in this chapter to differentiated SH-SY5Ys (Borgs et al., 2016; Sánchez-Danés et al., 2012).

In agreement with the hypothesis carbachol-evoked global  $\text{Ca}^{2+}$  signals (lysosome/TPC-dependent) in the LRRK2-GS SH-SY5Ys were potentiated but bradykinin-evoked  $\text{Ca}^{2+}$  signals (lysosome/TPC-independent) were not (Fig. 4.13). Intriguingly, the carbachol signal was potentiated at the plateau phase but not its initial peak. This plateau phase likely corresponds to  $\text{Ca}^{2+}$  entering the cell as it is non-existent in the absence of extracellular  $\text{Ca}^{2+}$  (Fig. 4.3A c.f. Fig 4.5A). As discussed earlier the mechanism responsible for carbachol-induced  $\text{Ca}^{2+}$  entry has been debated, with nAChR, SOCE, VOCCs and TRPC channels possibly being involved (Bollimuntha et al., 2006; Dajas-Bailador et al., 2002; Lambert and Nahorski, 1992; Ring et al., 2015). However, although it is the entry part of the carbachol-evoked  $\text{Ca}^{2+}$  signal that is potentiated in the LRRK2-GS SH-SY5Ys, this does not discount lysosomal involvement. Indeed there is some evidence that TPC2 is crucial to  $\text{Ca}^{2+}$  signals that are also dependent upon nAChR and VOCCs (Cheung et al., 2011; Kelu et al., 2015). Furthermore, it has been reported that global  $\text{Ca}^{2+}$  signals which can only be observed in the presence of extracellular  $\text{Ca}^{2+}$ , and therefore probably represent  $\text{Ca}^{2+}$  entry, require intracellular  $\text{Ca}^{2+}$  stores (Dajas-Bailador et al., 2002). It has also been proposed that NAADP-induced signalling promotes VOCC activation (Arredouani et al., 2015), and lysosomes appear to be required for action potential-induced  $\text{Ca}^{2+}$  signals (Padamsey et al., 2017). Alternatively, the plateau phase of carbachol-evoked  $\text{Ca}^{2+}$  signals may represent a



specialised lysosomal SOCE (aSOCE) involving N-type VOCCs (Hui et al., 2015). However, it is noted that muscarinic  $\text{Ca}^{2+}$  signalling inhibits N-type VOCCs in SH-SY5Ys (Reeve et al., 1995). In contrast, the bradykinin-evoked  $\text{Ca}^{2+}$  signal in LRRK2-GS SH-SY5Ys was not potentiated at the corresponding “plateau” phase (Fig. 4.13E and G).

To begin the investigation into what may be responsible for the potentiated carbachol-evoked  $\text{Ca}^{2+}$  signals in the LRRK2-GS SH-SY5Y cells I examined the expression of TPCs. Interestingly, there was no difference between the LRRK2 WT and LRRK2-GS cells but expression in both was reduced compared to the untransfected cells (Fig. 4.14). This reduction was more pronounced for TPC1, which resulted in a lower *TPC1/TPC2* ratio in the LRRK2-transfected cells. It is unknown whether this is due to LRRK2 overexpression or is an overexpression artefact. Expanding the family of SH-SY5Y lines to include some that are transfected with a putatively “inert” protein, or a LRRK2 kinase-dead mutant, would help to determine the cause.

In addition to investigating TPC expression levels I compared GPN-evoked  $\text{Ca}^{2+}$  signals in these cells to assess lysosomal  $\text{Ca}^{2+}$  content. Rather than being potentiated this signal was slightly reduced in the LRRK2-GS cells compared to the LRRK2 WT controls (Fig. 4.15.A and B). I also assessed ER  $\text{Ca}^{2+}$  content as it appeared to be a component of carbachol-evoked  $\text{Ca}^{2+}$  signals. Again, thapsigargin-induced  $\text{Ca}^{2+}$  responses were not potentiated in the LRRK2-GS SH-SY5Ys (Fig. 4.15C and D). Finally, SOCE was compared as it may be required to replenish a depleted ER  $\text{Ca}^{2+}$  store for sustained carbachol  $\text{Ca}^{2+}$  signalling (Lambert and Nahorski, 1992; Shen et al., 2011). Furthermore, involvement of TPC2 (but not TPC1) in SOCE has been reported (López et al., 2012). Although the preceding thapsigargin-induced responses showed no obvious difference between LRRK2 WT and LRRK2-GS cells there was a clear inhibition of SOCE in the LRRK2-GS population (Fig. 4.16A and B). This finding indicates that SOCE is not responsible for the potentiated plateau phase of carbachol-evoked  $\text{Ca}^{2+}$  signals in the SH-SY5Y LRRK2-GS PD model. Reports of impaired SOCE in PD are not widespread but in research published last year it was associated with autophagy defects and neuronal death in PD (Zhou et al., 2016). However, Zhou and colleagues demonstrated that this was also linked to a clear reduction in ER  $\text{Ca}^{2+}$  content which was not the case here.

Very recently it has been reported that in SH-SY5Ys with reduced TRPC1 expression thapsigargin-induced SOCE is inhibited but the thapsigargin signal itself is unchanged (Sun et al., 2017). In addition, these SH-SY5Ys or TRPC1<sup>-/-</sup> neurons exhibited potentiated VOCC currents that could be inhibited by knocking down Cav1.3 – the VOCC channel linked to pacemaking activity of the SNc

and mitochondrial oxidative stress in PD (Chan et al., 2007; Guzman et al., 2010; Surmeier et al., 2017b). Perhaps, in LRRK2-GS SH-SY5Ys TRPC1 is somehow inhibited causing reduced SOCE but promoting  $\text{Ca}^{2+}$  entry through VOCCs during carbachol-evoked  $\text{Ca}^{2+}$  signals. To the best of my knowledge there is no evidence that directly links LRRK2 to TRPC1 but it has been reported that LRRK2 WT and LRRK2-GS do potentiate currents through VOCCs (Bedford et al., 2016). This type of simultaneous differential regulation of SOCE and VOCCs has also been linked to STIM1 (Cahalan, 2010). Investigation of VOCC activity in these LRRK2-GS SH-SY5Y cells is therefore a rational next line of enquiry.

The type of potentiated global  $\text{Ca}^{2+}$  signals seen in the LRRK2-GS SH-SY5Ys may disrupt many  $\text{Ca}^{2+}$ -sensitive processes throughout neurons. This may be of significance to the aetiology of PD which has already been associated with potentially dangerous repetitive influxes of  $\text{Ca}^{2+}$  in the SNc. Furthermore, the selective potentiation of carbachol-evoked  $\text{Ca}^{2+}$  signals here is consistent with a gain of function of the TPCs. If this is the case the perception of these lysosomal  $\text{Ca}^{2+}$  channels in PD may change: Not only may they be important for maintaining lysosomal function and degradation of disease-related entities such as  $\alpha$ -synuclein or defective mitochondria, but be more active promoters of neuronal death by substantially derailing global  $\text{Ca}^{2+}$  signalling (La Rovere et al., 2016; Papkovskaia et al., 2012; Spillantini et al., 1997). This would also further highlight TPCs as potential therapeutic targets for the treatment of PD.

To summarise, global  $\text{Ca}^{2+}$  signals evoked by the cholinergic agonist carbachol are inhibited in undifferentiated SH-SY5Ys when they are treated with the lysosomotropic agent GPN, with the novel TPC blocker tetrandrine, or putative TPC blockers identified by *in silico* screens. In contrast,  $\text{Ca}^{2+}$  signals evoked by bradykinin were not inhibited, suggestive of an agonist-specific dependence upon lysosomes and TPCs. Furthermore, in a neuronal model of LRRK2-GS PD, carbachol-evoked  $\text{Ca}^{2+}$  signals were potentiated but bradykinin signals were not. This agonist-selective potentiation could not be attributed to enhanced TPC expression, lysosomal  $\text{Ca}^{2+}$  or ER  $\text{Ca}^{2+}$ . In addition, store-operated  $\text{Ca}^{2+}$  entry (SOCE) in this PD model was reduced. This data is consistent with a gain of function of the TPCs in LRRK2-GS PD, and presents a possible novel route to neurodegeneration.

## CHAPTER 5: Conclusions and Future Directions

In this thesis I have explored the relationship between lysosomal  $\text{Ca}^{2+}$  signalling, global  $\text{Ca}^{2+}$  signalling and neurodegenerative disease. The rationale for investigating such a relationship has been prompted by reports of altered TRPML1 and TPC activity in neurodegenerative diseases (Hockey et al., 2015; LaPlante et al., 2004; Shen et al., 2012), NAADP-evoked global  $\text{Ca}^{2+}$  signals that are dependent upon these lysosomal  $\text{Ca}^{2+}$  channels (Brailoiu et al., 2009; Calcraft et al., 2009; Jha et al., 2014; Zhang et al., 2011), and the potentially catastrophic effects of large  $\text{Ca}^{2+}$  fluxes in neurons (Mehta et al., 2013). For PD specifically, it has been suggested that the vulnerability of SNc neurons is compounded by repetitive  $\text{Ca}^{2+}$  influx (Chan et al., 2007; Guzman et al., 2010; Surmeier et al., 2017b). In addition, the more vulnerable ventral section of SNc has lower levels of the  $\text{Ca}^{2+}$  buffer calbindin-D28K (Foehring et al., 2009). Although much work remains to be done to support the idea that lysosomal  $\text{Ca}^{2+}$  channels control global  $\text{Ca}^{2+}$  signals, and that they contribute to neurodegeneration in this capacity, this thesis includes data to strengthen this concept and tools to aid further investigation.

The first lysosomal  $\text{Ca}^{2+}$  channel of focus in this thesis was TRPML1. In the neurodegenerative diseases Mucopolysaccharidosis type IV (MLIV) and Niemann-Pick type C (NPC) TRPML1 has been associated with impaired local  $\text{Ca}^{2+}$  signalling (LaPlante et al., 2004; Shen et al., 2012). However, the influence of TRPML1 on global  $\text{Ca}^{2+}$  signalling has not been directly addressed and was the focus of Chapter 2. Here I demonstrated that synthetic TRPML1 agonists could induce global  $\text{Ca}^{2+}$  signals. These could be dissected into a small intracellular  $\text{Ca}^{2+}$  release component and a large  $\text{Ca}^{2+}$  influx component. This influx unlikely corresponds to store-operated  $\text{Ca}^{2+}$  entry (SOCE) as the TRPML1-mediated global  $\text{Ca}^{2+}$  signals were minimally affected by SOCE blocker BTP2. Experiments examining TRPML1-mediated  $\text{Fe}^{2+}$  entry as a proxy for  $\text{Ca}^{2+}$  supported the notion that TRPML1 at the plasma membrane might directly mediate  $\text{Ca}^{2+}$  entry. This is surprising given that examination of TRPML1 by confocal microscopy revealed its predominantly lysosomal localisation. Now the physiological relevance of this type of global  $\text{Ca}^{2+}$  signal must be ascertained. There are a handful of reports that global  $\text{Ca}^{2+}$  signals evoked by extracellular agonists are modulated in TRPML1-deficient cells or in cells expressing mutant TRPML1 (LaPlante et al., 2004; Park et al., 2016; Soyombo et al., 2006; Zhang et al., 2009). Future studies in this vein may benefit from the use of synthetic TRPML1 inhibitor ML-SI3, which as shown in Chapter 2 can block TRPML1-mediated global  $\text{Ca}^{2+}$  signals.

An implication of the work presented in Chapter 2 is that where reduced TRPML1 activity is associated with neurodegeneration impaired global  $\text{Ca}^{2+}$  signalling should be considered as a conduit to disease as well as impaired local  $\text{Ca}^{2+}$  signalling. Perhaps for example, reduced TRPML1 activity results in smaller global  $\text{Ca}^{2+}$  signals which inhibit ATP synthesis and place neurons under energetic stress (Glancy and Balaban, 2012). Moreover, where experiments have been designed to examine TRPML1-mediated  $\text{Ca}^{2+}$  signals in disease these should be conducted in the presence of extracellular  $\text{Ca}^{2+}$ . Otherwise any large changes to TRPML1-mediated  $\text{Ca}^{2+}$  influx may be overlooked. The impact of augmented TRPML1 activity on global  $\text{Ca}^{2+}$  signalling in disease should also be determined. Indeed, upregulation of TRPML1 appears to improve trafficking defects in neurodegenerative disorders and is therefore of potential therapeutic benefit (Cao et al., 2015b; Chen et al., 2014; Shen et al., 2012). However, if global  $\text{Ca}^{2+}$  signals are augmented by this upregulation beyond healthy levels this could spell disaster in cells that are already vulnerable to degeneration. Certainly, rises in intracellular  $\text{Ca}^{2+}$  have already been established as the enemy in multiple neurodegenerative diseases (Mehta et al., 2013).

In Chapters 3 and 4 focus was turned to the TPC channels. As for TRPML1, TPC2 has been associated with disturbed local  $\text{Ca}^{2+}$  signalling in neurodegenerative disease (Gómez-Suaga et al., 2012; Hockey et al., 2015). For TPC2 though it is increased channel activity that is implied and the disorder is Parkinson's disease (PD). In fibroblasts from people with familial PD and the *LRRK2* G2019S (*LRRK2*-GS) mutation upregulated TPC2 activity has been linked to disturbed lysosome morphology. In Chapter 3 I independently verified this morphology defect and extended the investigation into sporadic PD. This was to gauge whether disturbed lysosome morphology might be a common phenotype in PD, perhaps indicative of a common pathogenic pathway. As sporadic PD constitutes ~90% of PD cases discovery of such a pathway has the potential to benefit millions through rational drug design (Dorsey et al., 2007; Gandhi and Wood, 2010). Indeed, I found that the lysosome population in sporadic PD fibroblasts comprised a greater proportion of large lysosomes and clusters of lysosomes when compared to age-matched controls. This was confirmed by data that was generated from automated *in silico* processing of LAMP1-immunofluorescence images. The cause of this morphology disturbance is unknown and the effects of knocking down TPC2, chelating local  $\text{Ca}^{2+}$  or inhibiting Rab7 should be assessed as has been done for the *LRRK2*-GS defect (Hockey et al., 2015). More information about the health of the endolysosomal system may also be gleaned by carrying out similar morphometric assays with endosome and autophagosome markers.

As knocking down TPC2 or chelating local  $\text{Ca}^{2+}$  improves trafficking defects in LRRK2 PD models, TPC2 is expected to mediate local  $\text{Ca}^{2+}$  release, drawing a parallel with TRPML1 (Gómez-Suaga et al., 2012; Hockey et al., 2015). The involvement of TPCs in global  $\text{Ca}^{2+}$  signalling is however more widely appreciated (Brailoiu et al., 2009; Calcraft et al., 2009; Jha et al., 2014). Where data surrounding TPCs and global  $\text{Ca}^{2+}$  signalling peters out is at the level of physiological global  $\text{Ca}^{2+}$  signals evoked by extracellular stimuli. In Chapter 3 I set out to advance this topic. When fibroblasts were challenged with  $\text{NH}_4\text{Cl}$  to compromise the lysosomes,  $\text{Ca}^{2+}$  signals evoked by the inflammatory mediator bradykinin were inhibited suggesting that the lysosomes are important for this physiological global  $\text{Ca}^{2+}$  signal. When they were subjected to TPC knockdown, the bradykinin-evoked  $\text{Ca}^{2+}$  signals were also inhibited indicating TPC involvement too. I then questioned whether such TPC-dependent  $\text{Ca}^{2+}$  signals might be potentiated in the LRRK-GS PD fibroblasts that have been associated with upregulated TPC2 activity. However, this was not the case. Neither was there any potentiation in the sporadic PD fibroblasts. There was though a modest reduction in the frequency of cells displaying oscillatory responses in LRRK2-GS PD, and in sporadic PD the signal was slightly smaller compared to controls.

It is appreciated that experiments in patient-derived fibroblasts serve as a valuable foundation from which to delineate pathogenic mechanisms of neurodegeneration. However, they are likely to fall short of recapitulating disease in neurons (Auburger et al., 2012; Ordonez et al., 2012). To bridge the conceivable gap between fibroblasts and the brain I extended the investigation into a neuronal cell line – SH-SY5Y. In this cell line compromise of the lysosomes using GPN blocked physiological global  $\text{Ca}^{2+}$  signals induced by the cholinergic agonist carbachol. However, in contrast to fibroblasts, bradykinin-evoked  $\text{Ca}^{2+}$  signals were not inhibited by lysosome compromise in the SH-SY5Y cells. The reason for this cell-type discrepancy is unknown but perhaps highlights the importance of choosing an appropriate cell-type to investigate mechanisms of disease. Experiments to assess the effect of multiple lysosomotropes on bradykinin-evoked  $\text{Ca}^{2+}$  signals, in both cell types, may confirm this cell-type specificity of lysosome-dependence.

Another area where fibroblasts and SH-SY5Ys differed was TPC knockdown. Unfortunately, TPC knockdown proved inefficient in SH-SY5Ys compared to the fibroblasts, and could not be resolved within the time frame of this project. Therefore, the TPC-dependence of physiological global  $\text{Ca}^{2+}$  signals was explored by pharmacological intervention. Notably, there are currently no selective TPC blockers to the detriment of the field. However, tetrandrine, an inhibitor of L-type voltage-operated  $\text{Ca}^{2+}$  channels (VOCC), has recently been identified as a TPC inhibitor

(Sakurai et al., 2015). In SH-SY5Ys tetrandrine selectively blocked carbachol-evoked  $\text{Ca}^{2+}$  signals; selectivity that was conferred by bradykinin-evoked  $\text{Ca}^{2+}$  signals that remained intact.

To find selective TPC blockers collaborators have screened drugs that are FDA-approved but not classed as  $\text{Ca}^{2+}$  channel antagonists. Encouragingly, in a similar manner to tetrandrine, putative TPC inhibitors from these screens selectively blocked carbachol-evoked  $\text{Ca}^{2+}$  signals in the SH-SY5Ys. As such this agonist-selective assay in human cells may form part of a working pipeline to identify or develop selective TPC blockers. Use of such blockers in the lab could propel TPC research and provide further insights into how TPC activity might contribute to diseases including PD. Importantly, by screening drugs that are already widely-approved for human use, the time between drug discovery and clinical use may be drastically cut. Furthermore, if the link between upregulated TPC activity and PD continues to hold, such drugs may serve to modify the disease (Gómez-Suaga et al., 2012; Hockey et al., 2015). However, there are obvious issues about the use of DA receptor inhibitors such as pimozide or fluphenazine in the treatment of PD which is characterised by a loss of DAergic activity (Brichta et al., 2013; Peters, 2013).

Further experiments are required to exclude the possibilities that tetrandrine and the putative TPC blockers selectively inhibit carbachol-evoked  $\text{Ca}^{2+}$  signals by blocking other  $\text{Ca}^{2+}$  channels or simply becoming trapped inside the lysosomes. Expanding this assay to comprise multiple cell types and agonists would also strengthen it and negate the hypothesis that these drugs are in fact carbachol antagonists. In this light, the inhibitory effect of tetrandrine upon physiological  $\text{Ca}^{2+}$  signals in fibroblasts has been examined during the close of this project. As shown in Figure 5.1 tetrandrine inhibited global  $\text{Ca}^{2+}$  signals evoked by bradykinin, although the effect was surprisingly modest. In contrast, global  $\text{Ca}^{2+}$  signals evoked by histamine were more substantially inhibited. This must now be followed up by stringent examination of the signals to determine their TPC dependence. This result may also have implications for the work on fibroblasts presented in Chapter 3: If global  $\text{Ca}^{2+}$  signals evoked by histamine are more TPC-dependent than those of bradykinin it might be expected that histamine-evoked  $\text{Ca}^{2+}$  signals are inhibited to a greater extent by TPC knockdown. Furthermore, in the LRRK2-GS PD fibroblasts, histamine-evoked  $\text{Ca}^{2+}$  signals may more clearly differ from age-matched control cells.

The differential effects of tetrandrine and putative TPC blockers in SH-SY5Ys suggested that global  $\text{Ca}^{2+}$  signals evoked by carbachol are TPC-dependent but that those evoked by bradykinin are not. Considering this, and the association between upregulated TPC2 activity and LRRK2-GS, it was hypothesised that carbachol-evoked  $\text{Ca}^{2+}$  signals would be augmented in SH-SY5Ys stably

expressing LRRK2-GS but that bradykinin-evoked  $\text{Ca}^{2+}$  signals would not be. This was proven to be the case. The cause of the potentiated carbachol-evoked  $\text{Ca}^{2+}$  signals in the presence of LRRK2-GS is unclear but is consistent with increased TPC activity. If this is confirmed it would diverge the perception of lysosomal  $\text{Ca}^{2+}$  signalling in neurodegenerative disease: In addition to disrupting local processes, disturbed lysosomal  $\text{Ca}^{2+}$  signalling may perturb  $\text{Ca}^{2+}$ -dependent processes throughout neurons, which may be an even greater threat to their survival.

The last finding here was that SOCE was reduced in the neuronal model of LRRK2-GS PD. This has recently been echoed in sporadic PD and *pl2g6* PD, and although it has not been a focus of this thesis, renewed attention to SOCE in PD may be warranted (Zhou et al., 2016). Indeed, a retrospective examination of SOCE in the sporadic and LRRK2-PD fibroblasts used in Chapter 3 may uncover a common  $\text{Ca}^{2+}$  signalling defect in PD.

As a final point, the future of this investigation should no doubt be directed towards neurons and neuron-glia co-cultures to substantiate these findings. For sporadic PD, where there is no known genetic predisposition, transformation of the patient fibroblasts into neurons would provide a valuable model (Sánchez-Danés et al., 2012).

In summary (Fig. 5.2), I demonstrated that the lysosomal  $\text{Ca}^{2+}$  channel TRPML1 is capable of mediating global  $\text{Ca}^{2+}$  signals although it has predominantly been associated with local  $\text{Ca}^{2+}$  flux. Building upon reports that TPCs mediate global  $\text{Ca}^{2+}$  signals, I demonstrated the physiological relevance of this by identifying extracellular agonists that elicit TPC-dependent global  $\text{Ca}^{2+}$  signals. Finally, I have shown that global  $\text{Ca}^{2+}$  signals evoked by these agonists are modulated in PD patient fibroblasts and in a neuronal PD model. These disturbances may have damaging consequences in PD although their TPC dependence requires further examination. During this process I also developed a method of automated image-processing to quantify lysosome size and frequency in fibroblasts (see Kilpatrick et al., 2017), and laid the foundations of a screen in human neuronal cells to facilitate the identification of novel TPC blockers.

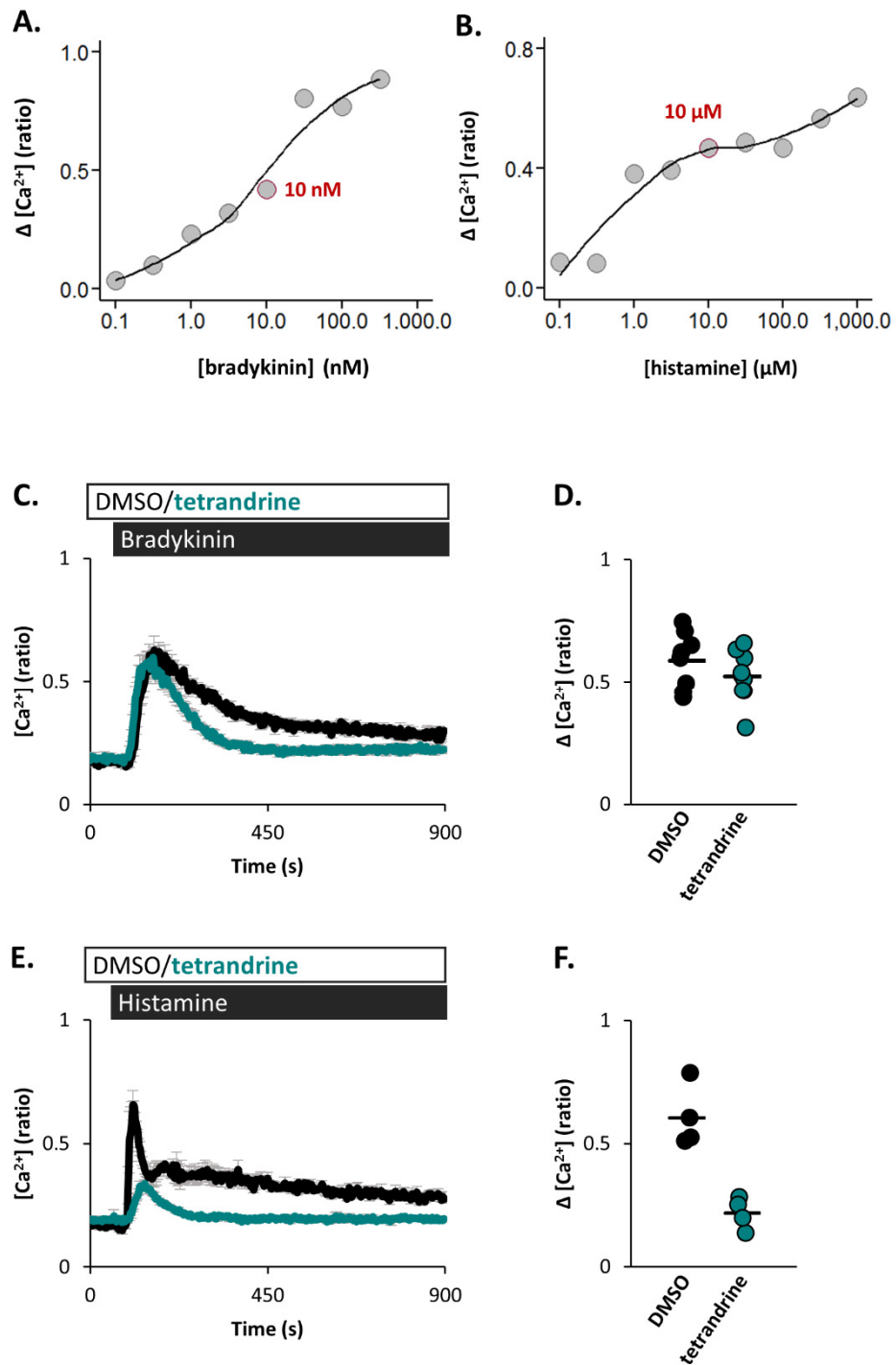


**Figure 5.1 Recently identified TPC inhibitor tetrandrine preferentially inhibits histamine-evoked  $Ca^{2+}$  signals in fibroblasts**

(A and B) Data quantifying magnitude of  $Ca^{2+}$  signals in Ctrl fibroblasts stimulated with (A) bradykinin (as appears in Fig. 3.4B) or (B) histamine at a range of concentrations. Each plot point represents one experiment. The bradykinin (10 nM) and histamine (10  $\mu$ M) concentrations used in C and E are outlined in red. (A) Data from 28-32 fibroblasts per experiment from 1 plating. (B) Data from 12-21 fibroblasts per experiment from 1 plating. (C) Average cytosolic  $Ca^{2+}$  traces (mean of experiments  $\pm$  S.E.M) of Ctrl fibroblasts stimulated with bradykinin (10 nM) in the presence of DMSO or tetrandrine (10  $\mu$ M). (D) Data quantifying magnitude of responses in C. Each plot point represents one



experiment, n=8/9 (DMSO/tetrandrine). A total of 209/255 (DMSO/tetrandrine) fibroblasts from 5 independent platings were analysed. **(E and F)** Same format as for (C and D), upon stimulation with histamine (10  $\mu$ M), n=4/4 (DMSO/tetrandrine). A total of 169/160 (DMSO/tetrandrine) fibroblasts from 2 independent platings were analysed. Methods as described in Chapters 2-4.

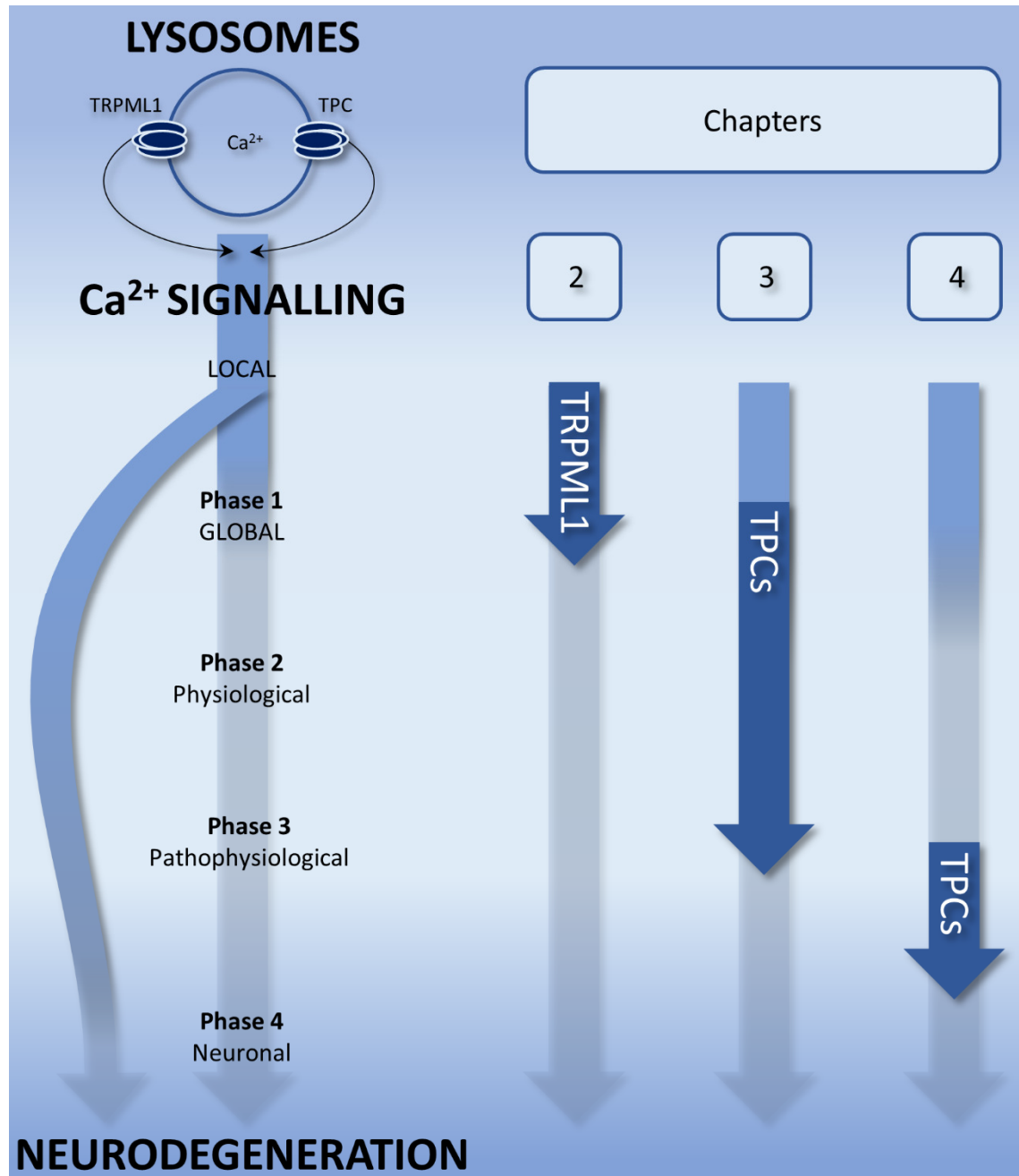


**Figure 5.2 Lysosomal Ca<sup>2+</sup> Signalling and Neurodegeneration – A Global View. Conclusions and Future Directions**

TRPML1 and TPC2 dysfunction has been associated with disrupted local Ca<sup>2+</sup> signalling in neurodegenerative diseases such as MLIV and PD. Such disruption may contribute to neurodegeneration (curved left-hand arrow). However, it is unknown whether global Ca<sup>2+</sup> signalling is also disturbed by their dysfunction and whether this contributes to neurodegeneration (straight

arrow on left). To investigate this, progress through 4 phases has been incremented in this thesis. Phase 1: verification that the lysosomal  $\text{Ca}^{2+}$  channel in question can mediate global  $\text{Ca}^{2+}$  signals. Phase 2: confirmation that the lysosomal  $\text{Ca}^{2+}$  channel mediates physiological global  $\text{Ca}^{2+}$  signals in response to extracellular stimuli. Phase 3: demonstration that these physiological signals are altered in models of neurodegenerative disease. Phase 4: investigation of phases 1-3 in a neuronal model of neurodegenerative disease.

The lysosomal  $\text{Ca}^{2+}$  channel under investigation, and the phases covered in each results chapter are indicated.

Topics of lysosomal  $\text{Ca}^{2+}$  signalling that are supported by the literature

Phases addressed in this thesis

Phases requiring further investigation



## Appendices

### Appendix A: Additional genes implicated in PD or parkinsonism

**PLA2G6:** Mutations in *PLA2G6* are associated with parkinsonism as well as infantile neuroaxonal dystrophy (INAD) and neurodegeneration with brain iron accumulation (NBIA) (Morgan et al., 2006; Paisan-Ruiz et al., 2009). *PLA2G6* has been linked to regulation of lipid peroxidation, oxidative stress and mitochondrial function (Kinghorn et al., 2015).  $Ca^{2+}$  signalling is also modulated by *PLA2G6*: In astrocytes mutant *PLA2G6* is associated with reduced  $Ca^{2+}$  signals in response to ATP (Strokin et al., 2012). Inhibited SOCE was also observed in fibroblasts from *PLA2G6*-PD patients and from sporadic PD patients (Zhou et al., 2016). This was recapitulated in *PLA2G6*<sup>-/-</sup> mice in which ER  $Ca^{2+}$  content appeared reduced. These mice exhibited motor dysfunction, autophagic dysfunction and loss of DA neurons in the SNc from 16 months.

**SYNJ1:** In 2013 mutant Synaptojanin-1 (encoded by *SYNJ1*) was linked to autosomal recessive, early-onset parkinsonism (Krebs et al., 2013; Quadri et al., 2013). Synaptojanin-1 is recruited by endophilin A to clathrin pits and is a phosphoinositide phosphatase. This function is important in the recycling of synaptic vesicles following clathrin-mediated endocytosis (Mani et al., 2007; McPherson et al., 1996; Milosevic et al., 2011). Synaptojanin-1, along with dynamin-1, is dephosphorylated by calcineurin in response to rises in  $Ca^{2+}$  during endocytosis (Cousin et al., 2001).

**HTRA2:** This protease appears to have a role in mitochondrial maintenance. A heterozygous mutation and a polymorphism in *HTRA2* that are associated with PD were shown to cause mitochondrial dysfunction when overexpressed in SH-SY5Y or HEK293 cells (Strauss et al., 2005). It is a regulator of apoptosis and autophagy and can be phosphorylated by PINK1 (Li et al., 2010; Plun-Favreau et al., 2007).

**FBX07:** *FBX07* mutations have been associated with autosomal recessive early onset pyramidal parkinsonism (Fonzo et al., 2009). Roles in ubiquitination and maintaining mitochondrial health have been proposed for *FBX07*: It is part of the PINK1-PARKIN team of mitophagy (Burchell et al., 2013) and ubiquitinates substrates including c-IAP1 (inhibitor of autophagy), GSK3 $\beta$  (a

component of Wnt signalling) and TOMM20 (an OMM protein) (Kuiken et al., 2012; Teixeira et al., 2016).

**UCLH1:** UCLH1 is reported to have both ubiquitin hydrolase and ligase activity, and is expressed predominantly in the brain (Day and Thompson, 2010; Liu et al., 2002). The exact functions of WT UCLH1 are unclear but it appears to add ubiquitin conjugates to  $\alpha$ -syn and may be important for axonal maintenance or as an antioxidant (Bishop et al., 2016; Liu et al., 2002). The I193 mutant form has been implicated in loss of dopaminergic neurons in the SNc (Setsuie and Wada, 2007). The relative importance of UCLH1 in PD aetiology is debatable, exemplified by two meta-analyses in disagreement as to whether the S18Y mutation is a protective factor against PD (Healy et al., 2006; Maraganore et al., 2004).

**VPS13C:** A single nucleotide polymorphism in the vicinity of *VPS13C* was picked up in GWAS meta-analysis by Nalls and many colleagues (Nalls et al., 2014). Very recently, loss of function truncated *VPS13C* mutants have been associated with autosomal recessive parkinsonism (Lesage et al., 2016). Endogenous *VPS13C* localises to the OMM, and *VPS13C* knockdown was associated with reduced mitochondrial membrane potential, increased respiration rate, increased PINK1/Parkin-mediated mitophagy, and transcriptional upregulation of Parkin, in response to mitochondrial damage.

**CHCHD2:** Mutations in *CHCHD2* have been associated with autosomal dominant PD (Funayama et al., 2015). The WT protein localises to the mitochondria and is protective against oxidative stress (Aras et al., 2015; Liu et al., 2015).

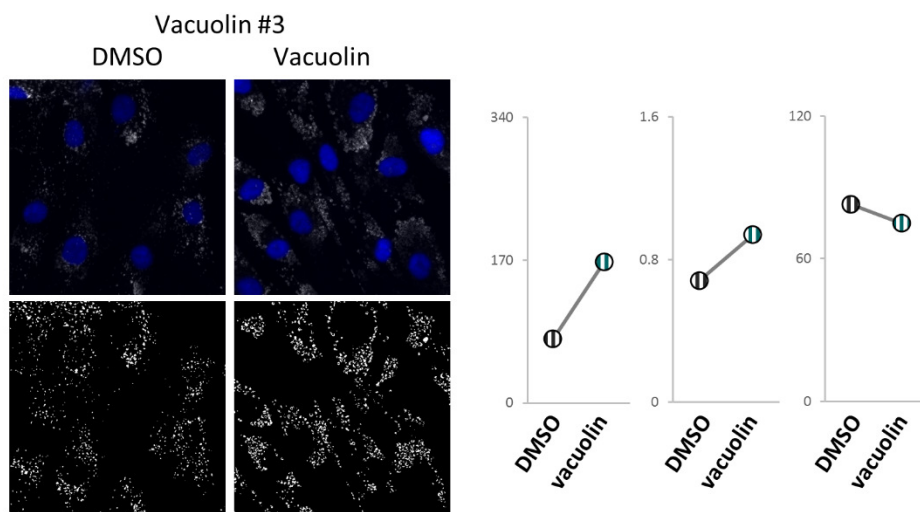
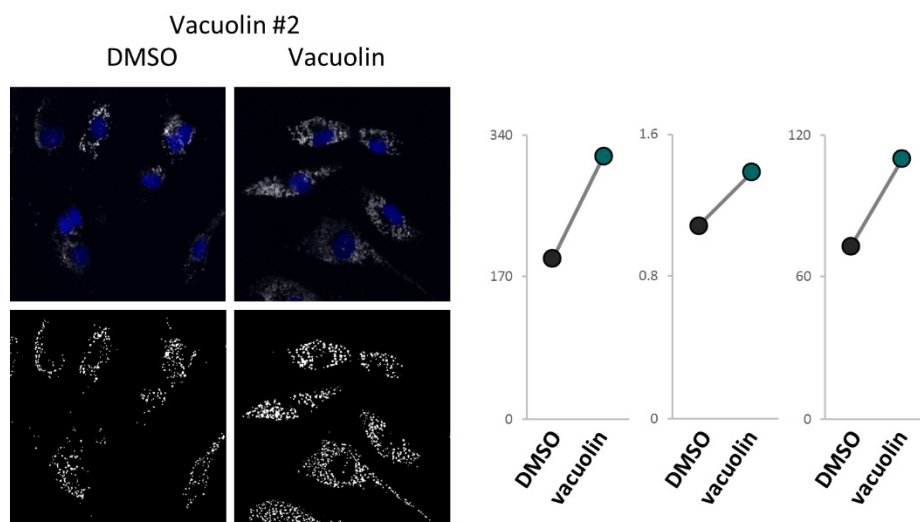
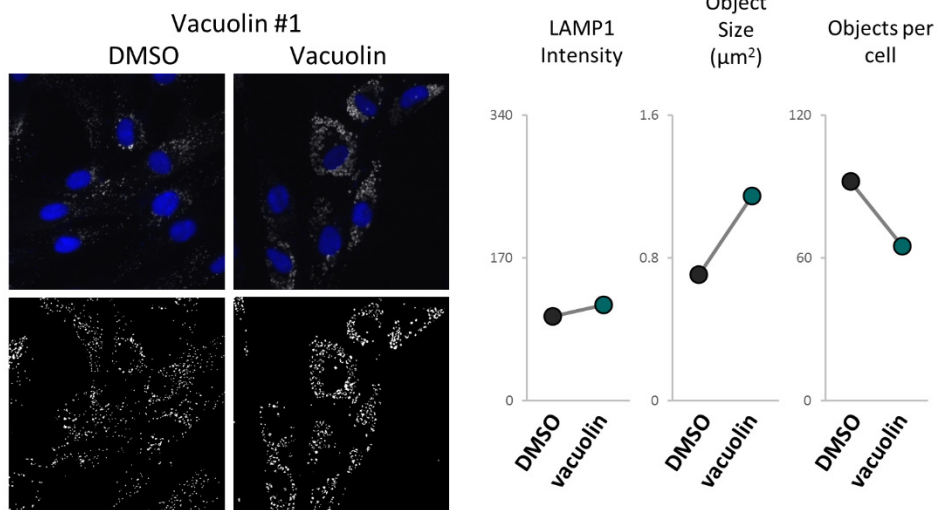
**EIF4G1:** The encoded EIF4G1 protein is the scaffold for the eukaryotic translation initiation complex eIF4F (Villa et al., 2013). Interestingly, LRRK2 phosphorylates 4E-BP which is a component of the same complex (Imai et al., 2008). *EIF4G1* mutations associated with parkinsonism cause reduced mitochondrial membrane potential in response to oxidative stress compared to WT (Chartier-Harlin et al., 2011). Elsewhere, depletion of EIF4G1 also resulted in reduced mitochondrial membrane potential as well as increased autophagy (Ramírez-Valle et al., 2008). Upregulation of EIF4G1 expression in conjunction with *VPS35* mutations is a toxic combination in yeast (Dhungel et al., 2015). In yeast expressing  $\alpha$ -syn upregulation of EIF4G1 suppressed associated toxicity. Neuronal death following *in vitro* ischemia was linked to degradation of EIF4G1 by calcium-activated calpain, thus indicating a neuroprotective role for EIF4G1 (Vosler et al., 2011).

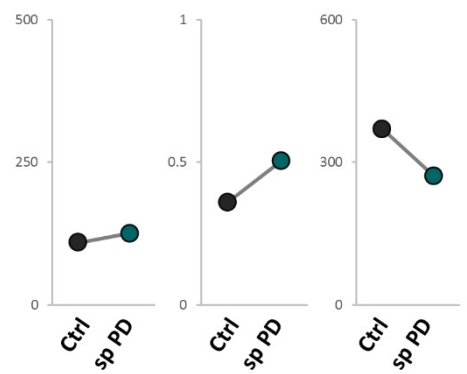
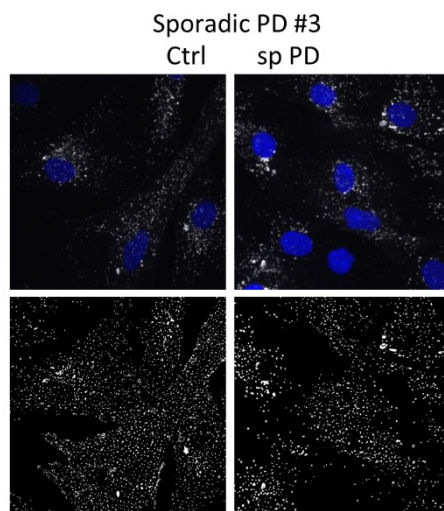
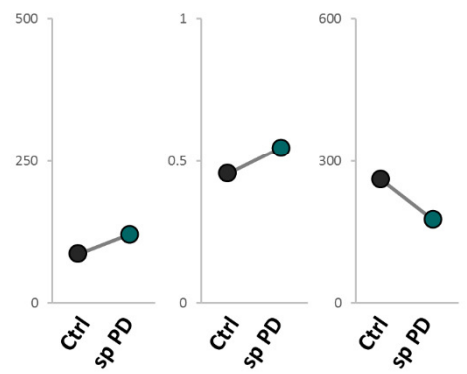
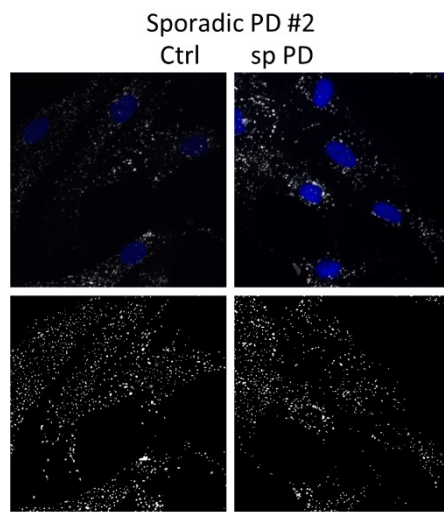
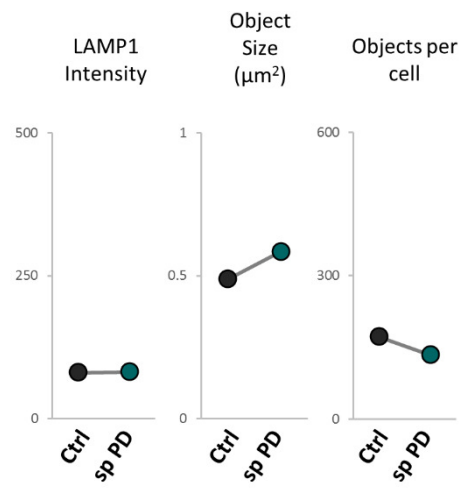
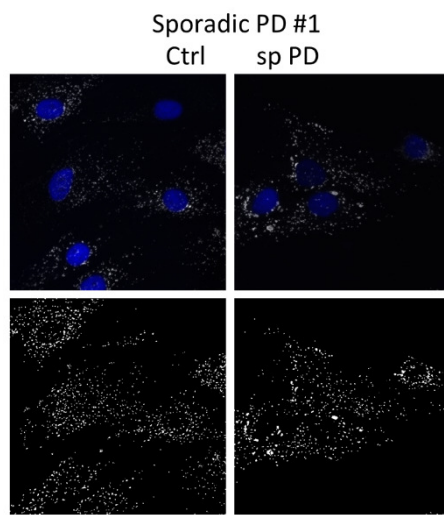
***DNAJC13***: *DNAJC13* binds Hsc70, is thought to regulate clathrin-mediated trafficking, and is associated with parkinsonism (Girard et al., 2005; Vilariño-Güell et al., 2014). Disrupted trafficking of the transferrin receptor has been demonstrated in cells overexpressing mutant *DNAJC13*. In cells subjected to *DNAJC13* knockdown trafficking of the EGF (epidermal growth factor) receptor, M6P receptor and cathepsin D is disturbed (Girard et al., 2005; Popoff et al., 2009).

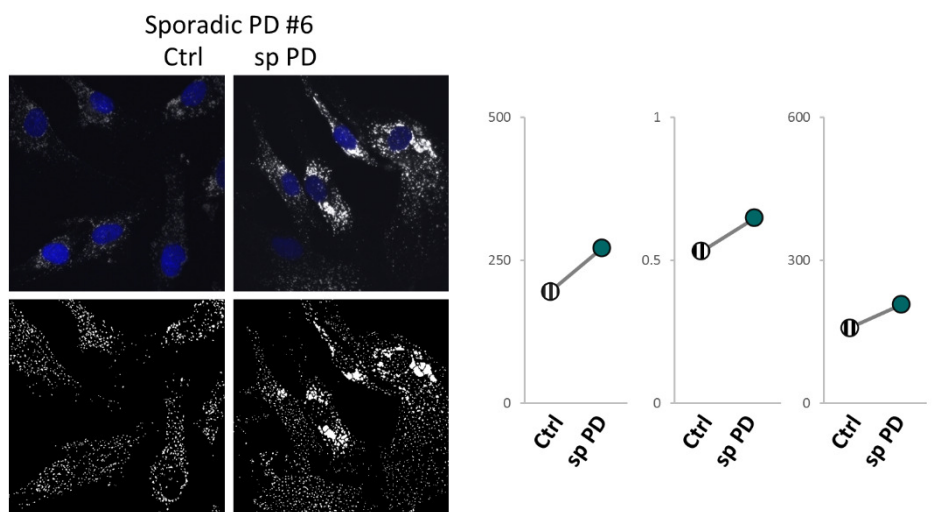
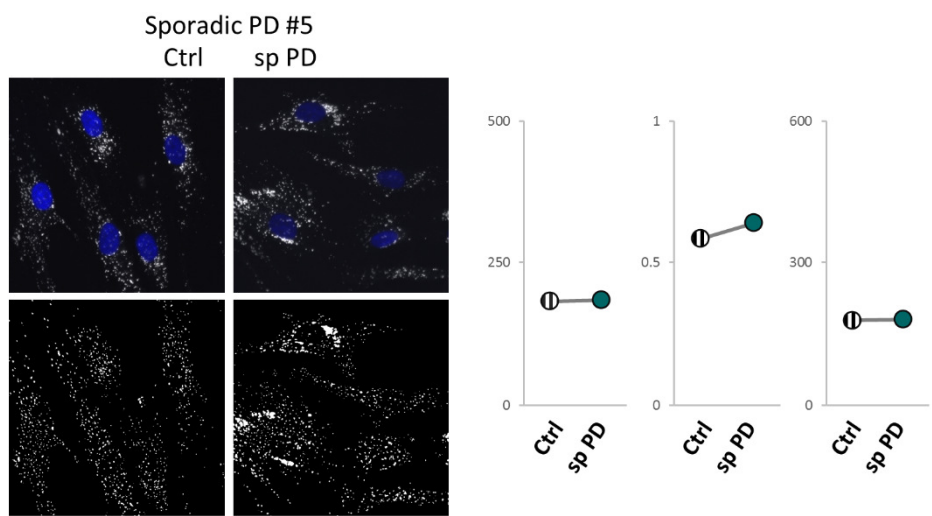
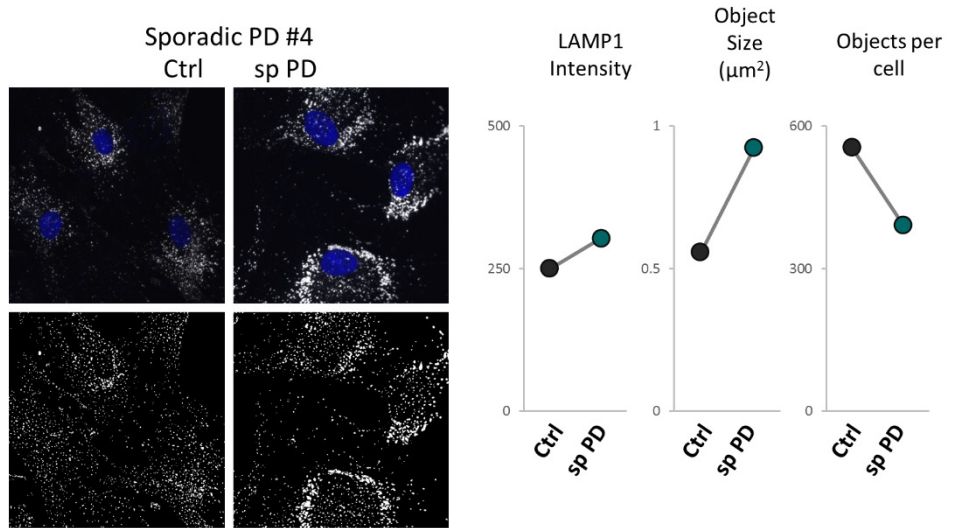
***DNAJC6***: Encoded by *DNAJC6*, Auxilin is restricted to neurons and has been associated with juvenile parkinsonism (Ahle and Ungewickell, 1990; Edvardson et al., 2012). Auxilin is thought to be important in clathrin-mediated endocytosis, and binds Hsc70 (Eisenberg and Greene, 2007).

***TMEM230***: *TMEM230* colocalises with the TGN, pre-synaptic vesicles and endosomes. Very recently *TMEM230* mutations were linked to autosomal dominant Parkinson's disease (Deng et al., 2016). This study showed that such PD mutations slowed movement of synaptic vesicles and that *TMEM230* was present in midbrain Lewy Body inclusions of sporadic PD patients. This work is part of an ongoing dispute between two groups studying the same pedigree. The opposing group was the first to link mutations in *DNAJC13* to PD (Farrer et al., 2017; Vilariño-Güell et al., 2014).

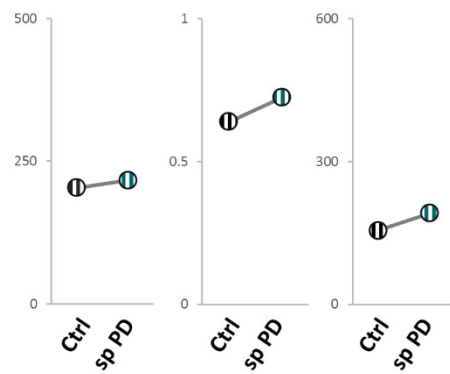
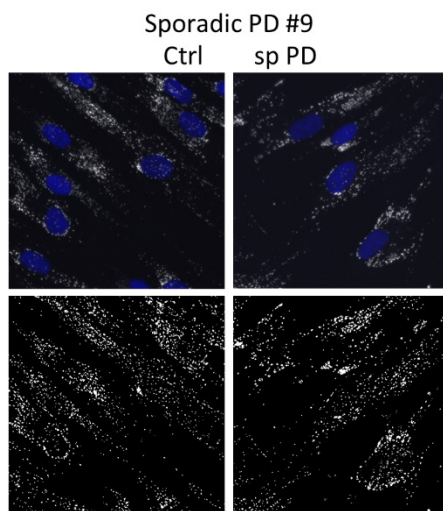
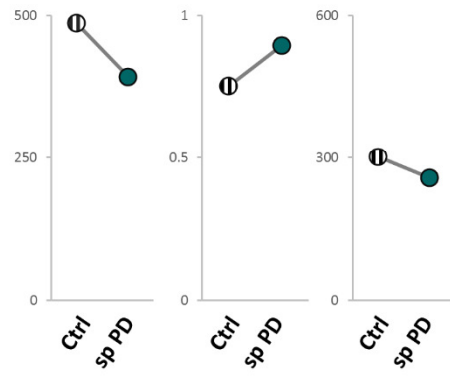
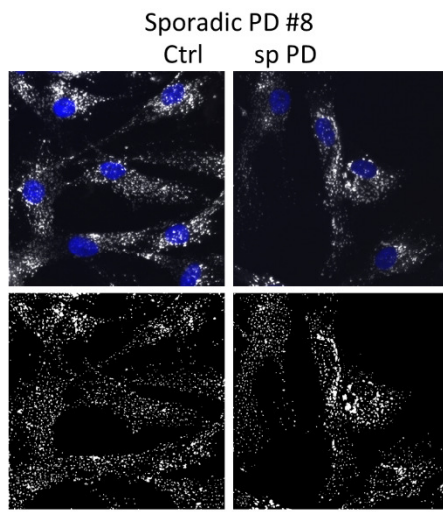
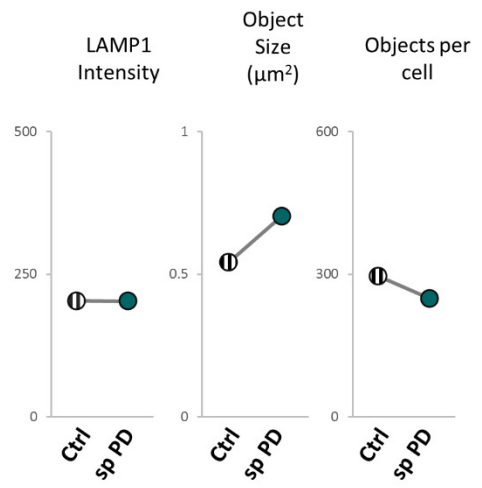
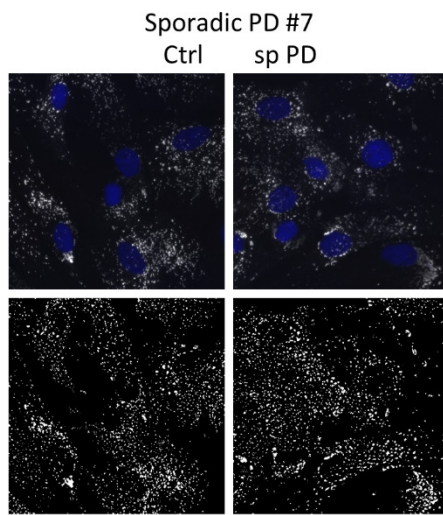
## Appendix B: Example binary images for lysosome size and frequency analysis

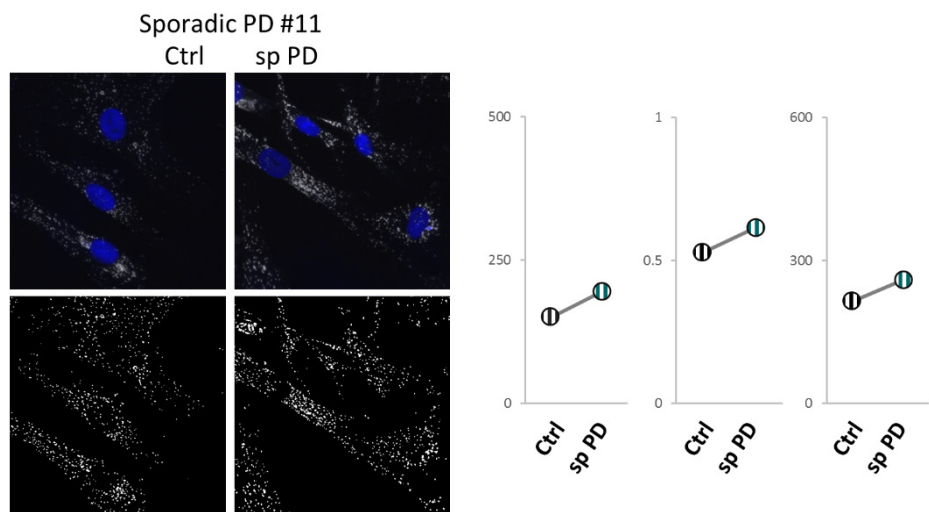
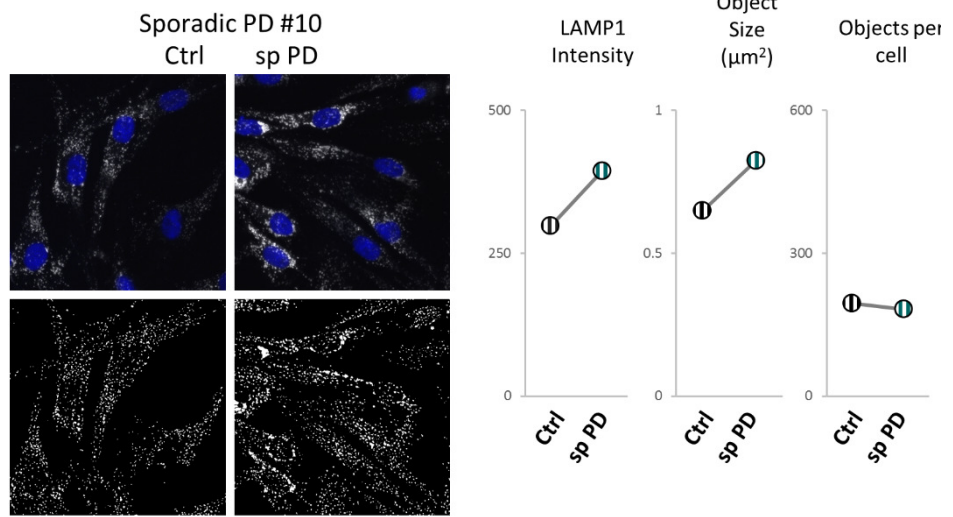








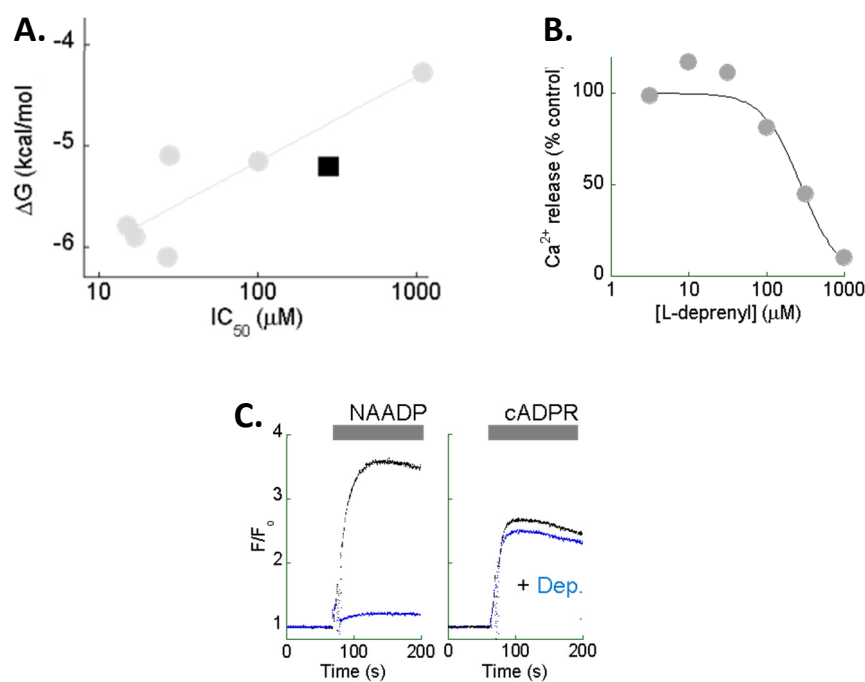




## Appendix C: *In silico*-based drug screens for FDA-approved, selective TPC blockers

### L-Deprenyl – Dr Taufiq Rahman and Professor Sandip Patel

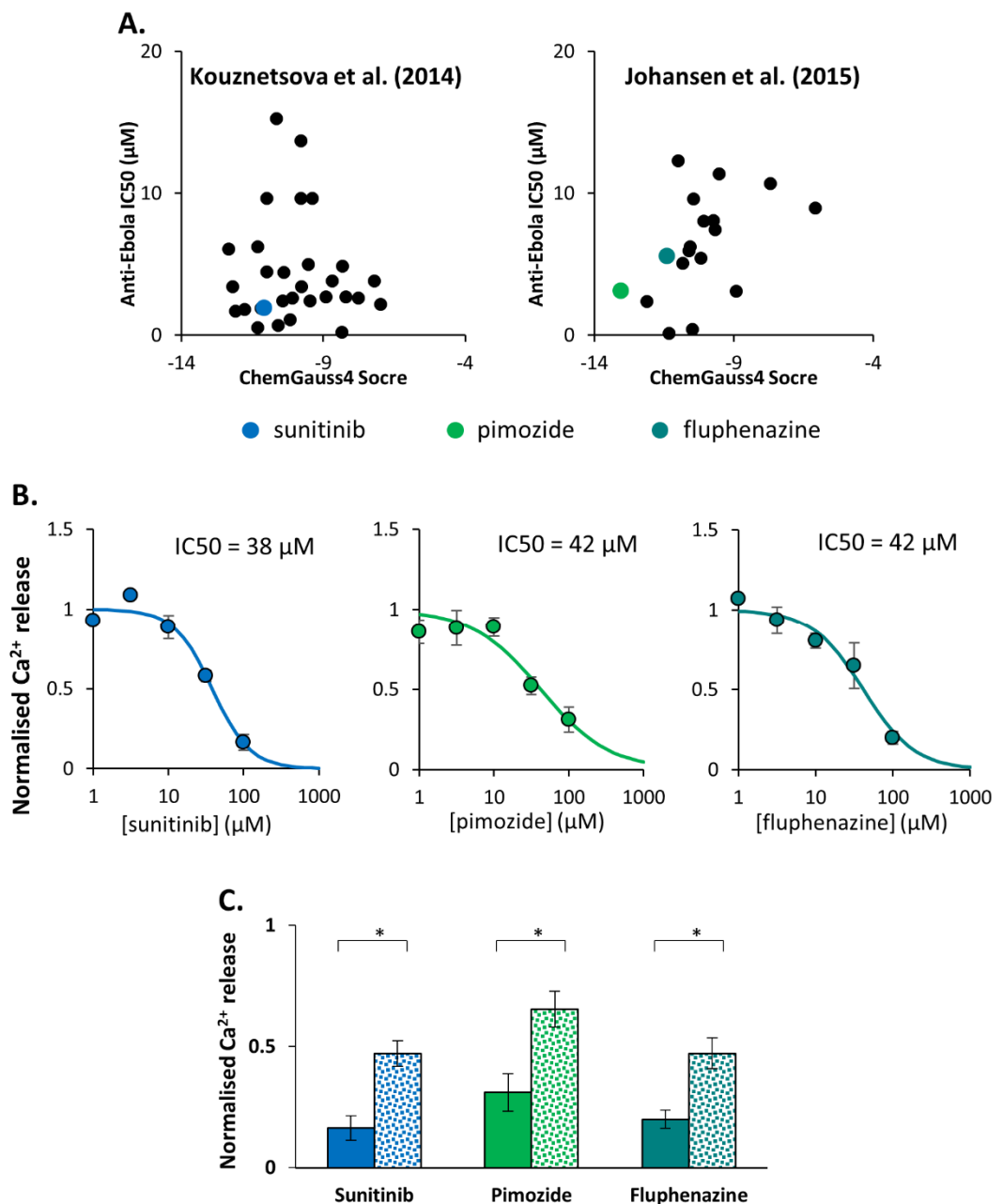
The voltage-operated Na<sup>+</sup> channel (VONC) antagonist bupivacaine has been identified as a TPC blocker (Rahman et al., 2014). Using ligand software, a conformer library of FDA-approved drugs was screened against bupivacaine for shape and electrostatic similarities. L-deprenyl was the highest-ranked drug that was not a VONC antagonist, and also docked to a TPC model as described (Rahman et al., 2014). L-deprenyl inhibited NAADP-induced Ca<sup>2+</sup> release in sea urchin egg homogenate in a concentration-dependent manner. L-deprenyl did not block cADPR-induced Ca<sup>2+</sup> signals.



**Identification of L-deprenyl as a putative TPC blocker** Figures provided by Dr Taufiq Rahman and Prof Sandip Patel. **(A)** The distribution of top hit FDA-approved drugs according to IC<sub>50</sub>s on NAADP-induced Ca<sup>2+</sup> release in sea urchin egg homogenate (x axis) and *in silico* TPC docking ( $\Delta G$ ; y axis). Grey circles represent VOCC and VONC antagonists. L-deprenyl is represented by the black square. **(B)** Inhibition curve showing concentration-dependent block of NAADP-induced Ca<sup>2+</sup> release in sea urchin egg homogenate. **(C)** Inhibition of Ca<sup>2+</sup> released by NAADP (1 μM) and cADPR (1 μM) in sea urchin egg homogenate. L-deprenyl was used at 1mM.

## Sunitinib, pimoziide and fluphenazine – Drs Christopher Penny and Taufiq Rahman

Human TPC2 was modelled on the recently reported structure of plant TPC1 as a template (Guo et al., 2016). Using docking software, a conformer library of FDA-approved drugs was screened, and drug interactions with the modelled pore were scored. These scores were cross-referenced with *in vitro* screens for Ebola infection inhibitors (Johansen et al., 2015; Kouznetsova et al., 2014). A handful of the best binders to the modelled TPC pore and the most potent inhibitors of Ebola infection were selected for screening in the sea urchin egg homogenate. Sunitinib, pimoziide and fluphenazine all blocked NAADP-induced  $\text{Ca}^{2+}$  release in a concentration-dependent manner, and selectively blocked this over cADPR-induced  $\text{Ca}^{2+}$  release.



Identification of sunitinib, pimoziide and fluphenazine as a putative TPC blockers (legend on next page)

All figures adapted from originals by Dr Penny. **(A)** The distribution of top hit FDA-approved drugs according to *in silico* TPC2 docking (ChemGauss4 score; x axis) and IC50s reported in in vitro Ebola screens (y axis). **(B)** Inhibition curves showing concentration-dependent block of NAADP (1  $\mu\text{M}$ )-induced  $\text{Ca}^{2+}$  release in sea urchin egg homogenate. **(C)** Inhibition of  $\text{Ca}^{2+}$  released by NAADP (1  $\mu\text{M}$ ; block colours) and cADPR (5  $\mu\text{M}$ ; coloured dots) in sea urchin egg homogenate. All three drugs were used at 100  $\mu\text{M}$ .  $\text{Ca}^{2+}$  release normalised to that in the absence of the indicated drug.

## References

- Ahle, S., and Ungewickell, E. (1990). Auxilin, a newly identified clathrin-associated protein in coated vesicles from bovine brain. *The Journal of Cell Biology* *111*, 19–29.
- Airaksinen, M.S., Eilers, J., Garaschuk, O., Thoenen, H., Konnerth, A., and Meyer, M. (1997). Ataxia and altered dendritic calcium signaling in mice carrying a targeted null mutation of the calbindin D28k gene. *PNAS* *94*, 1488–1493.
- Aley, P.K., Mikolajczyk, A.M., Munz, B., Churchill, G.C., Galione, A., and Berger, F. (2010a). Nicotinic acid adenine dinucleotide phosphate regulates skeletal muscle differentiation via action at two-pore channels. *Proc. Natl. Acad. Sci. U.S.A.* *107*, 19927–19932.
- Aley, P.K., Noh, H.J., Gao, X., Tica, A.A., Brailoiu, E., and Churchill, G.C. (2010b). A functional role for nicotinic acid adenine dinucleotide phosphate in oxytocin-mediated contraction of uterine smooth muscle from rat. *J. Pharmacol. Exp. Ther.* *333*, 726–735.
- Aley, P.K., Singh, N., Brailoiu, G.C., Brailoiu, E., and Churchill, G.C. (2013). Nicotinic acid adenine dinucleotide phosphate (NAADP) is a second messenger in muscarinic receptor-induced contraction of guinea pig trachea. *J. Biol. Chem.* *288*, 10986–10993.
- Ali, R.A., Camick, C., Wiles, K., Walseth, T.F., Slama, J.T., Bhattacharya, S., Giovannucci, D.R., and Wall, K.A. (2016). Nicotinic Acid Adenine Dinucleotide Phosphate Plays a Critical Role in Naive and Effector Murine T Cells but Not Natural Regulatory T Cells. *J. Biol. Chem.* *291*, 4503–4522.
- Alvarez-Dominguez, C., Roberts, R., and Stahl, P.D. (1997). Internalized *Listeria monocytogenes* modulates intracellular trafficking and delays maturation of the phagosome. *Journal of Cell Science* *110*, 731–743.
- Angelova, P.R., Ludtmann, M.H.R., Horrocks, M.H., Negoda, A., Cremades, N., Klenerman, D., Dobson, C.M., Wood, N.W., Pavlov, E.V., Gandhi, S., et al. (2016). Ca<sup>2+</sup> is a key factor in  $\alpha$ -synuclein-induced neurotoxicity. *J Cell Sci* *129*, 1792–1801.
- Appelmans, F., Wattiaux, R., and De Duve, C. (1955). Tissue fractionation studies. 5. The association of acid phosphatase with a special class of cytoplasmic granules in rat liver. *Biochem J* *59*, 438–445.
- Aras, S., Bai, M., Lee, I., Springett, R., Hüttemann, M., and Grossman, L.I. (2015). MNRR1 (formerly CHCHD2) is a bi-organelle regulator of mitochondrial metabolism. *Mitochondrion* *20*, 43–51.
- Arighi, C.N., Hartnell, L.M., Aguilar, R.C., Haft, C.R., and Bonifacino, J.S. (2004). Role of the mammalian retromer in sorting of the cation-independent mannose 6-phosphate receptor. *J Cell Biol* *165*, 123–133.
- Arredouani, A., Ruas, M., Collins, S.C., Parkesh, R., Clough, F., Pillinger, T., Coltart, G., Rietdorf, K., Royle, A., Johnson, P., et al. (2015). Nicotinic Acid Adenine Dinucleotide Phosphate (NAADP) and Endolysosomal Two-pore Channels Modulate Membrane Excitability and Stimulus-Secretion Coupling in Mouse Pancreatic  $\beta$  Cells. *J Biol Chem* *290*, 21376–21392.
- Ataei, F., Torkzadeh-Mahani, M., and Hosseinkhani, S. (2013). A novel luminescent biosensor for rapid monitoring of IP<sub>3</sub> by split-luciferase complementary assay. *Biosensors and Bioelectronics* *41*, 642–648.

- Auburger, G., Klinkenberg, M., Drost, J., Marcus, K., Morales-Gordo, B., Kunz, W.S., Brandt, U., Broccoli, V., Reichmann, H., Gispert, S., et al. (2012). Primary Skin Fibroblasts as a Model of Parkinson's Disease. *Mol Neurobiol* 46, 20–27.
- Aulestia, F.J., Alonso, M.T., and García-Sancho, J. (2015). Differential calcium handling by the cis and trans regions of the Golgi apparatus. *Biochemical Journal* 466, 455–465.
- Aumann, T., and Horne, M. (2012). Activity-dependent regulation of the dopamine phenotype in substantia nigra neurons. *Journal of Neurochemistry* 121, 497–515.
- Baba-Aissa, F., Raeymaekers, L., Wuytack, F., De Greef, C., Missiaen, L., and Casteels, R. (1996). Distribution of the organellar Ca<sup>2+</sup> transport ATPase SERCA2 isoforms in the cat brain. *Brain Research* 743, 141–153.
- Bach, G. (2005). Mucolipin 1: endocytosis and cation channel—a review. *Pflugers Arch - Eur J Physiol* 451, 313–317.
- Bach, G., Cohen, M.M., and Kohn, G. (1975). Abnormal ganglioside accumulation in cultured fibroblasts from patients with mucopolidosis IV. *Biochemical and Biophysical Research Communications* 66, 1483–1490.
- Bach, G., Ziegler, M., Kohn, G., and Cohen, M.M. (1977). Mucopolysaccharide accumulation in cultured skin fibroblasts derived from patients with mucopolidosis IV. *American Journal of Human Genetics* 29, 610.
- Bach, G., Chen, C.-S., and Pagano, R.E. (1999). Elevated lysosomal pH in Mucopolidosis type IV cells. *Clinica Chimica Acta* 280, 173–179.
- Bae, M., Patel, N., Xu, H., Lee, M., Tominaga-Yamanaka, K., Nath, A., Geiger, J., Gorospe, M., Mattson, M.P., and Haughey, N.J. (2014). Activation of TRPML1 clears intraneuronal A $\beta$  in preclinical models of HIV infection. *J. Neurosci.* 34, 11485–11503.
- Bahnassawy, L. 'a, Nicklas, S., Palm, T., Menzl, I., Birzele, F., Gillardon, F., and Schwamborn, J.C. (2013). The Parkinson's Disease-Associated LRRK2 Mutation R1441G Inhibits Neuronal Differentiation of Neural Stem Cells. *Stem Cells and Development* 22, 2487–2496.
- Balderhaar, H.J. kleine, and Ungermann, C. (2013). CORVET and HOPS tethering complexes – coordinators of endosome and lysosome fusion. *J Cell Sci* 126, 1307–1316.
- Ballard, P.A., Tetrud, J.W., and Langston, J.W. (1985). Permanent human parkinsonism due to 1-methy 1–4-phenyl-1,2,3,6-tetrahydropyridine (MPTP) Seven cases. *Neurology* 35, 949–949.
- Bancila, M., Copin, J.-C., Daali, Y., Schatlo, B., Gasche, Y., and Bijlenga, P. (2011). Two structurally different T-type Ca<sup>2+</sup> channel inhibitors, mibefradil and pimozide, protect CA1 neurons from delayed death after global ischemia in rats. *Fundamental & Clinical Pharmacology* 25, 469–478.
- Bandyopadhyay, D., Cyphersmith, A., Zapata, J.A., Kim, Y.J., and Payne, C.K. (2014). Lysosome Transport as a Function of Lysosome Diameter. *PLOS ONE* 9, e86847.
- Barceló-Torns, M., Lewis, A.M., Gubern, A., Barneda, D., Bloor-Young, D., Picatoste, F., Churchill, G.C., Claro, E., and Masgrau, R. (2011). NAADP mediates ATP-induced Ca<sup>2+</sup> signals in astrocytes. *FEBS Letters* 585, 2300–2306.
- Bardien, S., Lesage, S., Brice, A., and Carr, J. (2011). Genetic characteristics of leucine-rich repeat kinase 2 (LRRK2) associated Parkinson's disease. *Parkinsonism & Related Disorders* 17, 501–508.

- Bargal, R., and Bach, G. (1997a). Mucopolipidosis type IV: Abnormal transport of lipids to lysosomes. *J Inherit Metab Dis* 20, 625–632.
- Bargal, R., and Bach, G. (1997b). Mucopolipidosis type IV: abnormal transport of lipids to lysosomes. *J. Inherit. Metab. Dis.* 20, 625–632.
- Bargal, R., Avidan, N., Ben-Asher, E., Olender, Z., Zeigler, M., Frumkin, A., Raas-Rothschild, A., Glusman, G., Lancet, D., and Bach, G. (2000). Identification of the gene causing mucopolipidosis type IV. *Nat. Genet.* 26, 118–123.
- Bargal, R., Avidan, N., Olender, T., Ben Asher, E., Zeigler, M., Raas-Rothschild, A., Frumkin, A., Ben-Yoseph, O., Friedlender, Y., Lancet, D., et al. (2001). Mucopolipidosis type IV: novel MCOLN1 mutations in Jewish and non-Jewish patients and the frequency of the disease in the Ashkenazi Jewish population. *Hum. Mutat.* 17, 397–402.
- Barmada, S.J., Serio, A., Arjun, A., Bilican, B., Daub, A., Ando, D.M., Tsvetkov, A., Pleiss, M., Li, X., Peisach, D., et al. (2014). Autophagy induction enhances TDP43 turnover and survival in neuronal ALS models. *Nat Chem Biol* 10, 677–685.
- Bassi, M.T., Manzoni, M., Monti, E., Pizzo, M.T., Ballabio, A., and Borsani, G. (2000). Cloning of the Gene Encoding a Novel Integral Membrane Protein, Mucopolidin—and Identification of the Two Major Founder Mutations Causing Mucopolipidosis Type IV. *Am J Hum Genet* 67, 1110–1120.
- Baudhuin, P., Beaufay, H., and Duve, C. de (1965). Combined Biochemical and Morphological Study of Particulate Fractions from Rat Liver. *The Journal of Cell Biology* 26, 219–243.
- Bedford, C., Sears, C., Perez-Carrion, M., Piccoli, G., and Condliffe, S.B. (2016). LRRK2 Regulates Voltage-Gated Calcium Channel Function. *Front Mol Neurosci* 9.
- Beilina, A., Rudenko, I.N., Kaganovich, A., Civiero, L., Chau, H., Kalia, S.K., Kalia, L.V., Lobbstaël, E., Chia, R., Ndukwe, K., et al. (2014). Unbiased screen for interactors of leucine-rich repeat kinase 2 supports a common pathway for sporadic and familial Parkinson disease. *Proc Natl Acad Sci U S A* 111, 2626–2631.
- Bender, A., Krishnan, K.J., Morris, C.M., Taylor, G.A., Reeve, A.K., Perry, R.H., Jaros, E., Hersheson, J.S., Betts, J., Klopstock, T., et al. (2006). High levels of mitochondrial DNA deletions in substantia nigra neurons in aging and Parkinson disease. *Nat Genet* 38, 515–517.
- Bendor, J.T., Logan, T.P., and Edwards, R.H. (2013). The Function of  $\alpha$ -Synuclein. *Neuron* 79, 1044–1066.
- Bento, C.F., Ashkenazi, A., Jimenez-Sanchez, M., and Rubinsztein, D.C. (2016). The Parkinson's disease-associated genes ATP13A2 and SYT11 regulate autophagy via a common pathway. *Nature Communications* 7, 11803.
- Berg, I., Potter, B.V.L., Mayr, G.W., and Guse, A.H. (2000). Nicotinic Acid Adenine Dinucleotide Phosphate (Naadp+) Is an Essential Regulator of T-Lymphocyte Ca<sup>2+</sup>-Signaling. *J Cell Biol* 150, 581–588.
- Berridge, M.J., Lipp, P., and Bootman, M.D. (2000). The versatility and universality of calcium signalling. *Nat Rev Mol Cell Biol* 1, 11–21.
- Betarbet, R., Sherer, T.B., MacKenzie, G., Garcia-Osuna, M., Panov, A.V., and Greenamyre, J.T. (2000). Chronic systemic pesticide exposure reproduces features of Parkinson's disease. *Nat Neurosci* 3, 1301–1306.



- Bezprozvanny, I., Watras, J., and Ehrlich, B.E. (1991). Bell-shaped calcium-response curves of Ins(1,4,5)P<sub>3</sub>- and calcium-gated channels from endoplasmic reticulum of cerebellum. *Nature* *351*, 751–754.
- Bhagya, N., and Chandrashekar, K.R. (2016). Tetrandrine – A molecule of wide bioactivity. *Phytochemistry* *125*, 5–13.
- Biasutto, L., Azzolini, M., Szabò, I., and Zoratti, M. (2016). The mitochondrial permeability transition pore in AD 2016: An update. *Biochimica et Biophysica Acta (BBA) - Molecular Cell Research* *1863*, 2515–2530.
- Biedler, J.L., Helson, L., and Spengler, B.A. (1973). Morphology and growth, tumorigenicity, and cytogenetics of human neuroblastoma cells in continuous culture. *Cancer Res.* *33*, 2643–2652.
- Biedler, J.L., Roffler-Tarlov, S., Schachner, M., and Freedman, L.S. (1978). Multiple Neurotransmitter Synthesis by Human Neuroblastoma Cell Lines and Clones. *Cancer Res* *38*, 3751–3757.
- Bieniecki, W., and Grabowski, S. (2005). Multi-pass approach to adaptive thresholding based image segmentation (PDF Download Available).
- Bilgic, B., Pfefferbaum, A., Rohlfing, T., Sullivan, E.V., and Adalsteinsson, E. (2012). MRI Estimates of Brain Iron Concentration in Normal Aging Using Quantitative Susceptibility Mapping. *Neuroimage* *59*, 2625–2635.
- Bisaglia, M., Filograna, R., Beltrami, M., and Bubacco, L. (2014). Are dopamine derivatives implicated in the pathogenesis of Parkinson's disease? *Ageing Research Reviews* *13*, 107–114.
- Bishop, P., Rocca, D., and Henley, J.M. (2016). Ubiquitin C-terminal hydrolase L1 (UCH-L1): structure, distribution and roles in brain function and dysfunction. *Biochemical Journal* *473*, 2453–2462.
- Blackinton, J., Lakshminarasimhan, M., Thomas, K.J., Ahmad, R., Greggio, E., Raza, A.S., Cookson, M.R., and Wilson, M.A. (2009). Formation of a Stabilized Cysteine Sulfinic Acid Is Critical for the Mitochondrial Function of the Parkinsonism Protein DJ-1. *J Biol Chem* *284*, 6476–6485.
- Bollimuntha, S., Ebadi, M., and Singh, B.B. (2006). TRPC1 protects human SH-SY5Y cells against salsolinol-induced cytotoxicity by inhibiting apoptosis. *Brain Res* *1099*, 141–149.
- Bootman, M.D., Berridge, M.J., and Lipp, P. (1997). Cooking with Calcium: The Recipes for Composing Global Signals from Elementary Events. *Cell* *91*, 367–373.
- Borgs, L., Peyre, E., Alix, P., Hanon, K., Grobarczyk, B., Godin, J.D., Purnelle, A., Krusy, N., Maquet, P., Lefebvre, P., et al. (2016). Dopaminergic neurons differentiating from LRRK2 G2019S induced pluripotent stem cells show early neuritic branching defects. *Scientific Reports* *6*, 33377.
- Braak, H., Tredici, K.D., Rüb, U., de Vos, R.A.I., Jansen Steur, E.N.H., and Braak, E. (2003). Staging of brain pathology related to sporadic Parkinson's disease. *Neurobiology of Aging* *24*, 197–211.
- Brailoiu, E., Churamani, D., Pandey, V., Brailoiu, G.C., Tuluc, F., Patel, S., and Dun, N.J. (2006). Messenger-specific role for nicotinic acid adenine dinucleotide phosphate in neuronal differentiation. *J. Biol. Chem.* *281*, 15923–15928.

- Brailoiu, E., Churamani, D., Cai, X., Schrlau, M.G., Brailoiu, G.C., Gao, X., Hooper, R., Boulware, M.J., Dun, N.J., Marchant, J.S., et al. (2009). Essential requirement for two-pore channel 1 in NAADP-mediated calcium signaling. *J Cell Biol* 186, 201–209.
- Brailoiu, E., Rahman, T., Churamani, D., Prole, D.L., Brailoiu, G.C., Hooper, R., Taylor, C.W., and Patel, S. (2010a). An NAADP-gated two-pore channel targeted to the plasma membrane uncouples triggering from amplifying Ca<sup>2+</sup> signals. *J. Biol. Chem.* 285, 38511–38516.
- Brailoiu, G.C., Gurzu, B., Gao, X., Parkesh, R., Aley, P.K., Trifa, D.I., Galione, A., Dun, N.J., Madesh, M., Patel, S., et al. (2010b). Acidic NAADP-sensitive Calcium Stores in the Endothelium AGONIST-SPECIFIC RECRUITMENT AND ROLE IN REGULATING BLOOD PRESSURE. *J. Biol. Chem.* 285, 37133–37137.
- Branch, S.Y., Chen, C., Sharma, R., Lechleiter, J.D., Li, S., and Beckstead, M.J. (2016). Dopaminergic Neurons Exhibit an Age-Dependent Decline in Electrophysiological Parameters in the MitoPark Mouse Model of Parkinson’s Disease. *J. Neurosci.* 36, 4026–4037.
- Braulke, T., and Bonifacino, J.S. (2009). Sorting of lysosomal proteins. *Biochim. Biophys. Acta* 1793, 605–614.
- Brichta, L., Greengard, P., and Flajolet, M. (2013). Advances in the pharmacological treatment of Parkinson’s disease: targeting neurotransmitter systems. *Trends in Neurosciences* 36, 543–554.
- Brini, M., and Carafoli, E. (2009). Calcium Pumps in Health and Disease. *Physiological Reviews* 89, 1341–1378.
- Bristow, D. r., Arias-Montaña, J. a., and Young, J. m. (1991). Histamine-induced inositol phosphate accumulation in HeLa cells: lithium sensitivity. *British Journal of Pharmacology* 104, 677–684.
- de Brito, O.M., and Scorrano, L. (2008). Mitofusin 2 tethers endoplasmic reticulum to mitochondria. *Nature* 456, 605–610.
- Bucci, C., Parton, R.G., Mather, I.H., Stunnenberg, H., Simons, K., Hoflack, B., and Zerial, M. (1992). The small GTPase rab5 functions as a regulatory factor in the early endocytic pathway. *Cell* 70, 715–728.
- Burchell, V.S., Nelson, D.E., Sanchez-Martinez, A., Delgado-Camprubi, M., Ivatt, R.M., Pogson, J.H., Randle, S.J., Wray, S., Lewis, P.A., Houlden, H., et al. (2013). The Parkinson’s disease-linked proteins Fbxo7 and Parkin interact to mediate mitophagy. *Nat. Neurosci.* 16, 1257–1265.
- Burgoyne, T., Patel, S., and Eden, E.R. (2015). Calcium signaling at ER membrane contact sites. *Biochimica et Biophysica Acta (BBA) - Molecular Cell Research* 1853, 2012–2017.
- Burré, J., Sharma, M., Tsetsenis, T., Buchman, V., Etherton, M., and Südhof, T.C. (2010).  $\alpha$ -Synuclein Promotes SNARE-Complex Assembly in vivo and in vitro. *Science* 329, 1663–1667.
- Cahalan, M.D. (2010). How to STIMulate Calcium Channels. *Science* 330, 43–44.
- Calcraft, P.J., Ruas, M., Pan, Z., Cheng, X., Arredouani, A., Hao, X., Tang, J., Rietdorf, K., Teboul, L., Chuang, K.-T., et al. (2009). NAADP mobilizes calcium from acidic organelles through two-pore channels. *Nature* 459, 596–600.

- Cali, T., Ottolini, D., Negro, A., and Brini, M. (2013). Enhanced parkin levels favor ER-mitochondria crosstalk and guarantee Ca<sup>2+</sup> transfer to sustain cell bioenergetics. *Biochimica et Biophysica Acta (BBA) - Molecular Basis of Disease* 1832, 495–508.
- Cancela, J.M., Churchill, G.C., and Galione, A. (1999). Coordination of agonist-induced Ca<sup>2+</sup>-signalling patterns by NAADP in pancreatic acinar cells. *Nature* 398, 74–76.
- Cancela, J.M., Van Coppenolle, F., Galione, A., Tepikin, A.V., and Petersen, O.H. (2002). Transformation of local Ca<sup>2+</sup> spikes to global Ca<sup>2+</sup> transients: the combinatorial roles of multiple Ca<sup>2+</sup> releasing messengers. *EMBO J* 21, 909–919.
- Cane, M.C., Parrington, J., Rorsman, P., Galione, A., and Rutter, G.A. (2016). The two pore channel TPC2 is dispensable in pancreatic  $\beta$ -cells for normal Ca<sup>2+</sup> dynamics and insulin secretion. *Cell Calcium* 59, 32–40.
- Cang, C., Bekele, B., and Ren, D. (2014). The voltage-gated sodium channel TPC1 confers endolysosomal excitability. *Nat. Chem. Biol.* 10, 463–469.
- Cao, Q., Zhong, X.Z., Zou, Y., Murrell-Lagnado, R., Zhu, M.X., and Dong, X.-P. (2015a). Calcium release through P2X4 activates calmodulin to promote endolysosomal membrane fusion. *J Cell Biol* 209, 879–894.
- Cao, Q., Zhong, X.Z., Zou, Y., Zhang, Z., Toro, L., and Dong, X.-P. (2015b). BK Channels Alleviate Lysosomal Storage Diseases by Providing Positive Feedback Regulation of Lysosomal Ca<sup>2+</sup> Release. *Developmental Cell* 33, 427–441.
- Capel, R.A., Bolton, E.L., Lin, W.K., Aston, D., Wang, Y., Liu, W., Wang, X., Burton, R.-A.B., Bloor-Young, D., Shade, K.-T., et al. (2015). Two-pore Channels (TPC2s) and Nicotinic Acid Adenine Dinucleotide Phosphate (NAADP) at Lysosomal-Sarcoplasmic Reticular Junctions Contribute to Acute and Chronic  $\beta$ -Adrenoceptor Signaling in the Heart. *J Biol Chem* 290, 30087–30098.
- Cerny, J., Feng, Y., Yu, A., Miyake, K., Borgonovo, B., Klumperman, J., Meldolesi, J., McNeil, P.L., and Kirchhausen, T. (2004). The small chemical vacuolin-1 inhibits Ca<sup>2+</sup>-dependent lysosomal exocytosis but not cell resealing. *EMBO Rep* 5, 883–888.
- Chan, C.S., Guzman, J.N., Ilijic, E., Mercer, J.N., Rick, C., Tkatch, T., Meredith, G.E., and Surmeier, D.J. (2007). “Rejuvenation” protects neurons in mouse models of Parkinson’s disease. *Nature* 447, 1081–1086.
- Chandra, S., Kable, E.P., Morrison, G.H., and Webb, W.W. (1991). Calcium sequestration in the Golgi apparatus of cultured mammalian cells revealed by laser scanning confocal microscopy and ion microscopy. *Journal of Cell Science* 100, 747–752.
- Chandran, K., Sullivan, N.J., Felbor, U., Whelan, S.P., and Cunningham, J.M. (2005). Endosomal Proteolysis of the Ebola Virus Glycoprotein Is Necessary for Infection. *Science* 308, 1643–1645.
- Chartier-Harlin, M.-C., Kachergus, J., Roumier, C., Mouroux, V., Douay, X., Lincoln, S., Levecque, C., Larvor, L., Andrieux, J., Hulihan, M., et al. (2004).  $\alpha$ -synuclein locus duplication as a cause of familial Parkinson’s disease. *The Lancet* 364, 1167–1169.
- Chartier-Harlin, M.-C., Dachsel, J.C., Vilariño-Güell, C., Lincoln, S.J., Leprêtre, F., Hulihan, M.M., Kachergus, J., Milnerwood, A.J., Tapia, L., Song, M.-S., et al. (2011). Translation initiator EIF4G1 mutations in familial Parkinson disease. *Am. J. Hum. Genet.* 89, 398–406.

- Chen, T.-H., and Hsu, W.H. (1994). U-73122 inhibits carbachol-induced increases in  $[Ca^{2+}]_i$ , IP3, and insulin release in  $\beta$ -TC3 cells. *Life Sciences* 56, PL103-PL108.
- Chen, C.-C., Keller, M., Hess, M., Schiffmann, R., Urban, N., Wolfgardt, A., Schaefer, M., Bracher, F., Biel, M., Wahl-Schott, C., et al. (2014). A small molecule restores function to TRPML1 mutant isoforms responsible for mucopolidosis type IV. *Nat Commun* 5.
- Chen, C.S., Bach, G., and Pagano, R.E. (1998). Abnormal transport along the lysosomal pathway in mucopolidosis, type IV disease. *Proc. Natl. Acad. Sci. U.S.A.* 95, 6373–6378.
- Chen, H.-J., Anagnostou, G., Chai, A., Withers, J., Morris, A., Adhikaree, J., Pennetta, G., and de Belleruche, J.S. (2010). Characterization of the Properties of a Novel Mutation in VAPB in Familial Amyotrophic Lateral Sclerosis. *J Biol Chem* 285, 40266–40281.
- Chen, J., Raeymaecker, J.D., Hovgaard, J.B., Smaardijk, S., Vandecaetsbeek, I., Wuytack, F., Møller, J.V., Eggermont, J., Maeyer, M.D., Christensen, S.B., et al. (2017). Structure/activity Relationship of Thapsigargin Inhibition on the Purified Golgi/secretory Pathway  $Ca^{2+}/Mn^{2+}$  Transport ATPase (SPCA1a). *J. Biol. Chem.* jbc.M117.778431.
- Chen, R.H.C., Wislet-Gendebien, S., Samuel, F., Visanji, N.P., Zhang, G., Marsilio, D., Langman, T., Fraser, P.E., and Tandon, A. (2013).  $\alpha$ -Synuclein Membrane Association Is Regulated by the Rab3a Recycling Machinery and Presynaptic Activity. *J. Biol. Chem.* 288, 7438–7449.
- Cheng, B., Martinez, A.A., Morado, J., Scofield, V., Roberts, J.L., and Maffi, S.K. (2013). Retinoic acid protects against proteasome inhibition associated cell death in SH-SY5Y cells via the AKT pathway. *Neurochemistry International* 62, 31–42.
- Cheng, X., Zhang, X., Gao, Q., Ali Samie, M., Azar, M., Tsang, W.L., Dong, L., Sahoo, N., Li, X., Zhuo, Y., et al. (2014). The intracellular  $Ca^{2+}$  channel MCOLN1 is required for sarcolemma repair to prevent muscular dystrophy. *Nat Med* 20, 1187–1192.
- Cherra, S.J., Steer, E., Gusdon, A.M., Kiselyov, K., and Chu, C.T. (2013). Mutant LRRK2 elicits calcium imbalance and depletion of dendritic mitochondria in neurons. *Am. J. Pathol.* 182, 474–484.
- Cheung, C.Y., Webb, S.E., Love, D.R., and Miller, A.L. (2011). Visualization, characterization and modulation of calcium signaling during the development of slow muscle cells in intact zebrafish embryos. *Int. J. Dev. Biol.* 55, 153–174.
- Chinta, S.J., Mallajosyula, J.K., Rane, A., and Andersen, J.K. (2010). Mitochondrial alpha-synuclein accumulation impairs complex I function in dopaminergic neurons and results in increased mitophagy in vivo. *Neuroscience Letters* 486, 235–239.
- Chou, A.P., Maidment, N., Klintenberg, R., Casida, J.E., Li, S., Fitzmaurice, A.G., Fernagut, P.-O., Mortazavi, F., Chesselet, M.-F., and Bronstein, J.M. (2008). Ziram Causes Dopaminergic Cell Damage by Inhibiting E1 Ligase of the Proteasome. *J. Biol. Chem.* 283, 34696–34703.
- Choudhury, A., Sharma, D.K., Marks, D.L., and Pagano, R.E. (2004). Elevated Endosomal Cholesterol Levels in Niemann-Pick Cells Inhibit Rab4 and Perturb Membrane Recycling. *Mol Biol Cell* 15, 4500–4511.
- Christensen, K.A., Myers, J.T., and Swanson, J.A. (2002). pH-dependent regulation of lysosomal calcium in macrophages. *Journal of Cell Science* 115, 599–607.

- Churamani, D., Hooper, R., Brailoiu, E., and Patel, S. (2012). Domain assembly of NAADP-gated two-pore channels. *Biochem J* 441, 317–323.
- Churamani, D., Hooper, R., Rahman, T., Brailoiu, E., and Patel, S. (2013). The N-terminal region of two-pore channel 1 regulates trafficking and activation by NAADP. *Biochem. J.* 453, 147–151.
- Churchill, G.C., and Galione, A. (2001). NAADP induces Ca<sup>2+</sup> oscillations via a two-pool mechanism by priming IP<sub>3</sub>- and cADPR-sensitive Ca<sup>2+</sup> stores. *EMBO J* 20, 2666–2671.
- Churchill, G.C., Okada, Y., Thomas, J.M., Genazzani, A.A., Patel, S., and Galione, A. (2002). NAADP Mobilizes Ca<sup>2+</sup> from Reserve Granules, Lysosome-Related Organelles, in Sea Urchin Eggs. *Cell* 111, 703–708.
- Churchill, G.C., O’Neill, J.S., Masgrau, R., Patel, S., Thomas, J.M., Genazzani, A.A., and Galione, A. (2003). Sperm Deliver a New Second Messenger. *Current Biology* 13, 125–128.
- Cicchetti, F., Lapointe, N., Roberge-Tremblay, A., Saint-Pierre, M., Jimenez, L., Ficke, B.W., and Gross, R.E. (2005). Systemic exposure to paraquat and maneb models early Parkinson’s disease in young adult rats. *Neurobiology of Disease* 20, 360–371.
- Clapham, D.E. (2007). Calcium Signaling. *Cell* 131, 1047–1058.
- Clapper, D.L., Walseth, T.F., Dargie, P.J., and Lee, H.C. (1987). Pyridine nucleotide metabolites stimulate calcium release from sea urchin egg microsomes desensitized to inositol trisphosphate. *J. Biol. Chem.* 262, 9561–9568.
- Clayton, N., Marshall, F.H., Bountra, C., and O’Shaughnessy, C.T. (2002). CB1 and CB2 cannabinoid receptors are implicated in inflammatory pain. *Pain* 96, 253–260.
- Coblentz, J., Croix, C.S., and Kiselyov, K. (2014). Loss of TRPML1 promotes production of reactive oxygen species: is oxidative damage a factor in mucopolidosis type IV? *Biochemical Journal* 457, 361–368.
- Colin, E., Barth, M., BouSSION, F., Latour, P., Piguët-Lacroix, G., Guichet, A., Ziegler, A., Triau, S., Loisel, D., Sentilhes, L., et al. (2015). In Utero Diagnosis of Niemann–Pick Type C in the Absence of Family History. *JIMD Rep* 28, 105–110.
- Collin, T., Chat, M., Lucas, M.G., Moreno, H., Racay, P., Schwaller, B., Marty, A., and Llano, I. (2005). Developmental Changes in Parvalbumin Regulate Presynaptic Ca<sup>2+</sup> Signaling. *J. Neurosci.* 25, 96–107.
- Colombini, M. (1980). Structure and Mode of Action of a Voltage Dependent Anion-Selective Channel (vdac) Located in the Outer Mitochondrial Membrane Dependent Anion-Selective Channel (vdac)\*. *Annals of the New York Academy of Sciences* 341, 552–563.
- Comellas, G., Lemkau, L.R., Zhou, D.H., George, J.M., and Rienstra, C.M. (2012). Structural Intermediates during  $\alpha$ -Synuclein Fibrillogenesis on Phospholipid Vesicles. *J. Am. Chem. Soc.* 134, 5090–5099.
- Cosker, F., Cheviron, N., Yamasaki, M., Menteyne, A., Lund, F.E., Moutin, M.-J., Galione, A., and Cancela, J.-M. (2010). The Ecto-enzyme CD38 Is a Nicotinic Acid Adenine Dinucleotide Phosphate (NAADP) Synthase That Couples Receptor Activation to Ca<sup>2+</sup> Mobilization from Lysosomes in Pancreatic Acinar Cells. *J. Biol. Chem.* 285, 38251–38259.

- Cousin, M.A., Tan, T.C., and Robinson, P.J. (2001). Protein phosphorylation is required for endocytosis in nerve terminals: potential role for the dephosphins dynamin I and synaptojanin, but not AP180 or amphiphysin. *J. Neurochem.* *76*, 105–116.
- Csordás, G., Várnai, P., Golenár, T., Roy, S., Purkins, G., Schneider, T.G., Balla, T., and Hajnóczky, G. (2010). Imaging Interorganelle Contacts and Local Calcium Dynamics at the ER-Mitochondrial Interface. *Molecular Cell* *39*, 121–132.
- Cuervo, A.M., and Dice, J.F. (2000). When lysosomes get old☆ *Experimental Gerontology* *35*, 119–131.
- Cuervo, A.M., and Wong, E. (2014). Chaperone-mediated autophagy: roles in disease and aging. *Cell Res* *24*, 92–104.
- Cuervo, A.M., Stefanis, L., Fredenburg, R., Lansbury, P.T., and Sulzer, D. (2004). Impaired Degradation of Mutant  $\alpha$ -Synuclein by Chaperone-Mediated Autophagy. *Science* *305*, 1292–1295.
- Curcio-Morelli, C., Charles, F.A., Micsenyi, M.C., Cao, Y., Venugopal, B., Browning, M.F., Dobrenis, K., Cotman, S.L., Walkley, S.U., and Slaugenhaupt, S.A. (2010a). Regular Article Macroautophagy is Defective in Mucolipin 1-Deficient Mouse Neurons. *Neurobiol Dis* *40*, 370–377.
- Curcio-Morelli, C., Zhang, P., Venugopal, B., Charles, F.A., Browning, M.F., Cantiello, H.F., and Slaugenhaupt, S.A. (2010b). Functional multimerization of mucolipin channel proteins. *J. Cell. Physiol.* *222*, 328–335.
- Czerniczyniec, A., Bustamante, J., and Lores-Arnaiz, S. (2007). Improvement of mouse brain mitochondrial function after deprenyl treatment. *Neuroscience* *144*, 685–693.
- Dajas-Bailador, F.A., Mogg, A.J., and Wonnacott, S. (2002). Intracellular Ca<sup>2+</sup> signals evoked by stimulation of nicotinic acetylcholine receptors in SH-SY5Y cells: contribution of voltage-operated Ca<sup>2+</sup> channels and Ca<sup>2+</sup> stores. *Journal of Neurochemistry* *81*, 606–614.
- Danzer, K.M., Haasen, D., Karow, A.R., Moussaud, S., Habeck, M., Giese, A., Kretschmar, H., Hengerer, B., and Kostka, M. (2007). Different Species of  $\alpha$ -Synuclein Oligomers Induce Calcium Influx and Seeding. *J. Neurosci.* *27*, 9220–9232.
- Daugherty, A., and Raz, N. (2013). Age-Related Differences in Iron Content of Subcortical Nuclei Observed in vivo: A Meta-Analysis. *Neuroimage* *70*, 113–121.
- Davidson, C.D., Ali, N.F., Micsenyi, M.C., Stephney, G., Renault, S., Dobrenis, K., Ory, D.S., Vanier, M.T., and Walkley, S.U. (2009). Chronic Cyclodextrin Treatment of Murine Niemann-Pick C Disease Ameliorates Neuronal Cholesterol and Glycosphingolipid Storage and Disease Progression. *PLoS One* *4*.
- Davidson, S.M., Foote, K., Kunuthur, S., Gosain, R., Tan, N., Tyser, R., Zhao, Y.J., Graeff, R., Ganesan, A., Duchon, M.R., et al. (2015). Inhibition of NAADP signalling on reperfusion protects the heart by preventing lethal calcium oscillations via two-pore channel 1 and opening of the mitochondrial permeability transition pore. *Cardiovasc Res* *108*, 357–366.
- Davis, G.C., Williams, A.C., Markey, S.P., Ebert, M.H., Caine, E.D., Reichert, C.M., and Kopin, I.J. (1979a). Chronic parkinsonism secondary to intravenous injection of meperidine analogues. *Psychiatry Research* *1*, 249–254.

- Davis, L.C., Morgan, A.J., Chen, J.-L., Snead, C.M., Bloor-Young, D., Shenderov, E., Stanton-Humphreys, M.N., Conway, S.J., Churchill, G.C., Parrington, J., et al. (2012). NAADP Activates Two-Pore Channels on T Cell Cytolytic Granules to Stimulate Exocytosis and Killing. *Current Biology* 22, 2331–2337.
- Davis, W.L., Jones, R.G., and Hagler, H.K. (1979b). Calcium containing lysosomes in the normal chick duodenum: A histochemical and analytical electron microscopic study. *Tissue and Cell* 11, 127–138.
- Day, I.N.M., and Thompson, R.J. (2010). UCHL1 (PGP 9.5): Neuronal biomarker and ubiquitin system protein. *Progress in Neurobiology* 90, 327–362.
- De Duve, C., De Barse, T., Poole, B., Trouet, A., Tulkens, P., and Van Hoof, F. (1974). Lysosomotropic agents. *Biochemical Pharmacology* 23, 2495–2531.
- De Stefani, D., Raffaello, A., Teardo, E., Szabò, I., and Rizzuto, R. (2011). A 40 kDa protein of the inner membrane is the mitochondrial calcium uniporter. *Nature* 476, 336–340.
- De Vos, K.J., Mórotz, G.M., Stoica, R., Tudor, E.L., Lau, K.-F., Ackerley, S., Warley, A., Shaw, C.E., and Miller, C.C.J. (2012). VAPB interacts with the mitochondrial protein PTPIP51 to regulate calcium homeostasis. *Hum Mol Genet* 21, 1299–1311.
- Dehay, B., Ramirez, A., Martinez-Vicente, M., Perier, C., Canron, M.-H., Doudnikoff, E., Vital, A., Vila, M., Klein, C., and Bezdard, E. (2012). Loss of P-type ATPase ATP13A2/PARK9 function induces general lysosomal deficiency and leads to Parkinson disease neurodegeneration. *Proc. Natl. Acad. Sci. U.S.A.* 109, 9611–9616.
- Demaurex, N., and Frieden, M. (2003). Measurements of the free luminal ER Ca<sup>2+</sup> concentration with targeted “cameleon” fluorescent proteins. *Cell Calcium* 34, 109–119.
- Deng, H.-X., Shi, Y., Yang, Y., Ahmeti, K.B., Miller, N., Huang, C., Cheng, L., Zhai, H., Deng, S., Nuytemans, K., et al. (2016). Identification of TMEM230 mutations in familial Parkinson’s disease. *Nat Genet* 48, 733–739.
- Denton, R.M. (2009). Regulation of mitochondrial dehydrogenases by calcium ions. *Biochimica et Biophysica Acta (BBA) - Bioenergetics* 1787, 1309–1316.
- Dexter, D.T., Carayon, A., Javoy-Agid, F., Agid, Y., Wells, F.R., Daniel, S.E., Lees, A.J., Jenner, P., and Marsden, C.D. (1991). ALTERATIONS IN THE LEVELS OF IRON, FERRITIN AND OTHER TRACE METALS IN PARKINSON’S DISEASE AND OTHER NEURODEGENERATIVE DISEASES AFFECTING THE BASAL GANGLIA. *Brain* 114, 1953–1975.
- Dhungel, N., Eleuteri, S., Li, L., Kramer, N.J., Chartron, J.W., Spencer, B., Kosberg, K., Fields, J.A., Stafa, K., Adame, A., et al. (2015). Parkinson’s Disease Genes VPS35 and EIF4G1 Interact Genetically and Converge on  $\alpha$ -Synuclein. *Neuron* 85, 76–87.
- Dickinson, G.D., and Parker, I. (2013). Factors Determining the Recruitment of Inositol Trisphosphate Receptor Channels During Calcium Puffs. *Biophys J* 105, 2474–2484.
- Dickinson, G.D., Churchill, G.C., Brailoiu, E., and Patel, S. (2010). Deviant Nicotinic Acid Adenine Dinucleotide Phosphate (NAADP)-mediated Ca<sup>2+</sup> Signaling upon Lysosome Proliferation. *J Biol Chem* 285, 13321–13325.

Djarmati, A., Hagenah, J., Reetz, K., Winkler, S., Behrens, M.I., Pawlack, H., Lohmann, K., Ramirez, A., Tadić, V., Brüggemann, N., et al. (2009). ATP13A2 variants in early-onset Parkinson's disease patients and controls. *Mov. Disord.* *24*, 2104–2111.

Djerada, Z., and Millart, H. (2013). Intracellular NAADP increase induced by extracellular NAADP via the P2Y<sub>11</sub>-like receptor. *Biochemical and Biophysical Research Communications* *436*, 199–203.

Dodson, M.W., Zhang, T., Jiang, C., Chen, S., and Guo, M. (2012). Roles of the Drosophila LRRK2 homolog in Rab7-dependent lysosomal positioning. *Hum. Mol. Genet.* *21*, 1350–1363.

Dong, X., Cheng, X., Mills, E., Delling, M., Wang, F., Kurz, T., and Xu, H. (2008). The Type IV Mucopolidosis-Associated Protein TRPML1 is an Endo-lysosomal Iron Release Channel. *Nature* *455*, 992–996.

Dong, X., Wang, X., Shen, D., Chen, S., Liu, M., Wang, Y., Mills, E., Cheng, X., Delling, M., and Xu, H. (2009). Activating Mutations of the TRPML1 Channel Revealed by Proline-scanning Mutagenesis. *J Biol Chem* *284*, 32040–32052.

Dong, X., Shen, D., Wang, X., Dawson, T., Li, X., Zhang, Q., Cheng, X., Zhang, Y., Weisman, L.S., Delling, M., et al. (2010). PI(3,5)P<sub>2</sub> Controls Membrane Traffic by Direct Activation of Mucolipin Ca<sup>2+</sup> Release Channels in the Endolysosome. *Nat Commun* *1*.

Dorsey, E.R., Constantinescu, R., Thompson, J.P., Biglan, K.M., Holloway, R.G., Kieburtz, K., Marshall, F.J., Ravina, B.M., Schifitto, G., Siderowf, A., et al. (2007). Projected number of people with Parkinson disease in the most populous nations, 2005 through 2030. *Neurology* *68*, 384–386.

Dupont, G., Combettes, L., Bird, G.S., and Putney, J.W. (2011). Calcium Oscillations. *Cold Spring Harb Perspect Biol* *3*, a004226.

Durchfort, N., Verhoef, S., Vaughn, M.B., Shrestha, R., Adam, D., Kaplan, J., and Ward, D.M. (2012). The Enlarged Lysosomes in beige Cells Result From Decreased Lysosome Fission and Not Increased Lysosome Fusion. *Traffic* *13*, 108–119.

de Duve, C. (2005). The lysosome turns fifty. *Nat Cell Biol* *7*, 847–849.

de Duve, C., Pressman, B.C., Gianetto, R., Wattiaux, R., and Appelmans, F. (1955). Tissue fractionation studies. 6. Intracellular distribution patterns of enzymes in rat-liver tissue. *Biochem J* *60*, 604–617.

Dyall, J., Coleman, C.M., Hart, B.J., Venkataraman, T., Holbrook, M.R., Kindrachuk, J., Johnson, R.F., Olinger, G.G., Jahrling, P.B., Laidlaw, M., et al. (2014). Repurposing of Clinically Developed Drugs for Treatment of Middle East Respiratory Syndrome Coronavirus Infection. *Antimicrob Agents Chemother* *58*, 4885–4893.

Edelmann, L., Dong, J., Desnick, R.J., and Kornreich, R. (2002). Carrier screening for mucopolidosis type IV in the American Ashkenazi Jewish population. *Am. J. Hum. Genet.* *70*, 1023–1027.

Eden, E.R. (2016). The formation and function of ER-endosome membrane contact sites. *Biochim Biophys Acta* *1861*, 874–879.

Eden, E.R., Sanchez-Heras, E., Tsapara, A., Sobota, A., Levine, T.P., and Futter, C.E. (2016). Annexin A1 Tethers Membrane Contact Sites that Mediate ER to Endosome Cholesterol Transport. *Developmental Cell* *37*, 473–483.



- Edvardson, S., Cinnamon, Y., Ta-Shma, A., Shaag, A., Yim, Y.-I., Zenvirt, S., Jalas, C., Lesage, S., Brice, A., Taraboulos, A., et al. (2012). A Deleterious Mutation in DNAJC6 Encoding the Neuronal-Specific Clathrin-Uncoating Co-Chaperone Auxilin, Is Associated with Juvenile Parkinsonism. *PLoS One* 7.
- Edwards, Y.J.K., Beecham, G.W., Scott, W.K., Khuri, S., Bademci, G., Tekin, D., Martin, E.R., Jiang, Z., Mash, D.C., French-Mullen, J., et al. (2011). Identifying Consensus Disease Pathways in Parkinson's Disease Using an Integrative Systems Biology Approach. *PLoS One* 6.
- Eisenberg, E., and Greene, L.E. (2007). Multiple Roles of Auxilin and Hsc70 in Clathrin-Mediated Endocytosis. *Traffic* 8, 640–646.
- Elrick, M.J., Yu, T., Chung, C., and Lieberman, A.P. (2012). Impaired proteolysis underlies autophagic dysfunction in Niemann–Pick type C disease. *Hum Mol Genet* 21, 4876–4887.
- Enyeart, J.J., Dirksen, R.T., Sharma, V.K., Williford, D.J., and Sheu, S.S. (1990). Antipsychotic pimozide is a potent Ca<sup>2+</sup> channel blocker in heart. *Mol Pharmacol* 37, 752–757.
- Esposito, B., Gambarà, G., Lewis, A.M., Palombi, F., D'Alessio, A., Taylor, L.X., Genazzani, A.A., Ziparo, E., Galione, A., Churchill, G.C., et al. (2011). NAADP links histamine H1 receptors to secretion of von Willebrand factor in human endothelial cells. *Blood* 117, 4968–4977.
- Falardeau, J.L., Kennedy, J.C., Acierno, J.S., Sun, M., Stahl, S., Goldin, E., and Slaugenhaupt, S.A. (2002). Cloning and characterization of the mouse Mcoln1 gene reveals an alternatively spliced transcript not seen in humans. *BMC Genomics* 3, 3.
- Fang, Q., Zhong, N., Zhang, Y., and Zhou, Z. (2004). Tetrandrine inhibits Ca<sup>2+</sup>-activated chloride channel in cultured human umbilical vein endothelial cells. *Acta Pharmacol. Sin.* 25, 327–333.
- Farrer, M.J., Milnerwood, A.J., Follett, J., and Guella, I. (2017). TMEM230 is not a gene for Parkinson disease. *bioRxiv* 097030.
- Fassina, L., Magenes, G., Inzaghi, A., Palumbo, S., Allavena, G., Miracco, C., Pirtoli, L., Biggiogera, M., and Comincini, S. (2012). AUTOCOUNTER, an ImageJ JavaScript to analyze LC3B-GFP expression dynamics in autophagy-induced astrocytoma cells. *European Journal of Histochemistry* 56, 44.
- Favia, A., Desideri, M., Gambarà, G., D'Alessio, A., Ruas, M., Esposito, B., Bufalo, D.D., Parrington, J., Ziparo, E., Palombi, F., et al. (2014). VEGF-induced neoangiogenesis is mediated by NAADP and two-pore channel-2-dependent Ca<sup>2+</sup> signaling. *PNAS* 111, E4706–E4715.
- Fedorow, H., Halliday, G.M., Rickert, C.H., Gerlach, M., Riederer, P., and Double, K.L. (2006). Evidence for specific phases in the development of human neuromelanin. *Neurobiology of Aging* 27, 506–512.
- Feng, X., Huang, Y., Lu, Y., Xiong, J., Wong, C.-O., Yang, P., Xia, J., Chen, D., Du, G., Venkatachalam, K., et al. (2014a). Drosophila TRPML forms PI(3,5)P<sub>2</sub>-activated cation channels in both endolysosomes and plasma membrane. *J. Biol. Chem.* 289, 4262–4272.
- Feng, Y., He, D., Yao, Z., and Klionsky, D.J. (2014b). The machinery of macroautophagy. *Cell Res* 24, 24–41.
- Ferguson, S.M., and De Camilli, P. (2012). Dynamin, a membrane-remodelling GTPase. *Nat Rev Mol Cell Biol* 13, 75–88.

- Filadi, R., Greotti, E., Turacchio, G., Luini, A., Pozzan, T., and Pizzo, P. (2015). Mitofusin 2 ablation increases endoplasmic reticulum–mitochondria coupling. *PNAS* *112*, E2174–E2181.
- Filograna, R., Civiero, L., Ferrari, V., Codolo, G., Greggio, E., Bubacco, L., Beltramini, M., and Bisaglia, M. (2015). Analysis of the Catecholaminergic Phenotype in Human SH-SY5Y and BE(2)-M17 Neuroblastoma Cell Lines upon Differentiation. *PLOS ONE* *10*, e0136769.
- Foehring, R.C., Zhang, X.F., Lee, J.C.F., and Callaway, J.C. (2009). Endogenous Calcium Buffering Capacity of Substantia Nigral Dopamine Neurons. *J Neurophysiol* *102*, 2326–2333.
- Fonzo, A.D., Chien, H.F., Socal, M., Giraudo, S., Tassorelli, C., Iliceto, G., Fabbrini, G., Marconi, R., Fincati, E., Abbruzzese, G., et al. (2007). ATP13A2 missense mutations in juvenile parkinsonism and young onset Parkinson disease. *Neurology* *68*, 1557–1562.
- Fonzo, A.D., Dekker, M.C.J., Montagna, P., Baruzzi, A., Yonova, E.H., Guedes, L.C., Szczerbinska, A., Zhao, T., Dubbel-Hulsman, L.O.M., Wouters, C.H., et al. (2009). FBXO7 mutations cause autosomal recessive, early-onset parkinsonian-pyramidal syndrome. *Neurology* *72*, 240–245.
- Förster, C., and Kane, P.M. (2000). Cytosolic Ca<sup>2+</sup> Homeostasis Is a Constitutive Function of the V-ATPase in *Saccharomyces cerevisiae*. *J. Biol. Chem.* *275*, 38245–38253.
- Forster, J.I., Köglsberger, S., Trefois, C., Boyd, O., Baumuratov, A.S., Buck, L., Balling, R., and Antony, P.M.A. (2016). Characterization of Differentiated SH-SY5Y as Neuronal Screening Model Reveals Increased Oxidative Vulnerability. *J Biomol Screen* *21*, 496–509.
- Forsythe, I.D., Lambert, D.G., Nahorski, S.R., and Linsdell, P. (1992). Elevation of cytosolic calcium by cholinergic agonists in SH-SY5Y human neuroblastoma cells: estimation of the contribution of voltage-dependent currents. *British Journal of Pharmacology* *107*, 207–214.
- Foskett, J.K., White, C., Cheung, K.-H., and Mak, D.-O.D. (2007). Inositol trisphosphate receptor Ca<sup>2+</sup> release channels. *Physiol. Rev.* *87*, 593–658.
- Frei, K.P., Patronas, N.J., Crutchfield, K.E., Altarescu, G., and Schiffmann, R. (1998). Mucopolidosis type IV Characteristic MRI findings. *Neurology* *51*, 565–569.
- Funayama, M., Ohe, K., Amo, T., Furuya, N., Yamaguchi, J., Saiki, S., Li, Y., Ogaki, K., Ando, M., Yoshino, H., et al. (2015). CHCHD2 mutations in autosomal dominant late-onset Parkinson's disease: a genome-wide linkage and sequencing study. *The Lancet Neurology* *14*, 274–282.
- Furuichi, T., Cunningham, K.W., and Muto, S. (2001). A Putative Two Pore Channel AtTPC1 Mediates Ca<sup>2+</sup> Flux in Arabidopsis Leaf Cells. *Plant Cell Physiol* *42*, 900–905.
- Furukawa, K., Matsuzaki-Kobayashi, M., Hasegawa, T., Kikuchi, A., Sugeno, N., Itoyama, Y., Wang, Y., Yao, P.J., Bushlin, I., and Takeda, A. (2006). Plasma membrane ion permeability induced by mutant  $\alpha$ -synuclein contributes to the degeneration of neural cells. *Journal of Neurochemistry* *97*, 1071–1077.
- Gallop, J.L., Jao, C.C., Kent, H.M., Butler, P.J.G., Evans, P.R., Langen, R., and McMahon, H.T. (2006). Mechanism of endophilin N-BAR domain-mediated membrane curvature. *EMBO J* *25*, 2898–2910.
- Gambara, G., Billington, R.A., Debidda, M., D'Alessio, A., Palombi, F., Ziparo, E., Genazzani, A.A., and Filippini, A. (2008). NAADP-induced Ca<sup>2+</sup> signaling in response to endothelin is via the receptor subtype B and requires the integrity of lipid rafts/caveolae. *J. Cell. Physiol.* *216*, 396–404.

- Gandhi, S., and Wood, N.W. (2010). Genome-wide association studies: the key to unlocking neurodegeneration? *Nat Neurosci* 13, 789–794.
- Gandhi, S., Wood-Kaczmar, A., Yao, Z., Plun-Favreau, H., Deas, E., Klupsch, K., Downward, J., Latchman, D.S., Tabrizi, S.J., Wood, N.W., et al. (2009). PINK1-Associated Parkinson's Disease Is Caused by Neuronal Vulnerability to Calcium-Induced Cell Death. *Molecular Cell* 33, 627–638.
- Ganley, I.G., and Pfeffer, S.R. (2006). Cholesterol Accumulation Sequesters Rab9 and Disrupts Late Endosome Function in NPC1-deficient Cells. *J Biol Chem* 281, 17890–17899.
- García-Rúa, V., Feijóo-Bandín, S., Rodríguez-Penas, D., Mosquera-Leal, A., Abu-Assi, E., Beiras, A., María Seoane, L., Lear, P., Parrington, J., Portolés, M., et al. (2016). Endolysosomal two-pore channels regulate autophagy in cardiomyocytes. *J Physiol* 594, 3061–3077.
- Gasser, A., Bruhn, S., and Guse, A.H. (2006). Second Messenger Function of Nicotinic Acid Adenine Dinucleotide Phosphate Revealed by an Improved Enzymatic Cycling Assay. *J. Biol. Chem.* 281, 16906–16913.
- Gautier, C.A., Giaime, E., Caballero, E., Núñez, L., Song, Z., Chan, D., Villalobos, C., and Shen, J. (2012). Regulation of mitochondrial permeability transition pore by PINK1. *Mol Neurodegener* 7, 22.
- Gees, M., Colsoul, B., and Nilius, B. (2010). The Role of Transient Receptor Potential Cation Channels in Ca<sup>2+</sup> Signaling. *Cold Spring Harb Perspect Biol* 2.
- Gegg, M.E., Burke, D., Heales, S.J.R., Cooper, J.M., Hardy, J., Wood, N.W., and Schapira, A.H.V. (2012). Glucocerebrosidase Deficiency in Substantia Nigra of Parkinson Disease Brains. *Ann Neurol* 72, 455–463.
- Genazzani, A.A., and Galione, A. (1996). Nicotinic acid-adenine dinucleotide phosphate mobilizes Ca<sup>2+</sup> from a thapsigargin-insensitive pool. *Biochemical Journal* 315, 721–725.
- Gerasimenko, J.V., Charlesworth, R.M., Sherwood, M.W., Ferdek, P.E., Mikoshiba, K., Parrington, J., Petersen, O.H., and Gerasimenko, O.V. (2015). Both RyRs and TPCs are required for NAADP-induced intracellular Ca<sup>2+</sup> release. *Cell Calcium* 58, 237–245.
- Giasson, B.I., Murray, I.V.J., Trojanowski, J.Q., and Lee, V.M.-Y. (2001). A Hydrophobic Stretch of 12 Amino Acid Residues in the Middle of  $\alpha$ -Synuclein Is Essential for Filament Assembly. *J. Biol. Chem.* 276, 2380–2386.
- Giordano, F., Saheki, Y., Idevall-Hagren, O., Colombo, S.F., Pirruccello, M., Milosevic, I., Gracheva, E.O., Bagriantsev, S.N., Borgese, N., and De Camilli, P. (2013). PI(4,5)P<sub>2</sub>-Dependent and Ca<sup>2+</sup>-Regulated ER-PM Interactions Mediated by the Extended Synaptotagmins. *Cell* 153, 1494–1509.
- Giorgi, C., Ito, K., Lin, H.-K., Santangelo, C., Wieckowski, M.R., Lebiezinska, M., Bononi, A., Bonora, M., Duszyński, J., Bernardi, R., et al. (2010). PML Regulates Apoptosis at Endoplasmic Reticulum by Modulating Calcium Release. *Science* 330, 1247–1251.
- Girard, M., Poupon, V., Blondeau, F., and McPherson, P.S. (2005). The DnaJ-domain Protein RME-8 Functions in Endosomal Trafficking. *J. Biol. Chem.* 280, 40135–40143.
- Gitler, A.D., Chesi, A., Geddie, M.L., Strathearn, K.E., Hamamichi, S., Hill, K.J., Caldwell, K.A., Caldwell, G.A., Cooper, A.A., Rochet, J.-C., et al. (2009).  $\alpha$ -Synuclein is part of a diverse and highly

- conserved interaction network that includes PARK9 and manganese toxicity. *Nat Genet* *41*, 308–315.
- Giuliano, S., Cormerais, Y., Dufies, M., Grépin, R., Colosetti, P., Belaid, A., Parola, J., Martin, A., Lacas-Gervais, S., Mazure, N.M., et al. (2015). Resistance to sunitinib in renal clear cell carcinoma results from sequestration in lysosomes and inhibition of the autophagic flux. *Autophagy* *11*, 1891–1904.
- Glancy, B., and Balaban, R.S. (2012). Role of Mitochondrial Ca<sup>2+</sup> in the Regulation of Cellular Energetics. *Biochemistry* *51*, 2959–2973.
- Goldman, S.M. (2014). Environmental toxins and Parkinson's disease. *Annu. Rev. Pharmacol. Toxicol.* *54*, 141–164.
- Goldwurm, S., Tunesi, S., Tesei, S., Zini, M., Sironi, F., Primignani, P., Magnani, C., and Pezzoli, G. (2011). Kin-cohort analysis of LRRK2-G2019S penetrance in Parkinson's disease. *Mov. Disord.* *26*, 2144–2145.
- Gómez-Suaga, P., Luzón-Toro, B., Churamani, D., Zhang, L., Bloor-Young, D., Patel, S., Woodman, P.G., Churchill, G.C., and Hilfiker, S. (2012). Leucine-rich repeat kinase 2 regulates autophagy through a calcium-dependent pathway involving NAADP. *Hum Mol Genet* *21*, 511–525.
- Gómez-Suaga, P., Rivero-Ríos, P., Fdez, E., Blanca Ramírez, M., Ferrer, I., Aiastui, A., López De Munain, A., and Hilfiker, S. (2014). LRRK2 delays degradative receptor trafficking by impeding late endosomal budding through decreasing Rab7 activity. *Hum Mol Genet* *23*, 6779–6796.
- González-Polo, R.A., Niso-Santano, M., Ortiz-Ortiz, M.A., Gómez-Martín, A., Morán, J.M., García-Rubio, L., Francisco-Morcillo, J., Zaragoza, C., Soler, G., and Fuentes, J.M. (2007). Inhibition of Paraquat-Induced Autophagy Accelerates the Apoptotic Cell Death in Neuroblastoma SH-SY5Y Cells. *Toxicol Sci* *97*, 448–458.
- Greggio, E., and Cookson, M.R. (2009). Leucine-rich repeat kinase 2 mutations and Parkinson's disease: three questions. *ASN Neuro* *1*.
- Grimm, C., Cuajungco, M.P., van Aken, A.F.J., Schnee, M., Jörs, S., Kros, C.J., Ricci, A.J., and Heller, S. (2007). A helix-breaking mutation in TRPML3 leads to constitutive activity underlying deafness in the varitint-waddler mouse. *Proc Natl Acad Sci U S A* *104*, 19583–19588.
- Grimm, C., Jörs, S., Saldanha, S.A., Obukhov, A.G., Pan, B., Oshima, K., Cuajungco, M.P., Chase, P., Hodder, P., and Heller, S. (2010). Small molecule activators of TRPML3. *Chem Biol* *17*, 135–148.
- Grimm, C., Holdt, L.M., Chen, C.-C., Hassan, S., Müller, C., Jörs, S., Cuny, H., Kissing, S., Schröder, B., Butz, E., et al. (2014). High susceptibility to fatty liver disease in two-pore channel 2-deficient mice. *Nat Commun* *5*, 4699.
- Grove, J., and Marsh, M. (2011). The cell biology of receptor-mediated virus entry. *J Cell Biol* *195*, 1071–1082.
- Grynkiewicz, G., Poenie, M., and Tsien, R.Y. (1985). A new generation of Ca<sup>2+</sup> indicators with greatly improved fluorescence properties. *J. Biol. Chem.* *260*, 3440–3450.
- Gul, R., Park, D.-R., Shawl, A.I., Im, S.-Y., Nam, T.-S., Lee, S.-H., Ko, J.-K., Jang, K.Y., Kim, D., and Kim, U.-H. (2016). Nicotinic Acid Adenine Dinucleotide Phosphate (NAADP) and Cyclic ADP-

- Ribose (cADPR) Mediate Ca<sup>2+</sup> Signaling in Cardiac Hypertrophy Induced by  $\beta$ -Adrenergic Stimulation. *PLoS One* 11.
- Guo, J., Zeng, W., Chen, Q., Lee, C., Chen, L., Yang, Y., Cang, C., Ren, D., and Jiang, Y. (2016). Structure of the voltage-gated two-pore channel TPC1 from *Arabidopsis thaliana*. *Nature* 531, 196–201.
- Gusdon, A.M., Zhu, J., Van Houten, B., and Chu, C.T. (2012). ATP13A2 regulates mitochondrial bioenergetics through macroautophagy. *Neurobiology of Disease* 45, 962–972.
- Guzman, J.N., Sánchez-Padilla, J., Wokosin, D., Kondapalli, J., Ilijic, E., Schumacker, P.T., and Surmeier, D.J. (2010). Oxidant stress evoked by pacemaking in dopaminergic neurons is attenuated by DJ-1. *Nature* 468, 696–700.
- Hajnóczky, G., Robb-Gaspers, L.D., Seitz, M.B., and Thomas, A.P. (1995). Decoding of cytosolic calcium oscillations in the mitochondria. *Cell* 82, 415–424.
- Hales, C.M., Vaerman, J.-P., and Goldenring, J.R. (2002). Rab11 Family Interacting Protein 2 Associates with Myosin Vb and Regulates Plasma Membrane Recycling. *J. Biol. Chem.* 277, 50415–50421.
- Haller, O., Staeheli, P., Schwemmler, M., and Kochs, G. (2015). Mx GTPases: dynamin-like antiviral machines of innate immunity. *Trends in Microbiology* 23, 154–163.
- Haller, T., Dietl, P., Deetjen, P., and Völkl, H. (1996). The lysosomal compartment as intracellular calcium store in MDCK cells: a possible involvement in InsP<sub>3</sub>-mediated Ca<sup>2+</sup> release. *Cell Calcium* 19, 157–165.
- Hardie, R.C., and Franze, K. (2012). Photomechanical Responses in *Drosophila* Photoreceptors. *Science* 338, 260–263.
- He, L.-P., Hewavitharana, T., Soboloff, J., Spassova, M.A., and Gill, D.L. (2005). A Functional Link between Store-operated and TRPC Channels Revealed by the 3,5-Bis(trifluoromethyl)pyrazole Derivative, BTP2. *J. Biol. Chem.* 280, 10997–11006.
- Healy, D.G., Abou-Sleiman, P.M., Casas, J.P., Ahmadi, K.R., Lynch, T., Gandhi, S., Muqit, M.M.K., Foltynie, T., Barker, R., Bhatia, K.P., et al. (2006). UCHL-1 is not a Parkinson's disease susceptibility gene. *Annals of Neurology* 59, 627–633.
- Healy, D.G., Falchi, M., O'Sullivan, S.S., Bonifati, V., Durr, A., Bressman, S., Brice, A., Aasly, J., Zabetian, C.P., Goldwurm, S., et al. (2008). Phenotype, genotype, and worldwide genetic penetrance of LRRK2-associated Parkinson's disease: a case-control study. *Lancet Neurol* 7, 583–590.
- Heeman, B., Haute, C.V. den, Aelvoet, S.-A., Valsecchi, F., Rodenburg, R.J., Reumers, V., Debyser, Z., Callewaert, G., Koopman, W.J.H., Willems, P.H.G.M., et al. (2011). Depletion of PINK1 affects mitochondrial metabolism, calcium homeostasis and energy maintenance. *J Cell Sci* 124, 1115–1125.
- Hettiarachchi, N.T., Parker, A., Dallas, M.L., Pennington, K., Hung, C.-C., Pearson, H.A., Boyle, J.P., Robinson, P., and Peers, C. (2009).  $\alpha$ -Synuclein modulation of Ca<sup>2+</sup> signaling in human neuroblastoma (SH-SY5Y) cells. *Journal of Neurochemistry* 111, 1192–1201.

- Hockey, L.N., Kilpatrick, B.S., Eden, E.R., Lin-Moshier, Y., Brailoiu, G.C., Brailoiu, E., Futter, C.E., Schapira, A.H., Marchant, J.S., and Patel, S. (2015). Dysregulation of lysosomal morphology by pathogenic LRRK2 is corrected by TPC2 inhibition. *J Cell Sci* 128, 232–238.
- Höglinger, D., Haberkant, P., Aguilera-Romero, A., Riezman, H., Porter, F.D., Platt, F.M., Galione, A., and Schultz, C. (2015). Intracellular sphingosine releases calcium from lysosomes. *eLife* 4, e10616.
- Hooper, R., Churamani, D., Brailoiu, E., Taylor, C.W., and Patel, S. (2011). Membrane Topology of NAADP-sensitive Two-pore Channels and Their Regulation by N-linked Glycosylation. *J. Biol. Chem.* 286, 9141–9149.
- Hui, E., Johnson, C.P., Yao, J., Dunning, F.M., and Chapman, E.R. (2009). Synaptotagmin-mediated bending of the target membrane is a critical step in Ca<sup>2+</sup>-regulated fusion. *Cell* 138, 709–721.
- Hui, L., Geiger, N.H., Bloor-Young, D., Churchill, G.C., Geiger, J.D., and Chen, X. (2015). Release of calcium from endolysosomes increases calcium influx through N-type calcium channels: Evidence for acidic store-operated calcium entry in neurons. *Cell Calcium* 58, 617–627.
- Hurley, M.J., Brandon, B., Gentleman, S.M., and Dexter, D.T. (2013). Parkinson's disease is associated with altered expression of CaV1 channels and calcium-binding proteins. *Brain* 136, 2077–2097.
- Huynh, C., and Andrews, N.W. (2005). The small chemical vacuolin-1 alters the morphology of lysosomes without inhibiting Ca<sup>2+</sup>-regulated exocytosis. *EMBO Reports* 6, 843–847.
- Hwang, E.S., Yoon, G., and Kang, H.T. (2009). A comparative analysis of the cell biology of senescence and aging. *Cell. Mol. Life Sci.* 66, 2503–2524.
- Imai, Y., Gehrke, S., Wang, H.-Q., Takahashi, R., Hasegawa, K., Oota, E., and Lu, B. (2008). Phosphorylation of 4E-BP by LRRK2 affects the maintenance of dopaminergic neurons in *Drosophila*. *EMBO J* 27, 2432–2443.
- Infante, R.E., Wang, M.L., Radhakrishnan, A., Kwon, H.J., Brown, M.S., and Goldstein, J.L. (2008). NPC2 facilitates bidirectional transfer of cholesterol between NPC1 and lipid bilayers, a step in cholesterol egress from lysosomes. *Proc. Natl. Acad. Sci. U.S.A.* 105, 15287–15292.
- Ishibashi, K., Suzuki, M., and Imai, M. (2000). Molecular cloning of a novel form (two-repeat) protein related to voltage-gated sodium and calcium channels. *Biochem. Biophys. Res. Commun.* 270, 370–376.
- Ishibashi, S., Yamazaki, T., and Okamoto, K. (2009). Association of autophagy with cholesterol-accumulated compartments in Niemann-Pick disease type C cells. *Journal of Clinical Neuroscience* 16, 954–959.
- Ishida, S., Matsu-ura, T., Fukami, K., Michikawa, T., and Mikoshiba, K. (2014). Phospholipase C- $\beta$ 1 and  $\beta$ 4 Contribute to Non-Genetic Cell-to-Cell Variability in Histamine-Induced Calcium Signals in HeLa Cells. *PLOS ONE* 9, e86410.
- Ishikawa, J., Ohga, K., Yoshino, T., Takezawa, R., Ichikawa, A., Kubota, H., and Yamada, T. (2003). A Pyrazole Derivative, YM-58483, Potently Inhibits Store-Operated Sustained Ca<sup>2+</sup> Influx and IL-2 Production in T Lymphocytes. *The Journal of Immunology* 170, 4441–4449.

- Iv, W.H.H., Szymanski, C.J., and Payne, C.K. (2011). Endo-Lysosomal Vesicles Positive for Rab7 and LAMP1 Are Terminal Vesicles for the Transport of Dextran. *PLOS ONE* 6, e26626.
- Ivanova, H., Vervliet, T., Missiaen, L., Parys, J.B., De Smedt, H., and Bultynck, G. (2014). Inositol 1,4,5-trisphosphate receptor-isoform diversity in cell death and survival. *Biochimica et Biophysica Acta (BBA) - Molecular Cell Research* 1843, 2164–2183.
- Jadot, M., Colmant, C., Wattiaux-De Coninck, S., and Wattiaux, R. (1984). Intralysosomal hydrolysis of glycyl-L-phenylalanine 2-naphthylamide. *Biochem J* 219, 965–970.
- Jafari, S., Etminan, M., Aminzadeh, F., and Samii, A. (2013). Head injury and risk of Parkinson disease: A systematic review and meta-analysis. *Movement Disorders* 28, 1222–1229.
- Jaiswal, J.K., Andrews, N.W., and Simon, S.M. (2002). Membrane proximal lysosomes are the major vesicles responsible for calcium-dependent exocytosis in nonsecretory cells. *J Cell Biol* 159, 625–635.
- Jaleel, M., Nichols, R.J., Deak, M., Campbell, D.G., Gillardon, F., Knebel, A., and Alessi, D.R. (2007). LRRK2 phosphorylates moesin at threonine-558: characterization of how Parkinson's disease mutants affect kinase activity. *Biochem. J.* 405, 307–317.
- Jang, H., Boltz, D.A., Webster, R.G., and Smeyne, R.J. (2009). Viral Parkinsonism. *Biochim Biophys Acta* 1792, 714–721.
- Jefferies, H.B.J., Cooke, F.T., Jat, P., Boucheron, C., Koizumi, T., Hayakawa, M., Kaizawa, H., Ohishi, T., Workman, P., Waterfield, M.D., et al. (2008). A selective PIKfyve inhibitor blocks PtdIns(3,5)P<sub>2</sub> production and disrupts endomembrane transport and retroviral budding. *EMBO Rep* 9, 164–170.
- Jennings, A., Tyurikova, O., Bard, L., Zheng, K., Semyanov, A., Henneberger, C., and Rusakov, D.A. (2017). Dopamine elevates and lowers astroglial Ca<sup>2+</sup> through distinct pathways depending on local synaptic circuitry. *Glia* 65, 447–459.
- Jennings, J.J., Zhu, J., Rbaibi, Y., Luo, X., Chu, C.T., and Kiselyov, K. (2006). Mitochondrial Aberrations in Mucopolidosis Type IV. *J. Biol. Chem.* 281, 39041–39050.
- Jeong, H., Kim, M.-S., Kwon, J., Kim, K.-S., and Seol, W. (2006). Regulation of the transcriptional activity of the tyrosine hydroxylase gene by androgen receptor. *Neuroscience Letters* 396, 57–61.
- Jha, A., Ahuja, M., Patel, S., Brailoiu, E., and Muallem, S. (2014). Convergent regulation of the lysosomal two-pore channel-2 by Mg<sup>2+</sup>, NAADP, PI(3,5)P<sub>2</sub> and multiple protein kinases. *EMBO J.* 33, 501–511.
- Johansen, L.M., DeWald, L.E., Shoemaker, C.J., Hoffstrom, B.G., Lear-Rooney, C.M., Stossel, A., Nelson, E., Delos, S.E., Simmons, J.A., Grenier, J.M., et al. (2015). A screen of approved drugs and molecular probes identifies therapeutics with anti-Ebola virus activity. *Science Translational Medicine* 7, 290ra89-290ra89.
- John, L.M., Lechleiter, J.D., and Camacho, P. (1998). Differential Modulation of SERCA2 Isoforms by Calreticulin. *The Journal of Cell Biology* 142, 963–973.
- Johnson, L.N. (2009). Protein kinase inhibitors: contributions from structure to clinical compounds. *Quarterly Reviews of Biophysics* 42, 1–40.

- Johnson, J.D., and Misler, S. (2002). Nicotinic acid-adenine dinucleotide phosphate-sensitive calcium stores initiate insulin signaling in human beta cells. *Proc Natl Acad Sci U S A* *99*, 14566–14571.
- Johnson, C.L., Johnson, C.G., Bazan, E., Garver, D., Gruenstein, E., and Ahluwalia, M. (1990). Histamine receptors in human fibroblasts: inositol phosphates, Ca<sup>2+</sup>, and cell growth. *Am. J. Physiol.* *258*, C533-543.
- Johnson, D.E., Ostrowski, P., Jaumouillé, V., and Grinstein, S. (2016). The position of lysosomes within the cell determines their luminal pH. *J Cell Biol* *212*, 677–692.
- Jones, R.G., and Davis, W.L. (1982). Calcium-containing lysosomes in the outer mantle epithelial cells of *Amblema*, a fresh-water mollusc. *Anat. Rec.* *203*, 337–343.
- Jordens, I., Fernandez-Borja, M., Marsman, M., Dusseljee, S., Janssen, L., Calafat, J., Janssen, H., Wubbolts, R., and Neefjes, J. (2001). The Rab7 effector protein RILP controls lysosomal transport by inducing the recruitment of dynein-dynactin motors. *Current Biology* *11*, 1680–1685.
- Jouaville, L.S., Ichas, F., Holmuhamedov, E.L., Camacho, P., and Lechleiter, J.D. (1995). Synchronization of calcium waves by mitochondrial substrates in *Xenopus laevis* oocytes. *Nature* *377*, 438–441.
- Junn, E., Jang, W.H., Zhao, X., Jeong, B.S., and Mouradian, M.M. (2009). Mitochondrial Localization of DJ-1 Leads to Enhanced Neuroprotection. *J Neurosci Res* *87*, 123–129.
- Kahle, P.J., Waak, J., and Gasser, T. (2009). DJ-1 and prevention of oxidative stress in Parkinson's disease and other age-related disorders. *Free Radical Biology and Medicine* *47*, 1354–1361.
- Kaletsky, R.L., Simmons, G., and Bates, P. (2007). Proteolysis of the Ebola Virus Glycoproteins Enhances Virus Binding and Infectivity. *J Virol* *81*, 13378–13384.
- Kalinderi, K., Bostantjopoulou, S., and Fidani, L. (2016). The genetic background of Parkinson's disease: current progress and future prospects. *Acta Neurol Scand* *134*, 314–326.
- Kanaan, N.M., Kordower, J.H., and Collier, T.J. (2007). Age-related accumulation of Marinesco bodies and lipofuscin in rhesus monkey midbrain dopamine neurons: Relevance to selective neuronal vulnerability. *J. Comp. Neurol.* *502*, 683–700.
- Kaufmann, A.M., and Krise, J.P. (2007). Lysosomal Sequestration of Amine-Containing Drugs: Analysis and Therapeutic Implications. *Journal of Pharmaceutical Sciences* *96*, 729–746.
- Keely, S.J., Uribe, J.M., and Barrett, K.E. (1998). Carbachol Stimulates Transactivation of Epidermal Growth Factor Receptor and Mitogen-activated Protein Kinase in T84Cells IMPLICATIONS FOR CARBACHOL-STIMULATED CHLORIDE SECRETION. *J. Biol. Chem.* *273*, 27111–27117.
- Kelu, J.J., Chan, H.L.H., Webb, S.E., Cheng, A.H.H., Ruas, M., Parrington, J., Galione, A., and Miller, A.L. (2015). Two-Pore Channel 2 activity is required for slow muscle cell-generated Ca<sup>2+</sup> signaling during myogenesis in intact zebrafish. *Int. J. Dev. Biol.* *59*, 313–325.
- Ketteler, R., Freeman, J., Ferraro, F., Bata, N., Cutler, D.F., and Kriston-Vizi, J. (2017). Image-based siRNA screen to identify kinases regulating Weibel-Palade body size control using electroporation. *Scientific Data* *4*, 170022.



- Khan, S.Z., Longland, C.L., and Michelangeli, F. (2000). The effects of phenothiazines and other calmodulin antagonists on the sarcoplasmic and endoplasmic reticulum Ca<sup>2+</sup> pumps. *Biochemical Pharmacology* *60*, 1797–1806.
- Khan, S.Z., Dyer, J.L., and Michelangeli, F. (2001). Inhibition of the type 1 inositol 1,4,5-trisphosphate-sensitive Ca<sup>2+</sup> channel by calmodulin antagonists. *Cellular Signalling* *13*, 57–63.
- Khananshvili, D. (2014). Sodium-calcium exchangers (NCX): molecular hallmarks underlying the tissue-specific and systemic functions. *Pflugers Arch - Eur J Physiol* *466*, 43–60.
- Khwanraj, K., Phruksaniyom, C., Madlah, S., and Dharmasaroja, P. (2015). Differential Expression of Tyrosine Hydroxylase Protein and Apoptosis-Related Genes in Differentiated and Undifferentiated SH-SY5Y Neuroblastoma Cells Treated with MPP. *Neurology Research International* *2015*, e734703.
- Kilpatrick, B.S., Eden, E.R., Schapira, A.H., Futter, C.E., and Patel, S. (2013). Direct mobilisation of lysosomal Ca<sup>2+</sup> triggers complex Ca<sup>2+</sup> signals. *J Cell Sci* *126*, 60–66.
- Kilpatrick, B.S., Yates, E., Grimm, C., Schapira, A.H., and Patel, S. (2016a). Endo-lysosomal TRP mucolipin-1 channels trigger global ER Ca<sup>2+</sup> release and Ca<sup>2+</sup> influx. *J Cell Sci* *129*, 3859–3867.
- Kilpatrick, B.S., Magalhaes, J., Beavan, M.S., McNeill, A., Gegg, M.E., Cleeter, M.W.J., Bloor-Young, D., Churchill, G.C., Duchen, M.R., Schapira, A.H., et al. (2016b). Endoplasmic reticulum and lysosomal Ca<sup>2+</sup> stores are remodelled in GBA1-linked Parkinson disease patient fibroblasts. *Cell Calcium* *59*, 12–20.
- Kilpatrick, B.S., Eden, E.R., Hockey, L.N., Yates, E., Futter, C.E., and Patel, S. (2017). An Endosomal NAADP-Sensitive Two-Pore Ca<sup>2+</sup> Channel Regulates ER-Endosome Membrane Contact Sites to Control Growth Factor Signaling. *Cell Rep* *18*, 1636–1645.
- Kim, B.-J., Park, K.-H., Yim, C.-Y., Takasawa, S., Okamoto, H., Im, M.-J., and Kim, U.-H. (2008a). Generation of Nicotinic Acid Adenine Dinucleotide Phosphate and Cyclic ADP-Ribose by Glucagon-Like Peptide-1 Evokes Ca<sup>2+</sup> Signal That Is Essential for Insulin Secretion in Mouse Pancreatic Islets. *Diabetes* *57*, 868–878.
- Kim, H.J., Li, Q., Tjon-Kon-Sang, S., So, I., Kiselyov, K., and Muallem, S. (2007). Gain-of-function Mutation in TRPML3 Causes the Mouse Varitint-Waddler Phenotype. *J. Biol. Chem.* *282*, 36138–36142.
- Kim, H.J., Li, Q., Tjon-Kon-Sang, S., So, I., Kiselyov, K., Soyombo, A.A., and Muallem, S. (2008b). A novel mode of TRPML3 regulation by extracytosolic pH absent in the varitint-waddler phenotype. *EMBO J* *27*, 1197–1205.
- Kim, H.J., Soyombo, A.A., Tjon-Kon-Sang, S., So, I., and Muallem, S. (2009). The Ca<sup>2+</sup> Channel TRPML3 Regulates Membrane Trafficking and Autophagy. *Traffic* *10*, 1157–1167.
- Kim, S.-Y., Cho, B.H., and Kim, U.-H. (2010). CD38-mediated Ca<sup>2+</sup> Signaling Contributes to Angiotensin II-induced Activation of Hepatic Stellate Cells. *J Biol Chem* *285*, 576–582.
- King, V.F., Garcia, M.L., Himmel, D., Reuben, J.P., Lam, Y.K., Pan, J.X., Han, G.Q., and Kaczorowski, G.J. (1988). Interaction of tetrandrine with slowly inactivating calcium channels. Characterization of calcium channel modulation by an alkaloid of Chinese medicinal herb origin. *J. Biol. Chem.* *263*, 2238–2244.

- Kinghorn, K.J., Castillo-Quan, J.I., Bartolome, F., Angelova, P.R., Li, L., Pope, S., Cochemé, H.M., Khan, S., Asghari, S., Bhatia, K.P., et al. (2015). Loss of PLA2G6 leads to elevated mitochondrial lipid peroxidation and mitochondrial dysfunction. *Brain* 138, 1801–1816.
- Kinnear, N.P., Boittin, F.-X., Thomas, J.M., Galione, A., and Evans, A.M. (2004). Lysosome-Sarcoplasmic Reticulum Junctions A TRIGGER ZONE FOR CALCIUM SIGNALING BY NICOTINIC ACID ADENINE DINUCLEOTIDE PHOSPHATE AND ENDOTHELIN-1. *J. Biol. Chem.* 279, 54319–54326.
- Kintzer, A.F., and Stroud, R.M. (2016). Structure, inhibition, and regulatory sites of TPC1 from *Arabidopsis thaliana*. *Nature* 531, 258–262.
- Kip, S.N., Smelter, M., Iyanoye, A., Chini, E.N., Prakash, Y.S., Pabelick, C.M., and Sieck, G.C. (2006). Agonist-induced cyclic ADP ribose production in airway smooth muscle. *Archives of Biochemistry and Biophysics* 452, 102–107.
- Kirichok, Y., Krapivinsky, G., and Clapham, D.E. (2004). The mitochondrial calcium uniporter is a highly selective ion channel. *Nature* 427, 360–364.
- Kiselyov, K., Chen, J., Rbaibi, Y., Oberdick, D., Tjon-Kon-Sang, S., Shcheynikov, N., Muallem, S., and Soyombo, A. (2005). TRP-ML1 Is a Lysosomal Monovalent Cation Channel That Undergoes Proteolytic Cleavage. *J. Biol. Chem.* 280, 43218–43223.
- Kitada, T., Asakawa, S., Hattori, N., Matsumine, H., Yamamura, Y., Minoshima, S., Yokochi, M., Mizuno, Y., and Shimizu, N. (1998). Mutations in the parkin gene cause autosomal recessive juvenile parkinsonism. *Nature* 392, 605–608.
- Kiviluoto, S., Vervliet, T., Ivanova, H., Decuypere, J.-P., De Smedt, H., Missiaen, L., Bultynck, G., and Parys, J.B. (2013). Regulation of inositol 1,4,5-trisphosphate receptors during endoplasmic reticulum stress. *Biochimica et Biophysica Acta (BBA) - Molecular Cell Research* 1833, 1612–1624.
- Ko, D.C., Gordon, M.D., Jin, J.Y., and Scott, M.P. (2001). Dynamic Movements of Organelles Containing Niemann-Pick C1 Protein: NPC1 Involvement in Late Endocytic Events. *Mol Biol Cell* 12, 601–614.
- Kogot-Levin, A., Zeigler, M., Ornoy, A., and Bach, G. (2009). Mucopolipidosis Type IV: The Effect of Increased Lysosomal pH on the Abnormal Lysosomal Storage. *Pediatr Res* 65, 686–690.
- Kohn, G., Livni, N., Ornoy, A., Sekeles, E., Beyth, Y., Legum, C., Bach, G., and Cohen, M.M. (1977). Prenatal diagnosis of mucopolipidosis IV by electron microscopy. *The Journal of Pediatrics* 90, 62–66.
- Kolter, T., and Sandhoff, K. (2010). Lysosomal degradation of membrane lipids. *FEBS Letters* 584, 1700–1712.
- Korecka, J.A., Kesteren, R.E. van, Blaas, E., Spitzer, S.O., Kamstra, J.H., Smit, A.B., Swaab, D.F., Verhaagen, J., and Bossers, K. (2013). Phenotypic Characterization of Retinoic Acid Differentiated SH-SY5Y Cells by Transcriptional Profiling. *PLOS ONE* 8, e63862.
- Korkotian, E., Schwarz, A., Pelled, D., Schwarzmann, G., Segal, M., and Futerman, A.H. (1999). Elevation of intracellular glucosylceramide levels results in an increase in endoplasmic reticulum density and in functional calcium stores in cultured neurons. *J. Biol. Chem.* 274, 21673–21678.

Kornhuber, J., Muehlbacher, M., Trapp, S., Pechmann, S., Friedl, A., Reichel, M., Mühle, C., Terfloth, L., Groemer, T.W., Spitzer, G.M., et al. (2011). Identification of Novel Functional Inhibitors of Acid Sphingomyelinase. *PLOS ONE* 6, e23852.

Korolchuk, V.I., and Rubinsztein, D.C. (2011). Regulation of autophagy by lysosomal positioning. *Autophagy* 7, 927–928.

Kouznetsova, J., Sun, W., Martínez-Romero, C., Tawa, G., Shinn, P., Chen, C.Z., Schimmer, A., Sanderson, P., McKew, J.C., Zheng, W., et al. (2014). Identification of 53 compounds that block Ebola virus-like particle entry via a repurposing screen of approved drugs. *Emerg Microbes Infect* 3, e84.

Kraytsberg, Y., Kudryavtseva, E., McKee, A.C., Geula, C., Kowall, N.W., and Khrapko, K. (2006). Mitochondrial DNA deletions are abundant and cause functional impairment in aged human substantia nigra neurons. *Nat Genet* 38, 518–520.

Krebiehl, G., Ruckerbauer, S., Burbulla, L.F., Kieper, N., Maurer, B., Waak, J., Wolburg, H., Gizatullina, Z., Gellerich, F.N., Voitalla, D., et al. (2010). Reduced Basal Autophagy and Impaired Mitochondrial Dynamics Due to Loss of Parkinson's Disease-Associated Protein DJ-1. *PLoS One* 5.

Krebs, C.E., Karkheiran, S., Powell, J.C., Cao, M., Makarov, V., Darvish, H., Di Paolo, G., Walker, R.H., Shahidi, G.A., Buxbaum, J.D., et al. (2013). The Sac1 domain of SYNJ1 identified mutated in a family with early-onset progressive Parkinsonism with generalized seizures. *Hum. Mutat.* 34, 1200–1207.

Krebs, M., Beyhl, D., Görlich, E., Al-Rasheid, K.A.S., Marten, I., Stierhof, Y.-D., Hedrich, R., and Schumacher, K. (2010). Arabidopsis V-ATPase activity at the tonoplast is required for efficient nutrient storage but not for sodium accumulation. *Proc Natl Acad Sci U S A* 107, 3251–3256.

Kress, G.J., Dineley, K.E., and Reynolds, I.J. (2002). The Relationship between Intracellular Free Iron and Cell Injury in Cultured Neurons, Astrocytes, and Oligodendrocytes. *J. Neurosci.* 22, 5848–5855.

Krüger, R., Kuhn, W., Müller, T., Voitalla, D., Graeber, M., Kösel, S., Przuntek, H., Epplen, J.T., Schols, L., and Riess, O. (1998). AlaSOPro mutation in the gene encoding  $\alpha$ -synuclein in Parkinson's disease. *Nat Genet* 18, 106–108.

Kuiken, H.J., Egan, D.A., Laman, H., Bernards, R., Beijersbergen, R.L., and Dirac, A.M. (2012). Identification of F-box only protein 7 as a negative regulator of NF-kappaB signalling. *J Cell Mol Med* 16, 2140–2149.

Kukic, I., Lee, J.K., Coblentz, J., Kelleher, S.L., and Kiselyov, K. (2013). Zinc-dependent lysosomal enlargement in TRPML1-deficient cells involves MTF-1 transcription factor and ZnT4 (Slc30a4) transporter. *Biochemical Journal* 451, 155–163.

Kwon, H.J., Abi-Mosleh, L., Wang, M.L., Deisenhofer, J., Goldstein, J.L., Brown, M.S., and Infante, R.E. (2009). Structure of N-terminal Domain of NPC1 Reveals Distinct Subdomains for Binding and Transfer of Cholesterol. *Cell* 137, 1213–1224.

La Rovere, R.M.L., Roest, G., Bultynck, G., and Parys, J.B. (2016). Intracellular Ca<sup>2+</sup> signaling and Ca<sup>2+</sup> microdomains in the control of cell survival, apoptosis and autophagy. *Cell Calcium* 60, 74–87.

- Lakadamyali, M., Rust, M.J., and Zhuang, X. (2004). Endocytosis of influenza viruses. *Microbes Infect* 6, 929–936.
- Lambert, D.G., and Nahorski, S.R. (1990). Muscarinic-receptor-mediated changes in intracellular Ca<sup>2+</sup> and inositol 1,4,5-trisphosphate mass in a human neuroblastoma cell line, SH-SY5Y. *Biochem J* 265, 555–562.
- Lambert, D.G., and Nahorski, S.R. (1992). Carbachol-stimulated calcium entry in SH-SY5Y human neuroblastoma cells: which route? *J. Physiol. Paris* 86, 77–82.
- Lambert, D.G., Whitham, E.M., Baird, J.G., and Nahorski, S.R. (1990). Different mechanisms of Ca<sup>2+</sup> entry induced by depolarization and muscarinic receptor stimulation in SH-SY5Y human neuroblastoma cells. *Molecular Brain Research* 8, 263–266.
- LaPlante, J.M., Ye, C.P., Quinn, S.J., Goldin, E., Brown, E.M., Slaugenhaupt, S.A., and Vassilev, P.M. (2004). Functional links between mucolipin-1 and Ca<sup>2+</sup>-dependent membrane trafficking in mucopolipidosis IV. *Biochemical and Biophysical Research Communications* 322, 1384–1391.
- LaPlante, J.M., Sun, M., Falardeau, J., Dai, D., Brown, E.M., Slaugenhaupt, S.A., and Vassilev, P.M. (2006). Lysosomal exocytosis is impaired in mucopolipidosis type IV. *Molecular Genetics and Metabolism* 89, 339–348.
- LaPlante, J.M., Falardeau, J.L., Brown, E.M., Slaugenhaupt, S.A., and Vassilev, P.M. (2011). The cation channel mucolipin-1 is a bifunctional protein that facilitates membrane remodeling via its serine lipase domain. *Exp Cell Res* 317, 691–705.
- Larisch, N., Kirsch, S.A., Schambony, A., Studtucker, T., Böckmann, R.A., and Dietrich, P. (2016). The function of the two-pore channel TPC1 depends on dimerization of its carboxy-terminal helix. *Cell. Mol. Life Sci.* 73, 2565–2581.
- Lashuel, H.A., Overk, C.R., Oueslati, A., and Masliah, E. (2013). The many faces of  $\alpha$ -synuclein: from structure and toxicity to therapeutic target. *Nat Rev Neurosci* 14, 38–48.
- Lee, H.C. (2012). Cyclic ADP-ribose and Nicotinic Acid Adenine Dinucleotide Phosphate (NAADP) as Messengers for Calcium Mobilization. *J. Biol. Chem.* 287, 31633–31640.
- Lee, H.C., and Aarhus, R. (1995). A derivative of NADP mobilizes calcium stores insensitive to inositol trisphosphate and cyclic ADP-ribose. *J. Biol. Chem.* 270, 2152–2157.
- Lee, D., Zhao, X., Zhang, F., Eisenberg, E., and Greene, L.E. (2005). Depletion of GAK/auxilin 2 inhibits receptor-mediated endocytosis and recruitment of both clathrin and clathrin adaptors. *J. Cell. Sci.* 118, 4311–4321.
- Lee, H., Lee, J.K., Min, W.-K., Bae, J.-H., He, X., Schuchman, E.H., Bae, J., and Jin, H.K. (2010a). Bone Marrow-Derived Mesenchymal Stem Cells Prevent the Loss of Niemann-Pick Type C Mouse Purkinje Neurons by Correcting Sphingolipid Metabolism and Increasing Sphingosine-1-phosphate. *STEM CELLS* 28, 821–831.
- Lee, H., Lee, J.K., Park, M.H., Hong, Y.R., Marti, H.H., Kim, H., Okada, Y., Otsu, M., Seo, E.-J., Park, J.-H., et al. (2014). Pathological roles of the VEGF/SphK pathway in Niemann–Pick type C neurons. *Nat Commun* 5.
- Lee, J.-H., McBrayer, M.K., Wolfe, D.M., Haslett, L.J., Kumar, A., Sato, Y., Lie, P.P.Y., Mohan, P., Coffey, E.E., Kompella, U., et al. (2015). Presenilin 1 maintains lysosomal Ca<sup>2+</sup> homeostasis by regulating vATPase-mediated lysosome acidification. *Cell Rep* 12, 1430–1444.

- Lee, S., Liu, H.-P., Lin, W.-Y., Guo, H., and Lu, B. (2010b). LRRK2 Kinase Regulates Synaptic Morphology through Distinct Substrates at the Presynaptic and Postsynaptic Compartments of the *Drosophila* Neuromuscular Junction. *J. Neurosci.* *30*, 16959–16969.
- Lee, S.-H., Schwaller, B., and Neher, E. (2000). Kinetics of Ca<sup>2+</sup> binding to parvalbumin in bovine chromaffin cells: implications for [Ca<sup>2+</sup>] transients of neuronal dendrites. *J Physiol* *525*, 419–432.
- Leroy, E., Boyer, R., Auburger, G., Leube, B., Ulm, G., Mezey, E., Harta, G., Brownstein, M.J., Jonnalagada, S., Chernova, T., et al. (1998). The ubiquitin pathway in Parkinson's disease. *Nature* *395*, 451–452.
- Lesage, S., Drouet, V., Majounie, E., Deramecourt, V., Jacoupy, M., Nicolas, A., Cormier-Dequaire, F., Hassoun, S.M., Pujol, C., Ciura, S., et al. (2016). Loss of VPS13C Function in Autosomal-Recessive Parkinsonism Causes Mitochondrial Dysfunction and Increases PINK1/Parkin-Dependent Mitophagy. *Am J Hum Genet* *98*, 500–513.
- Lewis, A.M., Aley, P.K., Roomi, A., Thomas, J.M., Masgrau, R., Garnham, C., Shipman, K., Paramore, C., Bloor-Young, D., Sanders, L.E.L., et al. (2012).  $\beta$ -Adrenergic receptor signaling increases NAADP and cADPR levels in the heart. *Biochemical and Biophysical Research Communications* *427*, 326–329.
- Li, C. (1998). An Iterative Algorithm for Minimum Cross Entropy Thresholding.
- Li, B., Hu, Q., Wang, H., Man, N., Ren, H., Wen, L., Nukina, N., Fei, E., and Wang, G. (2010). Omi/HtrA2 is a positive regulator of autophagy that facilitates the degradation of mutant proteins involved in neurodegenerative diseases. *Cell Death Differ.* *17*, 1773–1784.
- Li, M., Yu, Y., and Yang, J. (2011). Structural Biology of TRP Channels. *Adv Exp Med Biol* *704*, 1–23.
- Li, M., Zhang, W.K., Benvin, N.M., Zhou, X., Su, D., Li, H., Wang, S., Michailidis, I.E., Tong, L., Li, X., et al. (2017). Structural basis of dual Ca<sup>2+</sup>/pH regulation of the endolysosomal TRPML1 channel. *Nat Struct Mol Biol* *24*, 205–213.
- Li, X., Rydzewski, N., Hider, A., Zhang, X., Yang, J., Wang, W., Gao, Q., Cheng, X., and Xu, H. (2016). A Molecular Mechanism to Regulate Lysosome Motility for Lysosome Positioning and Tubulation. *Nat Cell Biol* *18*, 404–417.
- Liao, G., Yao, Y., Liu, J., Yu, Z., Cheung, S., Xie, A., Liang, X., and Bi, X. (2007). Cholesterol Accumulation Is Associated with Lysosomal Dysfunction and Autophagic Stress in *Npc1*-/- Mouse Brain. *Am J Pathol* *171*, 962–975.
- Lieberman, L.A., and Higgins, D.E. (2009). A Small-Molecule Screen Identifies the Antipsychotic Drug Pimozide as an Inhibitor of *Listeria monocytogenes* Infection. *Antimicrob. Agents Chemother.* *53*, 756–764.
- Lin, P.-H., Duann, P., Komazaki, S., Park, K.H., Li, H., Sun, M., Sermersheim, M., Gumpper, K., Parrington, J., Galione, A., et al. (2015). Lysosomal Two-pore Channel Subtype 2 (TPC2) Regulates Skeletal Muscle Autophagic Signaling. *J. Biol. Chem.* *290*, 3377–3389.
- Lin-Moshier, Y., Walseth, T.F., Churamani, D., Davidson, S.M., Slama, J.T., Hooper, R., Brailoiu, E., Patel, S., and Marchant, J.S. (2012). Photoaffinity Labeling of Nicotinic Acid Adenine Dinucleotide Phosphate (NAADP) Targets in Mammalian Cells. *J Biol Chem* *287*, 2296–2307.

Lin-Moshier, Y., Keebler, M.V., Hooper, R., Boulware, M.J., Liu, X., Churamani, D., Abood, M.E., Walseth, T.F., Brailoiu, E., Patel, S., et al. (2014). The Two-pore channel (TPC) interactome unmasks isoform-specific roles for TPCs in endolysosomal morphology and cell pigmentation. *PNAS* *111*, 13087–13092.

Liou, J., Fivaz, M., Inoue, T., and Meyer, T. (2007). Live-cell imaging reveals sequential oligomerization and local plasma membrane targeting of stromal interaction molecule 1 after Ca<sup>2+</sup> store depletion. *PNAS* *104*, 9301–9306.

Lissandron, V., Podini, P., Pizzo, P., and Pozzan, T. (2010). Unique characteristics of Ca<sup>2+</sup> homeostasis of the trans-Golgi compartment. *PNAS* *107*, 9198–9203.

Liu, T., Liu, X., and Li, W. (2016). Tetrandrine, a Chinese plant-derived alkaloid, is a potential candidate for cancer chemotherapy. *Oncotarget* *7*, 40800–40815.

Liu, Y., Fallon, L., Lashuel, H.A., Liu, Z., and Lansbury Jr., P.T. (2002). The UCH-L1 Gene Encodes Two Opposing Enzymatic Activities that Affect  $\alpha$ -Synuclein Degradation and Parkinson's Disease Susceptibility. *Cell* *111*, 209–218.

Liu, Y., Clegg, H.V., Leslie, P.L., Di, J., Tollini, L.A., He, Y., Kim, T.-H., Jin, A., Graves, L.M., Zheng, J., et al. (2015). CHCHD2 inhibits apoptosis by interacting with Bcl-x L to regulate Bax activation. *Cell Death Differ* *22*, 1035–1046.

Liu, Z., Ma, C., Zhao, W., Zhang, Q., Xu, R., Zhang, H., Lei, H., and Xu, S. (2017). High Glucose Enhances Isoflurane-Induced Neurotoxicity by Regulating TRPC-Dependent Calcium Influx. *Neurochem Res* *42*, 1165–1178.

Lloyd-Evans, E., Pelled, D., Riebeling, C., Bodennec, J., de-Morgan, A., Waller, H., Schiffmann, R., and Futerman, A.H. (2003). Glucosylceramide and Glucosylsphingosine Modulate Calcium Mobilization from Brain Microsomes via Different Mechanisms. *J. Biol. Chem.* *278*, 23594–23599.

Lloyd-Evans, E., Morgan, A.J., He, X., Smith, D.A., Elliot-Smith, E., Sillence, D.J., Churchill, G.C., Schuchman, E.H., Galione, A., and Platt, F.M. (2008). Niemann-Pick disease type C1 is a sphingosine storage disease that causes deregulation of lysosomal calcium. *Nat Med* *14*, 1247–1255.

Lopes, F.M., Schröder, R., Júnior, M.L.C. da F., Zanotto-Filho, A., Müller, C.B., Pires, A.S., Meurer, R.T., Colpo, G.D., Gelain, D.P., Kapczinski, F., et al. (2010). Comparison between proliferative and neuron-like SH-SY5Y cells as an in vitro model for Parkinson disease studies. *Brain Research* *1337*, 85–94.

López, J.J., Camello-Almaraz, C., Pariente, J.A., Salido, G.M., and Rosado, J.A. (2005). Ca<sup>2+</sup> accumulation into acidic organelles mediated by Ca<sup>2+</sup>- and vacuolar H<sup>+</sup>-ATPases in human platelets. *Biochem. J.* *390*, 243–252.

López, J.J., Dionisio, N., Berna-Erro, A., Galán, C., Salido, G.M., and Rosado, J.A. (2012). Two-pore channel 2 (TPC2) modulates store-operated Ca<sup>2+</sup> entry. *Biochimica et Biophysica Acta (BBA) - Molecular Cell Research* *1823*, 1976–1983.

López-Otín, C., Blasco, M.A., Partridge, L., Serrano, M., and Kroemer, G. (2013). The Hallmarks of Aging. *Cell* *153*, 1194–1217.

- Lopez-Sanjurjo, C.I., Tovey, S.C., Prole, D.L., and Taylor, C.W. (2013). Lysosomes shape Ins(1,4,5)P<sub>3</sub>-evoked Ca<sup>2+</sup> signals by selectively sequestering Ca<sup>2+</sup> released from the endoplasmic reticulum. *J Cell Sci* 126, 289–300.
- Loulousis, M., Krager, S.L., Darcy, Y.L., Tischkau, S.A., and Copello, J.A. (2016). Drugs That Inhibit The Sarcoplasmic Reticulum Ca<sup>2+</sup> ATPase (SERCA) and Prevention of Breast Cancer Cell Proliferation. *FASEB J* 30, 768.4-768.4.
- Lu, Y., Hao, B.-X., Graeff, R., Wong, C.W.M., Wu, W.-T., and Yue, J. (2013). Two Pore Channel 2 (TPC2) Inhibits Autophagosomal-Lysosomal Fusion by Alkalinizing Lysosomal pH. *J. Biol. Chem.* 288, 24247–24263.
- Lu, Y., Dong, S., Hao, B., Li, C., Zhu, K., Guo, W., Wang, Q., Cheung, K.-H., Wong, C.W., Wu, W.-T., et al. (2014). Vacuolin-1 potently and reversibly inhibits autophagosome-lysosome fusion by activating RAB5A. *Autophagy* 10, 1895–1905.
- Luciani, D.S., Gwiazda, K.S., Yang, T.-L.B., Kalynyak, T.B., Bychkivska, Y., Frey, M.H.Z., Jeffrey, K.D., Sampaio, A.V., Underhill, T.M., and Johnson, J.D. (2009). Roles of IP<sub>3</sub>R and RyR Ca<sup>2+</sup> Channels in Endoplasmic Reticulum Stress and  $\beta$ -Cell Death. *Diabetes* 58, 422–432.
- Luzio, J.P., Pryor, P.R., and Bright, N.A. (2007a). Lysosomes: fusion and function. *Nat Rev Mol Cell Biol* 8, 622–632.
- Luzio, J.P., Bright, N.A., and Pryor, P.R. (2007b). The role of calcium and other ions in sorting and delivery in the late endocytic pathway. *Biochemical Society Transactions* 35, 1088–1091.
- Ma, S. y., Ciliax, B. j., Stebbins, G., Jaffar, S., Joyce, J. n., Cochran, E. j., Kordower, J. h., Mash, D. c., Levey, A. i., and Mufson, E. j. (1999). Dopamine transporter-immunoreactive neurons decrease with age in the human substantia nigra. *J. Comp. Neurol.* 409, 25–37.
- MacAskill, A.F., Rinholm, J.E., Twelvetrees, A.E., Arancibia-Carcamo, I.L., Muir, J., Fransson, A., Aspenstrom, P., Attwell, D., and Kittler, J.T. (2009). Miro1 Is a Calcium Sensor for Glutamate Receptor-Dependent Localization of Mitochondria at Synapses. *Neuron* 61, 541–555.
- Macgregor, A., Yamasaki, M., Rakovic, S., Sanders, L., Parkesh, R., Churchill, G.C., Galione, A., and Terrar, D.A. (2007). NAADP Controls Cross-talk between Distinct Ca<sup>2+</sup> Stores in the Heart. *J. Biol. Chem.* 282, 15302–15311.
- MacLeod, D.A., Rhinn, H., Kuwahara, T., Zolin, A., Di Paolo, G., McCabe, B.D., Clark, L.N., Small, S.A., and Abeliovich, A. (2013). RAB7L1 interacts with LRRK2 to modify intraneuronal protein sorting and Parkinson's disease risk. *Neuron* 77, 425–439.
- Maegawa, G.H.B., Tropak, M.B., Buttner, J.D., Rigat, B.A., Fuller, M., Pandit, D., Tang, L., Kornhaber, G.J., Hamuro, Y., Clarke, J.T.R., et al. (2009). Identification and Characterization of Ambroxol as an Enzyme Enhancement Agent for Gaucher Disease. *J. Biol. Chem.* 284, 23502–23516.
- Maetzel, D., Sarkar, S., Wang, H., Abi-Mosleh, L., Xu, P., Cheng, A.W., Gao, Q., Mitalipova, M., and Jaenisch, R. (2014). Genetic and Chemical Correction of Cholesterol Accumulation and Impaired Autophagy in Hepatic and Neural Cells Derived from Niemann-Pick Type C Patient-Specific iPS Cells. *Stem Cell Reports* 2, 866–880.
- Magalhaes, J., Gegg, M.E., Migdalska-Richards, A., Doherty, M.K., Whitfield, P.D., and Schapira, A.H.V. (2016). Autophagic lysosome reformation dysfunction in glucocerebrosidase deficient cells: relevance to Parkinson disease. *Hum. Mol. Genet.* ddw185.

- Malavasi, F., Deaglio, S., Funaro, A., Ferrero, E., Horenstein, A.L., Ortolan, E., Vaisitti, T., and Aydin, S. (2008). Evolution and Function of the ADP Ribosyl Cyclase/CD38 Gene Family in Physiology and Pathology. *Physiological Reviews* 88, 841–886.
- Mani, M., Lee, S.Y., Lucast, L., Cremona, O., Di Paolo, G., De Camilli, P., and Ryan, T.A. (2007). The dual phosphatase activity of Synaptojanin1 is required for both efficient synaptic vesicle internalization and re-availability at nerve terminals. *Neuron* 56.
- Manzoni, C., Mamais, A., Dihanich, S., Abeti, R., Soutar, M.P.M., Plun-Favreau, H., Giunti, P., Tooze, S.A., Bandopadhyay, R., and Lewis, P.A. (2013). Inhibition of LRRK2 kinase activity stimulates macroautophagy. *Biochimica et Biophysica Acta (BBA) - Molecular Cell Research* 1833, 2900–2910.
- Manzoni, C., Denny, P., Lovering, R.C., and Lewis, P.A. (2015). Computational analysis of the LRRK2 interactome. *PeerJ* 3.
- Maraganore, D.M., Lesnick, T.G., Elbaz, A., Chartier-Harlin, M.-C., Gasser, T., Krüger, R., Hattori, N., Mellick, G.D., Quattrone, A., Satoh, J.-I., et al. (2004). UCHL1 is a Parkinson's disease susceptibility gene. *Ann Neurol.* 55, 512–521.
- Marceau, F., and Regoli, D. (2004). Bradykinin receptor ligands: therapeutic perspectives. *Nat Rev Drug Discov* 3, 845–852.
- Marras, C., Lohmann, K., Lang, A., and Klein, C. (2012). Fixing the broken system of genetic locus symbols. *Neurology* 78, 1016–1024.
- Marras, C., Hincapié, C.A., Kristman, V.L., Cancelliere, C., Soklaridis, S., Li, A., Borg, J., af Geijerstam, J.-L., and Cassidy, J.D. (2014). Systematic Review of the Risk of Parkinson's Disease After Mild Traumatic Brain Injury: Results of the International Collaboration on Mild Traumatic Brain Injury Prognosis. *Archives of Physical Medicine and Rehabilitation* 95, S238–S244.
- Martin, I., Kim, J.W., Dawson, V.L., and Dawson, T.M. (2014a). LRRK2 pathobiology in Parkinson's disease. *J. Neurochem.* 131, 554–565.
- Martin, I., Kim, J.W., Lee, B.D., Kang, H.C., Xu, J.-C., Jia, H., Stankowski, J., Kim, M.-S., Zhong, J., Kumar, M., et al. (2014b). Ribosomal protein s15 phosphorylation mediates LRRK2 neurodegeneration in Parkinson's disease. *Cell* 157, 472–485.
- Masgrau, R., Churchill, G.C., Morgan, A.J., Ashcroft, S.J.H., and Galione, A. (2003). NAADP. *Current Biology* 13, 247–251.
- Matta, S., Van Kolen, K., da Cunha, R., van den Bogaart, G., Mandemakers, W., Miskiewicz, K., De Bock, P.-J., Morais, V.A., Vilain, S., Haddad, D., et al. (2012). LRRK2 Controls an EndoA Phosphorylation Cycle in Synaptic Endocytosis. *Neuron* 75, 1008–1021.
- Mcallister, B.S., Leeblundberg, L.M.F., Javors, M.A., and Olson, M.S. (1993). Bradykinin Receptors and Signal Transduction Pathways in Human Fibroblasts: Integral Role for Extracellular Calcium. *Archives of Biochemistry and Biophysics* 304, 294–301.
- McCaffrey, K., and Braakman, I. (2016). Protein quality control at the endoplasmic reticulum. *Essays In Biochemistry* 60, 227–235.
- McCarthy, S., Somayajulu, M., Sikorska, M., Borowy-Borowski, H., and Pandey, S. (2004). Paraquat induces oxidative stress and neuronal cell death; neuroprotection by water-soluble Coenzyme Q10. *Toxicology and Applied Pharmacology* 201, 21–31.



- McCartney, A.J., Zhang, Y., and Weisman, L.S. (2014). Phosphatidylinositol 3,5-bisphosphate: low abundance, high significance. *Bioessays* 36, 52–64.
- McCormack, A.L., Thiruchelvam, M., Manning-Bog, A.B., Thiffault, C., Langston, J.W., Cory-Slechta, D.A., and Di Monte, D.A. (2002). Environmental Risk Factors and Parkinson's Disease: Selective Degeneration of Nigral Dopaminergic Neurons Caused by the Herbicide Paraquat. *Neurobiology of Disease* 10, 119–127.
- McCue, H.V., Wardyn, J.D., Burgoyne, R.D., and Haynes, L.P. (2013). Generation and characterization of a lysosomally targeted, genetically encoded Ca<sup>2+</sup>-sensor. *Biochem J* 449, 449–457.
- McPherson, P.S., Garcia, E.P., Slepnev, V.I., David, C., Zhang, X., Grabs, D., Sossini, W.S., Bauerfeind, R., Nemoto, Y., and De Camilli, P. (1996). A presynaptic inositol-5-phosphatase. *Nature* 379, 353–357.
- Medina, D.L., Di Paola, S., Peluso, I., Armani, A., De Stefani, D., Venditti, R., Montefusco, S., Scotto-Rosato, A., Prezioso, C., Forrester, A., et al. (2015). Lysosomal calcium signalling regulates autophagy through calcineurin and TFEB. *Nat Cell Biol* 17, 288–299.
- Mehta, A., Prabhakar, M., Kumar, P., Deshmukh, R., and Sharma, P.L. (2013). Excitotoxicity: Bridge to various triggers in neurodegenerative disorders. *European Journal of Pharmacology* 698, 6–18.
- Meister, B., Grünebach, F., Bautz, F., Brugger, W., Fink, F.-M., Kanz, L., and Möhle, R. (1999). Expression of vascular endothelial growth factor (VEGF) and its receptors in human neuroblastoma. *European Journal of Cancer* 35, 445–449.
- Melchionda, M., Pittman, J.K., Mayor, R., and Patel, S. (2016). Ca<sup>2+</sup>/H<sup>+</sup> exchange by acidic organelles regulates cell migration in vivo. *J Cell Biol* 212, 803–813.
- Mendel, D.B., Laird, A.D., Xin, X., Louie, S.G., Christensen, J.G., Li, G., Schreck, R.E., Abrams, T.J., Ngai, T.J., Lee, L.B., et al. (2003). In Vivo Antitumor Activity of SU11248, a Novel Tyrosine Kinase Inhibitor Targeting Vascular Endothelial Growth Factor and Platelet-derived Growth Factor Receptors. *Clin Cancer Res* 9, 327–337.
- Menezes, A., Zeman, R., and Sabban, E. (1996). Involvement of Intracellular or Extracellular Calcium in Activation of Tyrosine Hydroxylase Gene Expression in PC12 Cells. *Journal of Neurochemistry* 67, 2316–2324.
- Mesaeli, N., Nakamura, K., Zvaritch, E., Dickie, P., Dziak, E., Krause, K.-H., Opas, M., MacLennan, D.H., and Michalak, M. (1999). Calreticulin Is Essential for Cardiac Development. *The Journal of Cell Biology* 144, 857–868.
- Miedel, M.T., Rbaibi, Y., Guerriero, C.J., Colletti, G., Weixel, K.M., Weisz, O.A., and Kiselyov, K. (2008). Membrane traffic and turnover in TRP-ML1-deficient cells: a revised model for mucopolidosis type IV pathogenesis. *J Exp Med* 205, 1477–1490.
- Millet, J.K., and Whittaker, G.R. (2015). Host cell proteases: Critical determinants of coronavirus tropism and pathogenesis. *Virus Research* 202, 120–134.
- Milosevic, I., Giovedi, S., Lou, X., Raimondi, A., Collesi, C., Shen, H., Paradise, S., O'Toole, E., Ferguson, S., Cremona, O., et al. (2011). Recruitment of endophilin to clathrin coated pit necks is required for efficient vesicle uncoating after fission. *Neuron* 72, 587–601.

- Mindell, J.A. (2012). Lysosomal Acidification Mechanisms. *Annual Review of Physiology* 74, 69–86.
- Missiaen, L., Van Acker, K., Van Baelen, K., Raeymaekers, L., Wuytack, F., Parys, J.B., De Smedt, H., Vanoevelen, J., Dode, L., Rizzuto, R., et al. (2004). Calcium release from the Golgi apparatus and the endoplasmic reticulum in HeLa cells stably expressing targeted aequorin to these compartments. *Cell Calcium* 36, 479–487.
- Miyamae, Y., Nishito, Y., Nakai, N., Nagumo, Y., Usui, T., Masuda, S., Kambe, T., and Nagao, M. (2016). Tetrandrine induces lipid accumulation through blockade of autophagy in a hepatic stellate cell line. *Biochemical and Biophysical Research Communications* 477, 40–46.
- Miyawaki, A., Llopis, J., Heim, R., McCaffery, J.M., Adams, J.A., Ikura, M., and Tsien, R.Y. (1997). Fluorescent indicators for Ca<sup>2+</sup> based on green fluorescent proteins and calmodulin. *Nature* 388, 882–887.
- Morgan, A.J. (2011). Sea urchin eggs in the acid reign. *Cell Calcium* 50, 147–156.
- Morgan, A.J. (2016). Ca<sup>2+</sup> dialogue between acidic vesicles and ER. *Biochemical Society Transactions* 44, 546–553.
- Morgan, A.J., Platt, F.M., Lloyd-Evans, E., and Galione, A. (2011). Molecular mechanisms of endolysosomal Ca<sup>2+</sup> signalling in health and disease. *Biochemical Journal* 439, 349–378.
- Morgan, A.J., Davis, L.C., Wagner, S.K.T.Y., Lewis, A.M., Parrington, J., Churchill, G.C., and Galione, A. (2013). Bidirectional Ca<sup>2+</sup> signaling occurs between the endoplasmic reticulum and acidic organelles. *J Cell Biol* 200, 789–805.
- Morgan, N.V., Westaway, S.K., Morton, J.E.V., Gregory, A., Gissen, P., Sonek, S., Cangul, H., Coryell, J., Canham, N., Nardocci, N., et al. (2006). PLA2G6, encoding a phospholipase A2, is mutated in neurodegenerative disorders with high brain iron. *Nat Genet* 38, 752–754.
- Moriguchi, S., Nishi, M., Komazaki, S., Sakagami, H., Miyazaki, T., Masumiya, H., Saito, S., Watanabe, M., Kondo, H., Yawo, H., et al. (2006). Functional uncoupling between Ca<sup>2+</sup> release and afterhyperpolarization in mutant hippocampal neurons lacking junctophilins. *Proc Natl Acad Sci U S A* 103, 10811–10816.
- Mosharov, E.V., Staal, R.G.W., Bové, J., Prou, D., Hananiya, A., Markov, D., Poulsen, N., Larsen, K.E., Moore, C.M.H., Troyer, M.D., et al. (2006).  $\alpha$ -Synuclein Overexpression Increases Cytosolic Catecholamine Concentration. *J. Neurosci.* 26, 9304–9311.
- Mullock, B.M., Bright, N.A., Fearon, C.W., Gray, S.R., and Luzio, J. (1998). Fusion of Lysosomes with Late Endosomes Produces a Hybrid Organelle of Intermediate Density and Is NSF Dependent. *The Journal of Cell Biology* 140, 591–601.
- Munsie, L.N., Milnerwood, A.J., Seibler, P., Beccano-Kelly, D.A., Tatarnikov, I., Khinda, J., Volta, M., Kadgien, C., Cao, L.P., Tapia, L., et al. (2015). Retromer-dependent neurotransmitter receptor trafficking to synapses is altered by the Parkinson's disease VPS35 mutation p.D620N. *Hum Mol Genet* 24, 1691–1703.
- Murphy, K.E., Gysbers, A.M., Abbott, S.K., Tayebi, N., Kim, W.S., Sidransky, E., Cooper, A., Garner, B., and Halliday, G.M. (2014). Reduced glucocerebrosidase is associated with increased  $\alpha$ -synuclein in sporadic Parkinson's disease. *Brain* 137, 834–848.

- Mushtaq, M., Nam, T.-S., and Kim, U.-H. (2011). Critical Role for CD38-mediated Ca<sup>2+</sup> Signaling in Thrombin-induced Procoagulant Activity of Mouse Platelets and Hemostasis. *J Biol Chem* 286, 12952–12958.
- Nadanaciva, S., Lu, S., Gebhard, D.F., Jessen, B.A., Pennie, W.D., and Will, Y. (2011). A high content screening assay for identifying lysosomotropic compounds. *Toxicology in Vitro* 25, 715–723.
- Nalls, M.A., Pankratz, N., Lill, C.M., Do, C.B., Hernandez, D.G., Saad, M., DeStefano, A.L., Kara, E., Bras, J., Sharma, M., et al. (2014). Large-scale meta-analysis of genome-wide association data identifies six new risk loci for Parkinson's disease. *Nat Genet* 46, 989–993.
- Naon, D., Zaninello, M., Giacomello, M., Varanita, T., Grespi, F., Lakshminaranayan, S., Serafini, A., Semenzato, M., Herkenne, S., Hernández-Alvarez, M.I., et al. (2016). Critical reappraisal confirms that Mitofusin 2 is an endoplasmic reticulum–mitochondria tether. *PNAS* 113, 11249–11254.
- Naraghi, M. (1997). T-jump study of calcium binding kinetics of calcium chelators. *Cell Calcium* 22, 255–268.
- Naylor, E., Arredouani, A., Vasudevan, S.R., Lewis, A.M., Parkesh, R., Mizote, A., Rosen, D., Thomas, J.M., Izumi, M., Ganesan, A., et al. (2009). Identification of a chemical probe for NAADP by virtual screening. *Nat Chem Biol* 5, 220–226.
- Nebel, M., Schwoerer, A.P., Warszta, D., Siebrands, C.C., Limbrock, A.-C., Swarbrick, J.M., Fliegert, R., Weber, K., Bruhn, S., Hohenegger, M., et al. (2013). Nicotinic Acid Adenine Dinucleotide Phosphate (NAADP)-mediated Calcium Signaling and Arrhythmias in the Heart Evoked by  $\beta$ -Adrenergic Stimulation. *J. Biol. Chem.* 288, 16017–16030.
- Nichols, W.C., Pankratz, N., Marek, D.K., Pauciulo, M.W., Elsaesser, V.E., Halter, C.A., Rudolph, A., Wojcieszek, J., Pfeiffer, R.F., Foroud, T., et al. (2009). Mutations in GBA are associated with familial Parkinson disease susceptibility and age at onset. *Neurology* 72, 310–316.
- Nilius, B., and Owsianik, G. (2011). The transient receptor potential family of ion channels. *Genome Biol* 12, 218.
- Notomi, T., Ezura, Y., and Noda, M. (2012). Identification of two-pore channel 2 as a novel regulator of osteoclastogenesis. *J. Biol. Chem.* 287, 35057–35064.
- Onyenwoke, R.U., Sexton, J.Z., Yan, F., Díaz, M.C.H., Forsberg, L.J., Major, M.B., and Brenman, J.E. (2015). The mucopolidosis IV Ca<sup>2+</sup> channel TRPML1 (MCOLN1) is regulated by the TOR kinase. *Biochemical Journal* 470, 331–342.
- Ordonez, M.P., Roberts, E.A., Kidwell, C.U., Yuan, S.H., Plaisted, W.C., and Goldstein, L.S.B. (2012). Disruption and therapeutic rescue of autophagy in a human neuronal model of Niemann Pick type C1. *Hum Mol Genet* 21, 2651–2662.
- Orenstein, S.J., Kuo, S.-H., Tasset, I., Arias, E., Koga, H., Fernandez-Carasa, I., Cortes, E., Honig, L.S., Dauer, W., Consiglio, A., et al. (2013). Interplay of LRRK2 with chaperone-mediated autophagy. *Nat Neurosci* 16, 394–406.
- Oueslati, A., Fournier, M., and Lashuel, H.A. (2010). Chapter 7 - Role of post-translational modifications in modulating the structure, function and toxicity of  $\alpha$ -synuclein: Implications for Parkinson's disease pathogenesis and therapies. In *Progress in Brain Research*, A.B. and M.A. Cenci, ed. (Elsevier), pp. 115–145.

- Pacelli, C., Giguère, N., Bourque, M.-J., Lévesque, M., Slack, R.S., and Trudeau, L.-É. (2015). Elevated Mitochondrial Bioenergetics and Axonal Arborization Size Are Key Contributors to the Vulnerability of Dopamine Neurons. *Current Biology* 25, 2349–2360.
- Pacheco, C.D., Kunkel, R., and Lieberman, A.P. (2007). Autophagy in Niemann-Pick C disease is dependent upon Beclin-1 and responsive to lipid trafficking defects. *Hum. Mol. Genet.* 16, 1495–1503.
- Padamsey, Z., McGuinness, L., Bardo, S.J., Reinhart, M., Tong, R., Hedegaard, A., Hart, M.L., and Emptage, N.J. (2017). Activity-Dependent Exocytosis of Lysosomes Regulates the Structural Plasticity of Dendritic Spines. *Neuron* 93, 132–146.
- Pagliero, R.J., D’Astolfo, D.S., Lelieveld, D., Pratiwi, R.D., Aits, S., Jaattela, M., Martin, N.I., Klumperman, J., and Egan, D.A. (2016). Discovery of Small Molecules That Induce Lysosomal Cell Death in Cancer Cell Lines Using an Image-Based Screening Platform. *ASSAY and Drug Development Technologies* 14, 489–510.
- Paisan-Ruiz, C., Bhatia, K.P., Li, A., Hernandez, D., Davis, M., Wood, N.W., Hardy, J., Houlden, H., Singleton, A., and Schneider, S.A. (2009). Characterization of PLA2G6 as a locus for dystonia-parkinsonism. *Ann. Neurol.* 65, 19–23.
- Palma, F.D., Belyantseva, I.A., Kim, H.J., Vogt, T.F., Kachar, B., and Noben-Trauth, K. (2002). Mutations in Mcoln3 associated with deafness and pigmentation defects in varitint-waddler (Va) mice. *PNAS* 99, 14994–14999.
- Palty, R., Silverman, W.F., Hershinkel, M., Caporale, T., Sensi, S.L., Parnis, J., Nolte, C., Fishman, D., Shoshan-Barmatz, V., Herrmann, S., et al. (2010). NCLX is an essential component of mitochondrial Na<sup>+</sup>/Ca<sup>2+</sup> exchange. *PNAS* 107, 436–441.
- Pandey, V., Chuang, C.-C., Lewis, A.M., Aley, P.K., Brailoiu, E., Dun, N.J., Churchill, G.C., and Patel, S. (2009). Recruitment of NAADP-sensitive acidic Ca<sup>2+</sup> stores by glutamate. *Biochemical Journal* 422, 503–512.
- Pankratov, Y., and Lalo, U. (2014). Calcium permeability of ligand-gated Ca<sup>2+</sup> channels. *European Journal of Pharmacology* 739, 60–73.
- Papkovskaia, T.D., Chau, K.-Y., Inesta-Vaquera, F., Papkovsky, D.B., Healy, D.G., Nishio, K., Staddon, J., Duchen, M.R., Hardy, J., Schapira, A.H.V., et al. (2012). G2019S leucine-rich repeat kinase 2 causes uncoupling protein-mediated mitochondrial depolarization. *Hum Mol Genet* 21, 4201–4213.
- Parihar, M.S., Parihar, A., Fujita, M., Hashimoto, M., and Ghafourifar, P. (2008). Mitochondrial association of alpha-synuclein causes oxidative stress. *Cell. Mol. Life Sci.* 65, 1272–1284.
- Paris, I., Martinez-Alvarado, P., Cárdenas, S., Perez-Pastene, C., Graumann, R., Fuentes, P., Olea-Azar, C., Caviedes, P., and Segura-Aguilar, J. (2005). Dopamine-Dependent Iron Toxicity in Cells Derived from Rat Hypothalamus. *Chem. Res. Toxicol.* 18, 415–419.
- Parisiadou, L., Xie, C., Cho, H.J., Lin, X., Gu, X.-L., Long, C.-X., Lobbestael, E., Baekelandt, V., Taymans, J.-M., Sun, L., et al. (2009). Phosphorylation of ezrin/radixin/moesin proteins by LRRK2 promotes the rearrangement of actin cytoskeleton in neuronal morphogenesis. *J. Neurosci.* 29, 13971–13980.

- Park, D.-R., Shawl, A.I., Ha, T.-G., Park, K.-H., Kim, S.-Y., and Kim, U.-H. (2015). Arginine Thiiazolidine Carboxylate Stimulates Insulin Secretion through Production of Ca<sup>2+</sup>-Mobilizing Second Messengers NAADP and cADPR in Pancreatic Islets. *PLoS One* 10.
- Park, J.-S., Mehta, P., Cooper, A.A., Veivers, D., Heimbach, A., Stiller, B., Kubisch, C., Fung, V.S., Krainc, D., Mackay-Sim, A., et al. (2011). Pathogenic effects of novel mutations in the P-type ATPase ATP13A2 (PARK9) causing Kufor-Rakeb syndrome, a form of early-onset parkinsonism. *Hum. Mutat.* 32, 956–964.
- Park, S., Ahuja, M., Kim, M.S., Brailoiu, G.C., Jha, A., Zeng, M., Baydyuk, M., Wu, L.-G., Wassif, C.A., Porter, F.D., et al. (2016). Fusion of lysosomes with secretory organelles leads to uncontrolled exocytosis in the lysosomal storage disease mucopolipidosis type IV. *EMBO Rep.* 17, 266–278.
- Parker, I., and Yao, Y. (1996). Ca<sup>2+</sup> transients associated with openings of inositol trisphosphate-gated channels in *Xenopus* oocytes. *J Physiol* 491, 663–668.
- Parkinson-Lawrence, E.J., Shandala, T., Prodoehl, M., Plew, R., Borlace, G.N., and Brooks, D.A. (2010). Lysosomal Storage Disease: Revealing Lysosomal Function and Physiology. *Physiology* 25, 102–115.
- Pasternak, B., Svanström, H., Nielsen, N.M., Fugger, L., Melbye, M., and Hviid, A. (2012). Use of Calcium Channel Blockers and Parkinson's Disease. *Am J Epidemiol* 175, 627–635.
- Patel, S., and Cai, X. (2015). Evolution of acidic Ca<sup>2+</sup> stores and their resident Ca<sup>2+</sup>-permeable channels. *Cell Calcium* 57, 222–230.
- Patel, S., and Docampo, R. (2010). Acidic calcium stores open for business: expanding the potential for intracellular Ca<sup>2+</sup> signaling. *Trends Cell Biol.* 20, 277–286.
- Patterson, M.C., Vecchio, D., Prady, H., Abel, L., and Wraith, J.E. (2007). Miglustat for treatment of Niemann-Pick C disease: a randomised controlled study. *The Lancet Neurology* 6, 765–772.
- Penny, C.J., Kilpatrick, B.S., Han, J.M., Sneyd, J., and Patel, S. (2014). A computational model of lysosome–ER Ca<sup>2+</sup> microdomains. *J Cell Sci* 127, 2934–2943.
- Pereira, G.J.S., Hirata, H., Fimia, G.M., do Carmo, L.G., Bincoletto, C., Han, S.W., Stilhano, R.S., Ureshino, R.P., Bloor-Young, D., Churchill, G., et al. (2011). Nicotinic acid adenine dinucleotide phosphate (NAADP) regulates autophagy in cultured astrocytes. *J. Biol. Chem.* 286, 27875–27881.
- Pereira, G.J.S., Hirata, H., do Carmo, L.G., Stilhano, R.S., Ureshino, R.P., Medaglia, N.C., Han, S.W., Churchill, G., Bincoletto, C., Patel, S., et al. (2014). NAADP-sensitive two-pore channels are present and functional in gastric smooth muscle cells. *Cell Calcium* 56, 51–58.
- Pereira, G.J.S., Antonioli, M., Hirata, H., Ureshino, R.P., Nascimento, A.R., Bincoletto, C., Vescovo, T., Piacentini, M., Fimia, G.M., Smalli, S.S., et al. (2016). Glutamate induces autophagy via the two-pore channels in neural cells. *Oncotarget* 8, 12730–12740.
- Perez-Reyes, E. (2003). Molecular Physiology of Low-Voltage-Activated T-type Calcium Channels. *Physiological Reviews* 83, 117–161.
- Periasamy, M., and Kalyanasundaram, A. (2007). SERCA pump isoforms: Their role in calcium transport and disease. *Muscle Nerve* 35, 430–442.

- Peters, J.-U. (2013). Polypharmacology – Foe or Friend? *J. Med. Chem.* *56*, 8955–8971.
- Peters, C., and Mayer, A. (1998). Ca<sup>2+</sup>/calmodulin signals the completion of docking and triggers a late step of vacuole fusion. *Nature* *396*, 575–580.
- Philippart, F., Destreel, G., Merino-Sepúlveda, P., Henny, P., Engel, D., and Seutin, V. (2016). Differential Somatic Ca<sup>2+</sup> Channel Profile in Midbrain Dopaminergic Neurons. *J. Neurosci.* *36*, 7234–7245.
- Phillips, M.J., and Voeltz, G.K. (2016). Structure and function of ER membrane contact sites with other organelles. *Nat Rev Mol Cell Biol* *17*, 69–82.
- Piccoli, G., Condliffe, S.B., Bauer, M., Giesert, F., Boldt, K., De Astis, S., Meixner, A., Sarioglu, H., Vogt-Weisenhorn, D.M., Wurst, W., et al. (2011). LRRK2 controls synaptic vesicle storage and mobilization within the recycling pool. *J. Neurosci.* *31*, 2225–2237.
- Pickrell, A.M., and Youle, R.J. (2015). The Roles of PINK1, Parkin, and Mitochondrial Fidelity in Parkinson’s Disease. *Neuron* *85*, 257–273.
- Piiper, A., Stryjek-Kaminska, D., Stein, J., Caspary, W.F., and Zeuzem, S. (1994). Tyrphostins inhibit secretagogue-induced 1,4,5-IP<sub>3</sub> production and amylase release in pancreatic acini. *American Journal of Physiology - Gastrointestinal and Liver Physiology* *266*, G363–G371.
- Pinton, P., Pozzan, T., and Rizzuto, R. (1998). The Golgi apparatus is an inositol 1,4,5-trisphosphate-sensitive Ca<sup>2+</sup> store, with functional properties distinct from those of the endoplasmic reticulum. *The EMBO Journal* *17*, 5298–5308.
- Pitt, S.J., Funnell, T.M., Sitsapesan, M., Venturi, E., Rietdorf, K., Ruas, M., Ganesan, A., Gosain, R., Churchill, G.C., Zhu, M.X., et al. (2010). TPC2 Is a Novel NAADP-sensitive Ca<sup>2+</sup> Release Channel, Operating as a Dual Sensor of Luminal pH and Ca<sup>2+</sup>. *J Biol Chem* *285*, 35039–35046.
- Pitt, S.J., Lam, A.K.M., Rietdorf, K., Galione, A., and Sitsapesan, R. (2014). Reconstituted human TPC1 is a proton-permeable ion channel and is activated by NAADP or Ca<sup>2+</sup>. *Sci Signal* *7*, ra46.
- Pitt, S.J., Reilly-O’Donnell, B., and Sitsapesan, R. (2016). Exploring the biophysical evidence that mammalian two-pore channels are NAADP-activated calcium-permeable channels. *J Physiol* *594*, 4171–4179.
- Pittman, J.K. (2011). Vacuolar Ca<sup>2+</sup> uptake. *Cell Calcium* *50*, 139–146.
- Plowey, E.D., Cherra, S.J., Liu, Y.-J., and Chu, C.T. (2008). Role of autophagy in G2019S-LRRK2-associated neurite shortening in differentiated SH-SY5Y cells. *J Neurochem* *105*, 1048–1056.
- Plun-Favreau, H., Klupsch, K., Moiso, N., Gandhi, S., Kjaer, S., Frith, D., Harvey, K., Deas, E., Harvey, R.J., McDonald, N., et al. (2007). The mitochondrial protease HtrA2 is regulated by Parkinson’s disease-associated kinase PINK1. *Nat Cell Biol* *9*, 1243–1252.
- Polymeropoulos, M.H., Lavedan, C., Leroy, E., Ide, S.E., Dehejia, A., Dutra, A., Pike, B., Root, H., Rubenstein, J., Boyer, R., et al. (1997). Mutation in the  $\alpha$ -Synuclein Gene Identified in Families with Parkinson’s Disease. *Science* *276*, 2045–2047.
- Popoff, V., Mardones, G.A., Bai, S.-K., Chambon, V., Tenza, D., Burgos, P.V., Shi, A., Benaroch, P., Urbé, S., Lamaze, C., et al. (2009). Analysis of articulation between clathrin and retromer in retrograde sorting on early endosomes. *Traffic* *10*, 1868–1880.

- Porras, P., Duesbury, M., Fabregat, A., Ueffing, M., Orchard, S., Gloeckner, C.J., and Hermjakob, H. (2015). A visual review of the interactome of LRRK2: Using deep-curated molecular interaction data to represent biology. *Proteomics* 15, 1390–1404.
- Poteser, M., Schleifer, H., Lichtenegger, M., Schernthaner, M., Stockner, T., Kappe, C.O., Glasnov, T.N., Romanin, C., and Groschner, K. (2011). PKC-dependent coupling of calcium permeation through transient receptor potential canonical 3 (TRPC3) to calcineurin signaling in HL-1 myocytes. *PNAS* 108, 10556–10561.
- Poulopoulos, M., Levy, O., and Alcalay, R. (2012). The Neuropathology of Genetic Parkinson's Disease. *Mov Disord* 27, 831–842.
- Pringsheim, T., Jette, N., Frolkis, A., and Steeves, T.D.L. (2014). The prevalence of Parkinson's disease: A systematic review and meta-analysis. *Movement Disorders* 29, 1583–1590.
- Prinz, W.A. (2014). Bridging the gap: Membrane contact sites in signaling, metabolism, and organelle dynamics. *J Cell Biol* 205, 759–769.
- Pryor, P.R., Mullock, B.M., Bright, N.A., Gray, S.R., and Luzio, J.P. (2000). The Role of Intraorganellar Ca<sup>2+</sup>In Late Endosome–Lysosome Heterotypic Fusion and in the Reformation of Lysosomes from Hybrid Organelles. *J Cell Biol* 149, 1053–1062.
- Pryor, P.R., Mullock, B.M., Bright, N.A., Lindsay, M.R., Gray, S.R., Richardson, S.C.W., Stewart, A., James, D.E., Piper, R.C., and Luzio, J.P. (2004). Combinatorial SNARE complexes with VAMP7 or VAMP8 define different late endocytic fusion events. *EMBO Rep* 5, 590–595.
- Pryor, P.R., Reimann, F., Gribble, F.M., and Luzio, J.P. (2006). Mucolipin-1 Is a Lysosomal Membrane Protein Required for Intracellular Lactosylceramide Traffic. *Traffic* 7, 1388–1398.
- Qiu, W., Su, M., Xie, F., Ai, J., Ren, Y., Zhang, J., Guan, R., He, W., Gong, Y., and Guo, Y. (2014). Tetrandrine blocks autophagic flux and induces apoptosis via energetic impairment in cancer cells. *Cell Death Dis* 5, e1123.
- Quadri, M., Fang, M., Picillo, M., Olgiati, S., Breedveld, G.J., Graafland, J., Wu, B., Xu, F., Erro, R., Amboni, M., et al. (2013). Mutation in the SYNJ1 gene associated with autosomal recessive, early-onset Parkinsonism. *Hum. Mutat.* 34, 1208–1215.
- Rah, S.-Y., Mushtaq, M., Nam, T.-S., Kim, S.H., and Kim, U.-H. (2010). Generation of Cyclic ADP-ribose and Nicotinic Acid Adenine Dinucleotide Phosphate by CD38 for Ca<sup>2+</sup> Signaling in Interleukin-8-treated Lymphokine-activated Killer Cells. *J Biol Chem* 285, 21877–21887.
- Rahman, T., Cai, X., Brailoiu, G.C., Abood, M.E., Brailoiu, E., and Patel, S. (2014). Two-pore channels provide insight into the evolution of voltage-gated Ca<sup>2+</sup> and Na<sup>+</sup> channels. *Sci. Signal.* 7, ra109-ra109.
- Raiborg, C., Wenzel, E.M., Pedersen, N.M., Olsvik, H., Schink, K.O., Schultz, S.W., Vietri, M., Nisi, V., Bucci, C., Brech, A., et al. (2015). Repeated ER–endosome contacts promote endosome translocation and neurite outgrowth. *Nature* 520, 234–238.
- Ramirez, A., Heimbach, A., Gründemann, J., Stiller, B., Hampshire, D., Cid, L.P., Goebel, I., Mubaidin, A.F., Wriekat, A.-L., Roeper, J., et al. (2006). Hereditary parkinsonism with dementia is caused by mutations in ATP13A2, encoding a lysosomal type 5 P-type ATPase. *Nat Genet* 38, 1184–1191.

- Ramírez-Valle, F., Braunstein, S., Zavadil, J., Formenti, S.C., and Schneider, R.J. (2008). eIF4GI links nutrient sensing by mTOR to cell proliferation and inhibition of autophagy. *J Cell Biol* *181*, 293–307.
- Ramonet, D., Podhajska, A., Stafa, K., Sonnay, S., Trancikova, A., Tsika, E., Pletnikova, O., Troncoso, J.C., Glauser, L., and Moore, D.J. (2012). PARK9-associated ATP13A2 localizes to intracellular acidic vesicles and regulates cation homeostasis and neuronal integrity. *Hum Mol Genet* *21*, 1725–1743.
- Raychowdhury, M.K., González-Perrett, S., Montalbetti, N., Timpanaro, G.A., Chasan, B., Goldmann, W.H., Stahl, S., Cooney, A., Goldin, E., and Cantiello, H.F. (2004). Molecular pathophysiology of mucopolidosis type IV: pH dysregulation of the mucolipin-1 cation channel. *Hum. Mol. Genet.* *13*, 617–627.
- Reddy, A., Caler, E.V., and Andrews, N.W. (2001). Plasma Membrane Repair Is Mediated by Ca<sup>2+</sup>-Regulated Exocytosis of Lysosomes. *Cell* *106*, 157–169.
- Reeve, A., Simcox, E., and Turnbull, D. (2014). Ageing and Parkinson's disease: Why is advancing age the biggest risk factor? *Ageing Res Rev* *14*, 19–30.
- Reeve, H. I., Vaughan, P.F.T., and Peers, C. (1995). Inhibition of N-type Ca<sup>2+</sup> channel currents in human neuroblastoma (SH-SY5Y) cells by muscarine via stimulation of M3 receptors. *Neuropharmacology* *34*, 319–326.
- Reinhardt, P., Schmid, B., Burbulla, L.F., Schöndorf, D.C., Wagner, L., Glatza, M., Höing, S., Hargus, G., Heck, S.A., Dhingra, A., et al. (2013). Genetic Correction of a LRRK2 Mutation in Human iPSCs Links Parkinsonian Neurodegeneration to ERK-Dependent Changes in Gene Expression. *Cell Stem Cell* *12*, 354–367.
- Rietdorf, K., Funnell, T.M., Ruas, M., Heinemann, J., Parrington, J., and Galione, A. (2011). Two-pore Channels Form Homo- and Heterodimers. *J. Biol. Chem.* *286*, 37058–37062.
- Ring, A., Strom, B.O., Turner, S.R., Timperley, C.M., Bird, M., Green, A.C., Chad, J.E., Worek, F., and Tattersall, J.E.H. (2015). Bispyridinium Compounds Inhibit Both Muscle and Neuronal Nicotinic Acetylcholine Receptors in Human Cell Lines. *PLOS ONE* *10*, e0135811.
- Rink, J., Ghigo, E., Kalaidzidis, Y., and Zerial, M. (2005). Rab conversion as a mechanism of progression from early to late endosomes. *Cell* *122*, 735–749.
- Rizk, A., Paul, G., Incardona, P., Bugarski, M., Mansouri, M., Niemann, A., Ziegler, U., Berger, P., and Sbalzarini, I.F. (2014). Segmentation and quantification of subcellular structures in fluorescence microscopy images using Squassh. *Nat. Protocols* *9*, 586–596.
- Rizzuto, R., De Stefani, D., Raffaello, A., and Mammucari, C. (2012). Mitochondria as sensors and regulators of calcium signalling. *Nat Rev Mol Cell Biol* *13*, 566–578.
- Robbins, E., Levine, E.M., and Eagle, H. (1970). Morphologic changes accompanying senescence of cultured human diploid cells. *J. Exp. Med.* *131*, 1211–1222.
- Rocha, N., Kuijl, C., van der Kant, R., Janssen, L., Houben, D., Janssen, H., Zwart, W., and Neefjes, J. (2009). Cholesterol sensor ORP1L contacts the ER protein VAP to control Rab7-RILP-p150 Glued and late endosome positioning. *J. Cell Biol.* *185*, 1209–1225.



- Roderick, H.L., Lechleiter, J.D., and Camacho, P. (2000). Cytosolic Phosphorylation of Calnexin Controls Intracellular Ca<sup>2+</sup> Oscillations via an Interaction with Serca2b. *The Journal of Cell Biology* *149*, 1235–1248.
- Rohacs, T. (2013). Regulation of Transient Receptor Potential channels by the phospholipase C pathway. *Adv Biol Regul* *53*, 341–355.
- Ron, I., and Horowitz, M. (2005). ER retention and degradation as the molecular basis underlying Gaucher disease heterogeneity. *Hum Mol Genet* *14*, 2387–2398.
- Rosenbaum, A.I., and Maxfield, F.R. (2011). Niemann-Pick type C disease: molecular mechanisms and potential therapeutic approaches. *J Neurochem* *116*, 789–795.
- Roskoski Jr., R. (2007). Sunitinib: A VEGF and PDGF receptor protein kinase and angiogenesis inhibitor. *Biochemical and Biophysical Research Communications* *356*, 323–328.
- Rott, R., Szargel, R., Haskin, J., Bandopadhyay, R., Lees, A.J., Shani, V., and Engelender, S. (2011).  $\alpha$ -Synuclein fate is determined by USP9X-regulated monoubiquitination. *Proc Natl Acad Sci U S A* *108*, 18666–18671.
- Ruas, M., Rietdorf, K., Arredouani, A., Davis, L.C., Lloyd-Evans, E., Koegel, H., Funnell, T.M., Morgan, A.J., Ward, J.A., Watanabe, K., et al. (2010). Purified TPC Isoforms Form NAADP Receptors with Distinct Roles for Ca<sup>2+</sup> Signaling and Endolysosomal Trafficking. *Current Biology* *20*, 703–709.
- Ruas, M., Chuang, K.-T., Davis, L.C., Al-Douri, A., Tynan, P.W., Tunn, R., Teboul, L., Galione, A., and Parrington, J. (2014). TPC1 Has Two Variant Isoforms, and Their Removal Has Different Effects on Endo-Lysosomal Functions Compared to Loss of TPC2. *Mol. Cell. Biol.* *34*, 3981–3992.
- Ruas, M., Davis, L.C., Chen, C.-C., Morgan, A.J., Chuang, K.-T., Walseth, T.F., Grimm, C., Garnham, C., Powell, T., Platt, N., et al. (2015). Expression of Ca<sup>2+</sup>-permeable two-pore channels rescues NAADP signalling in TPC-deficient cells. *EMBO J.* *34*, 1743–1758.
- Rutkowski, D.T., and Kaufman, R.J. (2004). A trip to the ER: coping with stress. *Trends in Cell Biology* *14*, 20–28.
- Rybalchenko, V., Ahuja, M., Coblentz, J., Churamani, D., Patel, S., Kiselyov, K., and Muallem, S. (2012). Membrane Potential Regulates Nicotinic Acid Adenine Dinucleotide Phosphate (NAADP) Dependence of the pH- and Ca<sup>2+</sup>-sensitive Organellar Two-pore Channel TPC1. *J Biol Chem* *287*, 20407–20416.
- Sah, D.W., and Bean, B.P. (1994). Inhibition of P-type and N-type calcium channels by dopamine receptor antagonists. *Mol Pharmacol* *45*, 84–92.
- Sakurai, Y., Kolokoltsov, A.A., Chen, C.-C., Tidwell, M.W., Bauta, W.E., Klugbauer, N., Grimm, C., Wahl-Schott, C., Biel, M., and Davey, R.A. (2015). Two pore channels control Ebolavirus host cell entry and are drug targets for disease treatment. *Science* *347*, 995–998.
- Samie, M., Wang, X., Zhang, X., Goschka, A., Li, X., Cheng, X., Gregg, E., Azar, M., Zhuo, Y., Garrity, A.G., et al. (2013). A TRP channel in the lysosome regulates large particle phagocytosis via focal exocytosis. *Dev. Cell* *26*, 511–524.
- Sampson, T.R., Debelius, J.W., Thron, T., Janssen, S., Shastri, G.G., Ilhan, Z.E., Challis, C., Schretter, C.E., Rocha, S., Gradinaru, V., et al. (2016). Gut Microbiota Regulate Motor Deficits and Neuroinflammation in a Model of Parkinson's Disease. *Cell* *167*, 1469–1480.e12.

- Sánchez-Danés, A., Richaud-Patin, Y., Carballo-Carbajal, I., Jiménez-Delgado, S., Caig, C., Mora, S., Di Guglielmo, C., Ezquerra, M., Patel, B., Giralt, A., et al. (2012). Disease-specific phenotypes in dopamine neurons from human iPS-based models of genetic and sporadic Parkinson's disease. *EMBO Molecular Medicine* 4, 380–395.
- Sanchez-Padilla, J., Guzman, J.N., Ilijic, E., Kondapalli, J., Galtieri, D.J., Yang, B., Schieber, S., Oertel, W., Wokosin, D., Schumacker, P.T., et al. (2014). Mitochondrial oxidant stress in locus coeruleus is regulated by activity and nitric oxide synthase. *Nat Neurosci* 17, 832–840.
- Sancho, R.M., Law, B.M.H., and Harvey, K. (2009). Mutations in the LRRK2 Roc-COR tandem domain link Parkinson's disease to Wnt signalling pathways. *Hum. Mol. Genet.* 18, 3955–3968.
- Sano, O., Kazetani, K., Funata, M., Fukuda, Y., Matsui, J., and Iwata, H. (2016). Vacuolin-1 inhibits autophagy by impairing lysosomal maturation via PIKfyve inhibition. *FEBS Lett* 590, 1576–1585.
- Sarkar, S., Carroll, B., Buganim, Y., Maetzel, D., Ng, A.H.M., Cassady, J.P., Cohen, M.A., Chakraborty, S., Wang, H., Spooner, E., et al. (2013). Impaired autophagy in the lipid-storage disorder Niemann-Pick type C1 disease. *Cell Rep* 5, 1302–1315.
- Schieder, M., Rötzer, K., Brüggemann, A., Biel, M., and Wahl-Schott, C.A. (2010). Characterization of Two-pore Channel 2 (TPCN2)-mediated Ca<sup>2+</sup> Currents in Isolated Lysosomes. *J. Biol. Chem.* 285, 21219–21222.
- Schöndorf, D.C., Aureli, M., McAllister, F.E., Hindley, C.J., Mayer, F., Schmid, B., Sardi, S.P., Valsecchi, M., Hoffmann, S., Schwarz, L.K., et al. (2014). iPSC-derived neurons from GBA1-associated Parkinson's disease patients show autophagic defects and impaired calcium homeostasis. *Nat Commun* 5, 4028.
- Schulz, C., Paus, M., Frey, K., Schmid, R., Kohl, Z., Mennerich, D., Winkler, J., and Gillardon, F. (2011). Leucine-Rich Repeat Kinase 2 Modulates Retinoic Acid-Induced Neuronal Differentiation of Murine Embryonic Stem Cells. *PLOS ONE* 6, e20820.
- Schulze, R.J., Weller, S.G., Schroeder, B., Krueger, E.W., Chi, S., Casey, C.A., and McNiven, M.A. (2013). Lipid droplet breakdown requires Dynamin 2 for vesiculation of autolysosomal tubules in hepatocytes. *J Cell Biol* 203, 315–326.
- Schwaller, B. (2010). Cytosolic Ca<sup>2+</sup> Buffers. *Cold Spring Harb Perspect Biol* 2, a004051.
- Seo, I., Jha, B.K., Lim, J.-G., Suh, S.-I., Suh, M.-H., and Baek, W.-K. (2014). Identification of lysosomotropic compounds based on the distribution and size of lysosomes. *Biochemical and Biophysical Research Communications* 450, 189–194.
- Seo, M.-D., Velamakanni, S., Ishiyama, N., Stathopoulos, P.B., Rossi, A.M., Khan, S.A., Dale, P., Li, C., Ames, J.B., Ikura, M., et al. (2012). Structural and functional conservation of key domains in InsP3 and ryanodine receptors. *Nature* 483, 108–112.
- Setsuie, R., and Wada, K. (2007). The functions of UCH-L1 and its relation to neurodegenerative diseases. *Neurochemistry International* 51, 105–111.
- Sezgin, M., and Sankur, B. (2004). Survey over image thresholding techniques and quantitative performance evaluation. *Journal of Electronic Imaging* 13, 146–165.
- Shao, J., Fu, Z., Ji, Y., Guan, X., Guo, S., Ding, Z., Yang, X., Cong, Y., and Shen, Y. (2016). Leucine zipper-EF-hand containing transmembrane protein 1 (LETM1) forms a Ca<sup>2+</sup>/H<sup>+</sup> antiporter. *Sci Rep* 6.

- Shawl, A.I., Park, K.-H., and Kim, U.-H. (2009). Insulin receptor signaling for the proliferation of pancreatic  $\beta$ -cells: Involvement of  $\text{Ca}^{2+}$  second messengers, IP<sub>3</sub>, NAADP and cADPR. *Islets* *1*, 216–223.
- Shawl, A.I., Park, K.-H., Kim, B.-J., Higashida, C., Higashida, H., and Kim, U.-H. (2012). Involvement of actin filament in the generation of  $\text{Ca}^{2+}$  mobilizing messengers in glucose-induced  $\text{Ca}^{2+}$  signaling in pancreatic  $\beta$ -cells. *Islets* *4*, 145–151.
- Shen, D., Wang, X., Li, X., Zhang, X., Yao, Z., Dibble, S., Dong, X., Yu, T., Lieberman, A.P., Showalter, H.D., et al. (2012). Lipid storage disorders block lysosomal trafficking by inhibiting a TRP channel and lysosomal calcium release. *Nat Commun* *3*, 731.
- Shen, W.-W., Frieden, M., and Demaurex, N. (2011). Remodelling of the endoplasmic reticulum during store-operated calcium entry. *Biology of the Cell* *103*, 365–380.
- Shi, B., Bhat, G., Mahesh, V.B., Brotto, M., Nosek, T.M., and Brann, D.W. (1999). Bradykinin Receptor Localization and Cell Signaling Pathways Used by Bradykinin in the Regulation of Gonadotropin-Releasing Hormone Secretion. *Endocrinology* *140*, 4669–4676.
- Shin, D.M., Dehoff, M., Luo, X., Kang, S.H., Tu, J., Nayak, S.K., Ross, E.M., Worley, P.F., and Muallem, S. (2003). Homer 2 tunes G protein-coupled receptors stimulus intensity by regulating RGS proteins and PLC $\beta$  GAP activities. *J Cell Biol* *162*, 293–303.
- Shin, N., Jeong, H., Kwon, J., Heo, H.Y., Kwon, J.J., Yun, H.J., Kim, C.-H., Han, B.S., Tong, Y., Shen, J., et al. (2008). LRRK2 regulates synaptic vesicle endocytosis. *Exp. Cell Res.* *314*, 2055–2065.
- Sidransky, E., Nalls, M.A., Aasly, J.O., Aharon-Peretz, J., Annesi, G., Barbosa, E.R., Bar-Shira, A., Berg, D., Bras, J., Brice, A., et al. (2009). Multi-center analysis of glucocerebrosidase mutations in Parkinson disease. *N Engl J Med* *361*, 1651–1661.
- Simms, B.A., and Zamponi, G.W. (2014). Neuronal Voltage-Gated Calcium Channels: Structure, Function, and Dysfunction. *Neuron* *82*, 24–45.
- Singh, A., Gebhart, M., Fritsch, R., Sinnegger-Brauns, M.J., Poggiani, C., Hoda, J.-C., Engel, J., Romanin, C., Striessnig, J., and Koschak, A. (2008). Modulation of Voltage- and  $\text{Ca}^{2+}$ -dependent Gating of  $\text{Ca}_v1.3$  L-type Calcium Channels by Alternative Splicing of a C-terminal Regulatory Domain. *J Biol Chem* *283*, 20733–20744.
- Sleat, D.E., Wiseman, J.A., El-Banna, M., Price, S.M., Verot, L., Shen, M.M., Tint, G.S., Vanier, M.T., Walkley, S.U., and Lobel, P. (2004). Genetic evidence for nonredundant functional cooperativity between NPC1 and NPC2 in lipid transport. *PNAS* *101*, 5886–5891.
- Smedler, E., and Uhlén, P. (2014). Frequency decoding of calcium oscillations. *Biochimica et Biophysica Acta (BBA) - General Subjects* *1840*, 964–969.
- Smith, I.F., Wiltgen, S.M., and Parker, I. (2009). Localization of puff sites adjacent to the plasma membrane: Functional and spatial characterization of  $\text{Ca}^{2+}$  signaling in SH-SY5Y cells utilizing membrane-permeant caged IP<sub>3</sub>. *Cell Calcium* *45*, 65–76.
- Soares, S., Thompson, M., White, T., Isbell, A., Yamasaki, M., Prakash, Y., Lund, F.E., Galione, A., and Chini, E.N. (2007). NAADP as a second messenger: neither CD38 nor base-exchange reaction are necessary for in vivo generation of NAADP in myometrial cells. *American Journal of Physiology - Cell Physiology* *292*, C227–C239.

- Sobo, K., Blanc, I.L., Luyet, P.-P., Fivaz, M., Ferguson, C., Parton, R.G., Gruenberg, J., and Goot, F.G. van der (2007). Late Endosomal Cholesterol Accumulation Leads to Impaired Intra-Endosomal Trafficking. *PLOS ONE* 2, e851.
- Song, E.-K., Lee, Y.-R., Kim, Y.-R., Yeom, J.-H., Yoo, C.-H., Kim, H.-K., Park, H.-M., Kang, H.-S., Kim, J.-S., Kim, U.-H., et al. (2012). NAADP Mediates Insulin-Stimulated Glucose Uptake and Insulin Sensitization by PPAR $\gamma$  in Adipocytes. *Cell Reports* 2, 1607–1619.
- Sousa, S.R., Vetter, I., Ragnarsson, L., and Lewis, R.J. (2013). Expression and Pharmacology of Endogenous Cav Channels in SH-SY5Y Human Neuroblastoma Cells. *PLoS One* 8.
- Soyombo, A.A., Tjon-Kon-Sang, S., Rbaibi, Y., Bashllari, E., Bisceglia, J., Muallem, S., and Kiselyov, K. (2006). TRP-ML1 Regulates Lysosomal pH and Acidic Lysosomal Lipid Hydrolytic Activity. *J. Biol. Chem.* 281, 7294–7301.
- Speak, A.O., te Vruchte, D., Davis, L.C., Morgan, A.J., Smith, D.A., Yanjanin, N.M., Simmons, L., Hartung, R., Runz, H., Mengel, E., et al. (2014). Altered distribution and function of natural killer cells in murine and human Niemann-Pick disease type C1. *Blood* 123, 51–60.
- Spillantini, M.G., Schmidt, M.L., Lee, V.M.-Y., Trojanowski, J.Q., Jakes, R., and Goedert, M. (1997).  $\alpha$ -Synuclein in Lewy bodies. *Nature* 388, 839–840.
- Spillantini, M.G., Crowther, R.A., Jakes, R., Hasegawa, M., and Goedert, M. (1998).  $\alpha$ -Synuclein in filamentous inclusions of Lewy bodies from Parkinson's disease and dementia with Lewy bodies. *Proc Natl Acad Sci U S A* 95, 6469–6473.
- Sreetama, S.C., Takano, T., Nedergaard, M., Simon, S.M., and Jaiswal, J.K. (2016). Injured astrocytes are repaired by Synaptotagmin XI-regulated lysosome exocytosis. *Cell Death Differ* 23, 596–607.
- Stathopoulos, P.B., Zheng, L., Li, G.-Y., Plevin, M.J., and Ikura, M. (2008). Structural and Mechanistic Insights into STIM1-Mediated Initiation of Store-Operated Calcium Entry. *Cell* 135, 110–122.
- Stefanis, L., Larsen, K.E., Rideout, H.J., Sulzer, D., and Greene, L.A. (2001). Expression of A53T Mutant But Not Wild-Type  $\alpha$ -Synuclein in PC12 Cells Induces Alterations of the Ubiquitin-Dependent Degradation System, Loss of Dopamine Release, and Autophagic Cell Death. *J. Neurosci.* 21, 9549–9560.
- Steger, M., Tonelli, F., Ito, G., Davies, P., Trost, M., Vetter, M., Wachter, S., Lorentzen, E., Duddy, G., Wilson, S., et al. (2016). Phosphoproteomics reveals that Parkinson's disease kinase LRRK2 regulates a subset of Rab GTPases. *eLife* 5, e12813.
- Stern, G. (2014). Niemann–Pick's and Gaucher's diseases. *Parkinsonism & Related Disorders* 20, Supplement 1, S143–S146.
- Storch, J., and Xu, Z. (2009). Niemann-Pick C2 (NPC2) and intracellular cholesterol trafficking. *Biochim. Biophys. Acta* 1791, 671–678.
- Strauss, K.M., Martins, L.M., Plun-Favreau, H., Marx, F.P., Kautzmann, S., Berg, D., Gasser, T., Wszolek, Z., Müller, T., Bornemann, A., et al. (2005). Loss of function mutations in the gene encoding Omi/HtrA2 in Parkinson's disease. *Hum Mol Genet* 14, 2099–2111.

- Strokin, M., Seburn, K.L., Cox, G.A., Martens, K.A., and Reiser, G. (2012). Severe disturbance in the Ca<sup>2+</sup> signaling in astrocytes from mouse models of human infantile neuroaxonal dystrophy with mutated Pla2g6. *Hum Mol Genet* 21, 2807–2814.
- Strübing, C., Krapivinsky, G., Krapivinsky, L., and Clapham, D.E. (2003). Formation of Novel TRPC Channels by Complex Subunit Interactions in Embryonic Brain. *J. Biol. Chem.* 278, 39014–39019.
- Sugiura, A., McLelland, G.-L., Fon, E.A., and McBride, H.M. (2014). A new pathway for mitochondrial quality control: mitochondrial-derived vesicles. *The EMBO Journal* 33, 2142–2156.
- Suh, B.-C., and Hille, B. (2005). Regulation of ion channels by phosphatidylinositol 4,5-bisphosphate. *Current Opinion in Neurobiology* 15, 370–378.
- Sulzer, D., and Surmeier, D.J. (2013). Neuronal vulnerability, pathogenesis and Parkinson's disease. *Mov Disord* 28, 41–50.
- Sun, M., Goldin, E., Stahl, S., Falardeau, J.L., Kennedy, J.C., Acierno, J.S., Bove, C., Kaneski, C.R., Nagle, J., Bromley, M.C., et al. (2000). Mucopolidosis type IV is caused by mutations in a gene encoding a novel transient receptor potential channel. *Hum. Mol. Genet.* 9, 2471–2478.
- Sun, Y., Zhang, H., Selvaraj, S., Sukumaran, P., Lei, S., Birnbaumer, L., and Singh, B.B. (2017). Inhibition of L-Type Ca<sup>2+</sup> Channels by TRPC1-STIM1 Complex Is Essential for the Protection of Dopaminergic Neurons. *J. Neurosci.* 37, 3364–3377.
- Surmeier, D.J., Schumacker, P.T., Guzman, J.D., Ilijic, E., Yang, B., and Zampese, E. (2017a). Calcium and Parkinson's disease. *Biochemical and Biophysical Research Communications* 483, 1013–1019.
- Surmeier, D.J., Obeso, J.A., and Halliday, G.M. (2017b). Selective neuronal vulnerability in Parkinson disease. *Nat Rev Neurosci* 18, 101–113.
- Suzuki, J., Kanemaru, K., Ishii, K., Ohkura, M., Okubo, Y., and Iino, M. (2014). Imaging intraorganelle Ca<sup>2+</sup> at subcellular resolution using CEPIA. *Nature Communications* 5, 4153.
- Svobodova, B., and Groschner, K. (2016). Mechanisms of lipid regulation and lipid gating in TRPC channels. *Cell Calcium* 59, 271–279.
- Szabadkai, G., Bianchi, K., Várnai, P., De Stefani, D., Wieckowski, M.R., Cavagna, D., Nagy, A.I., Balla, T., and Rizzuto, R. (2006). Chaperone-mediated coupling of endoplasmic reticulum and mitochondrial Ca<sup>2+</sup> channels. *J Cell Biol* 175, 901–911.
- Szalai, G., Csordás, G., Hantash, B.M., Thomas, A.P., and Hajnóczky, G. (2000). Calcium Signal Transmission between Ryanodine Receptors and Mitochondria. *J. Biol. Chem.* 275, 15305–15313.
- Tamari, F., Chen, F.W., Li, C., Chaudhari, J., and Ioannou, Y.A. (2013). PKC Activation in Niemann Pick C1 Cells Restores Subcellular Cholesterol Transport. *PLoS One* 8.
- Tang, F.-L., Erion, J.R., Tian, Y., Liu, W., Yin, D.-M., Ye, J., Tang, B., Mei, L., and Xiong, W.-C. (2015). VPS35 in Dopamine Neurons Is Required for Endosome-to-Golgi Retrieval of Lamp2a, a Receptor of Chaperone-Mediated Autophagy That Is Critical for  $\alpha$ -Synuclein Degradation and Prevention of Pathogenesis of Parkinson's Disease. *J. Neurosci.* 35, 10613–10628.

- Taylor, C.W., and Tovey, S.C. (2010). IP3 Receptors: Toward Understanding Their Activation. *Cold Spring Harb Perspect Biol* 2, a004010.
- Taymans, J.-M. (2012). The GTPase function of LRRK2. *Biochemical Society Transactions* 40, 1063–1069.
- Teixeira, F.R., Randle, S.J., Patel, S.P., Mevissen, T.E.T., Zenkeviciute, G., Koide, T., Komander, D., and Laman, H. (2016). Gsk3 $\beta$  and Tomm20 are substrates of the SCFFbxo7/PARK15 ubiquitin ligase associated with Parkinson's disease. *Biochemical Journal* 473, 3563–3580.
- Thai, T.L., Churchill, G.C., and Arendshorst, W.J. (2009). NAADP receptors mediate calcium signaling stimulated by endothelin-1 and norepinephrine in renal afferent arterioles. *Am J Physiol Renal Physiol* 297, F510–F516.
- Thastrup, O., Cullen, P.J., Drøbak, B.K., Hanley, M.R., and Dawson, A.P. (1990). Thapsigargin, a tumor promoter, discharges intracellular Ca<sup>2+</sup> stores by specific inhibition of the endoplasmic reticulum Ca<sup>2+</sup>(+)-ATPase. *Proc Natl Acad Sci U S A* 87, 2466–2470.
- Thomas, A.P. (2000). Sharing calcium opens new avenues of signalling. *Nat Cell Biol* 2, E126–E127.
- Thomas, K.J., McCoy, M.K., Blackinton, J., Beilina, A., van der Brug, M., Sandebring, A., Miller, D., Maric, D., Cedazo-Minguez, A., and Cookson, M.R. (2011). DJ-1 acts in parallel to the PINK1/parkin pathway to control mitochondrial function and autophagy. *Hum Mol Genet* 20, 40–50.
- Thompson, E.G., Schaheen, L., Dang, H., and Fares, H. (2007). Lysosomal trafficking functions of mucolipin-1 in murine macrophages. *BMC Cell Biol* 8, 54.
- Tian, X., Gala, U., Zhang, Y., Shang, W., Nagarkar Jaiswal, S., di Ronza, A., Jaiswal, M., Yamamoto, S., Sandoval, H., Duraine, L., et al. (2015). A Voltage-Gated Calcium Channel Regulates Lysosomal Fusion with Endosomes and Autophagosomes and Is Required for Neuronal Homeostasis. *PLoS Biol* 13.
- Treusch, S., Knuth, S., Slaugenhaupt, S.A., Goldin, E., Grant, B.D., and Fares, H. (2004). *Caenorhabditis elegans* functional orthologue of human protein h-mucolipin-1 is required for lysosome biogenesis. *Proc Natl Acad Sci U S A* 101, 4483–4488.
- Tsai, H.-H., Liou, H.-H., Muo, C.-H., Lee, C.-Z., Yen, R.-F., and Kao, C.-H. (2016). Hepatitis C virus infection as a risk factor for Parkinson disease A nationwide cohort study. *Neurology* 86, 840–846.
- Tugba Durlu-Kandilci, N., Ruas, M., Chuang, K.-T., Brading, A., Parrington, J., and Galione, A. (2010). TPC2 proteins mediate nicotinic acid adenine dinucleotide phosphate (NAADP)- and agonist-evoked contractions of smooth muscle. *J. Biol. Chem.* 285, 24925–24932.
- Turrens, J.F. (2003). Mitochondrial formation of reactive oxygen species. *J Physiol* 552, 335–344.
- T.W Ridler, and Calvard, S. (1978). Picture Thresholding Using an Iterative Selection Method. *IEEE Transactions on Systems, Man, and Cybernetics* 8, 630–632.
- Uhlén, P., and Fritz, N. (2010). Biochemistry of calcium oscillations. *Biochemical and Biophysical Research Communications* 396, 28–32.

- Usenovic, M., Tresse, E., Mazzulli, J.R., Taylor, J.P., and Krainc, D. (2012). Deficiency of ATP13A2 leads to lysosomal dysfunction,  $\alpha$ -synuclein accumulation and neurotoxicity. *J Neurosci* 32, 4240–4246.
- Vaarmann, A., Gandhi, S., and Abramov, A.Y. (2010). Dopamine Induces  $\text{Ca}^{2+}$  Signaling in Astrocytes through Reactive Oxygen Species Generated by Monoamine Oxidase. *J Biol Chem* 285, 25018–25023.
- Valente, E.M., Abou-Sleiman, P.M., Caputo, V., Muqit, M.M.K., Harvey, K., Gispert, S., Ali, Z., Turco, D.D., Bentivoglio, A.R., Healy, D.G., et al. (2004). Hereditary Early-Onset Parkinson's Disease Caused by Mutations in PINK1. *Science* 304, 1158–1160.
- Valenzano, K.J., Tafesse, L., Lee, G., Harrison, J.E., Boulet, J.M., Gottshall, S.L., Mark, L., Pearson, M.S., Miller, W., Shan, S., et al. (2005). Pharmacological and pharmacokinetic characterization of the cannabinoid receptor 2 agonist, GW405833, utilizing rodent models of acute and chronic pain, anxiety, ataxia and catalepsy. *Neuropharmacology* 48, 658–672.
- Vanier, M.T. (2010). Niemann-Pick disease type C. *Orphanet J Rare Dis* 5, 16.
- Vanoevelen, J., Raeymaekers, L., Parys, J.B., De Smedt, H., Van Baelen, K., Callewaert, G., Wuytack, F., and Missiaen, L. (2004). Inositol trisphosphate producing agonists do not mobilize the thapsigargin-insensitive part of the endoplasmic-reticulum and Golgi  $\text{Ca}^{2+}$  store. *Cell Calcium* 35, 115–121.
- Vanoevelen, J., Dode, L., Baelen, K.V., Fairclough, R.J., Missiaen, L., Raeymaekers, L., and Wuytack, F. The Secretory Pathway  $\text{Ca}^{2+}/\text{Mn}^{2+}$ -ATPase 2 Is a Golgi-localized Pump with High Affinity for  $\text{Ca}^{2+}$  Ions.
- Venkatachalam, K., and Montell, C. (2007). TRP Channels. *Annu Rev Biochem* 76, 387–417.
- Venkatachalam, K., Hofmann, T., and Montell, C. (2006). Lysosomal Localization of TRPML3 Depends on TRPML2 and the Mucopolipidosis-associated Protein TRPML1. *J Biol Chem* 281, 17517–17527.
- Venkatachalam, K., Wong, C.-O., and Zhu, M.X. (2015). The Role of TRPMLs in Endolysosomal Trafficking and Function. *Cell Calcium* 58, 48–56.
- Venugopal, B., Mesires, N.T., Kennedy, J.C., Curcio-Morelli, C., LaPlante, J.M., Dice, J.F., and Slaughter, S.A. (2009). Chaperone-mediated autophagy is defective in mucopolipidosis type IV. *J. Cell. Physiol.* 219, 344–353.
- Vergarajauregui, S., and Puertollano, R. (2006). Two Di-Leucine Motifs Regulate Trafficking of Mucolin-1 to Lysosomes. *Traffic* 7, 337–353.
- Vergarajauregui, S., Connelly, P.S., Daniels, M.P., and Puertollano, R. (2008). Autophagic dysfunction in mucopolipidosis type IV patients. *Hum Mol Genet* 17, 2723–2737.
- Vergarajauregui, S., Martina, J.A., and Puertollano, R. (2009). Identification of the Penta-EF-hand Protein ALG-2 as a  $\text{Ca}^{2+}$ -dependent Interactor of Mucolin-1. *J. Biol. Chem.* 284, 36357–36366.
- Vilariño-Güell, C., Rajput, A., Milnerwood, A.J., Shah, B., Szu-Tu, C., Trinh, J., Yu, I., Encarnacion, M., Munsie, L.N., Tapia, L., et al. (2014). DNAJC13 mutations in Parkinson disease. *Hum Mol Genet* 23, 1794–1801.

- Villa, N., Do, A., Hershey, J.W.B., and Fraser, C.S. (2013). Human Eukaryotic Initiation Factor 4G (eIF4G) Protein Binds to eIF3c, -d, and -e to Promote mRNA Recruitment to the Ribosome. *J. Biol. Chem.* *288*, 32932–32940.
- Visentin, S., Nuccio, C.D., Bernardo, A., Pepponi, R., Ferrante, A., Minghetti, L., and Popoli, P. (2013). The Stimulation of Adenosine A2A Receptors Ameliorates the Pathological Phenotype of Fibroblasts from Niemann-Pick Type C Patients. *J. Neurosci.* *33*, 15388–15393.
- Vosler, P.S., Gao, Y., Brennan, C.S., Yanagiya, A., Gan, Y., Cao, G., Zhang, F., Morley, S.J., Sonenberg, N., Bennett, M.V.L., et al. (2011). Ischemia-induced calpain activation causes eukaryotic (translation) initiation factor 4G1 (eIF4G1) degradation, protein synthesis inhibition, and neuronal death. *Proc Natl Acad Sci U S A* *108*, 18102–18107.
- Vruchte, D. te, Lloyd-Evans, E., Veldman, R.J., Neville, D.C.A., Dwek, R.A., Platt, F.M., Blitterswijk, W.J. van, and Sillence, D.J. (2004). Accumulation of Glycosphingolipids in Niemann-Pick C Disease Disrupts Endosomal Transport. *J. Biol. Chem.* *279*, 26167–26175.
- Wakabayashi, K., Tanji, K., Odagiri, S., Miki, Y., Mori, F., and Takahashi, H. (2013). The Lewy Body in Parkinson's Disease and Related Neurodegenerative Disorders. *Mol Neurobiol* *47*, 495–508.
- Wallingford, J.B., and Habas, R. (2005). The developmental biology of Dishevelled: an enigmatic protein governing cell fate and cell polarity. *Development* *132*, 4421–4436.
- Walseth, T.F., Lin-Moshier, Y., Weber, K., Marchant, J.S., Slama, J.T., and Guse, A.H. (2012a). Nicotinic Acid Adenine Dinucleotide 2'-Phosphate (NAADP) Binding Proteins in T-Lymphocytes. *Messenger (Los Angel)* *1*, 86–94.
- Walseth, T.F., Lin-Moshier, Y., Jain, P., Ruas, M., Parrington, J., Galione, A., Marchant, J.S., and Slama, J.T. (2012b). Photoaffinity Labeling of High Affinity Nicotinic Acid Adenine Dinucleotide Phosphate (NAADP)-Binding Proteins in Sea Urchin Egg. *J Biol Chem* *287*, 2308–2315.
- Walter, M., Davies, J.P., and Ioannou, Y.A. (2003). Telomerase immortalization upregulates Rab9 expression and restores LDL cholesterol egress from Niemann-Pick C1 late endosomes. *J. Lipid Res.* *44*, 243–253.
- Walter, M., Chen, F.W., Tamari, F., Wang, R., and Ioannou, Y.A. (2009). Endosomal lipid accumulation in NPC1 leads to inhibition of PKC, hypophosphorylation of vimentin and Rab9 entrapment. *Biology of the Cell* *101*, 141–153.
- Wang, M., and Kaufman, R.J. (2016). Protein misfolding in the endoplasmic reticulum as a conduit to human disease. *Nature* *529*, 326–335.
- Wang, H., Liu, T., Li, L., Wang, Q., Yu, C., Liu, X., and Li, W. (2015a). Tetrandrine is a potent cell autophagy agonist via activated intracellular reactive oxygen species. *Cell & Bioscience* *5*, 4.
- Wang, W., Gao, Q., Yang, M., Zhang, X., Yu, L., Lawas, M., Li, X., Bryant-Genevier, M., Southall, N.T., Marugan, J., et al. (2015b). Up-regulation of lysosomal TRPML1 channels is essential for lysosomal adaptation to nutrient starvation. *PNAS* *112*, E1373–E1381.
- Wang, W., Wang, X., Fujioka, H., Hoppel, C., Whone, A.L., Caldwell, M.A., Cullen, P.J., Liu, J., and Zhu, X. (2016). Parkinson's disease-associated mutant VPS35 causes mitochondrial dysfunction by recycling DLP1 complexes. *Nat Med* *22*, 54–63.



- Wang, X., Zhang, X., Dong, X.-P., Samie, M., Li, X., Cheng, X., Goschka, A., Shen, D., Zhou, Y., Harlow, J., et al. (2012). TPC proteins are phosphoinositide-activated sodium-selective ion channels in endosomes and lysosomes. *Cell* 151, 372–383.
- Ward, R.J., Zucca, F.A., Duyn, J.H., Crichton, R.R., and Zecca, L. (2014). The role of iron in brain ageing and neurodegenerative disorders. *The Lancet Neurology* 13, 1045–1060.
- Weibel, E.R., Stäubli, W., Gnägi, H.R., and Hess, F.A. (1969). CORRELATED MORPHOMETRIC AND BIOCHEMICAL STUDIES ON THE LIVER CELL. *J Cell Biol* 42, 68–91.
- Westermann, B. (2015). The mitochondria–plasma membrane contact site. *Current Opinion in Cell Biology* 35, 1–6.
- Williams, J.H., and Kauer, J.A. (1997). Properties of Carbachol-Induced Oscillatory Activity in Rat Hippocampus. *Journal of Neurophysiology* 78, 2631–2640.
- Wu, F., Xu, H.-D., Guan, J.-J., Hou, Y.-S., Gu, J.-H., Zhen, X.-C., and Qin, Z.-H. (2015a). Rotenone impairs autophagic flux and lysosomal functions in Parkinson’s disease. *Neuroscience* 284, 900–911.
- Wu, W.Y.-Y., Kang, K.-H., Chen, S.L.-S., Chiu, S.Y.-H., Yen, A.M.-F., Fann, J.C.-Y., Su, C.-W., Liu, H.-C., Lee, C.-Z., Fu, W.-M., et al. (2015b). Hepatitis C virus infection: a risk factor for Parkinson’s disease. *J Viral Hepat* 22, 784–791.
- Wu, Y., Kazumura, K., Maruyama, W., Osawa, T., and Naoi, M. (2015c). Rasagiline and selegiline suppress calcium efflux from mitochondria by PK11195-induced opening of mitochondrial permeability transition pore: a novel anti-apoptotic function for neuroprotection. *J Neural Transm* 122, 1399–1407.
- Xiao, H., Killip, M.J., Staeheli, P., Randall, R.E., and Jackson, D. (2013). The Human Interferon-Induced MxA Protein Inhibits Early Stages of Influenza A Virus Infection by Retaining the Incoming Viral Genome in the Cytoplasm. *J Virol* 87, 13053–13058.
- Xicoy, H., Wieringa, B., and Martens, G.J.M. (2017). The SH-SY5Y cell line in Parkinson’s disease research: a systematic review. *Mol Neurodegener* 12.
- Xie, X., Van Deusen, A.L., Vitko, I., Babu, D.A., Davies, L.A., Huynh, N., Cheng, H., Yang, N., Barrett, P.Q., and Perez-Reyes, E. (2007). Validation of High Throughput Screening Assays Against Three Subtypes of Cav3 T-Type Channels Using Molecular and Pharmacologic Approaches. *ASSAY and Drug Development Technologies* 5, 191–204.
- Xu, H., Delling, M., Li, L., Dong, X., and Clapham, D.E. (2007). Activating mutation in a mucolipin transient receptor potential channel leads to melanocyte loss in varitint–waddler mice. *Proc Natl Acad Sci U S A* 104, 18321–18326.
- Xu, M., Liu, K., Swaroop, M., Porter, F.D., Sidhu, R., Finkes, S., Ory, D.S., Marugan, J.J., Xiao, J., Southall, N., et al. (2012).  $\delta$ -Tocopherol Reduces Lipid Accumulation in Niemann-Pick Type C1 and Wolman Cholesterol Storage Disorders. *J. Biol. Chem.* 287, 39349–39360.
- Xu, M., Li, X.-X., Wang, L., Wang, M., Zhang, Y., and Li, P.-L. (2015). Contribution of Nrf2 to Atherogenic Phenotype Switching of Coronary Arterial Smooth Muscle Cells Lacking CD38 Gene. *Cell Physiol Biochem* 37, 432–444.

- Yamaguchi, S., Jha, A., Li, Q., Soyombo, A.A., Dickinson, G.D., Churamani, D., Brailoiu, E., Patel, S., and Muallem, S. (2011). Transient receptor potential mucolipin 1 (TRPML1) and two-pore channels are functionally independent organellar ion channels. *J. Biol. Chem.* *286*, 22934–22942.
- Yamasaki, M., Masgrau, R., Morgan, A.J., Churchill, G.C., Patel, S., Ashcroft, S.J.H., and Galione, A. (2004). Organelle Selection Determines Agonist-specific Ca<sup>2+</sup> Signals in Pancreatic Acinar and  $\beta$  Cells. *J. Biol. Chem.* *279*, 7234–7240.
- Yamasaki, M., Thomas, J.M., Churchill, G.C., Garnham, C., Lewis, A.M., Cancela, J.-M., Patel, S., and Galione, A. (2005). Role of NAADP and cADPR in the Induction and Maintenance of Agonist-Evoked Ca<sup>2+</sup> Spiking in Mouse Pancreatic Acinar Cells. *Current Biology* *15*, 874–878.
- Yamashiro, M. (1987). Kinetics of endosome acidification in mutant and wild-type Chinese hamster ovary cells. *J Cell Biol* *105*, 2713–2721.
- Yang, C., Guo, L., Liu, X., Zhang, H., and Liu, M. (2007). Determination of tetrandrine and fangchinoline in plasma samples using hollow fiber liquid-phase microextraction combined with high-performance liquid chromatography. *Journal of Chromatography A* *1164*, 56–64.
- Youdim, M.B.H., and Bakhle, Y.S. (2006). Monoamine oxidase: isoforms and inhibitors in Parkinson's disease and depressive illness. *British Journal of Pharmacology* *147*, S287–S296.
- Yu, L., McPhee, C.K., Zheng, L., Mardones, G.A., Rong, Y., Peng, J., Mi, N., Zhao, Y., Liu, Z., Wan, F., et al. (2010). Termination of autophagy and reformation of lysosomes regulated by mTOR. *Nature* *465*, 942–946.
- Yu, W., Gong, J.-S., Ko, M., Garver, W.S., Yanagisawa, K., and Michikawa, M. (2005). Altered cholesterol metabolism in Niemann-Pick type C1 mouse brains affects mitochondrial function. *J. Biol. Chem.* *280*, 11731–11739.
- Yuan, J.P., Kim, M.S., Zeng, W., Shin, D.M., Huang, G., Worley, P.F., and Muallem, S. (2009). TRPC channels as STIM1-regulated SOCs. *Channels* *3*, 221–225.
- Zacharias, D.A., and Kappen, C. (1999). Developmental expression of the four plasma membrane calcium ATPase (Pmca) genes in the mouse. *Biochimica et Biophysica Acta (BBA) - General Subjects* *1428*, 397–405.
- Zarranz, J.J., Alegre, J., Gómez-Esteban, J.C., Lezcano, E., Ros, R., Ampuero, I., Vidal, L., Hoenicka, J., Rodriguez, O., Atarés, B., et al. (2004). The new mutation, E46K, of  $\alpha$ -synuclein causes parkinson and Lewy body dementia. *Ann Neurol.* *55*, 164–173.
- Zavodszky, E., Seaman, M.N.J., Moreau, K., Jimenez-Sanchez, M., Breusegem, S.Y., Harbour, M.E., and Rubinsztein, D.C. (2014). Mutation in VPS35 associated with Parkinson's disease impairs WASH complex association and inhibits autophagy. *Nature Communications* *5*, 3828.
- Zecca, L., Fariello, R., Riederer, P., Sulzer, D., Gatti, A., and Tampellini, D. (2002). The absolute concentration of nigral neuromelanin, assayed by a new sensitive method, increases throughout the life and is dramatically decreased in Parkinson's disease. *FEBS Letters* *510*, 216–220.
- Zeevi, D.A., Frumkin, A., Offen-Glasner, V., Kogot-Levin, A., and Bach, G. (2009). A potentially dynamic lysosomal role for the endogenous TRPML proteins. *J. Pathol.* *219*, 153–162.
- Zeng, B.-Y., Medhurst, A.D., Jackson, M., Rose, S., and Jenner, P. (2005). Proteasomal activity in brain differs between species and brain regions and changes with age. *Mechanisms of Ageing and Development* *126*, 760–766.

- Zhang, F., Zhang, G., Zhang, A.Y., Koeberl, M.J., Wallander, E., and Li, P.-L. (2006). Production of NAADP and its role in Ca<sup>2+</sup> mobilization associated with lysosomes in coronary arterial myocytes. *Am. J. Physiol. Heart Circ. Physiol.* *291*, H274-282.
- Zhang, F., Jin, S., Yi, F., and Li, P.-L. (2009). TRP-ML1 functions as a lysosomal NAADP-sensitive Ca<sup>2+</sup> release channel in coronary arterial myocytes. *J. Cell. Mol. Med.* *13*, 3174–3185.
- Zhang, F., Xia, M., and Li, P.-L. (2010). Lysosome-dependent Ca<sup>2+</sup> release response to Fas activation in coronary arterial myocytes through NAADP: evidence from CD38 gene knockouts. *Am. J. Physiol., Cell Physiol.* *298*, C1209-1216.
- Zhang, F., Xu, M., Han, W.-Q., and Li, P.-L. (2011). Reconstitution of lysosomal NAADP-TRP-ML1 signaling pathway and its function in TRP-ML1(-/-) cells. *Am. J. Physiol., Cell Physiol.* *301*, C421-430.
- Zhang, X., Li, X., and Xu, H. (2012). Phosphoinositide isoforms determine compartment-specific ion channel activity. *Proc Natl Acad Sci U S A* *109*, 11384–11389.
- Zhang, X., Cheng, X., Yu, L., Yang, J., Calvo, R., Patnaik, S., Hu, X., Gao, Q., Yang, M., Lawas, M., et al. (2016). MCOLN1 is a ROS sensor in lysosomes that regulates autophagy. *Nature Communications* *7*, 12109.
- Zhang, Z.-H., Lu, Y.-Y., and Yue, J. (2013). Two Pore Channel 2 Differentially Modulates Neural Differentiation of Mouse Embryonic Stem Cells. *PLOS ONE* *8*, e66077.
- Zhitomirsky, B., and Assaraf, Y.G. (2014). Lysosomal sequestration of hydrophobic weak base chemotherapeutics triggers lysosomal biogenesis and lysosome-dependent cancer multidrug resistance. *Oncotarget* *6*, 1143–1156.
- Zhou, W., and Freed, C.R. (2005). DJ-1 Up-regulates Glutathione Synthesis during Oxidative Stress and Inhibits A53T  $\alpha$ -Synuclein Toxicity. *J. Biol. Chem.* *280*, 43150–43158.
- Zhou, Q., Yen, A., Rymarczyk, G., Asai, H., Trengrove, C., Aziz, N., Kirber, M.T., Mostoslavsky, G., Ikezu, T., Wolozin, B., et al. (2016). Impairment of PARK14-dependent Ca<sup>2+</sup> signalling is a novel determinant of Parkinson's disease. *Nat Commun* *7*, 10332.
- Zong, X., Schieder, M., Cuny, H., Fenske, S., Gruner, C., Rötzer, K., Griesbeck, O., Harz, H., Biel, M., and Wahl-Schott, C. (2009). The two-pore channel TPCN2 mediates NAADP-dependent Ca<sup>2+</sup>-release from lysosomal stores. *Pflugers Arch - Eur J Physiol* *458*, 891–899.
- Zoratti, C., Kipmen-Korgun, D., Osibow, K., Malli, R., and Graier, W.F. (2003). Anandamide initiates Ca<sup>2+</sup> signaling via CB2 receptor linked to phospholipase C in calf pulmonary endothelial cells. *Br J Pharmacol* *140*, 1351–1362.
- Zou, J., Hu, B., Arpag, S., Yan, Q., Hamilton, A., Zeng, Y.-S., Vanoye, C.G., and Li, J. (2015). Reactivation of Lysosomal Ca<sup>2+</sup> Efflux Rescues Abnormal Lysosomal Storage in FIG4-Deficient Cells. *J. Neurosci.* *35*, 6801–6812.
- Züchner, S., Mersiyanova, I.V., Muglia, M., Bissar-Tadmouri, N., Rochelle, J., Dadali, E.L., Zappia, M., Nelis, E., Patitucci, A., Senderek, J., et al. (2004). Mutations in the mitochondrial GTPase mitofusin 2 cause Charcot-Marie-Tooth neuropathy type 2A. *Nat Genet* *36*, 449–451.